Heteroleptic Dirhodium(II,II) Complexes: Synthesis, Spectroscopy and Applications in Hydroformylation and Hydroaminomethylation Catalytic Reactions

Stephen George de Doncker

University of Cape Town

DECEMBER 2023

Heteroleptic Dirhodium(II,II) Complexes: Synthesis, Spectroscopy and Applications in Hydroformylation and Hydroaminomethylation Catalytic Reactions

Thesis presented for the degree of

DOCTOR OF PHILOSOPHY

By

Stephen George de Doncker

Supervisors: **Doctor Siyabonga Ngubane (UCT)**

Professor Gregory S. Smith (UCT)

Department of Chemistry

Faculty of Science

University of Cape Town

DECEMBER 2023

Plagiarism Declaration

I, Stephen George de Doncker, hereby declare that I know the meaning of plagiarism and that all work contained in the document entitled,

"**Heteroleptic Dirhodium(II,II) Complexes: Synthesis, Spectroscopy and Applications in Hydroformylation and Hydroaminomethylation Catalytic Reactions"**,

is my own, original work and has not been submitted for examination for any degree at the University of Cape Town, or any other university. All sources of information contained herein are acknowledged, cited, and fully referenced. I authorise the University to reproduce for the purpose of research either the whole or any portion of the contents contained herein in any manner whatsoever.

Signature: Signed by candidate

Date: 31 December 2023

Acknowledgements

Firstly, I would like to extend thanks and gratitude to my supervisors, Dr Siyabonga Ngubane and Prof. Gregory Smith for the continuous support, encouragement, and guidance throughout the duration of both my MSc and PhD projects. I acknowledge that the constructive criticism, input, and discussion over the past few years, resulting in my general and academic growth has been of incredible valuable, and for this, I appreciate both of you enormously.

I would like to acknowledge Dr Marwaan Rylands for his expertise and advice on NMR related topics and Dr Marietjie Stander (University of Stellenbosch) for collection of ESI-MS data. Special mention must be given the members of the chemistry central admin office and to Deirdre Brooks for the meaningful chats, venting and much needed laughter and smiles.

To my friends, Desmond, Geoffrey, Jauhar, Dylan and Fernando, thank you for the friendship, support and good times over the years. The impact you guys have had on my life is immeasurable, and I hope that this synergy will continue over the coming years.

To my colleagues and friends, Athi Welsh, Taryn Golding, Dr Preshendren Govender, Dr Wade Petersen, Dr Shepherd Siangwata and Dr Daniel Kusza, thank you for the support, advice and the general atmosphere provided in and around the lab. We are significantly influenced by the company we keep, and in this regard, I feel that time could not have been spent more wisely in other company.

I would like to acknowledge the past and present members of the Smith and Ngubane research groups in the department of chemistry at UCT for the input and discussions throughout the duration of this degree.

Penultimately, to my family; Edgar, Emma, Lauren and Michelle, lessons learned through and with you have helped me throughout my life, with every challenge that has presented itself. Thank you for everything.

Finally, funding for this project was graciously provided by the National Research Foundation, the Department of Science and Technology, c*change, and SASOL group technology.

"Success is not final; failure is not fatal: It is the courage to continue that counts."

-Winston S. Churchill

Abstract

The synthesis of a series of bis-substituted heteroleptic dirhodium(II,II) complexes containing bridging acetate and chelating bipyridyl ligands is herein described. The protons at the 4- and 4'- positions of the bipyridyl ligands on the model complex **1** were substituted by either the electron withdrawing CF_3 (complex **2**) or electron donating OMe (complex **3**) groups, to observe the electronic influence on the metal complexes. As such, electroanalysis using cyclic voltammetry indicated variations in the metal-centred redox processes for the title complexes. The complexes obtained were used as pre-catalysts for the hydroformylation and hydroaminomethylation of olefins, an unprecedented homogenous catalysis system. Additionally, significant influence on the physicochemical properties of the complexes was determined using various analytical techniques. Factors such as (i) the hemi-lability of either the acetate (OAc^-) or hexafluorophosphate (PF_6^-) counter ion; (ii) substituents on the bipyridyl ligand; and (iii) the metathesis exchange between the OAc^- (complexes **1** - **3**) and PF_6^- (complexes **4** - **6**) counter ions, and their influence on the catalytic activity (hydroformylation and hydroaminomethylation) of the complexes is presented.

The series of complexes incorporate two known (**1** and **4**) and four new (**2**, **3**, **5**, and **6**) complexes. All complexes were characterised by spectroscopic (^1H, $^{13}C\{^1H\}$, ^{19}F, ^{31}P and DOSY NMR, FT-IR), electrochemical (cyclic voltammetry) and analytical (HPLC, conductivity and mass spectrometry) techniques where applicable.

The evaluation of the synthesised complexes in the hydroformylation reaction was initiated by comparison of model complex (**1**) and the fully substituted dirhodium(II,II) tetraacetate complex previously reported in the hydroformylation of 1-octene. Subsequently, further optimisation reactions were carried out under varying conditions (temperature, pressure and time). This resulted in optimal conditions of 85 °C, 40 bar syngas pressure and 4-hour reaction time being chosen. A catalyst loading of 2.87×10^{-3} mmol was employed for further catalytic reactions. Under the optimised conditions, the addition of mercury had no effects on the activity and selectivity indicating that the catalytic reaction is purely homogenous, the result of a molecular catalytic species. The complexes bearing acetate counter ions (**1** - **3**) showed near quantitative conversion (>97%) of 1-octene substrate with moderate to excellent activity. Excellent chemoselectivity toward aldehydes (>84%) with moderate regioselectivity towards

linear products (40 - 44%) were also observed in the hydroformylation of 1-octene. The incorporation of the hexafluorophosphate counter ions (**4 - 6**) were found to affect the chemo- and regioselectivity through both electronic, and steric factors.

The substrate scope was extended with catalyst precursor (complex **2**) showing the highest chemoselectivity for aldehyde in the hydroformylation of 1 octene. Long chain internal (7-tetradecene), cyclic (cyclohexene) and benzylic (styrene) olefins were explored as substrates. The catalyst showed moderate to excellent conversion (76 - 98%) under modified catalytic conditions, with chemo- and regioselectivity found to depend on the nature of the substrate. No hydrogenated products (alkanes and alcohols) were detected in any of the hydroformylation reactions carried out. Recyclability of the catalyst precursor was achieved, resulting from a combination of the PF_6^- counter ion and methoxy substituent (complex **6**) showing reproducible catalytic results over 5 cycles.

Prior to application in the hydroaminomethylation reaction, optimisation of the catalyst system toward hydrogenation of imines and enamines was carried out. As such, the optimised conditions of 105 °C, 40 bar H_2 pressure, 0.08 mol% catalyst loading, and 4-hour reaction time were applied to model substrates to determine the selectivity towards amine product(s). The applicability for the hydroaminomethylation reaction was explored with the trifluoromethyl congener (complex **5)**, varying the partial pressure of CO relative to H_2 in the syngas mixture to optimise the consumption of substrate and the formation of the target amine products. The use of aromatic amine substrates yielded low conversion to target products while aliphatic amine substrates showed good to excellent production of both secondary and tertiary amines, in combination with a range of olefin substrates.

Due to the multiple steps required for the conventional synthesis of pharmaceutically active compounds, incorporation of a catalytic step by way of hydroaminomethylation is a promising way of synthesising a library of compounds for structure-activity studies. To this end, the optimised catalyst and conditions were applied toward the hydroaminomethylation of a suitable substrate to afford two analogues of a known opioid analgesic, Tramadol® in low (34%) to excellent (74%) yields.

Publications, Conference Contributions and Awards

Journal article

Heteroleptic dirhodium(II,II) acetato-bipyridyl complexes: evaluation as catalyst precursors for hydroformylation reactions

Stephen de Doncker, Gregory S. Smith and Siyabonga Ngubane, *Appl. Catal. A Gen.*, 2023, **667**, 119440.

Conference Contributions

1. *Heteroleptic dirhodium(II,II) complexes as catalyst precursors toward the hydroformylation and hydroaminomethylation of alkenes* (oral presentation).
   CATSA Conference, Mossel Bay, (5 - 8 November 2023).
   Stephen de Doncker, Gregory S. Smith and Siyabonga Ngubane.

2. *Development of dirhodium(II,II) catalyst precursors toward the chemoselective hydroaminomethylation of alkenes* (flash oral presentation).
   Young Chemists' Symposium, University of Western Cape, (15 September 2023).
   Stephen de Doncker, Gregory S. Smith and Siyabonga Ngubane.

3. *Development of heteroleptic dirhodium(II,II) catalyst precursors toward the hydroformylation and hydroaminomethylation of Alkenes* (flash oral and poster presentation).
   XXV EuCOMC conference, Alcala de Henares, Madrid, Spain, (4 - 8 September 2023).
   Stephen de Doncker, Gregory S. Smith and Siyabonga Ngubane.

4. *Cationic dirhodium(II,II) acetate-bipyridyl chelate complexes: synthesis and application as catalytic precursors for the hydroformylation of 1-octene* (poster presentation).
   44th SACI National convention, Stellenbosch (8 - 13 January 2023).
   Stephen de Doncker, Gregory S. Smith and Siyabonga Ngubane.

5. *Cationic dirhodium(II,II) acetate-bipyridyl chelate complexes: synthesis and application as catalytic precursors for the hydroformylation of 1-octene* (poster presentation).
   CATSA conference, Champagne Sports Resort, Central Drakensberg (13 - 16 November 2022)
   Stephen de Doncker, Gregory S. Smith and Siyabonga Ngubane.

6. *Dirhodium(II,II) paddlewheel complexes: synthesis, structure, electrochemistry and hydroformylation activity* (oral presentation).
   Young Chemists' Symposium, University of Cape Town, (30 September 2020).
   Stephen de Doncker, Gregory S. Smith and Siyabonga Ngubane.

Awards

1. Vice Chancellor Research Scholarship award (2020 - 2022)
2. NRF Innovation Doctoral Scholarship (2020 - 2023)
3. Runner up prize for oral presentation, Young Chemists' Symposium (2020)

Abbreviations, Symbols, Formulas and Units

°	Degree(s)
δ	Chemical shift/partial charge
2D	Two-dimensional
°C	Degrees Celsius
μ	Mu(bridging)
API	Active pharmaceutical ingredient
Ar	Aromatic or aryl
ATR	Attenuated total reflectance
br	Broad signal (NMR); branched
$^{13}C\{^{1}H\}$	Proton decoupled carbon-13
cat.	Catalyst
$CDCl_3$	Deuterated chloroform
$CHCl_3$	Chloroform
cm^{-1}	Wavenumbers (reciprocal centimetres)
d	Doublet
dd	Doublet of doublets
DCM	Dichloromethane
DMSO	Dimethyl sulfoxide
DMSO-d_6	Deuterated dimethyl sulfoxide
EI	Electron impact
eq.	Equivalent(s)
ESI	Electrospray ionisation
EtOH	Ethanol
FT-IR	Fourier transform infrared spectroscopy
g	Gram(s)
GC	Gas chromatography
^{1}H	Proton
h	Hour(s)
HAM	Hydroaminomethylation
HETCOR	Heteronuclear correlation spectroscopy
HF	Hydroformylation

HPLC	High-performance liquid chromatography
HR	High resolution
HSQC	Heteronuclear single quantum correlation
Hz	Hertz
IR	Infrared
J	Coupling constant
kV	Kilovolt(s)
LC-MS	Liquid chromatography mass spectrometry
lin	Linear
m	Multiplet (NMR); medium intensity (IR)
MeOD	Deuterated methanol
MeOH	Methanol
MHz	Megahertz
mL	Millilitre(s)
mmol	Millimole(s)
mol	Mole(s)
MP	Melting Point
MS	Mass spectrometry
m/z	Mass to charge ratio
n	Normal
NMR	Nuclear magnetic resonance
o	Ortho-
p	Para-
Pet. Ether	Petroleum ether
PGM	Platinum group metals
Ph	Phenyl
ppm	Parts per million
^{31}P	Phosphorous
q	Quartet
rt	Room temperature
s	Singlet (NMR); strong intensity (IR)
SD	Standard deviation
SHOP	Shell higher olefin process

syngas	Synthesis gas
t	Triplet
TEPO	Triethyl phosphine oxide
TOF	Turnover frequency
vs	Versus
w	Weak intensity (IR)

Table of Contents

Chapter 1

Literature review

1.1 Catalysis

A catalyst, by definition, allows for a reaction to proceed *via* a reaction coordinate pathway presenting a lower activation energy barrier, without being consumed in the process.[1] Transition metal catalysed reactions form an important part of both synthetic and industrial chemical processes, providing an efficient and targeted method of producing value-added compounds for a variety of economic sectors.[2-4] Catalytic reactions provide a means of reduction or even the elimination of harmful by-products and/or generated waste from chemical processes, ordinarily associated with conventional stoichiometric syntheses, thereby facilitating more efficient synthetic procedures.[5] In recent years, the demand for industrial reactions which place less burden on the environment through more eco-friendly processes is increasing in various economic sectors, the most prominent including the pharmaceutical, automobile and petrochemical industries.[6-8]

The petrochemical industry produces a substantial amount of precursors for other economic sectors such as agrochemicals and textiles (produced from ethylene and propylene monomers, for example), in addition to fuel for bulk energy supply.[9-11] Furthermore, catalytic processes are used in the majority (around 90%) of syntheses toward the production of important goods and chemicals available for consumers over a broad scope of markets.[1,12] Therefore, there exists an ever-growing need for the design and development of new and improved catalysts and catalytic reactions. Research efforts toward reducing the environmental impact are an important consideration for 'greener' chemical reactions while increasing economic value, particularly in the fuel, pharmaceutical, fine chemical, and commodity chemical industries.[13-15] As described by Anastas and others, catalysis not only contributes to several Green Chemistry principles but is also the basis of one pillar in the Green Chemistry philosophy (Figure 1.1, *overleaf*).[15-17]

Additionally, the field of industrially applicable catalyst development is growing, with efforts to improve the activity, selectivity, atom economy and the recyclability of high-cost transition metal catalysts, predominantly for economic and environmental benefit.[15,18] Catalysts and catalytic reactions are divided into either heterogeneous or homogeneous classes, where a variety of metal-based compounds are used to effect the required molecular changes.

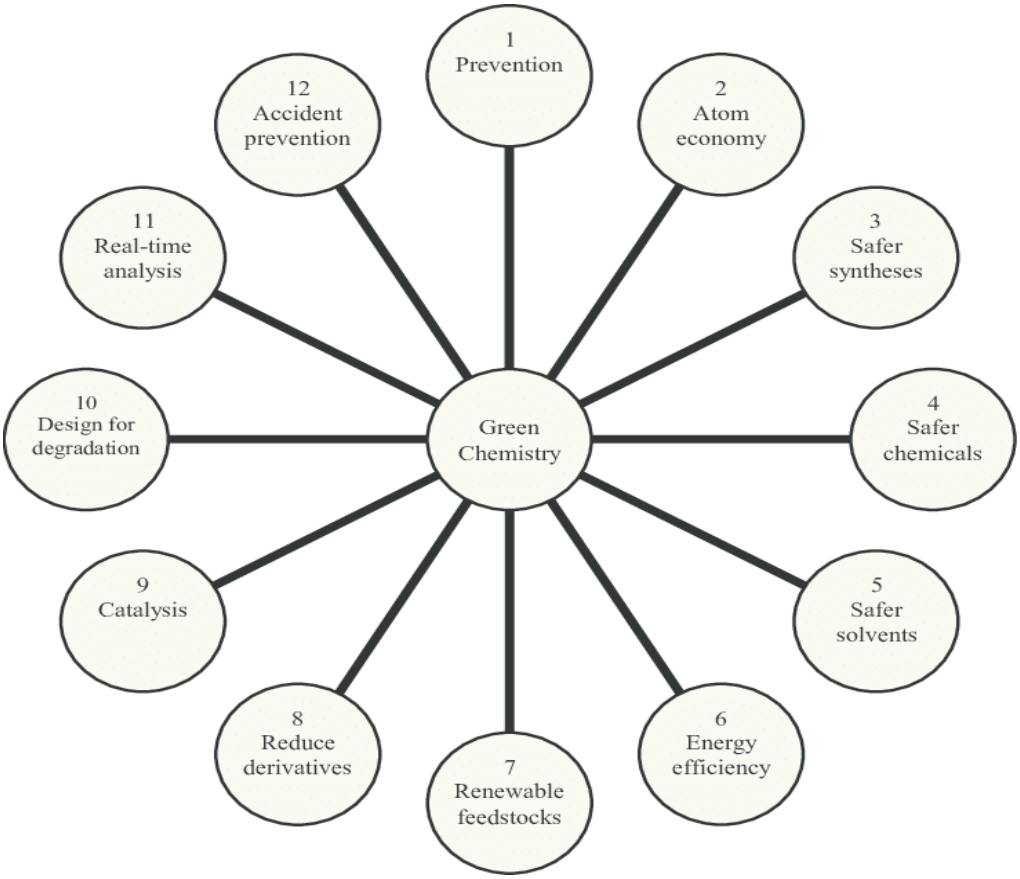

Figure 1.1. A graphic representation of the principles of green chemistry toward sustainable methods for producing economically valuable chemical compounds.[14,16]

1.1.1 Heterogeneous Catalysis

Heterogeneous catalysis is characterised by reactions where the catalytically active species is in a different phase to the reaction medium, relying on the ability of interactions on the catalyst surface to facilitate changes through the breaking and reforming of chemical bonds.[19] Furthermore, heterogeneous catalytic systems allow for relatively simplistic means of recovery of the catalyst. Catalyst recovery is important for several reasons, including the toxicity of the precious metals (cobalt and nickel for example) used in these processes and reducing the

economic impact involved when replacing spent catalytic species. By way of example, the conversion of synthesis gas (CO/H_2) to olefins and related products from the Fischer-Tropsch reaction using cobalt and the hydrogenation of C-C double bonds by carbon supported palladium catalysts involve disposal of toxic metal-based species that are widely used in industry and academia.[20,21] The major disadvantage of a heterogeneous catalytic system is restriction of the reaction to the contact surface between the phases, impacting the selectivity and reactivity negatively when compared to homogeneous catalytic reactions.

1.1.2 Homogeneous Catalysis

Homogeneous catalysis is characterised by reactions where the active catalyst or catalyst precursor and substrate are in the same phase. The distinction between the active catalyst and catalyst precursor is often described for homogeneous reactions, since the dissociation of a ligand to allow formation of the active species usually occurs *in-situ* after some induction period.[22] Some of the primary advantages associated with typical homogeneous catalytic systems include high selectivity and reactivity. This occurs due to favourable catalyst-substrate interactions which are maximised throughout the reaction medium. The modification of crucial properties such as steric influence around the catalytically active site is widely reported for enhancing aspects such as the chemoselectivity, regioselectivity and the enantioselectivity of the catalyst.[23-25] In addition to these structural changes, the electronic influence of the ligand is also exploited by varying appended functional groups, ligand donor atoms, as well as incorporating aromatic moieties to enhance catalytic activity. Some well-known examples of homogeneous catalytic reactions are allylic oxidation,[26,27] carbonylation,[28-30] hydrogenation,[31-34] hydroformylation,[35-37] hydroaminomethylation[38-41] and palladium-catalysed cross coupling.[42,43]

While these characteristics of homogeneous catalytic reactions are widely considered to be advantageous, a major disadvantage is encountered once separation of the desired product and the expensive, toxic or spent catalytic species from the reaction mixture is undertaken.[44,45] This is usually accomplished by energy intensive processes such as distillation, which may cause catalyst degradation if high temperatures are required.[46] Considerations into combining the high activity and selectivity associated with homogeneous catalysis, and the excellent recyclability characteristic of a heterogeneous catalytic system could circumvent this, whereby several strategies may be explored. Particularly, research efforts into improving the

recyclability of expensive precious metals used for industrially relevant catalytic reactions such as hydroformylation are therefore ongoing.

The industrial relevance of both homogeneous and heterogeneous catalytic reactions is large and continually evolving.[47-51] A major driving factor for the continued research and development of new and improved catalytic reactions is sustainability, in terms of both resources required to produce catalyst species and the use of renewable feedstocks. A summary of some important heterogeneous and homogeneous catalytic reactions is shown in Table 1.1.

Table 1.1: Outline of some important heterogeneous and homogeneous metal-based catalytic processes in academia and industry.[47-51]

Catalytic reaction	**Catalyst**	**Authored by (Year)**
Dehydrogenation of alcohols (ethanol)	Metal	Van Marum (1796)
Decomposition of H_2O_2 and NH_3	Metal	Thenard (1813)
Oxidation of SO_2 to SO_3 (contact process)	Pt	Phillips (1831)
$HCl + O_2 \rightarrow Cl_2$	Cu	Deacon (1875)
NH_3 synthesis from N_2 and H_2 under high pressure	Fe	Haber (1909)
$CO + H_2 \rightarrow CH_3OH$	ZnO-chromia	BASF (1923)
Hydrogenation of vegetable oils	Ni	Raney (1926)
Fischer-Tropsch Synthesis	Fe, Co	Fischer, Tropsch (1923)
Hydroformylation	Co, Rh	Roelen (1938)

1.2 The hydroformylation reaction

The hydroformylation reaction involves the addition of a formyl group to an olefin substrate using a transition-metal catalyst (Scheme 1.1, *overleaf*). This reaction was discovered by Otto Roelen in 1938, while carrying out investigation of the conversion of olefins formed from the Fischer-Tropsch process, into oxygenated byproducts.[52,53] Although aldehydes are the major product of the hydroformylation reaction, the hydrogenation of the alkene substrates to form alkanes, and the hydrogenation of the aldehyde products to produce alcohols can also occur.[29]

Additionally, the isomerisation of the alkene substrate may occur, producing further isomeric aldehydes which may then undergo hydrogenation, substantially lowering the selectivity of the reaction if a particular aldehyde is the intended target product.

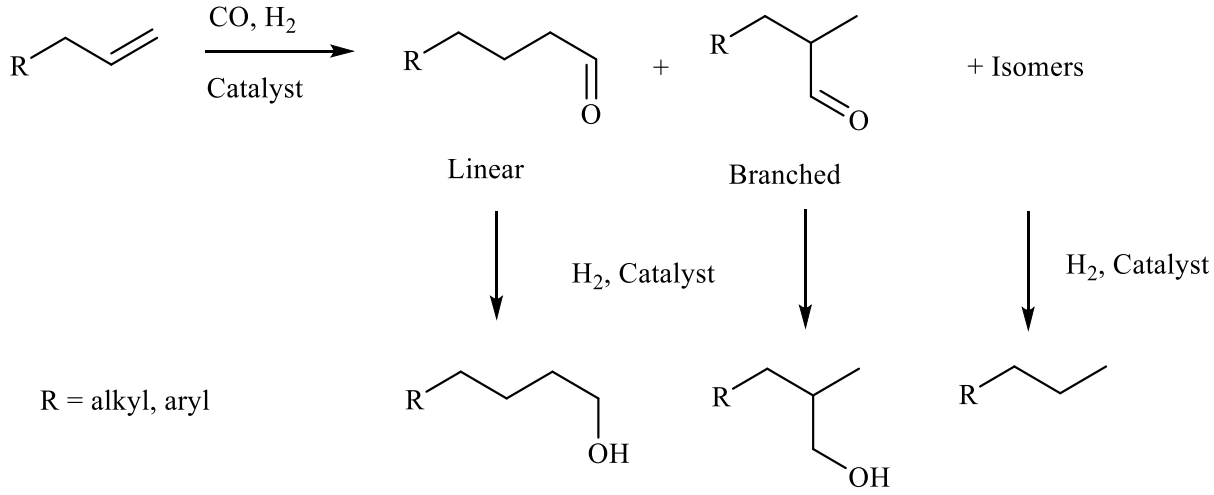

Scheme 1.1. Outline of possible products formed during the hydroformylation reaction.

The catalytic functionalisation of alkene feedstocks is the focus of some of the largest industrial processes, transforming lower-value substrates obtained from the refining of crude oil by the petroleum and chemical processing industries into higher value aldehyde products with many synthetic applications.[51] By way of example, aldehyde products obtained from the hydroformylation of these available feedstocks can be used as precursors for acrolein, alcohols, carboxylic acids, acetals, amines and pyrans toward further valorisation for the flavour, fragrance and surfactant markets.[54-57]

Since its inception, various transition metals have been evaluated as potential catalyst precursors in the hydroformylation reaction, including platinum, iridium, ruthenium, iron, cobalt, and rhodium.[58] Catalyst precursors containing cobalt and rhodium are subject to extensive study due to their high activity and selectivity in both modified and unmodified forms.[28,29,59] First-generation hydroformylation reactions exploited the findings of Otto Roelen, using cobalt-based carbonyl (CO) containing catalyst precursors almost entirely.[51] The formation of the active catalyst, a cobalt hydrido species $[Co(CO)_4H]$ occurs *in-situ* under the high temperatures (>160 °C) and pressures (> 30 MPa) required for the reaction to proceed.

These catalyst precursors initially provided adequate reaction rates and target product yield and are more colloquially known as unmodified cobalt catalysts.[60]

It is widely accepted that the primary disadvantages associated with unmodified cobalt catalyst systems are comparably harsh reaction conditions, requiring high temperatures and syngas pressures to negate catalyst deactivation. Additionally, the formation of hydrogenated products, such as alcohols and alkanes, leads to a substantial reduction in the selectivity of the reaction and poor aldehyde product yield. Furthermore, degradation of the cobalt-based catalyst leads to the formation of metallic cobalt, a toxic by-product, requiring further purification steps before separation of the products from the reaction mixture, by distillation for example.[61] Ligand modification of cobalt-based catalysts was achieved by the introduction of phosphine ligands coordinated to the cobalt metal centre, affording the modified second-generation cobalt catalysts, mostly utilised in the Shell Higher Olefin Process.[62]

Comparatively, rhodium-based catalysts have undergone similar modifications and typically require milder reaction conditions in terms of temperature and pressure to effect the formation of the desired aldehyde products.[63] Hydroformylation reactions utilising rhodium catalysts require no additional metal separation steps, show a decrease in the formation of alcohols and alkanes and an increase in the activity and selectivity toward aldehydes compared to cobalt catalysts.[64,65] The combination of milder reaction conditions, greater selectivity for aldehydes and the lack of steps required for by-product separation has resulted in an ever growing number of rhodium-based catalysts studied for hydroformylation. Further improvements toward regio- (linear vs branched) and chemoselectivity (aldehydes vs alcohols vs *iso*-octenes) can be achieved by ligand modification. This is conventionally carried out by altering steric factors (regioselectivity) and/or tuning the electronic character of the metal centre toward more efficient production of the target aldehyde products increasing the chemoselectivity of the reaction.[66]

Mechanistically the hydroformylation catalytic cycle may proceed *via* two mechanisms, namely associative and dissociative, differing only in the loss of a carbonyl ligand (dissociative mechanism) in the step preceding olefin coordination. The associative mechanism proceeds as described in Scheme 1.2 (*overleaf*), illustrating a route to the formation of both linear and branched aldehydes. In both cases the formation of the active catalyst, a 5-coordinate rhodium

hydrido species (a), is succeeded by the coordination of the alkene substrate to form a coordinatively saturated octahedral complex (b). The formation of regio-isomers and therefore the regioselectivity of the reaction is determined by the hydride migration step, producing the corresponding linear or branched rhodium alkyl intermediates (c) or (f).

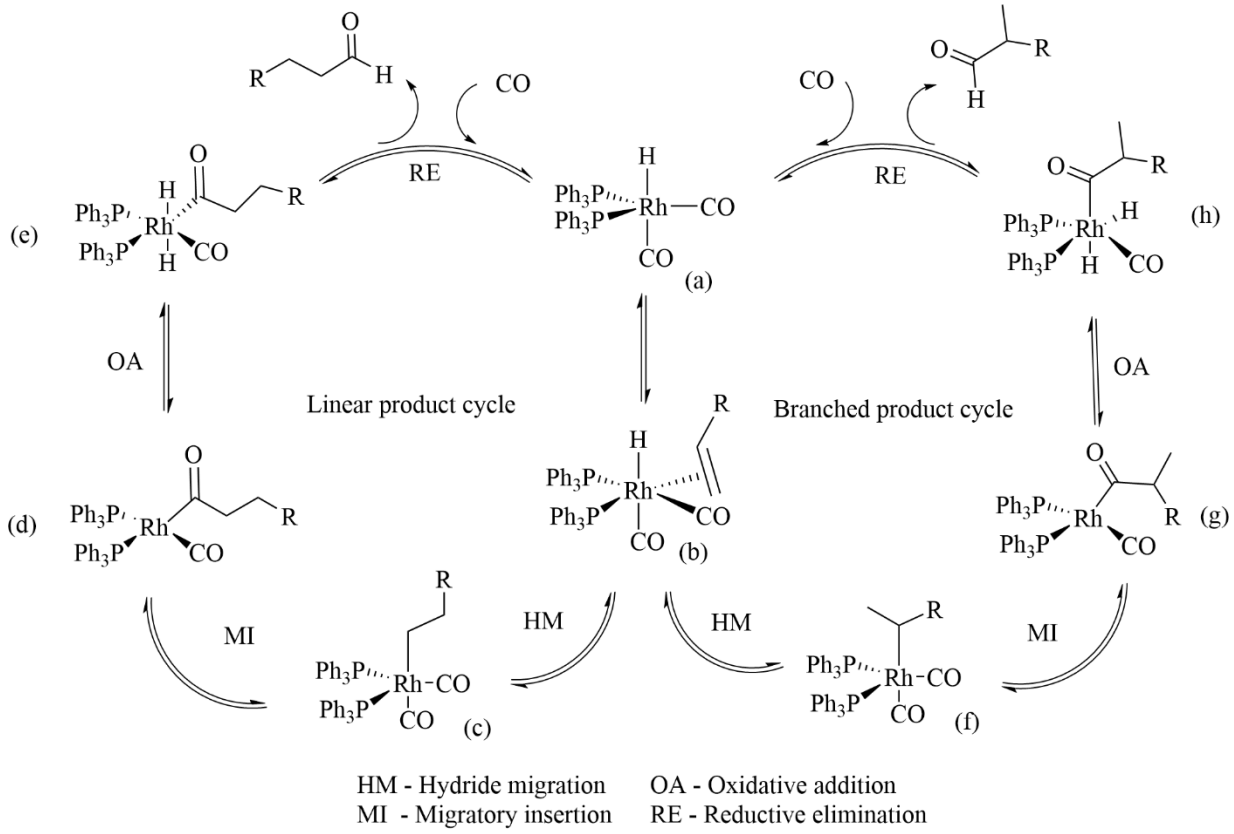

Scheme 1.2. Representation of the accepted associative mechanism for the catalytic cycle of the hydroformylation reaction, forming branched and linear aldehydes.[67]

The migratory insertion of a carbonyl ligand results in the formation of coordinatively unsaturated rhodium-acyl species (d) or (g) before the oxidative addition step. The addition of molecular hydrogen to the catalyst *via* oxidative addition results in octahedral acyl-dihydride complexes (e) and/or (h) being formed. In the reductive elimination step that follows, the aldehyde products are liberated with the synchronous reforming of the active catalyst species by coordination of a carbonyl ligand, from the reaction atmosphere (CO/H_2). The understanding of mechanistic influence as well as the effect of the reaction conditions on the formation of intermediates and final products is imperative for optimising the reaction. Therefore, variation of reaction conditions such as temperature, pressure, catalyst

concentration and the addition of complementary ligands in varying equivalents must be explored as a combination to further tune the chemo- and regioselectivity of the hydroformylation reaction. By way of example, experimental evidence shows that increasing the CO partial pressure favours the formation of metal-acyl intermediates resulting in higher production of linear aldehydes while supressing the isomerisation of substrate.[68,69] The introduction of a suitable ligand under these conditions may be used to control the regioselectivity simultaneously. Conventionally, this is achieved through the steric influence of a ligand such as triphenylphosphine (PPh_3), favouring the formation of linear aldehyde through interactions between the bulky phenyl groups and the branched acyl intermediates. The lowering of the CO partial pressure may be required in such a case, since competition for metal binding is likely to occur between the carbonyl and phosphine ligands. However, substantial lowering of the CO partial pressure may have a detrimental effect on the hydroformylation process, since there is a direct correlation between the formation of aldehydes and the concentration of CO in the reaction medium.[39] Consequently, optimisation regarding the partial pressure of CO in the reaction atmosphere would need to be carried out to ensure efficient hydroformylation of the substrate, with minimal isomerisation occurring to enhance the selectivity of the reaction.

As described in the example of triphenylphosphine, regioselectivity is primarily controlled through steric influence around the rhodium metal centre, favouring the formation of the linear intermediate (c) over the more sterically demanding intermediate (f) in Scheme 1.2, ultimately yielding linear aldehyde products.[70] Therefore, the design of efficient catalytic systems often includes multiple optimisation experiments to determine whether any sensitivity on the selectivity and activity of the reaction regarding these factors is evident.[71,72]

Furthermore, the electronic nature of the metal centre is an important factor to consider for overall catalyst performance. Ligands having different σ-donor and π-acceptor properties may significantly increase the stability of the complex intermediates throughout the catalytic cycle, resulting in lower temperatures and pressures required to effect the necessary molecular changes. Additionally, influencing the stability of intermediary species in the catalytic cycle has a significant effect on the ability of the metal centre to undergo reductive elimination or oxidative addition. Tucci and coworkers reported the effects of ligands bearing group 15 donor atoms, whereby a trend in the reactivity and selectivity of the hydroformylation reaction was

noted.[73] Extrapolation of the observed trend to ligands containing nitrogen donor atoms suggests that the formation of more stable complexes may be possible with nitrogen donor ligands. Although this study described the effects of monodentate ligands, the use of chelating ligands is well known to further increase the stability of metal complexes. Therefore, literature describing rhodium-based complexes bearing *N,O* and *N,N* chelating ligands are well reported for hydroformylation reactions (Figure 1.2, *vida infra*).[40,71,74,75] The general trend when considering both monophasic and biphasic systems is that the *N,N*- based complexes outperform the *N,O* complexes by up to 10% in terms of aldehyde production for the same Rh(I) loading and ancillary ligand.[35,71,72,75] Further improvements were noted when the ancillary ligand was changed from 1,5-cylooctadiene to carbonyl and chlorido ligands. Considerations into the rational design of catalysts should incorporate factors such as discussed here to improve the activity, selectivity, and notably for recyclability of the catalyst precursor in homogeneous hydroformylation reactions where expensive PGMs are used. The functional changes may also be employed for tandem reactions such as hydrohydroxymethylation and hydroaminomethylation, for which hydroformylation is a crucial step.

1.3 The hydroaminomethylation reaction

An extension of the hydroformylation reaction to produce secondary and tertiary amines, known as hydroaminomethylation, was first described by Reppe and Vetter in the mid-20th century.[76] This process involves the reaction of the aldehyde(s), produced from a hydroformylation reaction, with an amine reagent through an *in-situ* condensation reaction. This produces intermediary imines if primary amine substrates are used, or enamines if secondary amine substrates are used. The formed imines or enamines are subsequently catalytically reduced in the presence of the catalyst and H_2 to form the product amines (Scheme 1.3). This reaction allows for a facile conversion of alkene substrates into amines, opposed to the conventional synthetic procedures requiring multiple steps for overall reductive amination. Such conventional reductive amination reactions often require multiple purification steps and introducing the possibility of unwanted by-products by stoichiometric synthetic procedures, often employing harsh reagents.

Amines are widely used for the synthesis of biologically active compounds, agricultural feedstocks and dyes.[77,78] Therefore, the application of catalytic processes to produce amines such as the combination of hydroformylation and hydrogenation for overall

hydroaminomethylation are widely considered as 'greener' alternatives to conventional synthetic procedures.[79-81]

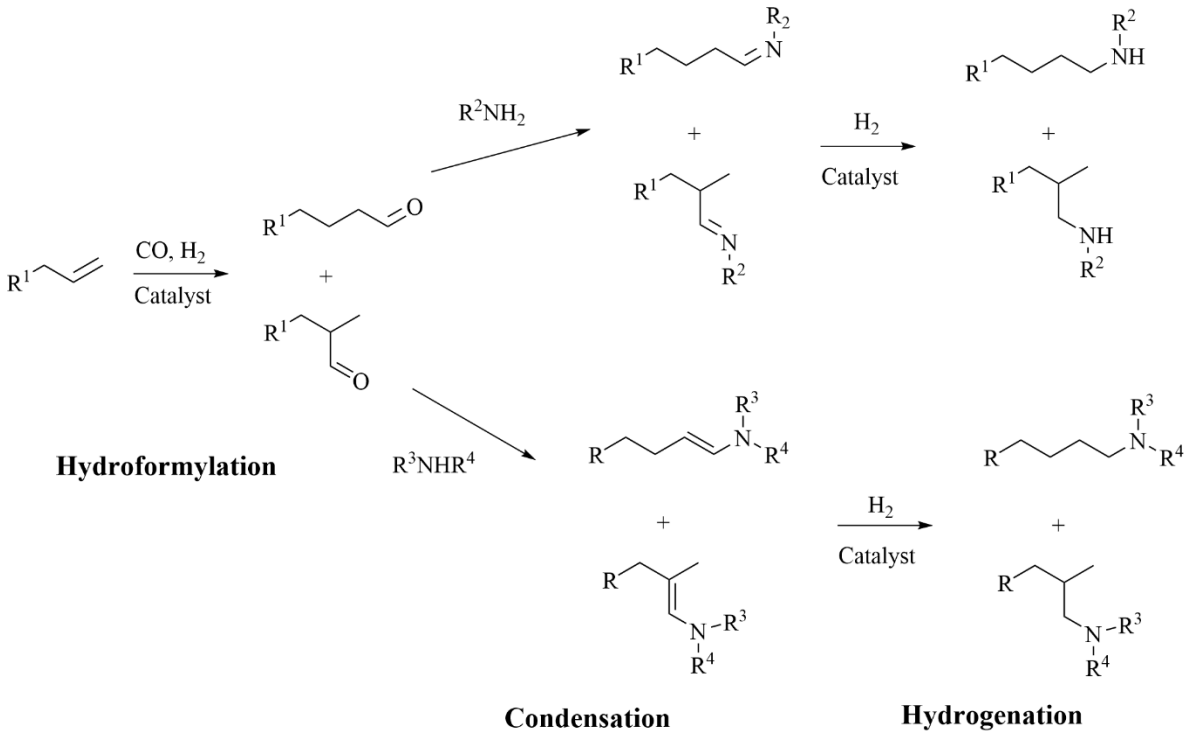

Scheme 1.3. Graphic representation of the hydroaminomethylation process including the hydroformylation, condensation and hydrogenation steps depicted with primary or secondary amine substrates.

By way of comparison, a synthetic procedure for the opioid painkiller Tramadol® was achieved through a Mannich reaction followed by a subsequent reaction of the resulting Mannich base with organolithium or Grignard reagents. Finally, resolution of the desired compound may be achieved *via* palladium-catalysed hydrogenolysis or crystallisation of the hydrochloride salt.[82] In contrast to this multi-step stoichiometric procedure, the selection of a suitable substrate for hydroaminomethylation may allow for directly obtaining the product in fewer steps, exploiting the advantages of catalytic reactions in synthetic procedures toward obtaining active pharmaceutical ingredients (API's).

Furthermore, efficient means of synthesis may be achieved through this type of incorporation of a single catalytic step to a suitable substrate, reducing the derivatives and waste produced from a known stochiometric synthetic procedure. The advantage of the hydroaminomethylation reaction on olefin substrates over more classical substitution methodologies is the production of amines with high atom economy and the reduction in toxic products *via* a reaction containing

two catalytic steps, with water being the primary by-product.[83] Therefore, the reaction may require the design of a catalyst which is stable under both the optimised reaction conditions, and in the presence of molecules capable of coordination such as liberated water and amine substrate. Furthermore, the catalyst must favour the selectivity needs of the reaction, usually achieved by varying the transition metal used.[77]

Several transition metal catalysts have been investigated for use in hydroaminomethylation. These include cobalt, rhodium and ruthenium, however, typical catalyst precursors designed as efficient hydroformylation agents do not guarantee activity in the hydrogenation step required for hydroaminomethylation.[77,84-87] Consequentially, hetero-bimetallic rhodium/iridium or rhodium/ruthenium catalyst systems have shown an increased efficiency compared to homo-metallic complexes, utilising rhodium as the primary hydroformylation catalyst, and iridium or ruthenium as the primary hydrogenation catalyst.[77,88-90] The design of an efficient rhodium-based hydroaminomethylation catalyst needs to incorporate selectivity toward the hydrogenation of amines and enamines over aldehydes and alkenes in order to maximise the amine product yield.

The addition of phosphine ligands and other additives to enhance the selectivity of rhodium-based hydroaminomethylation is well reported in literature, however, fewer reports on preformed nitrogen-containing complex catalysts exist to date.[91-95] Recently, October and coworkers reported the synthesis and evaluation of Rh(I) imino-pyridyl complexes with good activity and selectivity for amine products in hydroaminomethylation reactions.[39] Comparable conversions with good regioselectivity under milder conditions and at lower catalyst loading were obtained when compared with analogous work.[39] In a subsequent study, the substrate scope was extended and coupled to a hydrogenolysis step, employing the same Rh(I) centred imino-pyridyl complexes at 0.5 mol% catalyst loading under reaction conditions of 50 bar syngas (1:3 $CO:H_2$) pressure at 85 °C and a reaction duration of 6 hours. Sequential palladium-catalysed hydrogenolysis of the reaction products afforded valuable amines from olefins in moderate to high yields, illustrating the utility of homogeneous rhodium-catalysed hydroaminomethylation.[94] As is the case for most homogeneous catalysed reactions using catalyst precursors containing PGMs, the recyclability of these catalysts remains an important area of ongoing research.

1.4 Enhancing the recyclability of catalyst precursors in homogeneous catalytic reactions such as hydroformylation

Improvements toward the efficient recovery of expensive platinum group metal (PGM)-based catalysts in homogeneous reactions have been attempted by a variety of methods. These efforts are primarily carried out through modification of molecular interaction and/or suitable phase separation of the desired reaction products with the catalyst species.[96] Some reported strategies include immobilisation of the catalyst onto an insoluble support,[18] the incorporation of dendritic frameworks for separation using nano-filtration,[97,98] liquid-liquid phase separations such as aqueous- or fluorous-biphasic catalysis[99,100] or combinations of macromolecules functionalised with solubilising groups to enhance aqueous recyclability.[101,102] In all cases, modifying the physicochemical properties of the catalyst is carried out, which may affect the chemo- and regioselectivity and activity of the catalytic reaction whilst achieving enhanced catalyst recovery.

Immobilisation of the catalyst precursor through host-guest interactions where intermolecular forces such as Van der Waals forces, hydrogen bonding, electrostatic interactions as well as charge transfer can be used to good effect. Such research efforts are reported for inclusion complexes with cyclodextrins for catalysis in aqueous media.[103] This requires the addition of host molecules to the reaction, necessitating further investigation into the effects on reactivity and selectivity of the catalytic process in question.

Aqueous-organic biphasic catalytic reactions are well known, reporting suitable modification of the ancillary ligands with so-called water 'solubilising' functionalities with high polarity including sulfonate, carboxylate or quaternary ammonium moieties [104-107] Modification of the prototypical rhodium-based catalyst precursor, $[Rh(PPh_3)_3(CO)H]$, with additional sulfonate groups to promote aqueous solubility was first commercially used for the biphasic hydroformylation of short chain olefins (propene and butene) in the Ruhrchemie/Rhône-Poulenc process.[107] The modification of rhodium(I)-based complexes incorporating both solubilising and macromolecular strategies has been extensively studied. By way of example, the addition of sulfonate groups to a trimeric Rh(I)-based dendritic catalyst precursor by Hager and coworkers showed substantial enhancement on the recyclability in aqueous biphasic hydroformylation reactions compared to similar complexes.[94]

The principle of biphasic catalysis relies on the hydroformylation reaction occurring at the boundary between the catalyst-containing aqueous phase and the substrate-containing phase or suitable activation of the catalyst precursor which then enters the substrate-containing phase. This often requires vigorous stirring and heat to allow for suitable interphase interaction. After completion of the reaction and venting of syngas, the mixture is cooled to ambient temperature whereby phase separation occurs, and aspiration of the organic layer is carried out to isolate the products. The aqueous layer may then be reintroduced into a reaction vessel containing fresh olefin substrate, hence allowing for recyclability of the catalyst. This process is outlined schematically in Scheme 1.4.

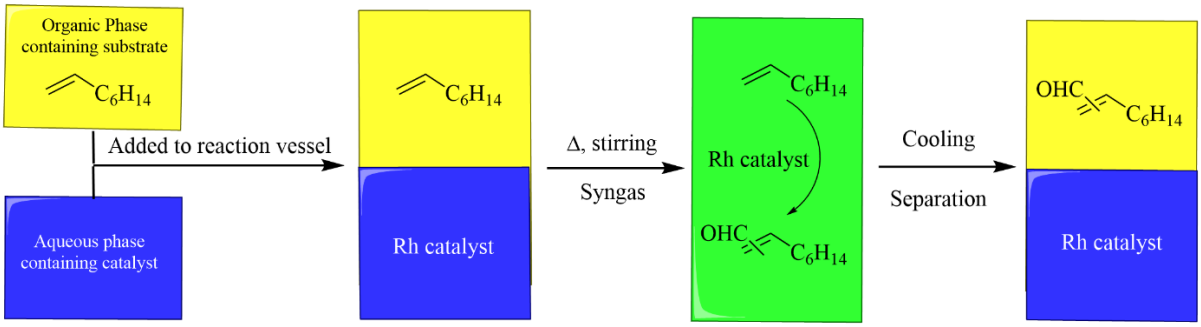

Scheme 1.4. Outline of the principle of aqueous biphasic catalysis of 1-octene as an example, with a water-soluble rhodium catalyst.

The use of fluorous-biphasic catalytic systems exploits similar characteristics as aqueous-biphasic systems, where compounds containing groups with appended fluorine atoms show enhanced temperature-dependant solubility in a fluorous-hydrocarbon phase compared to inorganic or organic phases.[108] This employs the characteristic that at elevated temperature, the fluorous phase is miscible with the organic phase, thereby allowing substantial contact between the catalyst and substrate, resulting in enhanced reaction efficiency and higher product yield. Fluorous-biphasic systems have been explored in various catalytic reactions, with some evidence of their applicability reported in the hydroformylation reaction.[109-111] Some examples of rhodium-based catalyst precursors for aqueous or fluorous-biphasic hydroformylation are shown in Figure 1.2 below. The applicability of each strategy to aid in the recyclability of the catalyst has a common trait; namely the tuning of specific characteristics and physicochemical properties of the metal complexes to enhance separation of the catalyst from the bulk medium.

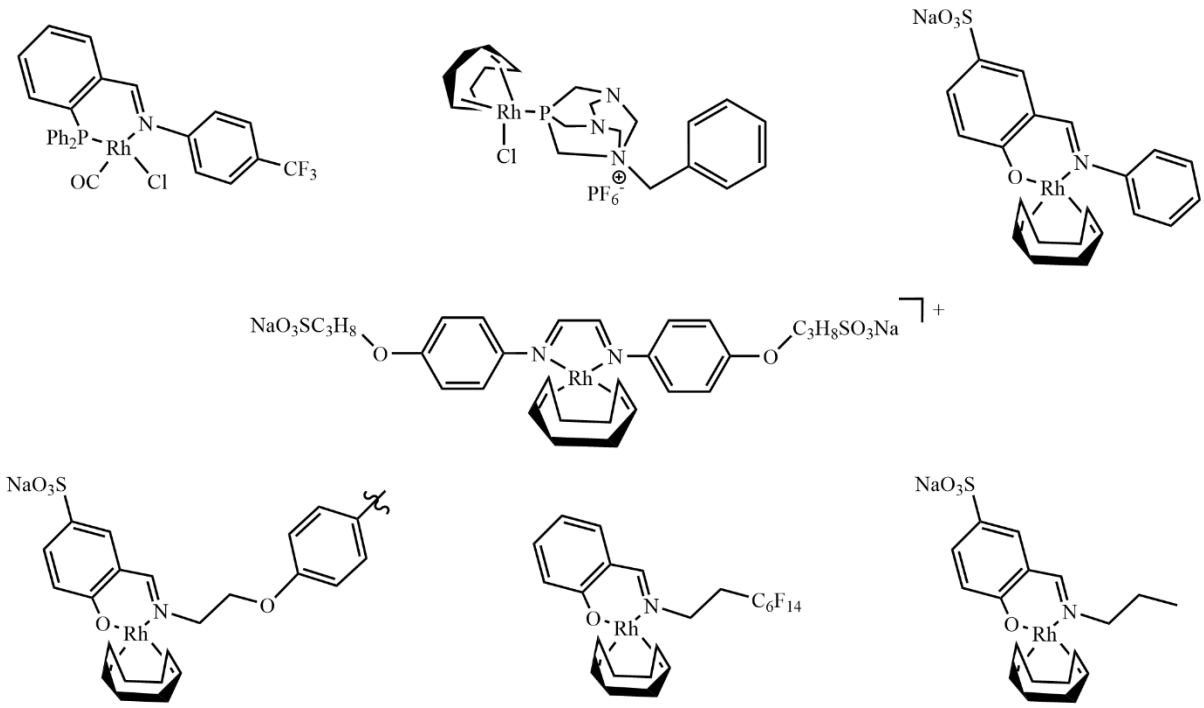

Figure 1.2. Some examples of rhodium(I)-derived catalyst precursors applied to biphasic hydroformylation reactions.[71,72,75,106,111]

The recycling strategy and the resulting catalyst modifications carried out to increase the solubility of the catalyst should minimise catalyst degradation, while maintaining the selectivity and activity of the reaction. To this end, the rational design of a catalyst with increased solubility under reaction conditions relative to ambient conditions may be beneficial for catalyst recovery. Furthermore, modifications made to the catalyst precursor should be carried out in such a way that minimises prospective negative influences on the chemo- and/or regioselectivity and does not promote catalyst degradation once applied to homogeneous catalytic reactions such as hydroformylation and hydroaminomethylation.

Subsequently, it has been shown that multinuclear complexes exhibit comparable or enhanced catalytic capabilities, such as chemoselectivity in hydroformylation compared to their mononuclear counterparts for example.[35,106] In this regard, multinuclear complexes are of interest since most studies involve discrete metal centres dispersed throughout a molecular structure for both rhodium-based mono-nuclear, low-valent, and larger macromolecular compounds.

1.5 Multinuclear complexes in catalytic reactions

The presence of more than one active metal centre in a molecule has been shown to significantly influence reactivity and selectivity in catalytic applications. In recent times, the utilisation of metallodendrimers in homogeneous catalysis has been primarily utilised for enhancing activity and recyclability. Metallodendrimers are three-dimensional molecules centred around a core, expanding into a periphery which becomes larger with increasing generation number. These branched, monodisperse macromolecules may contain metal atoms at the core, interspersed throughout the molecular framework or on the periphery of the dendritic structure (Figure 1.3, *overleaf*).[111,112] The incorporation of transition metals into dendritic frameworks to form metallodendrimers was initiated by Newkome and co-workers in the 1990s.[113] They reported the use and modification of dendrimers containing suitable donor atoms appended to functional groups on the periphery of the macromolecular scaffolds capable of binding to metallic complexes.[113]

The application of these macromolecules to afford catalytically active species in the form of metallodendrimers may be used as a method of catalyst immobilisation *via* dative interactions as previously described.[114] The corresponding increase in the concentration of metal atoms at defined sites in the macromolecule has a profound effect in terms of factors such as reactivity, selectivity and the ability to be separated, a recurring motif in the catalysis research area.[115] Interestingly, the inclusion of multiple metal centres is not always represented by a corresponding increase in the activity of a catalyst precursor, resulting in catalytic activity which may be higher than expected.[71,101,115] This is attributed to a cooperative effect between the metal centres, in addition to the increased nuclearity of catalytically active sites per molecule.[116,117] The separation of large macromolecular structures such as metallodendrimers may be achieved through nanofiltration of the catalyst from the reaction medium and products formed, in a manner such as described by Siangwata and co-workers (Figure 1.3, overleaf).[72]

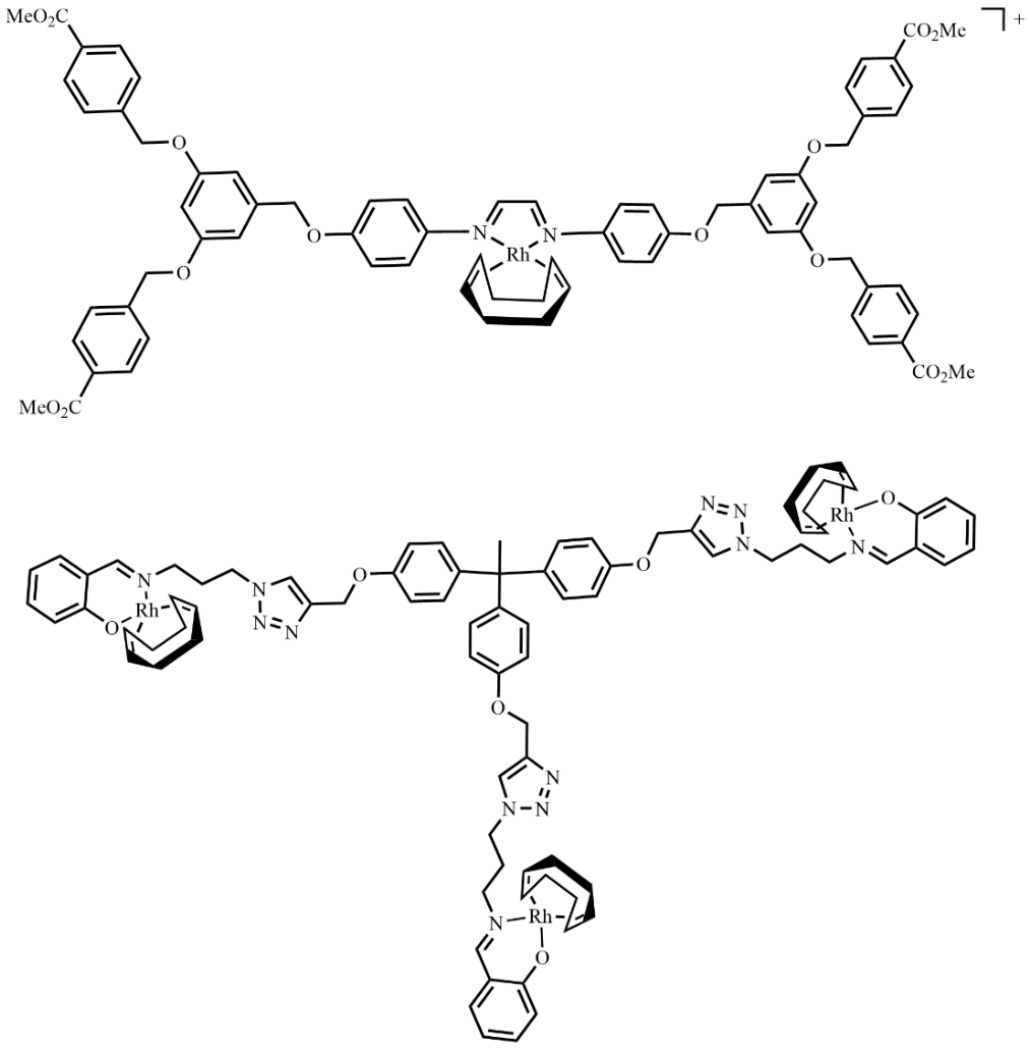

Figure 1.3. Examples of cationic and neutral rhodium(I)-centred metallodendrimers used in hydroformylation reactions with metal atoms located in the core, or on the periphery.[71,72]

Furthermore, dendritic frameworks may contribute to the stabilisation of metal complexes through functional groups in the molecular structure or shielding of the metal centre through multiple conformational arrangements of the arms.[35,71] The latter is expected to be enhanced for metallodendrimers containing metal atoms in the core, such as described by Omosun and coworkers (Figure 1.3, above), which may be utilised for enhanced regioselectivity with increasing generation number as these contain one catalytic centre with numerous arms providing increased steric influence.[71]

The addition of different functional groups of various types to the ligand allows for the prospect of inclusion of metal centres with different oxidation states in one discrete molecule. In terms of hydroformylation, Govender and coworkers showed that the incorporation of mono-metallic

mixed valent Rh(I) and Rh(III) metal centres into a molecule resulted in a complex precursor with high selectivity for linear aldehydes.[118] Additionally, it was shown that these mixed valent complexes showed comparable chemoselectivity to Rh(I)-based complexes containing *N*,*N* or *N*,*P* donor ligands.[75,119] The combination of the Rh(I) and Rh(III) metal centres suggest that a complex containing an intermediary oxidation state may benefit from the high reactivity of a Rh(III) metal centre combined with the greater stability of Rh(I)-based catalyst precursors by incorporating important oxidation states required at different points in the catalytic cycle.[118] In this regard, metal-metal bonded dirhodium(II,II) complexes may be considered as excellent candidates for catalyst precursors in the hydroformylation of olefins.

1.6 Metal-metal bonded dirhodium(II,II) complexes

The effects of multiple metal centres on the catalytic activity of a reaction may be further explored through complexes with a bimetallic core as opposed to those containing two discrete metal centres. The first report of a complex with a metal-metal bond was in 1935 by Brosset, describing a $W_2Cl_9^{3-}$ anion with atomic distances between the tungsten atoms so small that they must 'in some way be bound together'.[120,121] Since this account, metal-metal bonded complexes containing a variety of metal atoms such as vanadium, chromium, niobium, rhenium, molybdenum, ruthenium, iron, cobalt, iridium and rhodium have been reported with bond orders varying between the metal atoms located in the core.[107] Figure 1.4 (*overleaf*) shows some examples of donor atom motifs and the general structure of complexes in this class. Homoleptic dirhodium(II,II) paddlewheel complexes have structural nuances such as a metal-metal bond, D_{4h} symmetry and vacant axial sites available for coordination.[122] These complexes have been studied for their interesting physicochemical and electrochemical properties, such as the accessibility of geometries and oxidation states not ordinarily observed for mono-nuclear complexes.[123-125] Modification to the bridging ligands may be carried out to tune the electronic character of the metal centres, allowing for stabilisation of higher or lower oxidation states of the bimetallic core, not seen for mono-nuclear rhodium complexes.[125]

Early dirhodium(II,II) complexes were obtained by reacting a hexachlorido rhodate species in formic acid to obtain the dirhodium(II,II) tetraformate complex.[126] More recently, dirhodium(II,II) tetraacetate is efficiently obtained through a reaction of $RhCl_3 \cdot 3H_2O$ with sodium acetate in a mixture of ethanol and acetic acid.[36,127] Further dirhodium(II,II) complexes are usually obtained through ligand metathesis reactions by reacting suitable ligands containing

functionalities such as carboxylic acids, formamidines, benzamidines, and oxopyridines for example (Figure 1.4).[39,128,129]

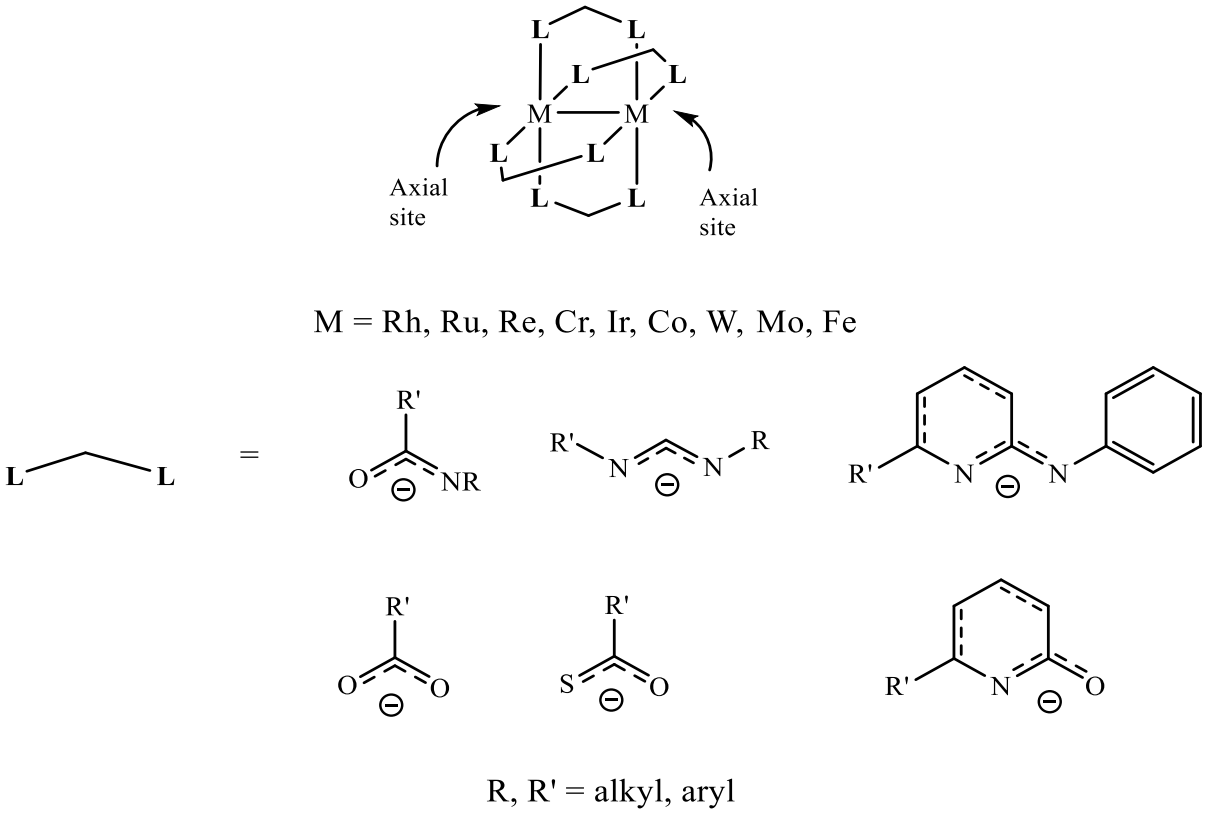

Figure 1.4. Some examples of bimetallic paddlewheel structured complexes with examples of different types of bridging ligands in their anionic form.

The presence of vacant axial sites allows for additional ligation after formation of the complex is carried out. These sites may be occupied by solvent molecules containing suitable donor atoms, additional pre-formed ligands or modified bridging ligands containing a suitable tether or substituent.[36,130] By way of example, the 2-fluoro-substituted diphenyl formamidinate complex in our previous study showed the highest regioselectivity for linear aldehydes, with confirmation of a metal-fluoro interaction through solid state analysis strongly supporting the influence of axial interactions on regioselectivity (Figure 1.5).[36] Furthermore, Darko and co-workers described the synthesis and catalytic properties of a dirhodium complex containing a ligand-modified with a thioether tether for applications in the cyclopropanation of alkenes, with the tethered thioether moiety reported as essential for high yields and the suppression of catalytic byproducts.[130]

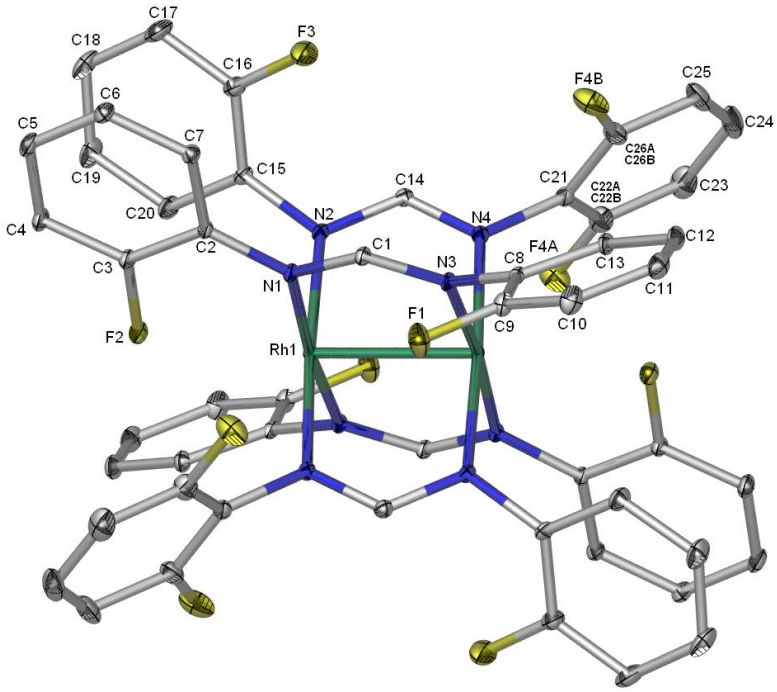

Figure 1.5. Previously reported homoleptic dirhodium(II,II) diphenylformamidinate complex structure showing the Rh-F axial interaction.[36]

The coordination of auxiliary ligands to the vacant axial sites of the complex often results in visible changes to the complex, mediated by the changes in the electronic properties imposed by these ligands.[131,132] This occurs due to changes in the electronic transitions, which in turn affects the redox behaviour of the complexes. Comparatively the intermediary +2 oxidation state on each rhodium atom in such paddlewheel complexes is observed, in relation to the more conventional rhodium(I) centred complexes utilised as hydroformylation catalytic precursors. This may allow for more facile oscillation between the Rh(I) and Rh(III) oxidation states required in the catalytic cycle, combined with the high stability exhibited by the metal-metal bonded dirhodium(II,II) complex with the appropriate ligands. Furthermore, the overall charge may result in more efficient CO ligand exchange during catalytic processes such as hydroaminomethylation, allowing for the binding of comparably 'softer' imine ligands in preference to CO. Additionally, the presence of the rhodium-rhodium bond may allow for delocalisation of charge in the core, in combination with the electronic effects imparted by coordinated ligands. The stability of this rhodium-rhodium bond is attributed to suitable orbital mixing between each metal atom and the bridging ligands.[133] Altering the extent of the orbital mixing could further allow for better accessibility to higher and/or lower oxidation states as required, without significant catalyst degradation occuring.[132]

Thus far, the discussion has centred around homoleptic dirhodium(II,II) complexes, however, heteroleptic complexes have been isolated with varying degrees of substitution by introducing 1,2 or 3 alternate bridging ligands. The synthesis and isolation of heteroleptic dirhodium(II,II) complexes incorporating bridging ligands is not always a straightforward process, due to the formation of *cis*- and *trans*-isomers depending on the incoming ligand type.[134] The challenge of separation of isomers is further compounded when unsymmetrical bridging ligands are used, since coordination may occur allowing for *syn*- and *anti*-isomer formation, and further complexity is introduced if ligands bearing chiral motifs are used.[135]

The use of chelating ligands toward the formation of heteroleptic complexes further demonstrates a facet of dirhodium(II,II) compounds not exhibited by mono-nuclear rhodium counterparts, by means of combining bridging and chelating ligands in a discrete complex. The synthesis of heteroleptic bis-substituted dirhodium(II,II) chelate complexes may proceed directly *via* reactions with an appropriately structured ligand,[36,136,137] sequentially through stripping of the bridging ligands by an alkylating agent such as Et_3OBF_4,[138] or by the oxidation of a dirhodium(I,I) complex with a suitable oxidising agent such as $AgPF_6$. By way of example, the latter procedure is reported as part of the synthesis for several heteroleptic complexes, from di-μ-chlorobis[(1,2,5,6-η)-1,5-cyclooctadiene]dirhodium(I) with a ligand such as bis-(4-methylphenyl)formamidine. The corresponding intermediates may then undergo reactions with an appropriate ligand such as bipyridine, phenanthroline, naphthyridine or an azobenzene to afford heteroleptic complexes. Catalan and co-workers described such a synthetic procedure to afford bis-substituted heteroleptic naphthyridyl-containing complexes from formation of a dirhodium(I,I) complex, oxidised by $AgBF_4$ in acetonitrile,[139] following substitution by modified pyridyl-naphthyridine ligands.[131] The overall structure and some examples of complexes of this class are shown in Figure 1.5 (*overleaf*).

Due to their appreciable diverse geometrical and electronic characteristics, dirhodium(II,II) complexes have shown good applicability in catalytic reactions such as allylic oxidation, carbonylation, hydrogenation and hydroformylation.[36,140-143] As such, the investigation into modification of complexes in this class may be useful in the design of catalyst precursors for additional reactions such as hydroaminomethylation.

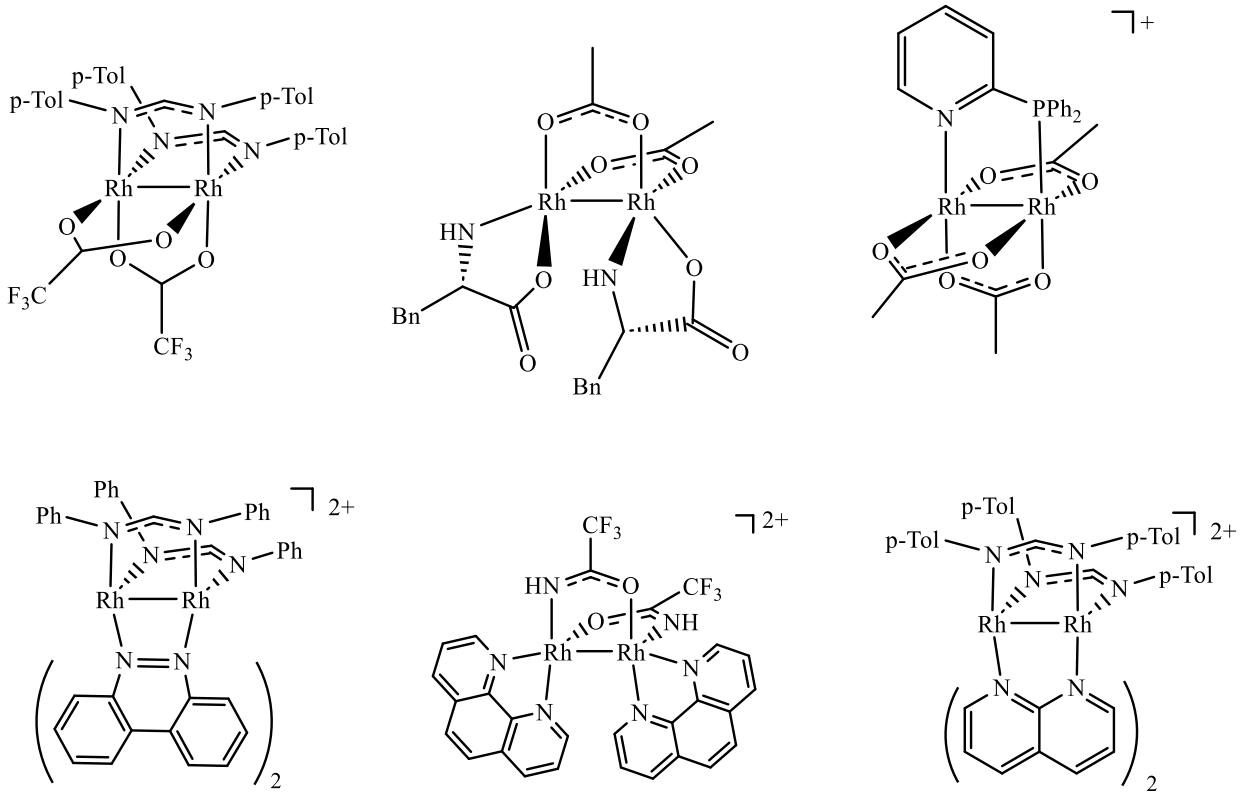

Figure 1.5. Some examples of bis-substituted heteroleptic bimetallic paddlewheel structured complexes combining bridging and chelating ligands.[129,144-148]

1.7 Research rationale and motivation

Research and investigation into more effective and reusable catalyst precursors for homogeneous reactions such as hydroformylation and hydroaminomethylation is ongoing, due to the need for producing precursors for consumer markets and the rising cost of platinum-group metals used for catalytic chemical transformations.

Dirhodium(II,II) complexes have shown activity in the hydroformylation of olefins with the additional ability to catalyse hydrogenation only under specific conditions. To date, there are no reports of heteroleptic dirhodium(II,II) complexes with applications in hydroformylation explicitly describing the involvement of axially coordinated ligand on the catalytic product distribution. Additionally, these complexes have not been investigated for application in the hydroaminomethylation of olefins. Therefore, the careful design of such complexes to favour the hydrogenation of imines under hydroaminomethylation reaction conditions could lead to highly effective and efficient hydroaminomethylation catalysts. Furthermore, producing

dirhodium catalysts within the scope of homogeneous catalytic reactions such as hydroformylation and hydroaminomethylation with favourable characteristics including chemoselectivity, and particularly recyclability without immobilisation is unexplored, creating a niche area for investigation.

The effect of introducing a means of recycling cationic dirhodium(II,II) complexes in hydroformylation by exploiting temperature-dependent solubility or an aqueous biphasic approach may be beneficial in this research area. This may be achieved through the tailoring of physicochemical properties by combining chelating and bridging ligands, based on the highly effective dirhodium tetraacetate complex in the hydroformylation reaction. Key features such as solubility in aqueous media for biphasic catalysis or temperature variable solubility for monophasic systems could provide insight into catalyst recovery. To date, no studies on the use of dirhodium(II,II) complexes as hydroaminomethylation catalysts exist. Appreciable activity is observed when these complexes are used as catalytic precursors in the hydroformylation reaction with no detectable hydrogenation of aldehyde products reported.[36] This provides a good starting point for the development of an efficient dirhodium(II,II) complex for highly selective hydroaminomethylation catalysts.

As discussed in section 1.3, the recyclability aspect remains a challenge for homogeneous catalytic systems, however, the nature of dirhodium complexes bearing chelate ligands may be exploited to increase the aqueous solubility as described for biphasic catalysts. Additionally, the introduction of solubilising moieties to the equatorial ligands of dirhodium(II,II) complexes may be useful in the recyclability of catalyst precursors. In hydroaminomethylation reactions, the proposed amine products should display a lower solubility in water, providing a means of catalyst separation from the organic phase and product in a biphasic reaction system. In this project, the physicochemical characteristics of bis-substituted heteroleptic dirhodium(II,II) acetato-bipyridyl complexes and the effects of these changes on the catalytic applicability toward the efficient hydroformylation and hydroaminomethylation of olefins are explored.

1.8 Research Aims and Objectives

1.8.1. General aims

The overall aim of this project is to synthesise and characterise a series of heteroleptic dirhodium(II,II) acetato-bipyridyl complexes and evaluate them as catalyst precursors in the hydroformylation and hydroaminomethylation reactions.

1.8.2 Specific objectives

- To synthesise a series of dirhodium(II,II) acetato-bipyridyl complexes containing hemi-labile acetate ligands, with substituents varied in the 4 and 4’ positions of the bipyridyl ligand (Scheme 1.5).

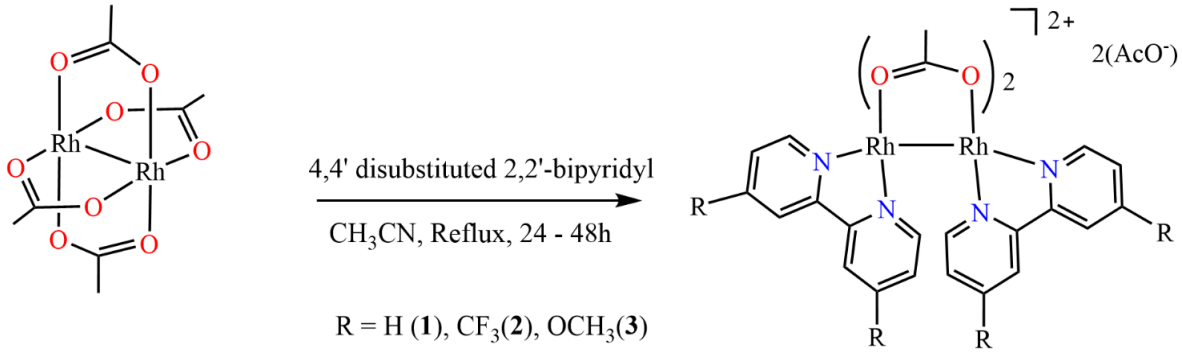

Scheme 1.5. Synthetic outline for the target dirhodium complexes in this study.[149]

- To synthesise a series of dirhodium(II) acetato-bipyridyl complexes containing hexafluorophosphate counter ions, with varied substituents in the 4- and 4’-positions of the bipyridyl ligands (Scheme 1.6).

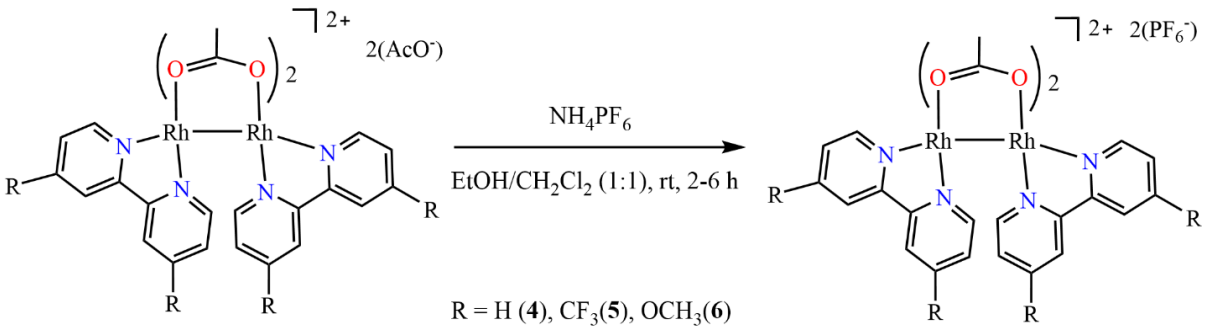

Scheme 1.6. Synthetic outline for the target hexafluorophosphate dirhodium complexes in this study.[150]

Characterisation and identification of the complexes will be carried out by spectroscopic and analytical techniques such as:

- Nuclear magnetic resonance (NMR) analysis such as ^{1}H, $^{13}C\{^{1}H\}$, ^{19}F, ^{31}P and DOSY.
- Infrared (IR) spectroscopy.
- UV-Vis and Electrochemical analyses.
- HPLC.
- Melting point analysis.
- Mass Spectrometry.
- Conductivity.

- To explore the effects of the bipyridyl and acetate ligands on the catalytic activity and product distribution and sensitivity to substrate variation in monophasic hydroformylation reactions.

- Evaluation of synthesised complexes as catalysts in the hydroformylation of 1-octene, styrene, cyclohexene and 7-tetradecene and analysing the product distribution by gas chromatography.

- To determine the applicability of the synthesised complexes in biphasic hydroformylation or induce temperature dependent characteristics to effect catalyst recyclability.

- The development of the synthesised complexes as catalyst precursors for chemoselective hydrogenation of imines and enamines toward the hydroaminomethylation reaction with olefin substrates (styrene, cyclohexene, cyclohex-2-en-1-one and cyclohex-2-en-1-ol) with primary and secondary amine substrates. This optimised catalytic reaction will then be applied toward the synthesis of analogues of the available opioid class drug, Tramadol®. The reaction products will be isolated and characterised by gas chromatography, NMR and LC-MS where applicable.

1.9 References

1. I. Chorkendorff and J. W. Niemantsverdriet, *Concepts of Modern Catalysis and Kinetics*, Wiley-VCH Verlag GmbH & Co. KGaA, Weinheim, 2nd edn., 2007.

2. I. Fleischer, L. Wu, I. Profir, R. Jackstell, R. Franke and M. Beller, *Chem. - Eur. J.*, 2013, **19**, 10589-10594.

3. L. Wu, I. Fleischer, R. Jackstell, and M. Beller, *J. Am. Chem. Soc.*, 2013, **135**, 3989-3996.

4. I. Profir, M. Beller and I. Fleischer, *Org. Biomol. Chem.*, 2014, **12**, 6972-6976.

5. P. J. Baricelli, M. Rodriguez, L. G. Melean, M. M. Alonso, M. Borusiak, M. Rosales, B. Gonzalez, K. C. B. De Oliveira, E. V. Gusevskaya and E. N. Dos Santos, *Appl. Catal. A: Gen.*, 2015, **490**, 163-169.

6. J. M. Hawkins and T. J. N. Watson, *Angew. Chem. Int. Ed.*, 2004, **43**, 3224–3228.

7. Y. Nishihata, J. Mizuki, H. Tanaka, M. Uenishi and M. Kimura, *J. Phys. Chem. Solids*, 2005, **66**, 274-282.

8. C. Marcilly, *J. Catal.*, 2003, **216**, 47-62.

9. J. Crosby, *Pestic. Sci.*, 1996, **46**, 11-31.

10. R. Geyer, J. R. Jambeck and K. L. Law, *Sci. Adv.*, 2017, **3**, 1-5**.**

11. D. L. Klass, *Biomass for renewable energy, fuels, and chemicals*. Elsevier, 1998, pp. 2-27.

12. American Chemical Society Report, Technology Vision 2020, the Chemical Industry, December 1996, http://www/chemicalvision2020.com/

13. J. Heveling, *J. Chem. Educ.*, 2012, **89**, 1530-1536.

14. P. T. Anastas, L. B. Bartlett, M. M. Kirchhoff and T. C. Williamson, *Catal. Today.*, 2000, **55** (2), 11-22.

15. P. T. Anastas, M. M. Kirchhoff and T. C. Williamson, *Appl. Catal. A*, 2001, **221**, 3-13.

16. P. T. Anastas and E. S. Beach, *Green Chem. Lett. Rev.*, 2007, **1** (1), 9-24.

17. S. E. Manahan, *Green Chemistry and the ten Commandments of Sustainability*, ChemChar Research, Columbia, Missouri U.S.A., 2nd edn., 2006.

18. D. J. Cole-Hamilton, *Science.*, 2003, **299**, 1702-1706.

19. O. Deutschmann, H. Knözinger, K. Kochloefl and T. Turek, in *Heterogeneous Catalysis and Solid Catalysts*, Wiley-VCH Verlag GmbH & Co. KGaA, 2011, pp. 54-59.

20. E. Van Steen and M. Claeys, *Chem. Eng. Technol.*, 2008, **31** (5), 655-666.

21. R. M. Mironenko, O. B. Belskaya, V. P. Talsi and V. A. Likholobov, *J. Catal.*, 2020, **389**, 721-734.

22. A. Martínez-Carrión, M. G. Howlett, C. Alamillo-Ferrer, A. D. Clayton, R. A. Bourne, A Codina, A Vidal-Ferran, R W. Adams and J. Burés, *Angew. Chem. Int. Ed.*, 2019, **58**, 10189-10193.

23. N. Karodia, S. Guise, C. Newlands and J. A. Andersen, *Chem. Commun.*, 1998, 2341-2342.

24. R. Franke, D. Selent and A. Börner, *Chem. Rev.*, 2012, **112** (11), 5675-5732.

25. K. Tsutomo and K. Barry Sharpless, *J. Am. Chem. Soc.*, 1980, **102,** 5974-5976.

26. J. P. Collman, M. Kubota and J. W. Hosking, *J. Am. Chem. Soc.*, 1967, **89**, 4809-4811.

27. R. A. Miller, W. Li and G. R. Humphrey, *Tetrahedron Lett.*, 1996, **37** (20) 3429-3432.

28. N. Yoneda, S. Kusano, M. Yasui, P. Pujado and S. Wilcher, *Appl. Catal. A Gen.*, 2001, **221**, 253-265.

29. G. J. Sunley and D. J. Watson, *Catal. Today.*, 2000, **58**, 293-307.

30. T. L. Church, Y. D. Y. L. Getzler, C. M. Byrne and G. W. Coates, *Chem. Commun.*, 2007, 657-674.

31. J. A. Osborn, F. H. Jardine, J. F. Young and G. Wilkinson, *J. Chem. Soc.*, 1966, 1711-1732.

32. H. M. Lee, D. C. Smith, Z. He, E. D. Stevens, C. S. Yi and S. P. Nolan, *Organometallics.*, 2001, **20** (4), 794-797.

33. H. Alawisi, H. D. Arman and Z. J. Tonzetich, O*rganometallics.*, 2021, **40** (8), 1062-1070.

34. M. Beller, B. Cornils, C. D. Frohning and C. W. Kohlpaintner, *J. Mol. Catal. A Chem.*, 1995, **104**, 17-85.

35. C. Williams, M. Ferreira, E. Monflier, S. L. Mapolie and G. S. Smith, *Dalton Trans.*, 2018, **47**, 9418-9429.

36. S. de Doncker, A. Casimiro, I. A. Kotze, S. Ngubane and G. S. Smith, *Inorg. Chem.*, 2020, **59**, 12928-12940.

37. S. M. Mercer, T. Robert, D. V. Dixon and P. G. Jessop, *Catal. Sci. Technol.*, 2012, **2**, 1315-1318.

38. W. Alsalahi, R. Grzybek and A. M. Trzeciak, *Catal. Sci. Technol.*, 2017, **7**, 3097-3103.

39. J. October and S. F. Mapolie, *Catal. Lett.*, 2020, **150**, 998-1010.

40. A. Schmidt, M. Marchetti and P. Eilbracht, *Tetrahedron.*, 2004, **60**, 11487-11492.

41. M. A. Subhani, K. S. Müller and P. Eilbracht, *Adv. Synth. Catal*., 2009, **351**, 2113-2123.

42. A. R. Hajipour and Z. Khorsandi, *Nanochem Res.*, 2019, **4** (2), 132-139.

43. T. E. Barder, S. D. Walker, J. R. Martinelli, and S. L. Buchwald, *J. Am. Chem. Soc.*, 2005, **127** (13), 4685-4696.

44. E. Farnetti, R. Di Monte and J. Kašpar, *Homogeneous and Heterogeneous Catalysis*, Encyclopaedia of Life Support Systems, Paris, Volume 2, 1999.

45. X. Cui, W. Li, P. Ryabchuk, K. Junge and M. Beller, *Nat. Catal.*, 2018, **1**, 385-397.

46. S. C. Bourque, F. Maltais, W. J. Xiao, O. Tardif, H. Alper, P. Arya and L. E. Manzer, *J. Am. Chem. Soc.*, 1999, **121**, 3035-3038.

47. E. Jones, *Ind. Eng. Chem.*, 1950, **42** (11), 2208-2210.

48. J. Berzelius, *Annales de chimie et de physique*, 1863, **61**, 146.

49. F. Fischer and H. Tropsch, *Brennst. Chem*., 1923, **4**, 276-285.

50. D. Sanfilippo, in *Catalytic Industrial Processes*, EOLSS Publishers, Paris, 2009.

51. J. N. Armor, *Catal. Today*, 2011, **163**, 3-9.

52. O. Roelen, DE Patent DE 849 548 C (1938).

53. B. Cornils, W. A. Herrmann and M. Rasch, *Angew. Chem. Int. Ed.*, 1994, **33**, 2144-2163.

54. A. Behr, Y. Brunsch and A. Lux, *Tetrahedron Lett.*, 2012, **53**, 2680-2683.

55. A. Behr and L. Johnen, *Chem Sus. Chem.*, 2009, **2**, 1072-1095.

56. K. A. D. Swift, *Top. Catal.*, 2004, **27**, 143-155.

57. T. A. Faßbach, T. Gaide, M. Terhorst, A. Behr and A. J. Vorhol, *Chem. Cat. Chem.*, 2017, **9** 1359-1362.

58. S. Gladiali, J. Carles Bayón and C. Claver, *Tetrahedron: Asymmetry.*, 1995, **6**, 1453-1474.

59. F. P. Pruchnik, and S. A. Duraj, *Organometallic Chemistry of the Transition Elements. Modern Inorganic Chemistry*, Springer, Boston, MA, 1990, p. 691.

60. A. Chalk and J. Harrod, *Adv. Organomet. Chem.*, 1968, **6**, 119-170.

61. S. L. Desset, Doctoral dissertation, University of St. Andrews, St Andrews, 2009.

62. W. Keim, *Chem. Ing. Tech*., 1984, **56**, 850.

63. D. Evans, J. A. Osborn and G. Wilkinson, *J. Am. Chem. Soc.*, 1968, **90**, 3133-3142.

64. T. Mizugaki, M. Ooe, K. Ebitani and K. Kaneda, *J. Mol. Catal. Chem.*, 1999, **145**, 329-333.

65. J. Pospech, I. Fleischer, R. Franke, S. Buchholz and M. Beller, *Angew. Chem. Int. Ed*., 2013, **52**, 2852-2872.

66. M. Vilches-Herrera, L. Domke and A. Börner, *ACS Catal.*, 2014, **4**, 1706-1724.

67. W. R. Moser, C. J. Papile, D. A. Brannon, R. A. Duwell and S. J. Weininger, *J. Mol. Catal.*, 1987, **41**, 271-292.

68. F. Zhou, L. Zhang, Q. Wu, F. Guo, S. Tang, B. Xu, M. Yuan, H. Fu, R. Li, X. Zheng and H. Chen, *Appl. Organomet. Chem.*, 2018, **33**, 4646-4658.

69. W. Gil and A. M. Trzeciak, *Coord. Chem. Rev.*, 2011, **255**, 473-483.

70. R. L. Pruett, *Adv. Organomet. Chem*., 1979, **17**, 1-60.

71. N. N. Omosun, S. Ngubane, G. S. Smith, *Appl. Catal. A Gen.*, 2021, **610**, 117950.

72. S. Siangwata, N. J. Goosen and G. S. Smith, *Appl. Catal. A Gen*., 2020, **603**, 117736.

73. E. R. Tucci, *Ind. Eng. Chem., Prod. Res. Dev*., 1971, **9**, 516.

74. E. B. Hager, B. C. E. Makhubela and G. S. Smith, *Dalton Trans.*, 2012, **41**, 13927-13935.

75. B. C. E. Makhubela, A. M. Jardine, G. Westman and G. S. Smith, *Dalton Trans.*, 2012, **41**, 10715-10723.

76. W. Reppe and H. Vetter, *Ann. Chem.*, 1953, **582**, 133-163.

77. H. Liu, D. Yang, Y. Yao, Y. Xu, H. Shang and X. Lin, *Mol. Catal.*, 2020, **485**, 1-8.

78. S. Li, K. Huang, J. Zhang, W. Wu and X. Zhang, *Org. Lett.*, 2013, **15**, 1036-1039.

79. C. Michon, M. A. Abadie and F. Medina, *J. Organomet. Chem.*, 2017, **847**,13-27.

80. J. Hannedouche and E. Schulz, *Organometallics.*, 2018, **37**, 4313-4326.

81. L. Huang, M. Arndt, K. Gooßen, H. Heydt and L. J. Gooßen, *Chem. Rev.*, 2015,**115**, 2596-2697.

82. Q. Shen, Y. Qian, X. Xu, W. Li, J. Liu and W. Fu, *Acta Pharmacol. Sin*., 2015, **36**, 887-894.

83. M. J. Schneider, M. Lijewski, R. Woelfel, M. Haumann and P. Wasserscheid, *Angew. Chem. Int. Ed.*, 2013, **52**, 6996-6999.

84. D. M. Hood, R. A. Johnson, A. E. Carpenter, J. M. Younker, D. J. Vinyard and G. G. Stanley, *Science.*, 2020, **367**, 542-548.

85. S. Hanna, J. C. Holder and J. F. Hartwig, *Angew. Chem., Int. Ed.*, 2019, **58**, 3368-3372.

86. S. Gűlak, L. Wu, Q. Liu, R. Franke, R. Jackstell and M. Beller, *Angew. Chem., Int. Ed*., 2014, **53**, 7320-7323.

87. T. Rische, L. Barfacker and P. Eilbracht, *Eur. J. Org. Chem.*, 1999, **3**, 653-660.

88. B. Zimmermann, J. Herwig and M. Beller, *Angew. Chem. Int. Ed.*, 1999, **38**, 2372-2375.

89. S. Fuchs, T. Rösler, B. Grabe, A. Kampwerth, G. Meier, H. Strutz, A. Behr and A. J. Vorholt, *Appl. Catal. A. Gen.*, 2018, **550**, 198-205.

90. J. Bianga, K. U. Künnemann, L. Goclik, L. Schurm, D. Vogt and T. Seidensticker, *ACS Catal.*, 2020, **10**, 6463-6472.

91. Z. Nairoukh and J. Blum, *J. Chem. Org.*, 2014, **79**, 2397-2403.

92. T. O. Vieira and H. Alper, *Chem. Commun.*, 2007, **26**, 2710-2711.

93. L. Routaboul, C. Buch, H. Klein, R. Jackstell and M. Beller, *Tetrahedron Lett.*, 2005, **46**, 7401-7405.

94. J. October and S. F. Mapolie, *Tetrahedron. Lett.*, 2021, **70**, 153018.

95. F. Zeng and S. C. Zimmerman, *Chem. Rev.*, 1997, **97**, 1681-1712.

96. P. Tundo and A. Perosa, *Chem. Soc. Rev.*, 2007, **36**, 532-550.

97. M. Priske, K. Wiese, A. Drews, M. Kraume and G. Baumgarten, *J. Memb. Sci.*, 2010, **360**, 77-83.

98. W. L. Peddie, J. N. van Rensburg, H. C. M. Vosloo and P. van der Gryp, *Chem. Eng. Res. Des.*, 2017, **121**, 219-232.

99. L. P. Barthel-Rosa and J. A. Gladysz, *Coord. Chem. Rev.*, 1999, **190-192**, 587-605.

100. P. J. Dyson, D. J. Ellis and T. Welton, *Platin. Met. Rev.*, 1998, **42**, 135-140.

101. J. October and S. F. Mapolie, *J. Organomet. Chem.*, 2017, **840**, 1-10.

102. L. C. Matsinha, P. Malatji, A. T. Hutton, G. A. Venter, S. F. Mapolie and G. S. Smith, *Eur. J. Inorg. Chem*., 2013, 4318-4328.

103. F. Hapiot, S. Tilloy and E. Monflier, *Chem. Rev.*, 2006, **106**, 767-781.

104. L. C. Matsinha, S. F. Mapolie and G. S. Smith, *Dalton Trans.*, 2015, **44**, 1240-1248.

105. G. Fremy, R. Grzybek, E. Monflier, A. Mortreux, A. M. Trzeciak and J. Ziolkowski, *J. Organomet. Chem.*, 1995, **505**, 11-16.

106. D. S. Ramarou, B. C. E. Makhubela and G. S. Smith, *J. Organomet. Chem.*, 2018, **870**, 23-31.

107. C. W. Kohlpaintner, R. W. Fischer and B. Cornils, *Appl. Catal. A Gen.*, 2001, **221**, 219-225.

108. D. J. Adams, D. J. Cole-Hamilton, E. G. Hope, P. J. Pogorzelec and A. M. Stuart, *J. Organomet. Chem.*, 2004, **689**, 1413-1417.

109. I. T. Horvath and J. Rabai, *Science.*, 1994, **266** (5182), 72-75.

110. I. T. Horvath, G. Kiss, R. A. Cook, J. E. Bond, P. A. Stevens, J. Rabai and E. Mozeleski, *J. Am. Chem. Soc.*, 1998, **120**, 3133-3143.

111. L. Maqeda, B. C. E. Makhubela and G. S. Smith, *Polyhedron.*, 2015, **91**, 128-135.

112. N. C. Antonels, J. R. Moss and G. S. Smith, *J. Organomet. Chem.*, 2001, **696**, 2003.

113. G. R. Newkome, C. N. Moorefield, G. R. Baker, A. L. Johnson and R. K. Bahera, *Angew. Chem. Int. Ed. Eng.*, 1991, **30**, 1689.

114. R. Malgas, S. F. Mapolie, S. O. Ojwach, G. S. Smith and J. Darkwa, *Cat. Commun*., 2008, **9,** 1612.

115. S. Siangwata, C. Williams, N. Omosun, S. Ngubane and G. S. Smith, *Appl. Catal. A Gen.*, 2021, **626**, 118362.

116. P. Antoni, D. Nyström, C.J. Hawker, A. Hult and M. Malkoch, *Chem. Commun.*, 2007, 22, 2249-2251.

117. J. Park and S. Hong, *Chem. Soc. Rev.*, 2012, **41**, 6931-6943.

118. P. Govender, S. Ngubane, B. Therrien and G. S. Smith, *J. Organomet. Chem.*, 2017, **848**, 281-287.

119. B. C. E. Makhubela, A. M. Jardine and G. S. Smith, *Green Chem.*, 2012, **14**, 338-347.

120. C. Brosset, *Arkiv Kemi, Miner. Geol.*, 1935, **128**, 7.

121. C. Brosset, *Nature.*, 1935, **135**, 874.

122. R. Hrdina, E*ur. J. Inorg. Chem.,* 2021, 501-528.

123. F. A Cotton, C. Murillo and R. Walton, *Multiple bonds between metal atoms*, Springer, Boston, MA, 2005, 3rd edition, Chapter 12, pp. 465-589.

124. J. L. Bear, B. Han, Y. Li, S. Ngubane, E. Van Caemelbecke and K. M. Kadish, *Polyhedron.*, 2009, **28** (8), 1551-1555.

125. J. L. Bear, E. Van Caemelbecke, S. Ngubane, V. Da-Riz, and K. M. Kadish, *Dalton Trans.*, 2011, **40** (11), 2486-2490.

126. T. A. Stephenson, S. M. Morehouse, A. R. Powell, J. P. Heffer and G. Wilkinson, *J. Chem. Soc.*, 1965, 3632.

127. G. A. Rempel, P. Legzdins, H. Smith and G. Wilkinson, *Inorg. Synth.*, 1972, **13**, 90-91.

128. F. A. Cotton, E. V. Dikarev and S. E. Stiriba, *Inorg. Chem.*, 1999, **38**, 4877-4881.

129. T. Ren, C. Lin, E. J. Valente and J. D. Zubkowski, *Inorg. Chim. Acta.*, 2000, **297**, 283-290.

130. B. G. Anderson, D. Cressy, J. J. Patel, C. F. Harris, G. P. A. Yap, J. F. Berry and A. Darko, *Inorg. Chem.*, 2019, **58** (3), 1728-1732.

131. T. J. Whittemore, H. J. Sayre, C. Xue, T. A. White, J. C. Galucci and C. Turro, *J. Am. Chem. Soc.*, 2017, **139**, 14724-14732.

132. A. Cassimiro, Masters dissertation, University of Cape Town, Cape Town, 2018.

133. J. Lloret, J. J. Carbo, C. Bo, A. Lledos and J. Perez-Prieto, *Organometallics.*, 2008, **27**, 2873-2876.

134. Y. Lou, T. P. Remarchuk and E. J. Corey, *J. Am. Chem. Soc.*, 2005, **127**, 14223-14230.

135. P. Lahuerta, J. Paya, X. Solans and M. A. Ubeda, *Inorg. Chem.*, 1992, **31**, 385-391.

136. T. Yoshimura, K. Umakoshi and Y. Sasaki, *Inorg. Chem.*, 2003, **42** (22), 7106-7115.

137. H. T. Chifotides, K. V. Catalan and K. R. Dunbar, *Inorg. Chem.*, 2003, **42**, 8739-8747.

138. M. E. Prater, L. E. Pence, R. Clérac, G. M. Finniss, C. Campana, P. Auban-Senzier, D. Jérome, E. Canadell and K. R. Dunbar, *J. Am. Chem. Soc.*, 1999, **121**, 8005-8016.

139. K. V. Catalan, D. J. Mindiola, D. L. Ward, and K. R. Dunbar, *Inorg. Chem*., 1997, **36**, 2458-2460.

140. A. J. Catino, R. E. Forslund and M. P. Doyle, *J. Am. Chem. Soc*., 2004, **126**, 13622-13623.

141. H. M. L. Davies, A. M. Walji and T. Nagashima, *J. Am. Chem. Soc.*, 2004, **126**, 4271-4280.

142. M. Nowotny, T. Maschmeyer, B. F. G. Johnson, P. Lahuerta, J. M. Thomas and J. E. Davies, *Angew. Chem. Int. Ed.*, 2001, **40,** 955-958.

143. H. K. Kisan and R. B. Sunoj, *J. Org. Chem.*, 2015, **80,** 2192-2197.

144. V. Fimiani, T. Ainis, A. Cavallaro, and P. Piraino, *J. Chemother.*, 1990, **2**, 319-326.

145. R. F. M. Frade, N. R. Candeias, C. M. M. Duarte, V. Andre, M. T. Duarte, P. M. P. Gois and C. A. M. Afonso, *Bioorg. Med. Chem. Lett.*, 2010, **20**, 3413-3415.

146. R. Ohnishi, H. Ohta, S. Mori and M. Hayashi, *Organometallics*., 2021, **40**, 2678-2690.

147. T. J. Whittemore, C. Xue, J. Huang, J. C. Gallucci, and C. Turro, *Nat. Chem.*, 2020, **12**, 180-185.

148. H. D. Manamperi, C. E. Moore and C. Turro, *Chem. Commun.*, 2021, **57**, 1635-1638.

149. C. A. Crawford, J. H. Matonic, J. C. Huffman, K. Folting, K. R. Dunbar and G. Christou, *Inorg. Chem.*, 1997, **36**, 2361-2371.

150. A. Welsh, L. Rylands, V. B. Arion, S. Prince and G. S. Smith, *Dalton Trans.*, 2020, **49**, 1143-1156.

Chapter 2

Synthesis and characterisation of heteroleptic dirhodium(II,II) acetato-bipyridyl complexes

This chapter forms part of a publication entitled "*Heteroleptic dirhodium(II,II) acetato-bipyridyl complexes: evaluation as catalyst precursors for hydroformylation reactions",* cited as: **S. de Doncker**, G. S. Smith and S. Ngubane, *Appl. Catal. A Gen.*, 2023, **667**, 119440.

2.1 Introduction

The reaction of rhodium trichloride with suitable carboxylate salts is a widely known protocol for obtaining the corresponding metal-metal bonded dirhodium(II,II) tetracarboxylate complexes.[1-3] Homoleptic dirhodium(II,II) carboxylate complexes are well known, and by reacting them with appropriate ligands, allows access to both homo- and heteroleptic dirhodium(II,II) complexes with varying degrees of substitution.[1,2] Heteroleptic dirhodium(II,II) paddlewheel complexes may be obtained by ligand metathesis reactions directly, or by forming solvated intermediates which may then undergo ligand substitution. Reactions carried out between dirhodium(II,II) tetraacetate [$Rh_2(OAc)_4$], and ligands with suitable geometric structure and donor atoms such as carboxylic acids, amino pyridines, formamidines, bipyridines and amides are well reported in the literature.[3]

The structural and electronic character of these bimetallic complexes are routinely manipulated by varying the degree of ligand substitution in combination with types of ligand donor atoms and substituents. Modifications of this nature result in the stabilization of higher or lower oxidation states often playing a crucial role in applications such as catalysis.[4] The isolation of neutral or cationic dirhodium(II,II) complexes is achieved by the introduction of charged or neutral ligands respectively, with the oxidation state of the rhodium atoms maintained in the core.

Additionally, the group of heteroleptic dirhodium(II,II) complexes may be subdivided into two, namely those where the bridging ligands vary in nature, or those utilising a combination of both bridging and chelating ligands.[5,6] The latter results in disruption of the paddlewheel structure and associated D_{4h} symmetry around the bimetallic core. Complexes bearing *N*,*N*-donor ligands with a suitable spatial arrangement of the nitrogen atoms, such as those containing the pyridine heterocyclic motif, is well documented.[6-9] The extension of ligand π electron systems through incorporation of additional aromatic and/or heteroaromatic moieties are also known, resulting in the formation of an array of heteroleptic complexes, some examples of which are shown in Figure 2.1.[9-12] These complexes incorporate the pyridine motif and have been reported for their favourable characteristics when combined with acetate or formamidinate bridging ligands for various applications, including some catalytic reactions.[7,8]

Unlike heteroleptic complexes containing only bridging-type ligands, the inclusion of chelating ligands such as bipyridine with a degree of substitution higher than two is not observed. This provides a straightforward means of obtaining bis-substituted heteroleptic dirhodium(II,II) complexes without preparative separation of a mixture of isomers or compounds with different degrees of substitution.[13,14]

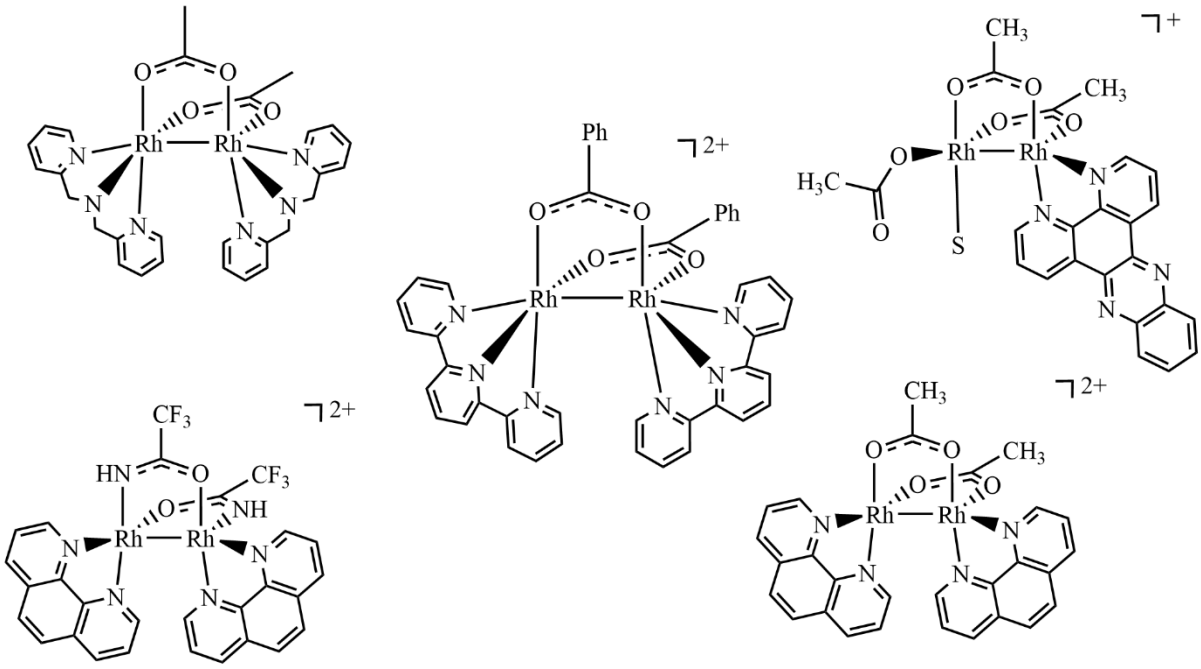

Figure 2.1. Examples of heteroleptic mono- and bis-substituted dirhodium(II,II) complexes containing bridging ligands only or bridging and chelating ligands with the pyridine motif, counter ions omitted for clarity.[6,9-12]

As previously alluded to, reports on the extension of the aromatic system for bipyridyl-based ligands are regularly explored. However, substituent variation of the ancillary bipyridyl ligands in heteroleptic dirhodium(II,II) acetato-bipyridyl complexes and their effects in thermally activated catalysis are unreported. To this end, the synthesis and characterisation of a series of dirhodium(II,II) acetato-bipyridyl complexes containing either acetate (**1 - 3**) or hexafluorophosphate (**4 - 6**) counter ions and the effects of axial interaction, substituent and counter ion are described.

2.2 Synthesis and characterisation of dirhodium(II,II) bis-κ-bipyridyl- μ-di-acetato diacetate complexes (1 - 3)

The synthesis of the target heteroleptic bis-substituted dirhodium(II,II) acetato-bipyridyl compounds containing acetate counter ions was achieved by a modified literature procedure, as depicted in Scheme 2.1.[11] The known compound **1**[11] and new compounds **2** and **3** were obtained in moderate to good yields (85 - 96%) by reacting 1 equivalent of the fully substituted dirhodium(II,II) tetraacetate [$Rh_2(OAc)_4$] with 2.1 equivalents of either 2,2'-bipyridyl, 4,4'-bis(trifluoromethyl)-2,2'-bipyridyl or 4,4'-bis(methoxy)-2,2'-bipyridyl (Scheme 2.1).

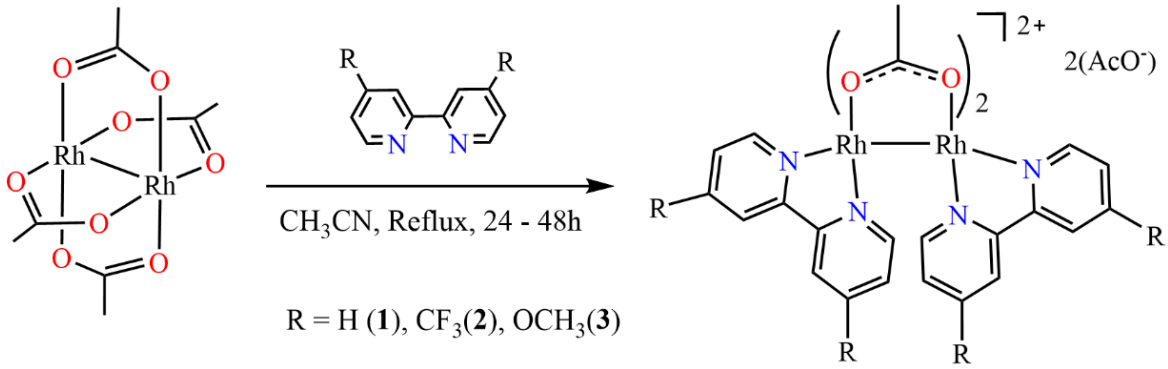

Scheme 2.1. Synthetic outline for reactions carried out to afford heteroleptic dirhodium(II,II) acetato-bipyridyl complexes.

The reactants were dissolved in anhydrous acetonitrile under inert atmosphere and heated to reflux for 24 to 48 hours to maximise yield. Due to a plethora of possible coordination modes and the varying symmetrical implications of these modes, the reaction time is important to consider regarding modification of the synthetic method. There are numerous reports of isolated complexes and adducts with various coordination modes and geometries for these

dirhodium(II,II) complexes.[7,15] However, the prolonged reaction time under reflux with above two equivalents of the bipyridyl ligand described below (Scheme 2.2) ensures that conversion to the target *bis*-substituted chelate complexes is achieved.[7,11,15] The sequence of steps in the proposed mechanism (Scheme 2.2) is initiated by the coordination of the acetonitrile solvent through the nitrogen donor atom to the bimetallic core of the $Rh_2(OAc)_4$ precursor complex. Experimentally, this is visualised by a vivid colour change of the solution, from green to purple in acetonitrile which occurs as the axial ligation takes place.

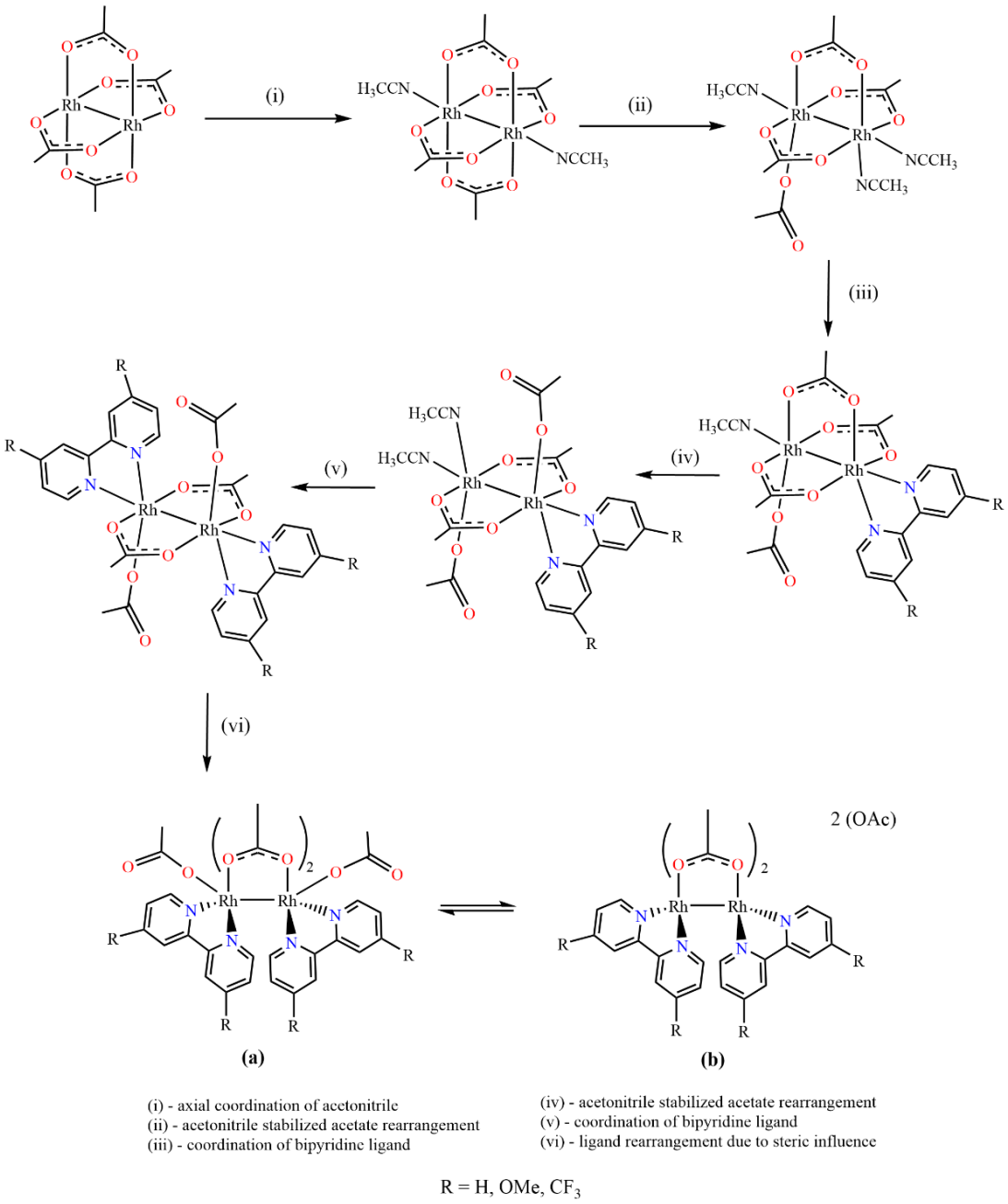

Scheme 2.2. Proposed reaction mechanism for the formation of the target heteroleptic dirhodium(II,II) acetato-bipyridyl complexes (**1 - 3**).

This is supported by reported findings of the role of axial ligation on the electronic excitations in the fully substituted dirhodium(II,II) tetraacetate complex.[16] The success of the reaction is strongly dependent on the nature of the solvent, where coordinating solvents such as methanol and acetonitrile are recommended as they stabilise the intermediates and facilitate the substitution of the acetate ligands.

An example of the stabilising effect of acetonitrile is reported by Prater and co-workers, demonstrating the removal of the bridging acetate ligands with an alkylating agent, Et_3OBF_4, resulting in a completely solvated dirhodium species, of the form $Rh_2(NCCH_3)_{10}$ while maintaining the metal-metal bond.[17] The stabilising effect imparted by the coordinated acetonitrile increases the lability of the bridging acetate ligand. This allows for binding of additional acetonitrile molecules, additional solvent molecules or ligand molecules such as 2,2'-bipyridyl. Should the incoming bipyridyl ligand bind, the lability of the Rh-O bond results in a stepwise substitution of the acetate ligand. This is illustrated by the corresponding decrease in hapticity of the bridging acetate ligand as shown in step (ii).

Although both the solvent and incoming ligands contain nitrogen donor atoms, subsequent rearrangement and formation of the more stable *N*,*N*-chelate system favours the formation of the intermediate resulting from step (iii). Unsymmetrical coordination of the acetate ligand may also occur, however in this instance the torsional strain imposed on the complex increases the reactivity toward further substitution of the additional bipyridyl ligand under these reaction conditions.

Successive substitution of the second bipyridyl ligand results in the formation of the heteroleptic complex, which may exist in several forms depending on the binding mode of the acetate ligands. Two examples of this are shown in Scheme 2.2, highlighted as species (a) or (b), which may exist as either form depending on external factors such as stability in solution or the presence of other molecules capable of coordination. Complexes **1** - **3** were isolated as red solids in good yields of 71 - 96% with excellent solubility observed in H_2O, MeOH, acetonitrile, toluene and DMSO with partial solubility noted in EtOH and acetone.

2.2.1 ^{1}H-NMR spectroscopy

The characterisation of complexes **1** - **3** were initially carried out by NMR spectroscopy, the experimental details of which are outlined in section 2.5. The successful formation of the complexes is suggested initially by comparison of the NMR spectra obtained for the complex and the corresponding precursor ligand. The binding of the ligands to the metal atoms usually presents with shifts in the proton signals of ligands due to changes in the distribution of electron density and its effect on the magnetic fields experienced by nuclei such as ^{1}H or ^{13}C. By way of example, a comparison of the spectra obtained for 4,4'-bipyridyl and complex **1** is shown in Figure 2.2. In this case, distinct chemical shift differences in the bipyridyl and acetate proton signals are observed upon complex formation.

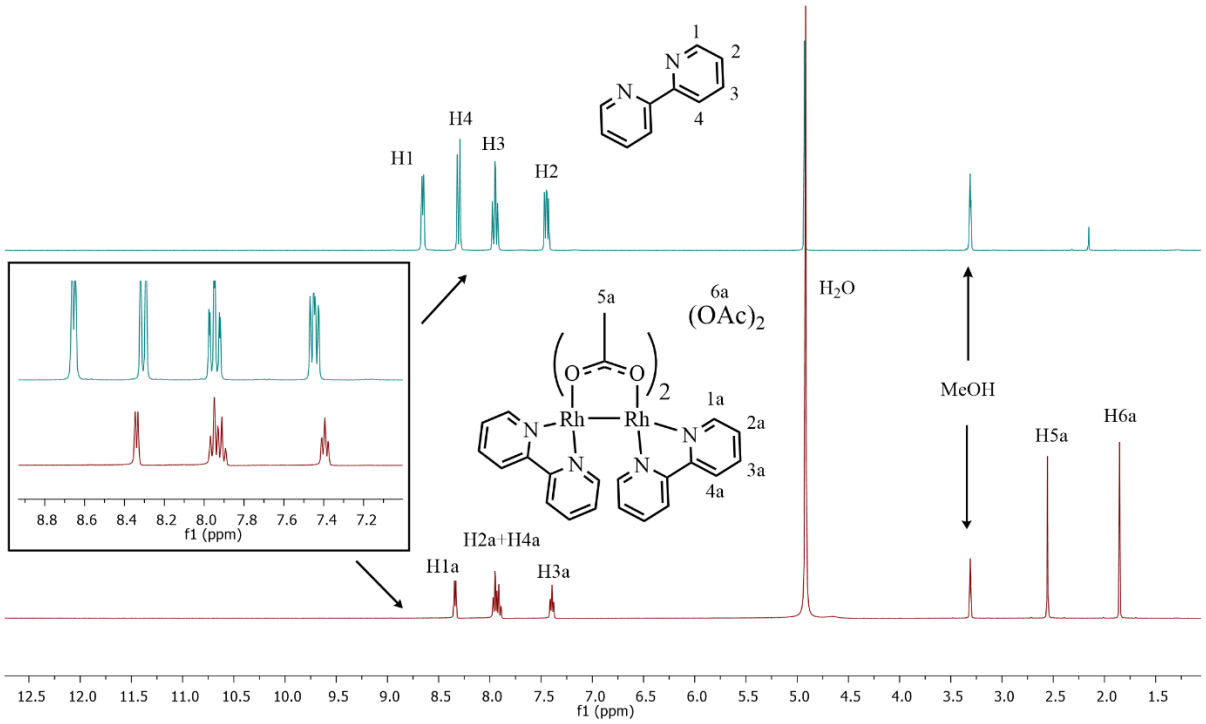

Figure 2.2. ^{1}H-NMR spectral comparison of the aromatic proton signals of 4,4'-bipyridyl (above) and complex **1** (below) recorded in MeOD.

A characteristic upfield shift from 8.68 ppm to 8.34 ppm is observed for the doublet signal corresponding to the proton (H_1) adjacent to the nitrogen heteroatom in the bipyridyl ligand upon binding to the respective rhodium atom (H_{1a}). This arises due to back-bonding of the π^* orbital of the bipyridyl ligand with the rhodium metal atom, resulting in a shift in electron density from the metal centre toward the aromatic system, thereby causing a shielding effect

and the upfield shift observed in the spectrum. Due to the bicyclic heteroaromatic system structure, a negligible shift is observed for the protons in the *para* position relative to the nitrogen atom (H_3, H_{3a}), shifting from 7.94 to 7.93 ppm. Interestingly, the signals corresponding to the protons in the *meta* positions relative to the nitrogen atom present an upfield shift of 0.4 ppm for H_{4a} and a downfield shift of 0.5 ppm observed for H_{2a}. This results in the signals corresponding to these protons overlapping in the spectrum obtained for the complex. The integration of 8H for signals corresponding to protons assigned to H_{2a} and H_{4a} and the 4H integration for each of the signals assigned to H_{1a} and H_{3a} relative to the bridging acetate proton signal H_{5a} (6H) resonating at 2.56 ppm is observed. The proton signals observed for complex **1** correspond with those reported in the literature,[11] supporting the formation of the bis-substituted complex.

The deshielding observed for the specific aromatic proton signals can be explained by resonance, whereby the increased electron density at the *ortho* and *para* positions is usually accompanied by relatively lower electron density at the *meta* position. Additionally, the shielding effect observed for proton H_{4a} relative to H_4 is due to the presence of the aromatic group bound at the 2-position. The singlet resonating at 1.79 ppm, differentiated from the bridging acetate signal by the change in chemical shift, is assigned to the remaining acetate moiety with the expected relative integration of 6H and correlates with the previously reported data.[11] The upfield shift of this signal relative to the signal corresponding to the bridging acetate group may be due to two factors; (i) binding to the axial site in a monodentate coordination mode, or (ii) the acetate group existing as a counter ion. Although some interplay between these states may occur, this proposed dynamic effect may be of relevance once the complexes are applied as catalyst precursors.

The ^{1}H-NMR spectra recorded for complexes **2** and **3** (Figure 2.3, *overleaf*) shows the effects of substitution at the 4 and 4' positions of the bipyridyl ligand on both the bridging and counter ion acetate proton signals, relative to complex **1**. Generally, the expected shifts in the bipyridyl proton signals are observed with respect to the electron-withdrawing trifluoromethyl and electron-donating methoxy substituents in complexes **2** and **3** respectively.

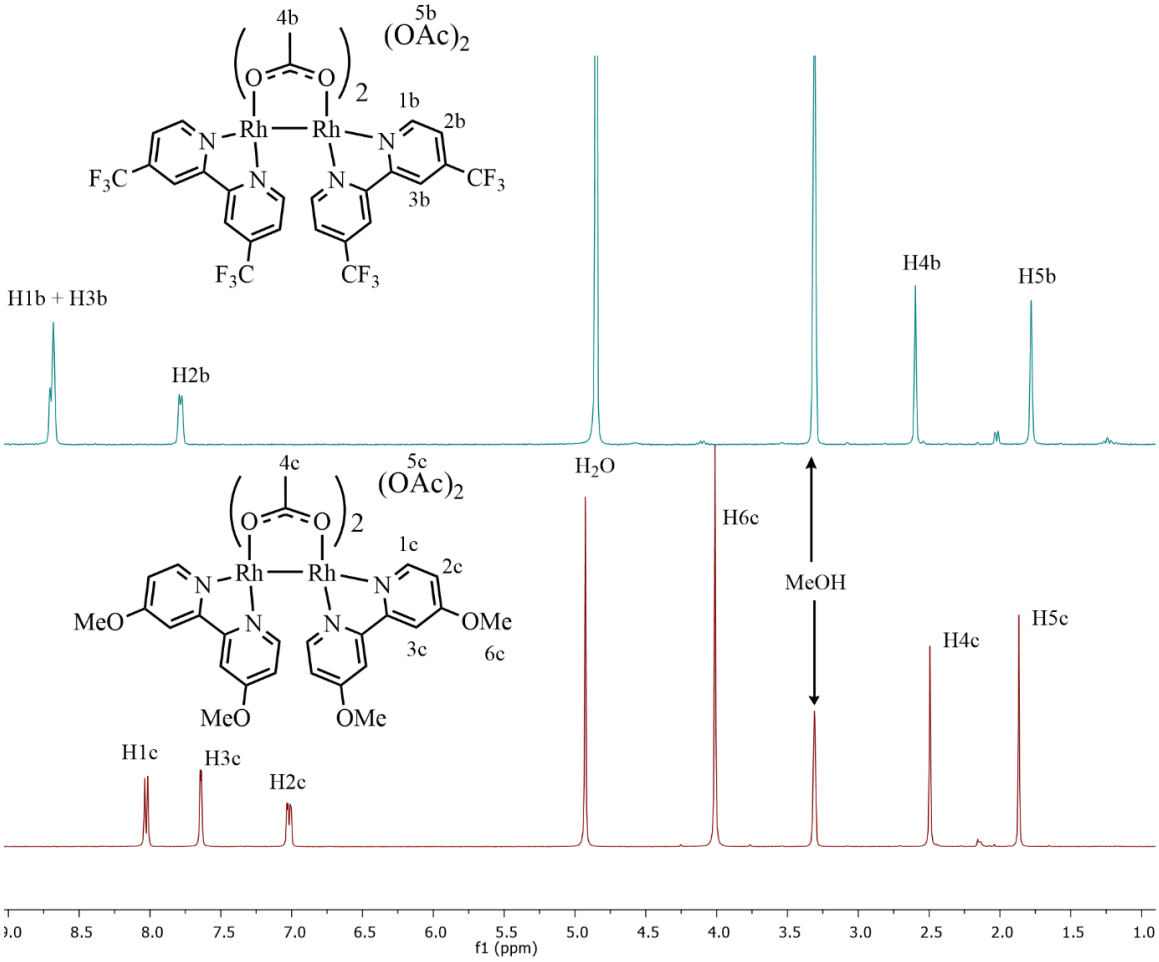

Figure 2.3. ^{1}H-NMR spectral comparison of complex **2** and **3** recorded in MeOD.

The doublet, singlet and doublet multiplicities observed correspond to signals resonating in the aromatic region as expected for the 4,4'-disubtituted heterocyclic bipyridyl motif. The correct relative integration of 4H is observed for each aromatic signal compared to the bridging acetate signal, integrating for the expected 6H. The influence of the electron-withdrawing and electron-donating effects imparted by the respective substituents is further supported by significant deshielding observed for signal H_{1b}, and the shielding observed for H_{1c}, resonating at 8.71 and 8.02 ppm respectively, relative to analogous signals in complex **1**. This shielding occurs due to the methoxy substituent imparting mesomeric donation (*np*-π) into the heteroaromatic system.

The signals corresponding to protons H_{3b} and H_{3c} present the largest difference in chemical shift, resonating at 8.69 and 7.64 ppm, observed with respective broad singlet and doublet multiplicity. This is due to the proximity of the electron withdrawing trifluoromethyl substituent and the deshielding effect of the adjacent aromatic group. The comparison of the coupling constants was used to aid the assignment of the observed signals for complex **3**, where

coupling between both H_{1c} and H_{3c} to H_{2c} is observed. The coupling constants for the proton interactions were calculated as ^{2}J = 6.6 Hz and ^{3}J = 2.7 Hz respectively. A schematic representation of the effects of the substituent on electron distribution, and the corresponding changes magnetic environments of the aromatic protons upon coordination to the metal is shown in Scheme 2.3.

The bridging acetate signal in complex **2** with the electron-withdrawing trifluoromethyl substituent is observed resonating at 2.60 ppm relative to the analogous signal in the spectrum of complex **3**, observed at 2.49 ppm. This is due to the mesomeric electron donating effect emanating from the methoxy substituent. Conversely, comparison of the signals corresponding to the counter ion acetate protons displays increased shielding for the counter ion signal for complex **2** (1.78 ppm) relative to complex **3** (1.88 ppm). This is attributed to the affinity for axial site of the acetate counter ion, where more favourable interactions between the counter ion and metal centre result in higher probability of binding. This therefore results in significant deshielding of the protons in the axially bound acetate ligand in complex **3**.

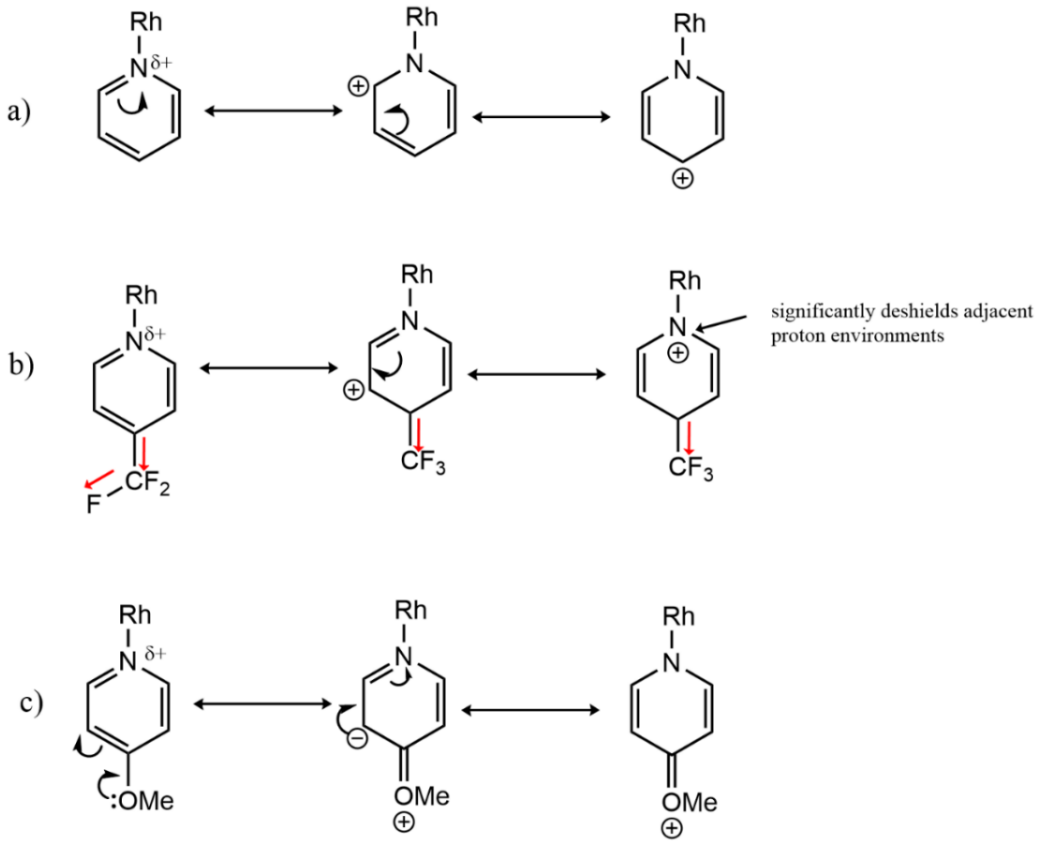

Scheme 2.3. Proposed effects of the electron donating (OMe) and withdrawing (CF_3) substituents and unsubstituted bipyridyl ligand on the shielding and deshielding of proton signals observed for complexes **1**, **2** and **3**.

2.2.2 Diffusion ordered (DOSY) NMR spectroscopy

The observed trend in the chemical shift of the acetate counter ion signals and their proposed interaction with the bimetallic core was further probed by diffusion ordered NMR spectroscopy (DOSY). The fundamental principle of DOSY is that the NMR signals of a compound can be separated based on their diffusion coefficients, not unlike those reported in the use of HPLC-NMR as an analytical technique.[18] In this context, should the acetate counter ion ligand be axially bound, the signals corresponding to the bridging acetate signal would be observed having the same diffusion order, observed in a single line on the 2-D spectrum. The obtained DOSY spectra for complexes **1** and **2** recorded in MeOD are shown in Figures 2.4 and 2.5 respectively.

The spectrum recorded for complex **1** displays signals corresponding to the bipyridyl (8.50-7.20 ppm) and acetate (2.56 ppm) protons of ligands bound to the core in the same diffusion range (9.21 ppm, Figure 2.4, vertical axis). The signal corresponding to the counter ion is observed resonating at 1.79 ppm with different diffusion order (9.10 ppm, Figure 2.4, vertical axis). This suggests that the acetate group corresponding to this signal, referred to as the counter ion from this point, is not strongly bound to the axial site in the presence of methanol, inferring that some lability of the Rh-OAc axial bond exists in solution.

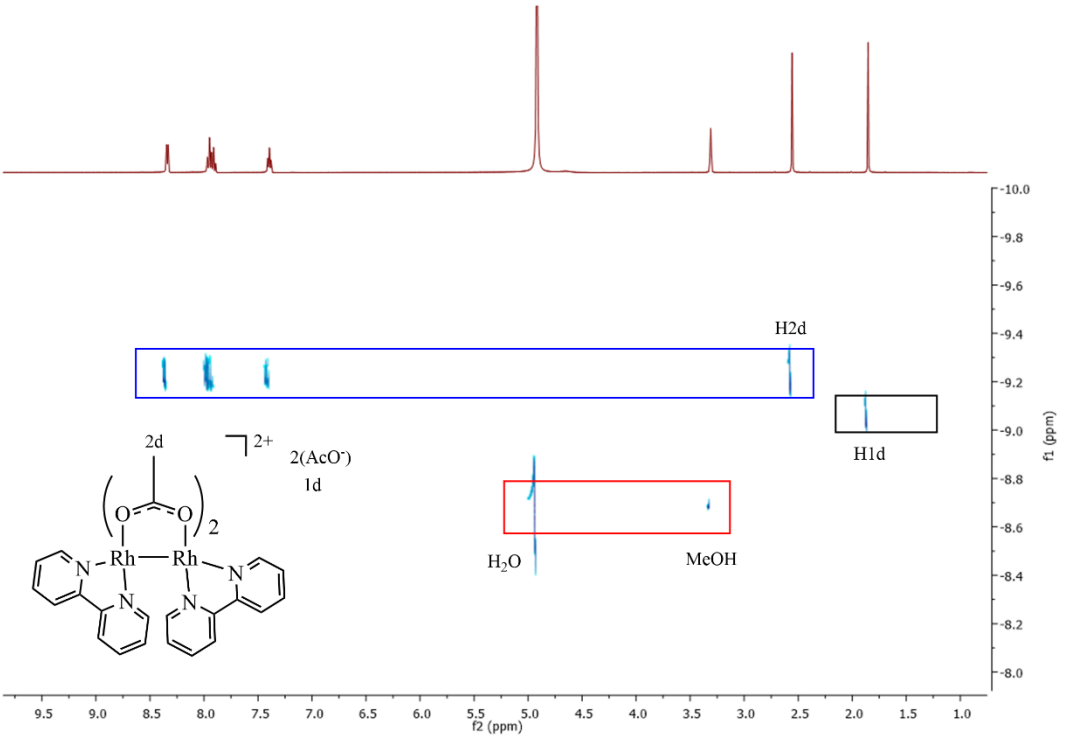

Figure 2.4. DOSY spectrum obtained for complex **1** recorded in MeOD.

The separation of the residual MeOH and H_2O from the inner coordination sphere signals suggest that no exclusive binding of these molecules occurs, likely a consequence of the axial interaction of the counter ion acetate group with the bimetallic core. Interestingly, the spectrum obtained for complex **2** (Figure 2.5) shows larger differences in the diffusion order between the inner coordination sphere and the counter ion proton signals. The bridging acetate proton signal (H_{2e}) is observed at 2.60 ppm, while the counter ion signal (H_{1e}) is observed resonating at 1.78 ppm, with diffusion order differences of 9.26 to 9.08 ppm.

The larger observed difference in the diffusion of the counter ion for complex **2**, compared to complex **1** is ascribed to changes in the electronics of the dirhodium(II,II) core resulting from the change in bipyridyl substituent (H *vs.* CF_3). The lower axial binding of the acetate counter ion is supported by the previously obtained spectrum whereby the signals observed for complex **2** showed greater shielding of the acetate proton signal H_{5b} (Figure 2.3, *vida supra*) compared to the analogous protons in complexes **1** and **3**. Corroborating experiments and further details on the investigation of the axial site interactions is discussed in detail in section 2.4.

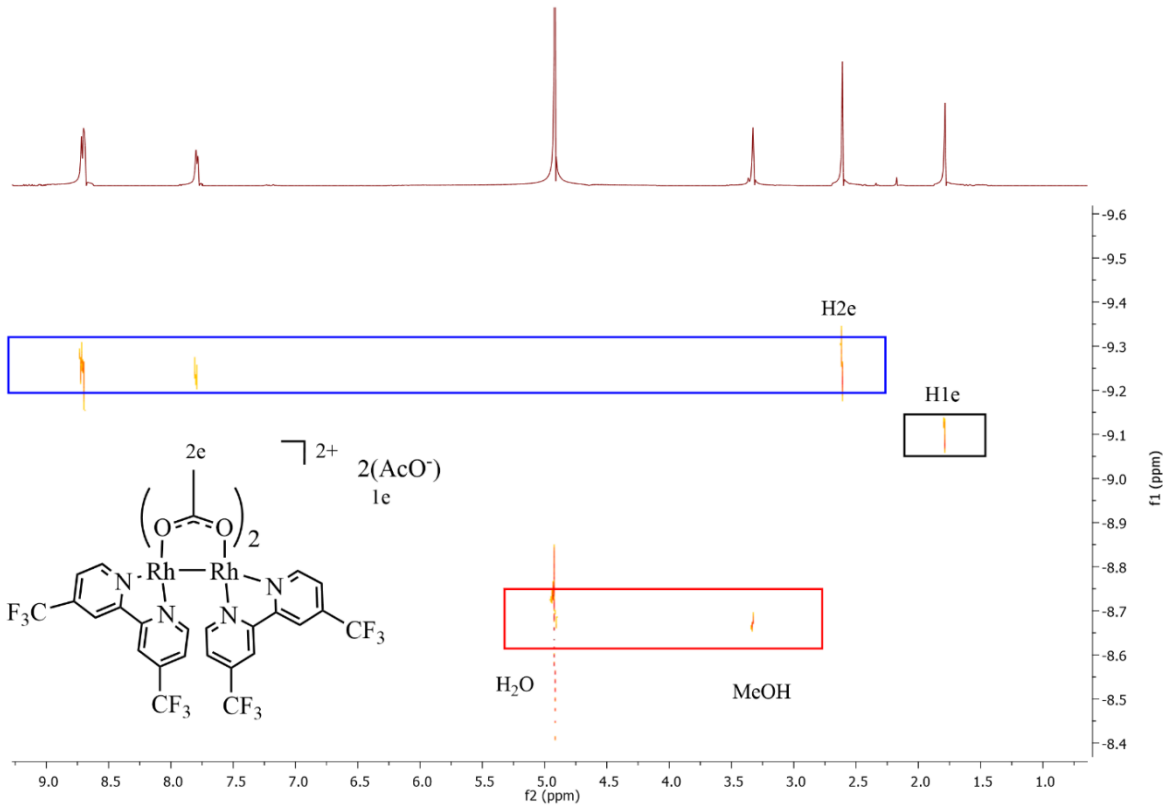

Figure 2.5. DOSY spectrum of complex **2** recorded in MeOD.

2.2.3 $^{13}C\{^{1}H\}$- and ^{19}F- NMR spectroscopy

The successful synthesis of complexes **1** - **3** is further supported by the presence of characteristic signals observed in the $^{13}C\{^{1}H\}$ NMR spectra recorded. The spectrum obtained for complex **1** (Figure 2.6) displays nine distinct carbon signals corresponding to the proposed structure. The characteristic signals observed at 191.8 and 180.3 ppm are assigned to the carbonyl carbon atoms in the bridging and counter ion acetate moieties respectively, in agreement with the previous findings.[11]

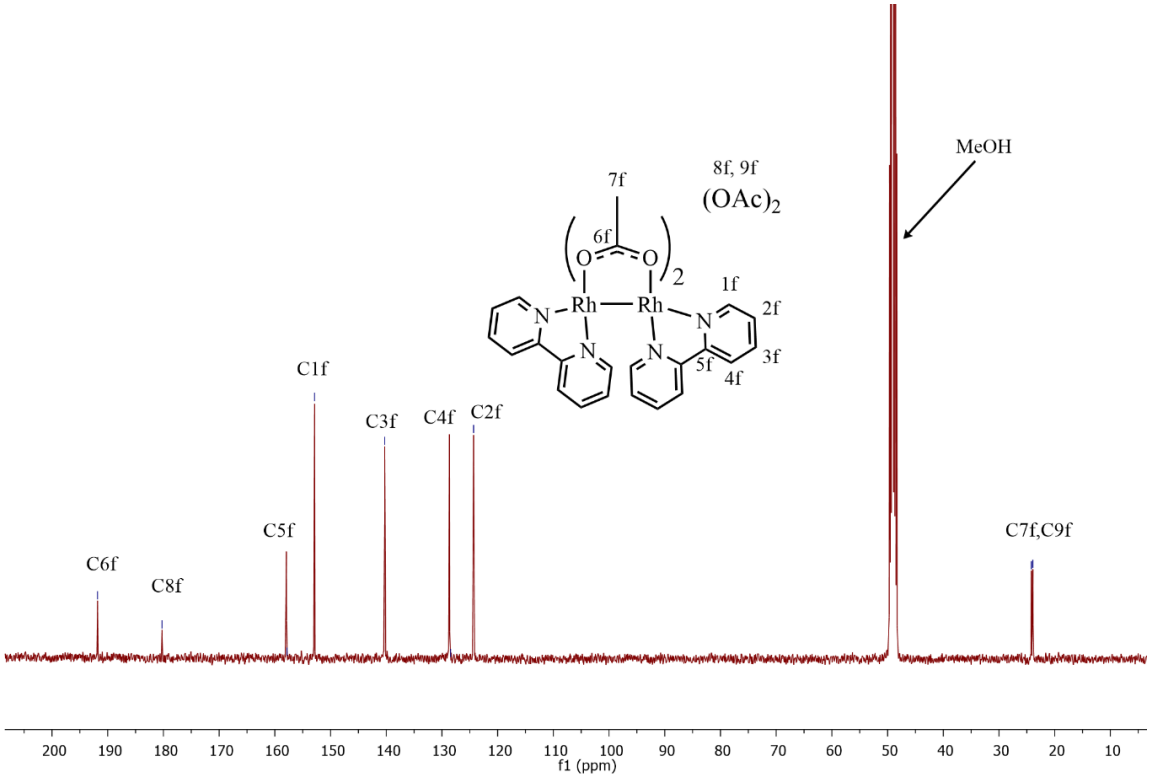

Figure 2.6. $^{13}C\{^{1}H\}$ NMR spectrum of complex **1** recorded in MeOD.

The five signals observed in the 158 - 124 ppm region are assigned to the bipyridyl carbon atoms, with the most deshielded signal corresponding to the quaternary carbon (C_{5f}) followed by the signal corresponding to C_{1f} resonating at 152.8 ppm. The remaining aromatic signals resonating at 140.3, 128.4 and 124.3 ppm were assigned to carbons C_{4f}, C_{2f} and C_{3f} respectively, due to the shielding and deshielding effects observed in the ^{1}H-NMR spectrum. The signals corresponding to the acetyl CH_3 groups are observed as singlets in close proximity, resonating at 24.2 and 23.9 ppm, assigned to the bridging (C_{7f}) and counter ion acetate (C_{9f}) carbons respectively. This is due to the previously stated shielding and deshielding effects as illustrated in the ^{1}H-NMR spectrum previously recorded.

The $^{13}C\{^{1}H\}$ spectra obtained for complexes **2** and **3** (Figure 2.7) shows the expected number of signals, with further splitting observed in complex **2** due to coupling with the fluorine atoms of the trifluoromethyl group.[19] As observed in the spectrum recorded for complex **1**, the most deshielded carbon signal is assigned to the bridging acetate carbonyl carbon atom, resonating at 192.7 and 191.5 ppm for complexes **2** and **3** respectively. A small shielding effect (*ca.* 0.3 ppm) is observed in the carbonyl carbon signal of complex **3** due to the electron-donating effects of the methoxy group, relative to the corresponding carbon signal in the unsubstituted complex **1**.

Similarly, a deshielding effect of approximately 0.9 ppm is exhibited by the signal observed for the analogous carbon atom in complex **2**, due to the electron-withdrawing trifluoromethyl substituent. Furthermore, shifts in the counter ion acetate carbonyl signals are observed resonating at 180.5 and 180.2 ppm for C_{9h} and C_{9g} in complexes **2** and **3** respectively. This small difference in the chemical shifts can be attributed to the lower interaction of the acetate counter ion to the bimetallic core.

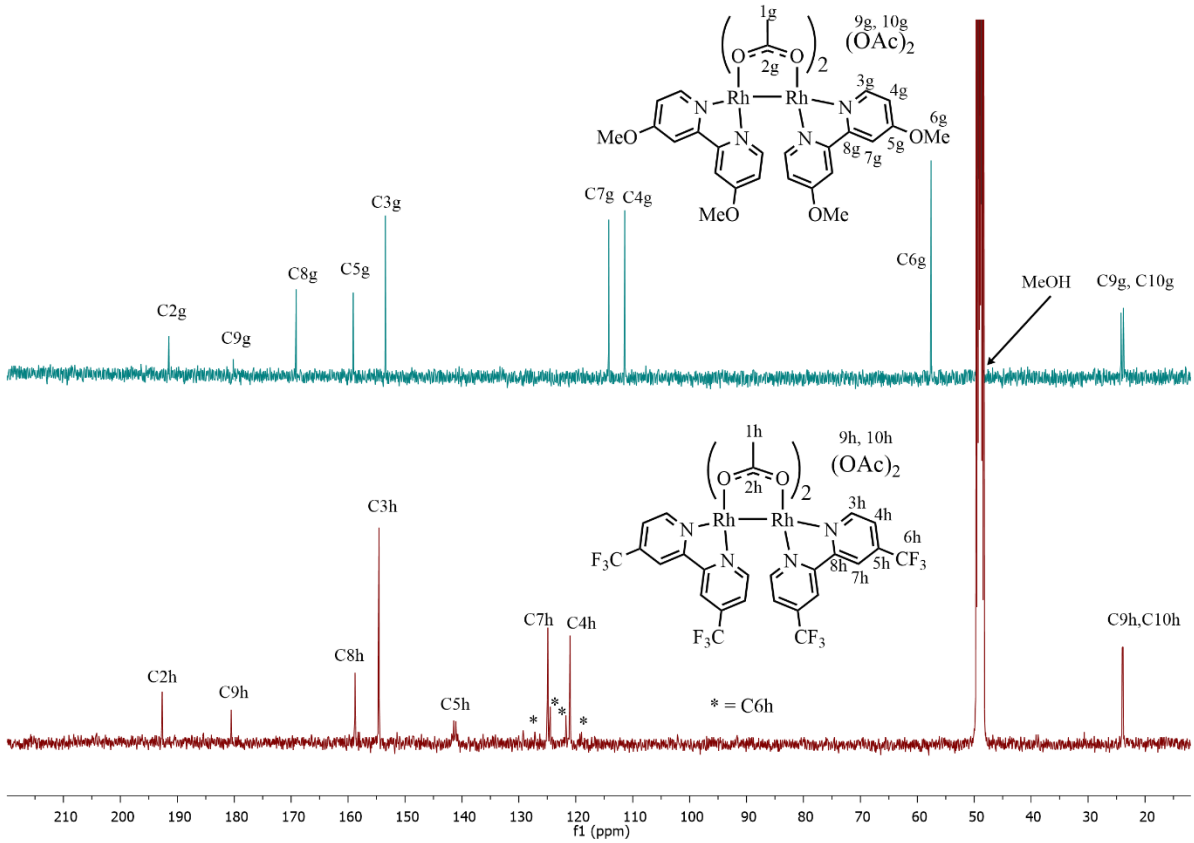

Figure 2.7. Stacked $^{13}C\{^{1}H\}$ NMR spectra of complexes **2** (below) and **3** (above) recorded in MeOD.

The signals corresponding to quarternary carbon atoms C_{8g} and C_{8h} are observed at significantly distinct chemical shifts, resonating at 141.2 ppm for complex **2**, compared to 169.1 ppm in complex **3**. This occurs due to the *ortho*- and *para*-directing nature of the substituents in addition to the effects of coordination of the pyridyl nitrogen atom and appended aromatic group. This results in a relative shielding (complex **2**) and deshielding (complex **3**) effect of carbon atoms at the *ortho*-position relative to the pyridyl nitrogen atom. By way of example, the electron-withdrawing effect of the trifluoromethyl substituent in complex **2** is expected to cause deshielding at the *ortho*-positions, C_4 and C_7, and at the binding nitrogen atom accompanied by a shielding effect at the carbon atom at the *ipso*-position. This distribution of electrons in the heteroaromatic system results in significant electronic effects at the C_8 position, observed as a more shielded signal relative to the analogous atom in complex **3**. The quartet signals observed at 141.2 and 123.1 ppm are assigned to the C_{5h} and C_{6h} atoms, with the associated coupling constants of 37 and 274 Hz respectively.[19] The combination of the electronic effects observed are minimal for the C_3 carbon atom at the *meta*-position relative to the substituent, where C_{3g} and C_{3h} are observed resonating at 153.4 and 154.6 ppm respectively.

Additionally, the ^{19}F NMR spectrum (Figure 2.8) recorded for complex **2** displays a single signal, observed as a singlet resonating at -66.2 ppm confirming a single magnetic environment for fluorine atoms, supporting the proposed structure.

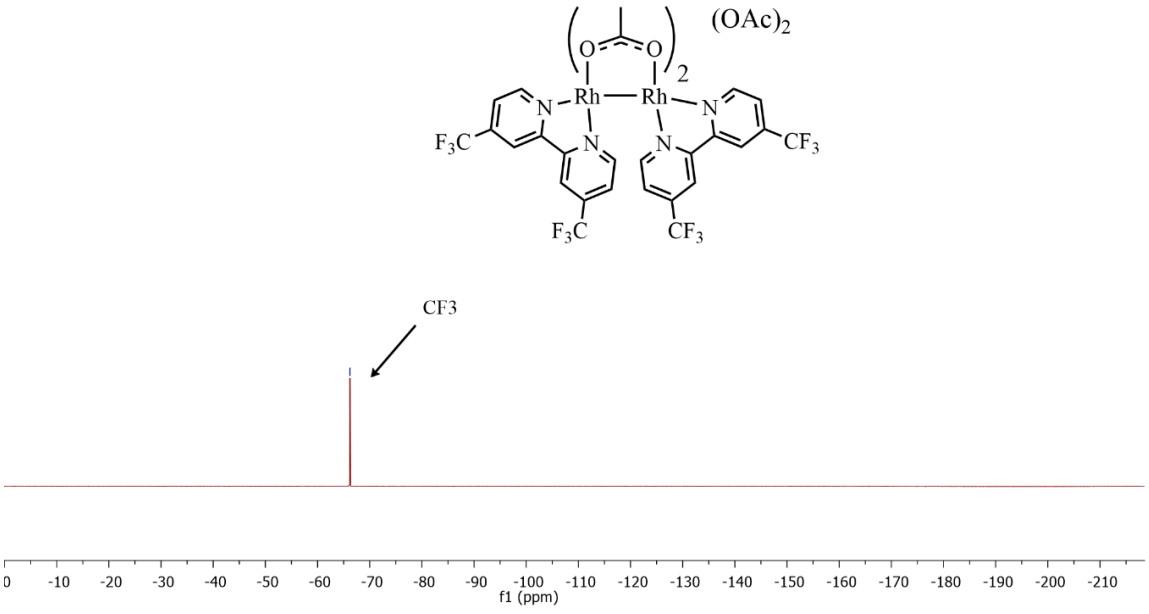

Figure 2.8. ^{19}F-NMR spectrum of complex **2** recorded in MeOD.

2.2.4 Infrared (IR) spectroscopy

Infrared spectroscopy was used to confirm coordination of the bipyridyl ligand to the dirhodium core. The recorded IR spectra support the NMR spectroscopic data, whereby distinct shifts in the characteristic C=N absorption bands are observed, from the 1590 cm^{-1} to the 1560 cm^{-1} region. This shift in the absorption band confirms that the coordination of the bipyridyl ligand through the nitrogen and rhodium atoms occurs (Appendix, Figure A1). The shift to a lower wavenumber combined with the shielding of the aromatic signals observed in the ^{1}H-NMR spectra upon formation of the complexes, substantiates the previous speculation of back-bonding occurring. Additionally, broad and shouldered absorption bands are observed in the 1550 - 1420 cm^{-1} region corresponding to the axially bound and bridging acetate ligands in all cases. Furthermore, the spectra obtained for complexes **2** and **3** displays intense absorption bands at 1182 and 1282 cm^{-1} corresponding to the C-F and C-OMe stretching modes for the respective bipyridyl substituent.

2.2.5 Mass spectrometry

The mass spectrometry data supports the ^{1}H, ^{13}C-, ^{19}F- and DOSY spectral data, further confirming formation of the new complexes. Base peaks are observed at *m/z* = 492.9715 and 378.0120 corresponding to $[M+DMSO-2(OAc)]^{2+}$ and $[M-2(OAc)]^{2+}$ molecular ion peaks for new complexes **2** and **3** respectively (Appendix, Figures A2 and A3).

2.3 Synthesis and characterisation of dirhodium(II,II) bis-κ-bipyridyl- μ-di-acetato bis-hexafluorophosphate complexes (4 - 6)

To explore the effects of the axial interaction of the acetate counter ions on the physicochemical characteristics of the complexes, anion exchange reactions were carried out by reacting complexes **1** - **3** with ammonium hexafluorophosphate (Scheme 2.4, *overleaf*) to afford di-cationic complexes **4** - **6** in moderate yields of 68 - 80%. Although complex **4** has previously been reported as a hydrate, incorporating axial adducts,[11] the method outlined here enables isolation of the complex without adduct formation, necessary for determining any differences between acetate and hexafluorophosphate-containing complexes in this context.

This method was adapted from a previously reported anion exchange reaction,[20] culminating in the isolation of complexes **4** - **6** as a bright yellow, bright red crystalline powder and a flaky green solid respectively. Complexes **4** and **5** were found to be soluble in methanol, H_2O, acetonitrile, dimethyl sulfoxide and acetone, with partial solubility noted in toluene and ethanol. Complex **6** was determined to be partially soluble in methanol, acetonitrile, and acetone, sparingly soluble in water, ethanol, and toluene and soluble in dimethyl sulfoxide.

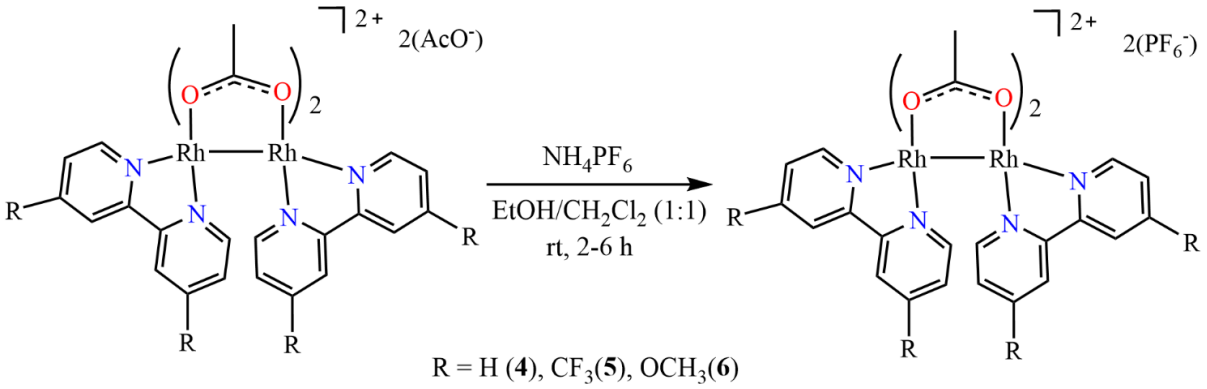

Scheme 2.4. Outline of the synthetic method applied for the synthesis of complexes **4** - **6**.

2.3.1 ^{1}H-, $^{13}C\{^{1}H\}$-, ^{19}F- and ^{31}P-NMR spectroscopy

The characterisation of the complexes was carried out as described for complexes **1** - **3**, with the absence of the characteristic counter ion acetate signals, confirming successful exchange of the acetate with the hexafluorophosphate counter ion, observed in the spectra obtained for complexes **4** - **6**. Comparison of the ^{1}H-NMR spectrum obtained for complex **4** to the previously recorded spectrum for complex **1** (Figure 2.9, *overleaf*) shows negligible upfield shifts (<0.05 ppm) in the signals corresponding to the bipyridyl protons in complex **1** (H_{1i}-H_{4i}) opposed to the analogous protons in complex **4** (H_{1j}-H_{4j}). Additionally, an observed downfield shift of 0.07 ppm is observed for the signal corresponding to bridging acetate proton upon counter ion exchange (H_{5j}). This supports the previous speculation of significant electronic effects arising from the axial interaction of the acetate counter ion to the bimetallic core in complex **1**.

Similarly, the absence of the counter ion acetate proton signal upon comparison of the ^{1}H-NMR spectra of complexes **2** and **5** is evident (Figure 2.10, *overleaf*). However, the signals corresponding to the bipyridyl ligand show no distinguishable shift, and a small upfield shift is

observed for the bridging acetate signal from 2.60 to 2.55 ppm. These observations support the proposed lower acetate-metal interaction observed for complex **2** compared to complex **1**, illustrated by the observed differences in the DOSY NMR spectra.

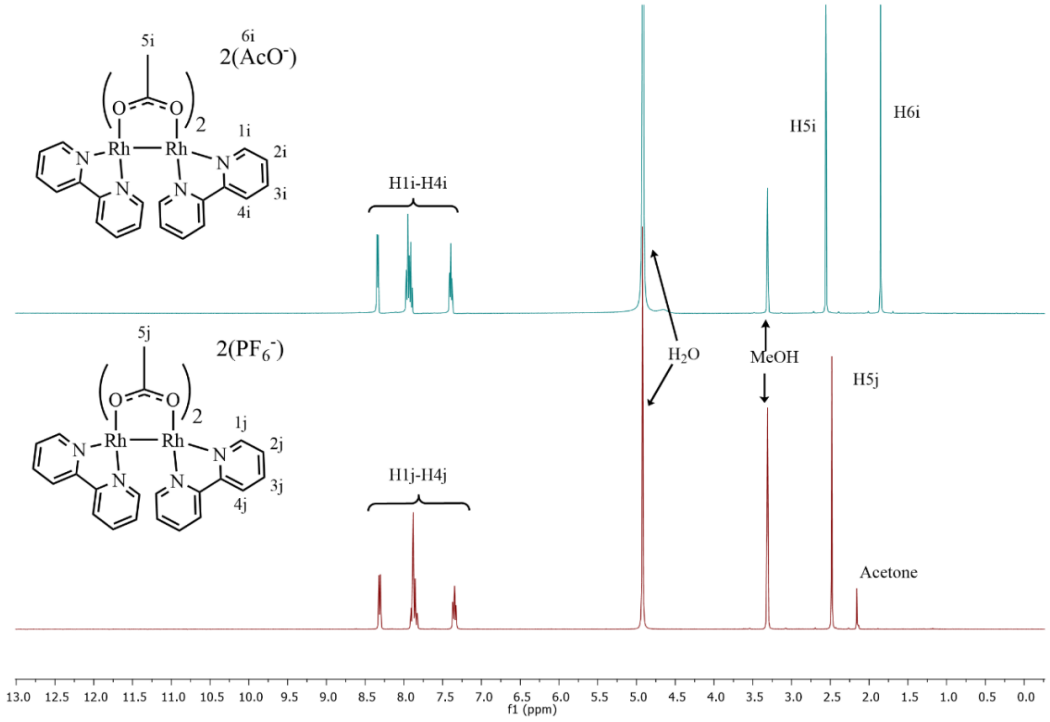

Figure 2.9. Comparison of the ^{1}H-NMR spectra of complexes **1** (upper) and **4** (lower) recorded in MeOD.

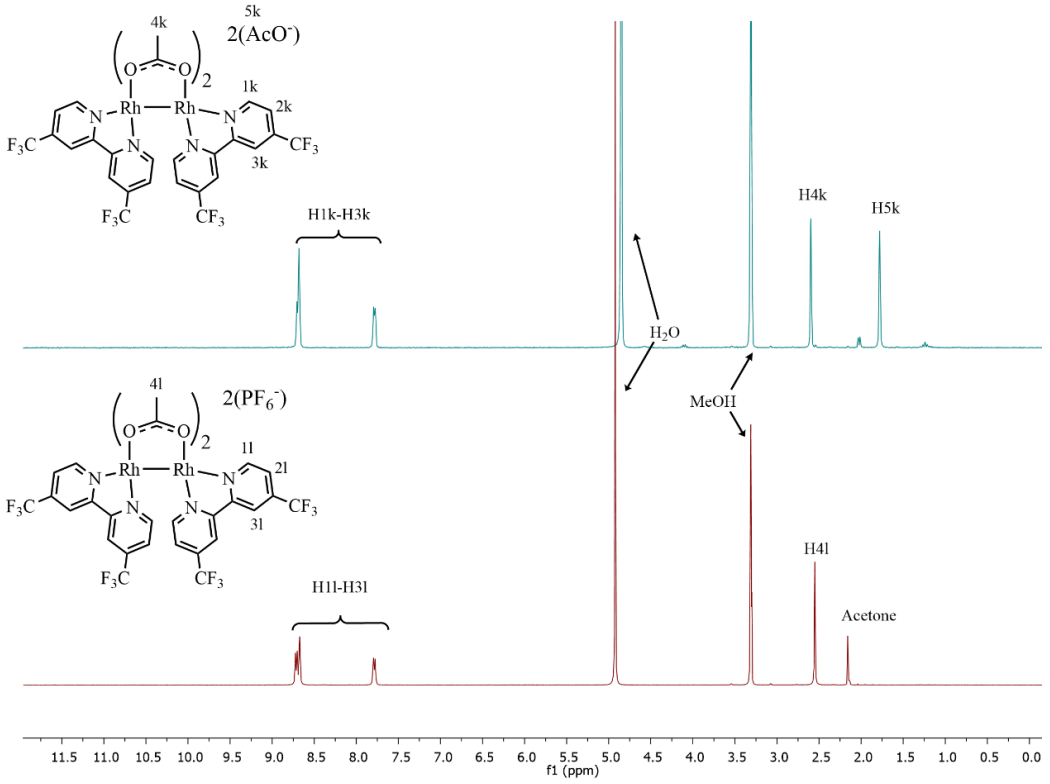

Figure 2.10. ^{1}H-NMR spectral comparison of complexes **2** (upper) and **5** (lower) recorded in MeOD.

Due to unsuitable solubility of complex **6** in methanol for spectral analysis, the ^{1}H spectrum was recorded in DMSO-d_6 and compared to the spectrum obtained for complex **3** in DMSO-d_6. Comparison of the stacked ^{1}H-NMR spectra is shown in Figure 2.11. A singlet signal is observed resonating at 1.47 ppm and integrating for 3H, corresponding to the counter ion acetate proton (complex **3**). This signal is not present in the spectrum recorded for complex **6**, thereby confirming successful counter ion exchange as in the case of complexes **4** and **5**.

Additionally, comparison of the obtained spectra for complexes **3** and **6** in DMSO shows negligible shifts in the signals corresponding to the methoxy substituent, bridging acetate and bipyridyl proton (H_{1m} and H_{1n}) resonating at 3.96, 2.37 and 7.83 ppm respectively. Interestingly, a downfield shift in the bipyridyl proton signal (H_{3m}) is observed upon counter ion exchange. This supports the strong influence of the counter ion on the electronic and magnetic properties of complex **3**. The expected relative integration is observed for the bipyridyl aromatic proton signals, integrating for 4H each and the methoxy substituent signal, integrating for the expected 12H, relative to the bridging acetate signal (6H).

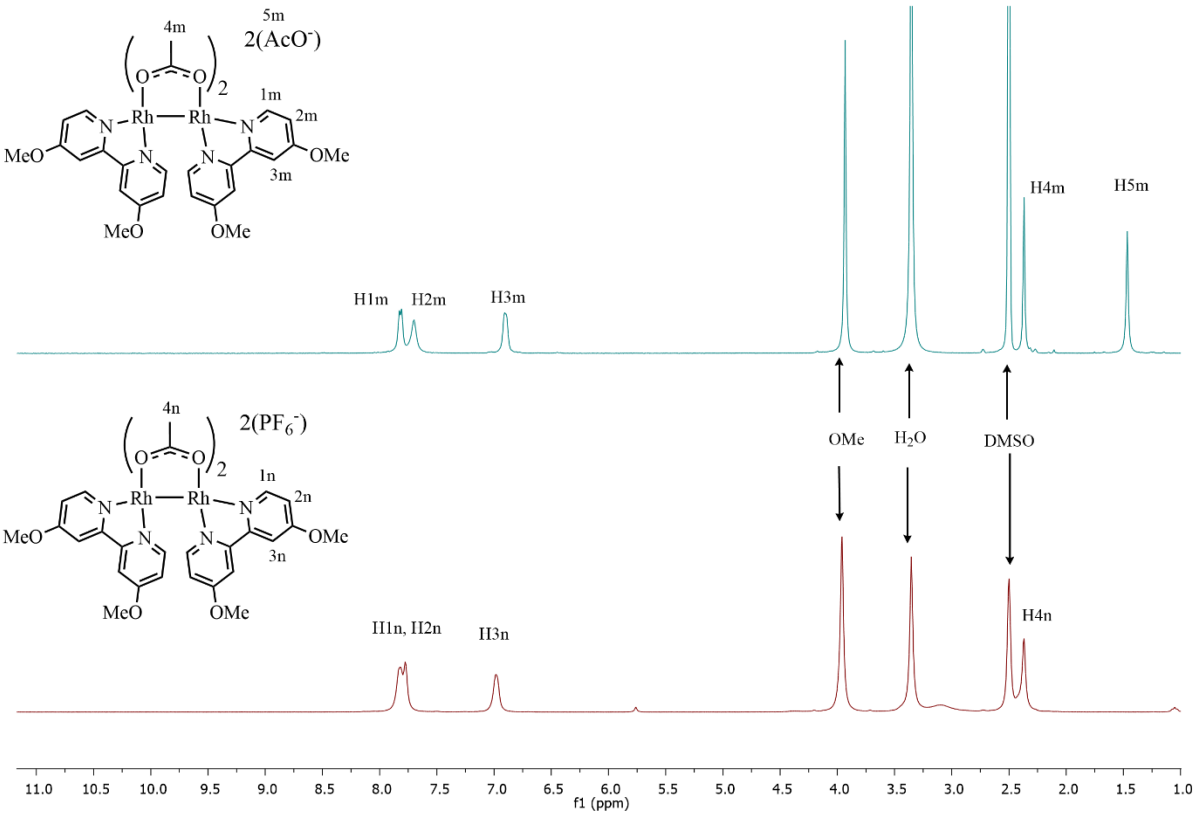

Figure 2.11. Comparison of the ^{1}H-NMR spectra obtained for complexes **3** (upper) and **6** (lower) recorded in DMSO-d_6.

Furthermore, notable downfield shifts in the bipyridyl signals from 7.70 ppm and 6.90 ppm in complex **3** (H_{2m}, H_{3m}) to 7.78 and 6.98 ppm (H_{2n}, H_{3n}) in complex **6** are observed upon counter ion exchange. This observation further supports that significant electronic effects are imposed on the complex upon removal of the counter ion acetate ligand. The combination of these observations confirms that the most prominent axial interaction for the acetate counter ion is observed for complex **3**, as speculated from the ^{1}H-NMR spectral comparison of complexes **1** - **3**.

The $^{13}C\{^{1}H\}$-NMR spectra recorded for complexes **4** - **6** show the expected signals corresponding to the bipyridyl carbon atoms with negligible differences observed in the chemical shifts between acetate and hexafluorophosphate congeners. By way of example, the stacked spectra of complexes **1** and **4** (Figure 2.12) illustrates the characteristic differences observed in the spectra upon anion exchange.

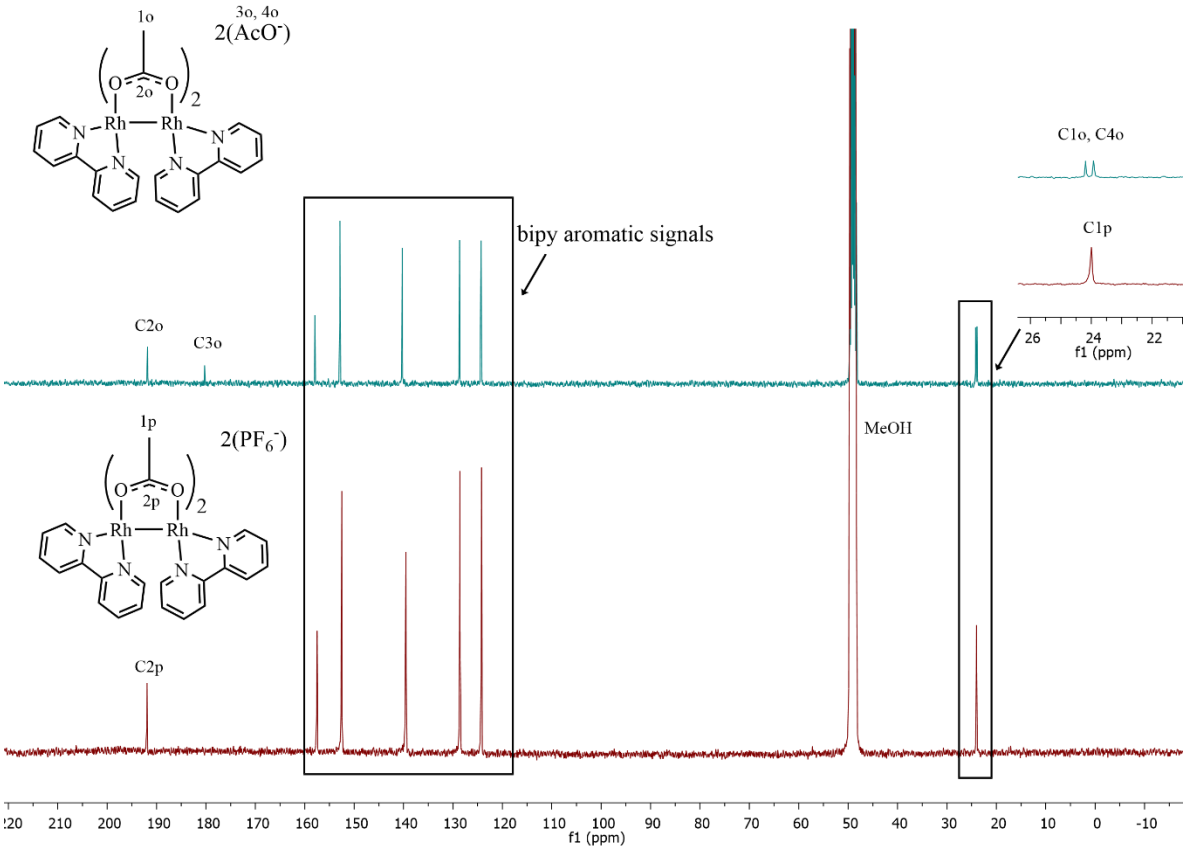

Figure 2.12. Comparison of the $^{13}C\{^{1}H\}$-NMR spectra obtained for complexes **1** (above) and **4** (below) recorded in MeOD.

The $^{13}C\{^{1}H\}$ spectral comparison supports the observations in the ^{1}H-NMR spectra regarding successful counter ion exchange, where the signals corresponding to the carbonyl and acetyl carbon atoms in the 180 and 24 ppm regions are not observed in the spectrum for **4**.

The ^{19}F-NMR spectra for complexes **4 - 6** were recorded as further evidence of counter ion exchange. This can be observed by a doublet signal for the hexafluorophosphate counter ion, expected due to coupling between the NMR active phosphorous and fluorine nuclei. The stacked spectra (Figure 2.13) display the expected doublet signals at -74.32, -74.11 and -70.11 ppm respectively, corresponding to the presence of the PF_6 counter ion. Additionally, the spectrum recorded for complex **5** displays a singlet resonating at -66.2 ppm. This corresponds to the bipyridyl trifluoromethyl substituent, unchanged relative to the signal observed for the precursor complex **2**.

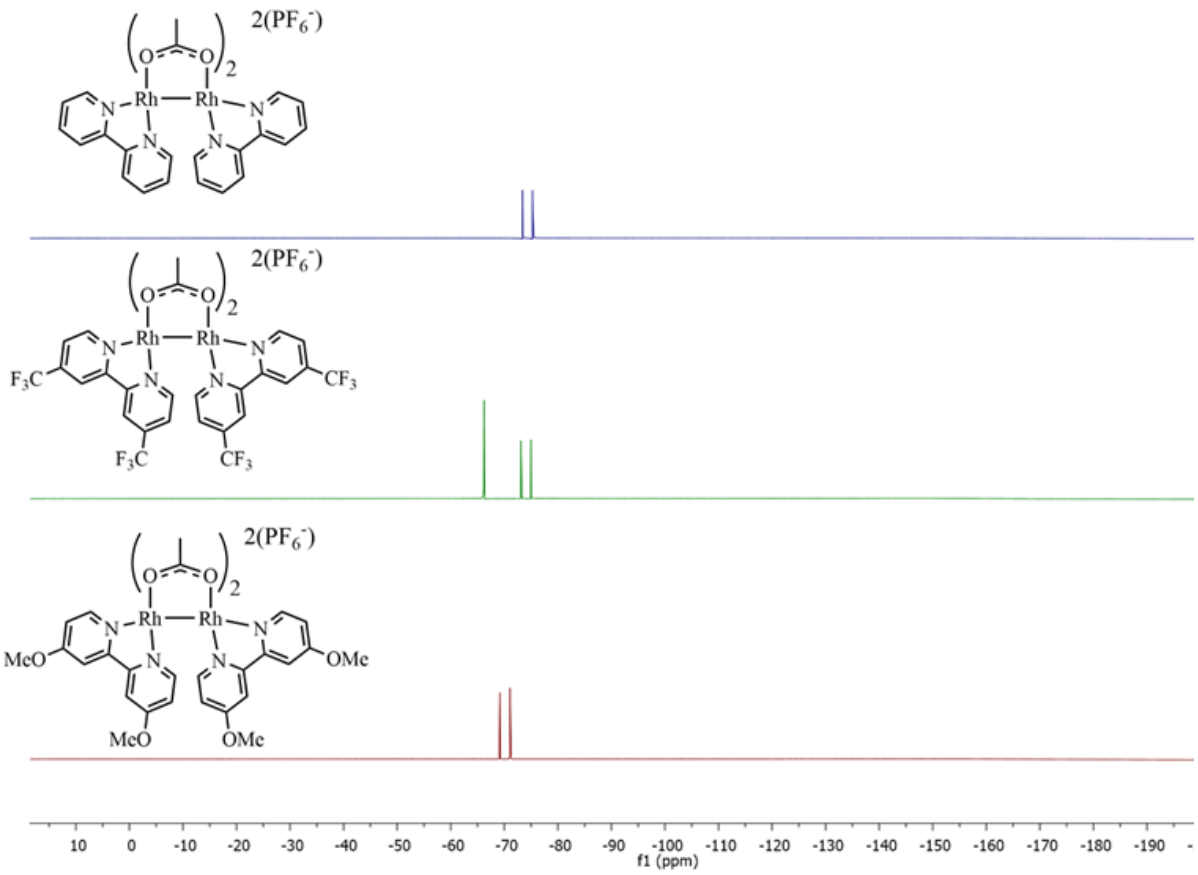

Figure 2.13. Comparison of the ^{19}F-NMR spectra recorded for complexes **4** (top)**, 5** (centre) and **6** (below), displaying characteristic signals corresponding to the fluorine nuclei in the respective complexes.

Similarly, the ^{31}P-NMR spectra obtained for complexes **4 - 6** (Figure 2.14) show a single signal with heptet multiplicity, resonating at -144.2 ppm due to coupling with the NMR active fluorine nuclei. The combination of the ^{19}F and ^{31}P-NMR data confirms that the hexafluorophosphate counter ions are present for each complex.

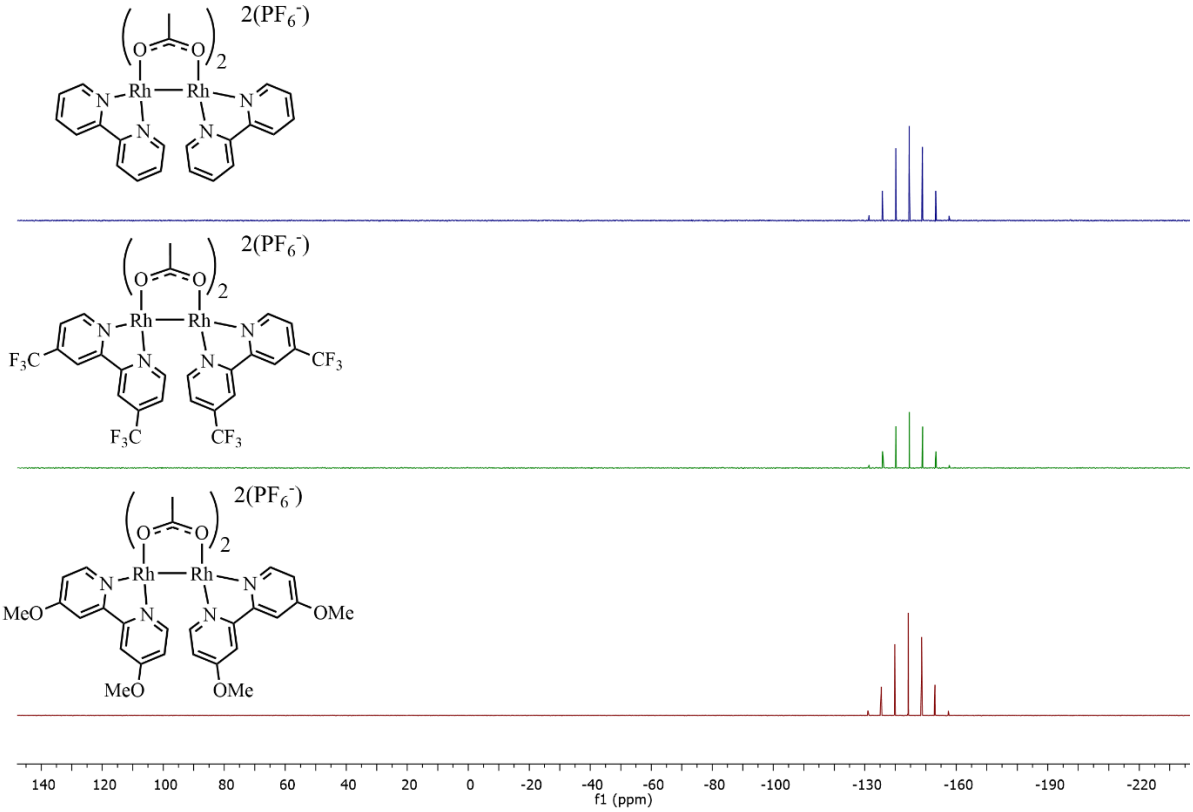

Figure 2.14. Comparison of the ^{31}P-NMR spectra recorded for complexes **4** (top), **5** (centre) and **6** (bottom) displaying the characteristic heptet signal, corresponding to the PF_6 anion.

2.3.2 Infrared (IR) spectroscopy

The infrared spectral data collected for complexes **4 - 6** (Appendix, Figure A4) support the discussed spectral data, with negligible shifts of absorption bands corresponding to the C=N, C=O and C-O functionalities observed in the 1590, 1450 and 1320 cm^{-1} regions for precursor complexes **1 - 3** respectively. The presence of a strong absorption band in the 800 cm^{-1} region is observed in all cases, assigned to the P-F stretching mode supporting the spectral data regarding the presence of the hexafluorophosphate counter ions.

2.3.3 Mass spectrometry

The mass spectrometry data supports the successful formation of the proposed structures, in agreement with the ^{1}H-, ^{13}C{^{1}H}-, ^{19}F- and ^{31}P-NMR and Infrared spectral data. Base peaks are observed at *m/z* = 317.9878, 492.9715 and 378.0121 corresponding to $[M\text{-}2(PF_6)]^{2+}$ molecular ions for complexes **4**, **5** and **6** respectively (Appendix, Figures A5-A7).

2.4 Electrochemical characterisation and axial interaction of hemi-labile acetate counter ions

Cyclic voltammetry was used to determine the redox behaviour of complexes **1 - 3** in relation to any significant influence imparted by the bipyridyl substituent (the electron-withdrawing trifluoromethyl or the electron-donating methoxy) on the reductive potential of the complexes. Furthermore, the effects of the counter ion acetate on the electronic character of the complexes may be elucidated using cyclic voltammetry. The voltammograms recorded (Figure 2.15, *overleaf*) show metal-centred 1-electron reduction potentials for the Rh_2^{4+} to Rh_2^{3+} event at -0.91, -0.85 and -0.95 V, observed for complexes **1**, **2** and **3** respectively (Figure 2.15 (a)).

Additionally, the obtained voltammograms show the expected shift in the reduction potential influenced by the nature of the bipyridyl substituent, with the trifluoromethyl-substituted complex **2** presenting the lowest reduction potential. This is attributed to the stabilizing effect emanating by strong inductive electron withdrawal of the CF_3 group upon reduction. Furthermore, figure 2.15 (a) shows only the metal-centred redox events and the irreversible redox behaviour exhibited by complex **2** may be due to electron transfer to the CF_3-substituted bipyridyl ligand. Additionally, the irreversible redox process observed for complex **2** may occur due to several reasons including (i) reactions between the formed Rh_2^{3+} species and the solvent, (ii) the formation of an unstable species and/or (iii) transfer of the electron from the metal centre to the ligands during the electrochemical process. Considering these factors, and the observed ligand-centred reductions observed for complex **2** only, it is likely that the electron transfer is taking place.

The observed shoulder and broad cathodic current observed in the voltammograms obtained for complexes **1** and **3** respectively are ascribed to anion exchange between the acetate counter ion with the hexafluorophosphate anions present in the supporting electrolyte ($TBAPF_6$). This

was verified by comparison of the voltammograms obtained for complexes **1** and **4** (Figure 2.15 (b)) isolated explicitly with acetate or hexafluorophosphate anions. The voltammogram obtained for complex **4** displays no shoulder, ascribed to the involvement of the acetate counter ion exchange for complex **1**. Additionally, the comparison illustrates the effect of the hemi-labile acetate on the electronic nature of the complex, whereby a corresponding cathodic shift in the reduction potential of approximately 50mV is observed upon hexafluorophosphate exchange. This observation further supports the previously obtained spectral data and the influence of axial interactions on the electronic nature for complexes.

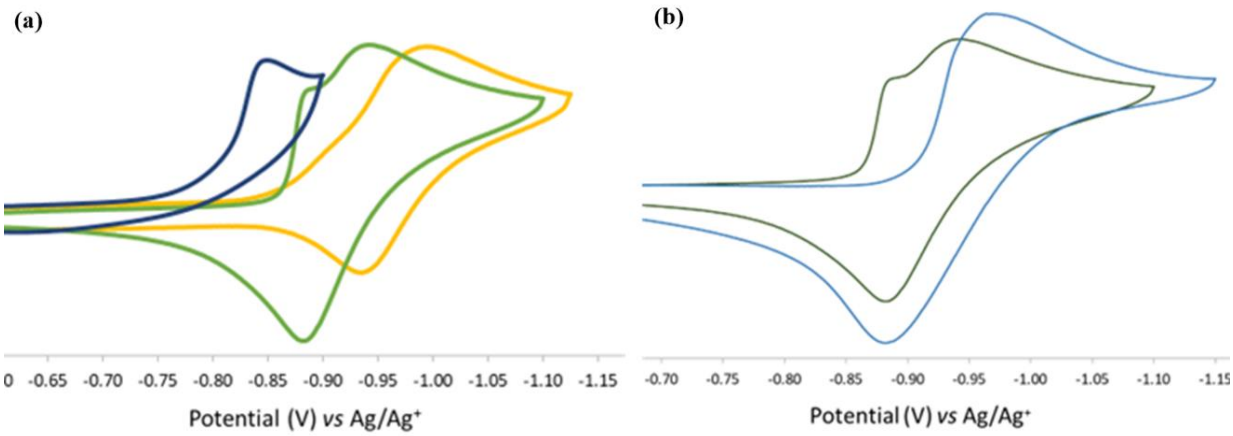

Figure 2.15 (a): Cyclic voltammograms for complexes **1** (green), **2** (blue) and **3** (yellow) illustrating the Rh_2^{4+} to Rh_2^{3} reduction, and **(b)**: Comparison of the cyclic voltammograms obtained for complexes **1** (green) and **4** (blue) illustrating the effects of the hemi-labile acetate on the Rh_2^{4+} to Rh_2^{3+} redox couple. All measurements recorded relative to Ag/Ag^+ recorded in $TBAPF_6$/acetonitrile.

This counter ion interaction was further substantiated by analysis of the signals observed in the ^{31}P NMR spectrum, specifically the signal corresponding to triethyl phosphine oxide (TEPO), when introduced to unsubstituted complexes containing the hemilabile acetate (complex **1**) and hexafluorophosphate (complex **4**) counter ions. The method for the use of TEPO was modified from previously reported literature methods, describing the analysis and evaluation of the Lewis' acidity of complexes by monitoring observed differences in the TEPO phosphorous NMR signal.[21,22]

The rationale behind this experiment is that presence of the acetate ligand binding in an axial mode competes for coordination to the rhodium atoms with the TEPO additive. This

competition thereby hinders the binding of the phosphorous additive to the bimetallic core, resulting in no observable changes in the shift and presentation of the TEPO phosphorous signal. The experiments were carried out by preparing solutions of complexes **1** and **4** with 1 equivalent of TEPO in MeOD at ambient temperature and comparing the spectra obtained to a reference spectrum recorded for TEPO in MeOD. The spectrum obtained for complex **1** + TEPO shows no signal shift or change in splitting observed when compared to TEPO (multiplet, 59.5 ppm), suggesting that no coordination of TEPO to the axial site of complex **1** has occurred (Figure 2.16, *overleaf*).

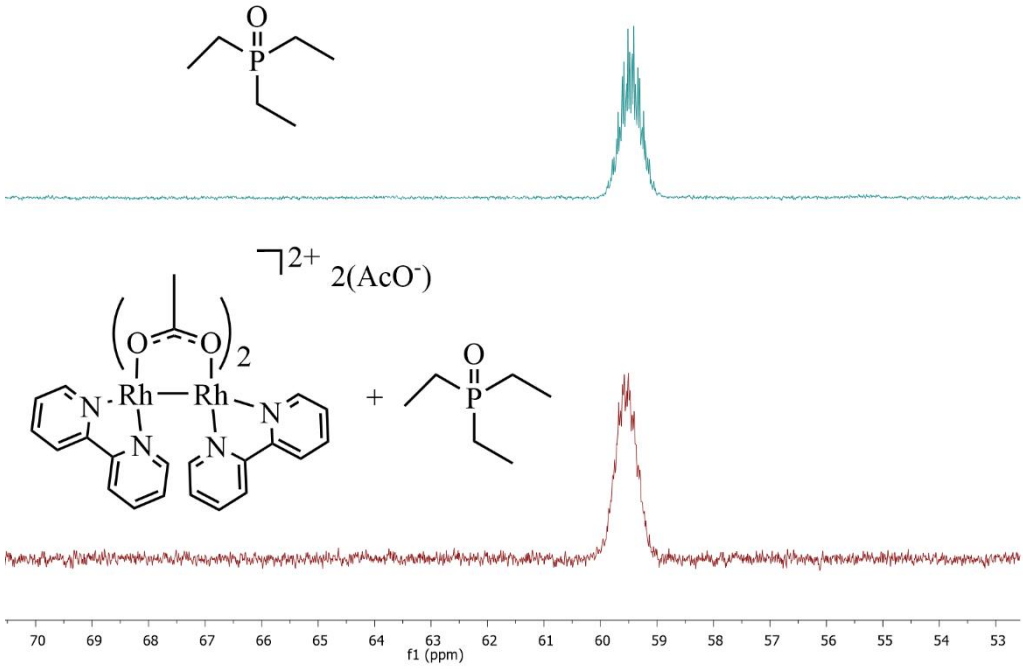

Figure 2.16. ^{31}P-NMR spectra recorded for TEPO (upper) and complex **1** + TEPO (lower) illustrating no changes to the phosphorous signal.

This supports the speculated hemi-lability of the acetate ligand, axially binding to the bimetallic core of the dirhodium complex. Conversely, a singlet signal (59.5 ppm) is observed in the spectrum obtained for complex **4** + TEPO, displaying negligible chemical shift differences observed compared to the analogous TEPO signal recorded in MeOD. However, comparison of the spectra obtained for complexes **1** and **4** with the TEPO additive show distinctive differences in the presentation of the signal (Figure 2.17, *overleaf*). The observed singlet indicates that the environment around the phosphorous atom is likely sterically restricted, reducing the possible conformational arrangements in the ethyl chains of the TEPO molecule,

implying interaction with the metal centre in complex **4**. This occurs unhindered since no acetate counter ion is present for competitive axial binding.

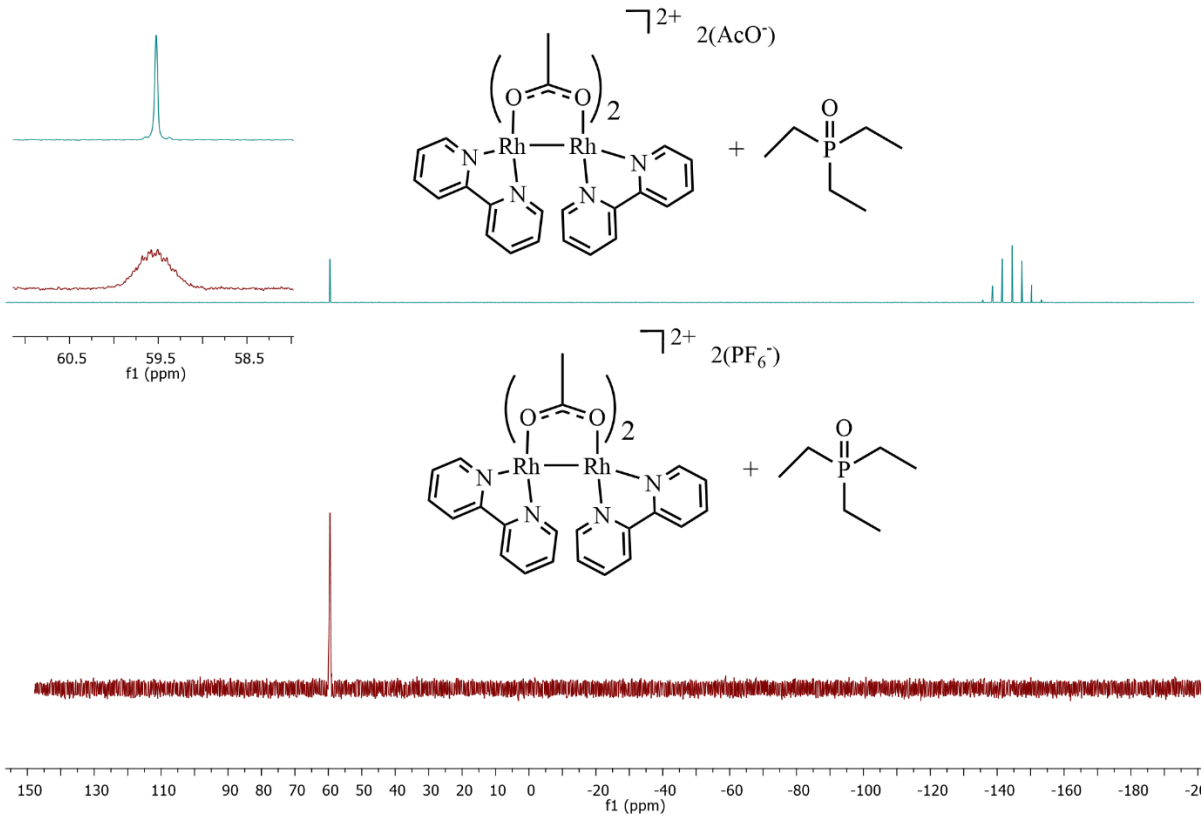

Figure 2.17. ^{31}P-NMR spectra recorded for **1** + TEPO (upper) and **4** + TEPO (lower) illustrating changes to the presentation of the TEPO phosphorous signal (expansion).

Further evidence of the effects of the axial site interaction of the counter ion was determined by measuring differences in the molar conductivity of acetate and hexafluorophosphate congeners of the unsubstituted complexes (**1** and **4**) and trifluoromethyl-substituted complexes (**2** and **5**). Binding of the acetate counter ion causes significant changes in the ionic nature of the complex, and therefore the conductivity of the solution. The results (Table 2.1) show a drastic increase in the recorded molar conductivity of complex **4** compared to complex **1**, providing strong support to the electrochemical and spectral data regarding axial binding of the acetate. Conversely, a less pronounced difference in the molar conductivity is observed for trifluoromethyl-substituted congeners (complexes **2** and **5**), supporting the speculation of weak axial binding of the acetate counter ion. This corroborates the larger differences in the diffusion of the signals observed in the DOSY spectrum obtained for complex **2** relative to complex **1**.

Complex	Counter ion	Substituent	Mols ($x10^{-6}$)	Measured Conductivity (µS)	Molar Conductivity ($S.cm^2/mol$)
1	^{-}OAc	H	5.8	246	42
4	$^{-}PF_6$		4.7	396	84
2	^{-}OAc	CF_3	2.3	161	70
5	$^{-}PF_6$		2.6	179	68

Table 2.1. Conductivity measurement results for complexes **1**, **2**, **4** and **5** in deionised water.

2.5 Summary

In summary, the synthesis and isolation of acetate (**1** - **3**) and hexafluorophosphate (**4** - **6**) congeners of heteroleptic bis-substituted dirhodium(II,II) acetato-bipyridyl complexes was achieved in moderate to excellent yields (68 - 96%) with full spectroscopic and analytical characterisation carried out. Spectral analysis of the synthesised complexes shows distinctive differences in the presentation of a counter ion/axially bound acetate ligand. A trend in the shielding and deshielding of this signal was observed and correlated to the electron withdrawing and electron donating nature of the bipyridyl substituent. The recorded DOSY spectra displayed a difference in the diffusion order of the counter ion acetate proton signal compared to the bridging acetate counter ion signal, inferring the hemilabile nature of the counter ion. Furthermore, the degree of the differences in the DOSY spectra support observations in the proton spectra collected for compounds **1** and **2**, with a more shielded counter ion acetate signal resulting in a large difference in diffusion order. Upon anion exchange, the comparison of analogous proton signals between congeners showed the absence of the counter ion acetate signals in the ^{1}H- and $^{13}C\{^{1}H\}$ spectra, supporting the successful substitution of the hexafluorophosphate for the acetate counter ion. Additionally, small chemical shift differences in the signals corresponding to the inner coordination sphere between the congeners was observed. The largest observable difference was noted for methoxy-substituted complexes **3** and **6**, supporting the speculation of the largest axial interaction observed upon comparison of the spectral data recorded for complexes **1** - **3**. Electrochemical characterisation was carried out by cyclic voltammetry, showing the expected

trend in the reduction potential of complexes **1** - **3**. The electron-withdrawing trifluoromethyl-substituted complex presented the lowest reduction potential in the series. Comparison of the voltammograms obtained for complexes **1** and **4** show that a cathodic shift is observed upon counter ion exchange, illustrating the effects of exchanging the axially labile acetate for the hexafluorophosphate counter ion. The axial interactions were then substantiated through an interaction study with triethylphosphine oxide and conductivity measurements, supporting the spectral data regarding effects of the hemi-labile acetate counter ions on the nature of the complexes. This hemi-labile phenomenon was found to be influenced by the nature of the bipyridyl substituent and is rationalised by the changes in the electronic environment of the metal centre by either electron-donating or electron-withdrawing groups. Unfortunately, solid state characterisation by means of single crystal x-ray diffraction was unable to be carried out due to the unsuitable quality of crystals grown upon further analysis.

2.6 Experimental details and instrumentation

2.6.1 Materials

All chemicals/reagents were purchased from Merck and used without purification unless stated otherwise. Rhodium(III) trichloride trihydrate was purchased from Heraeus SA. Solvents of analytical grade were used as received or freshly distilled, where necessary, and were stored over molecular sieves. All reactions were carried out under Ar or N_2 inert conditions, with apparatus prepared using standard Schlenk line techniques.

2.6.2 Equipment and instrumentation

Nuclear magnetic resonance (NMR) spectra were recorded on either a Bruker X600 (^{1}H at 599.95 MHz and ^{13}C{^{1}H} at 151.0 MHz), a Bruker X400 (^{1}H: 400.22 MHz, ^{13}C{^{1}H}: 100.65 MHz, ^{19}F: 377 MHz, ^{31}P{^{1}H}: 162 MHz) or a Varian Mercury 300 (^{1}H: 300.08 MHz, ^{13}C{^{1}H}:75.46 MHz) spectrometer. Chemical shifts for ^{1}H and ^{13}C{^{1}H} NMR were recorded using tetramethylsilane (TMS) as the internal standard. Coupling constants are reported in Hz and chemical shifts are reported in ppm relative to residual solvent signals. Infrared (IR) absorptions were recorded on a Perkin-Elmer Spectrum 100 FT-IR spectrometer using an Attenuated Total Reflectance Infrared spectroscopy (ATR-IR) attachment. High resolution mass spectrometry (HRMS) was carried out using Electron Impact (EI) on a JEOL GCmatell instrument with data recorded in positive mode. Melting Points were determined using a Büchi

B-540 melting point apparatus, reported without correction. Purity of the complexes was determined using an Agilent HPLC 1260 equipped with an Agilent 1260 UV/Vis diode array detector (DAD) and an Agilent Pursuit 5 C18 column (5 μM, 150 mm × 4.6 mm). The compounds were eluted using a mixture of solvent A (0.1% TFA in H_2O) and solvent B (MeOH) at a flow rate of 0.5 mL/min. The gradient elution conditions were as follows: 90% solvent A between 0 and 2 min, 90 - 10% solvent A from 2 to 8 min and 10% solvent A from 8 to 20 min. Conductivity measurements were carried out on a Jenway benchtop 4510 conductivity meter with a glass probe ($\kappa = 0.96$).

2.6.3 Instrumentation for electrochemical analysis

Cyclic voltametric measurements were carried out at ambient temperature under an inert Argon atmosphere using a three-electrode system on a BASi® Epsilon Eclipse potentiostat/galvanostat electrochemical workstation. All experiments were carried out in anhydrous acetonitrile, containing a solution of 0.10 M tetra-n-butylammonium hexafluorophosphate ($TBAPF_6$) as the supporting electrolyte. The C-3 cell stand equipped with a glassy carbon working electrode, $Ag/AgNO_3$ (0.01M $TBAPF_6$/acetonitrile) reference electrode and a Pt wire auxiliary electrode was used to carry out electrochemical measurements.

*2.6.4 General method for the synthesis of dirhodium(II,II) acetato-bipyridyl diacetate complexes (**1** - **3**)*

The synthesis of dirhodium(II,II) complexes with acetate counter ions was achieved through adaptation of the procedure reported for obtaining the known complex **1**.[11] A reaction vessel equipped with a stirrer bar was charged with dirhodium(II,II) tetraacetate (1 eq.) followed by anhydrous acetonitrile (10 mL). The mixture was stirred for up to 20 min until full dissolution was achieved. The required bis-4,4'-disubstituted 2,2'-bipyridyl ligand was added to the stirring solution (2 eq.) followed by an additional aliquot of anhydrous acetonitrile (5 mL). The reaction vessel was heated to reflux under N_2 atmosphere and stirred for an additional 24 hours, after which observed colour change from purple to red-brown was noted. The mixture was cooled to ambient temperature, before cooling in an ice bath for 1 h, resulting in the formation of a red precipitate, which was separated from the filtrate via suction filtration, washed with diethyl ether (3 x 10 mL) and dried in vacuo resulting in the isolation of a red-orange powder.

*2.6.4.1 Dirhodium(II,II) bis-κ-(2,2'-bipyridyl)-μ-bis-(di-acetato) diacetate (**1**)* [11]

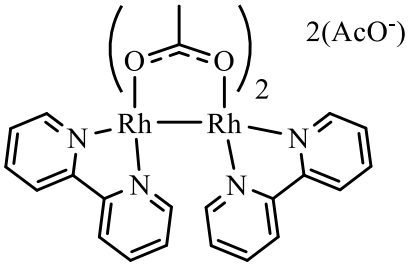

Dirhodium(II,II) tetraacetate (0.100 g, 0.226 mmol) was reacted with 2,2'-bipyridyl (0.099 g, 0.46 mmol) in anhydrous acetonitrile (15 mL) under reflux and N_2 atmosphere and for 24 hours. **Yield**: 0.170 g (0.220 mmol, 96%). **Melting Point:** Decomposition without melting, onset at 287 ˚C. **^{1}H NMR (300 MHz, CD_3OD)**: δ (ppm) = 8.34 (4H, d, ^3J = 5.6 Hz, C-**H**$_{ar}$), 7.90 (8H, m, C-**H**$_{ar}$), 7.40 (4H, t, ^3J = 6.5 Hz, C-**H**$_{ar}$), 2.56 (6H, s, μ-$O_2CC\mathbf{H}_3$), 1.85 (6H, s, $^-O_2CC\mathbf{H}_3$). **^{13}C NMR (101 MHz, CD_3OD)**: δ (ppm) = 191.8 (μ-$O_2\mathbf{C}CH_3$), 180.3 ($^-O_2\mathbf{C}CH_3$), 157.8 (**C**$_{ar}$), 152.9 (**C**$_{ar}$), 140.3 (**C**$_{ar}$), 128.4 (**C**$_{ar}$), 124.3 (**C**$_{ar}$), 24.2 (μ-$O_2C\mathbf{C}H_3$), 23.9 ($^-O_2C\mathbf{C}H_3$). **IR (ATR)**: (ν max/cm^{-1}) 1560 (C=N), 1438 (C=O), 1384 (C=C). **Purity** (HPLC): 97.06%, (t_R = 2.75 min).

*2.6.4.2 Dirhodium(II,II) bis-κ-(4,4'-(trifluoromethyl)-2,2'-bipyridyl)-μ-bis-(di-acetato) diacetate (**2**)*

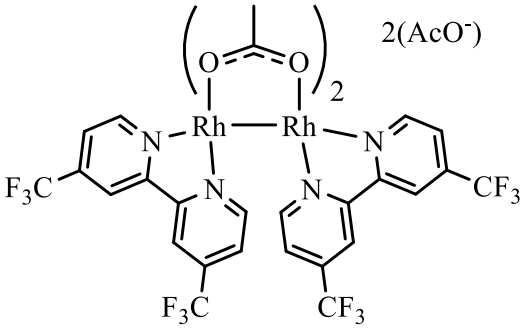

Dirhodium(II,II) tetraacetate (98 mg, 0.23 mmol) was reacted with 4,4'-bis(trifluoromethyl)-2,2'-bipyridyl (0.13 g, 0.46 mmol) in anhydrous acetonitrile (15 mL) under reflux and N_2 atmosphere for 24 hours. **Yield**: 197 mg (0.192 mmol, 85%). **Melting Point:** Decomposition without melting, onset at 278 ˚C. **^{1}H NMR (300 MHz, CD_3OD)**: δ (ppm) = 8.70 (4H, d, ^3J = 5.9 Hz, C-**H**$_{ar}$), 8.68 (4H, s, C-**H**$_{ar}$), 7.78 (4H, d, ^3J = 5.8 Hz, C-**H**$_{ar}$), 2.60 (6H, s, μ-$O_2CC\mathbf{H}_3$), 1.78 (6H, s, $^-O_2CC\mathbf{H}_3$). **^{13}C{^{1}H} NMR (101 MHz, CD_3OD)**: δ (ppm) = 191.2 (s, μ-$O_2\mathbf{C}CH_3$), 179.1 (s, $^-O_2\mathbf{C}CH_3$), 157.4 (s, **C**$_{ar}$), 153.1 (s, **C**$_{ar}$), 140.0 (d, $^2J_{FC}$ = 38 Hz, **C**$_{ar}$), 123.5 (**C**$_{ar}$),

121.7 (d, $^{1}J_{FC}$ = 274 Hz, **C**$_{ar}$), 119.6 (s, **C**$_{ar}$), 22.6 (s, μ-O_2C**C**H_3), 22.5 (s, $^{-}O_2C$**C**H_3). **^{19}F NMR (377 MHz, D_2O)**: δ (ppm) = -66.2. **HRMS (ESI, m/z)**: 492.9715 (100%, [M+DMSO-2OAc]$^{2+}$), calculated 493.0250. **IR (ATR)**: (ν_{max}/cm^{-1}) 1562 (C=N), 1418 (C=O), 1182 (C-F) **Purity** (HPLC): 95.78%, (t_R = 2.35 min).

*2.6.4.3 Dirhodium(II,II) bis-κ-(4,4'-(dimethoxy)-2,2'-bipyridyl)-μ-bis-(di-acetato) diacetate (**3**)*

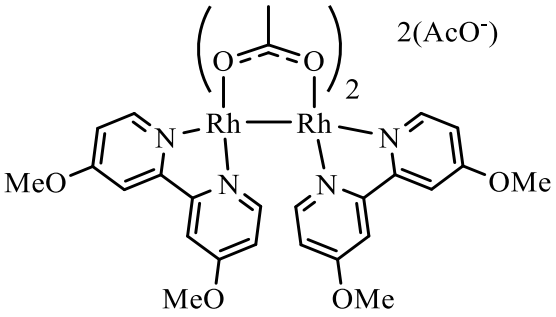

Dirhodium(II,II) tetraacetate (96 mg, 0.21 mmol) was reacted with 4,4'-dimethoxy-2,2'-bipyridyl (99 mg, 0.43 mmol) in anhydrous acetonitrile (15 mL) under reflux and N_2 atmosphere for 24 hours. **Yield**: 0.15 g (0.17 mmol, 79%). **Melting Point**: Decomposition without melting, onset at 396 ˚C. **^{1}H NMR (300 MHz, CD_3OD)**: δ (ppm) = 8.03 (4H, d, ^{3}J = 6.6 Hz, C-**H**$_{ar}$), 7.62 (4H, d, ^{4}J = 2.4 Hz, C-**H**$_{ar}$), 7.02 (4H, dd, ^{3}J = 6.6 Hz, ^{4}J = 2.4 Hz, C-**H**$_{ar}$), 4.01 (12H, s, OC**H**$_3$), 2.49 (6H, s, μ-O_2CC**H**$_3$), 1.86 (6H, s, $^{-}O_2$CC**H**$_3$). **^{13}C{^{1}H} NMR (101 MHz, CD_3OD)**: δ (ppm) = 191.5 (s, μ-O_2**C**CH_3), 180.2 (s, $^{-}O_2$**C**CH_3), 169.1 (s, **C**$_{ar}$), 159.1 (s, **C**$_{ar}$), 153.5 (s, **C**$_{ar}$), 114.2 (s, **C**$_{ar}$), 111.4 (s, **C**$_{ar}$), 57.6 (s, O**C**H_3), 24.2 (s, μ-O_2C**C**H_3), 23.8 (s, $^{-}O_2$**C**CH_3). **HRMS (ESI, m/z)**: 378.0120 (100%, [M-2OAc]$^{2+}$), calculated 378.0100. **IR (ATR)**: (ν_{max}/cm^{-1}) 1554 (C=N), 1422 (C=O), 1282 (H_3C-O). **Purity** (HPLC): 96.76%, (t_R = 2.45 min).

*2.6.5 General method for the synthesis of dirhodium(II,II) acetato-bipyridyl bis-hexafluorophosphate complexes (**4** - **6**)*

The method utilised for the anion exchange reactions was adapted and modified from a reported procedure.[20] A bis-axial adduct of complex **4** was previously reported[11] however, the alternate synthetic method outlined herein describes the isolation of complexes without axial adducts. To this end, a reaction vessel equipped with a stirrer bar was charged with either complex **1**, **2** or **3** (1 eq.) and NH_4PF_6 (2.1 equivalents). To the reaction vessel was added 10 mL of an

EtOH/DCM solution in a 1:1 ratio. The reaction mixture was stirred under N_2 atmosphere and ambient temperature (16 - 20 ˚C) for 2-6 hours, after which a colour changes from red to yellow (**1**), orange (**2**) or green (**3**) was observed. The reaction mixture was concentrated under reduced pressure to ca. 5 mL resulting in the formation of a precipitate. The mixture was filtered under reduced pressure, washed with diethyl ether (2 x 10 mL) and dried in vacuo resulting in the isolation of either a yellow (**4**), orange (**5**) or green (**6**) solid.

*2.6.5.1 Dirhodium(II,II) bis-κ-(2,2'-bipyridyl)-μ-bis-(di-acetato) bis(hexafluorophosphate) (**4**)*

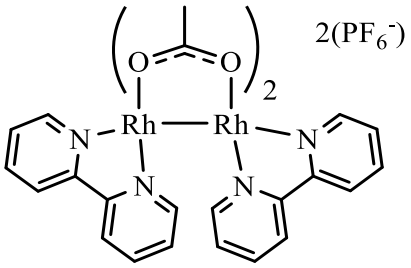

Complex **1** (50 mg, 0.066 mmol) was reacted with ammonium hexafluorophosphate (23 mg, 0.14 mmol) in an EtOH/DCM solution in a ratio of 1:1 under N_2 atmosphere for 2 hours. **Yield**: 49 mg (0.053 mmol, 80%). **Melting Point**: Decomposition without melting, onset at 189 ˚C. **^{1}H NMR (300 MHz, CD_3OD)**: δ (ppm) = 8.31 (4H, d, ^3J = 5.5 Hz, C-**H**$_{ar}$), 7.87 (8H, m, C-**H**$_{ar}$), 7.34 (4H, t, ^3J = 6.6 Hz C-**H**$_{ar}$), 2.48 (6H, s, μ-$O_2CC\mathbf{H}_3$). **^{13}C{^{1}H} NMR (101 MHz, CD_3OD)**: δ (ppm) = 191.9 (s, μ-$O_2C\mathbf{C}H_3$), 157.5 (s, **C**$_{ar}$), 152.5 (s, **C**$_{ar}$), 139.5 (s, **C**$_{ar}$), 128.6 (s, **C**$_{ar}$), 124.2 (s, **C**$_{ar}$), 24.0 (s, μ-$O_2C\mathbf{C}H_3$). **^{19}F NMR** (**377 MHz, CD_3OD**): δ (ppm) = -74.32 (d, $^1J_{FP}$ = 707.4 Hz, P**F**$_6$) **^{31}P{^{1}H} NMR** (**162 MHz, CD_3OD**): δ (ppm) = -144.51 (hept, $^1J_{PF}$ = 708.2 Hz, **P**F$_6$). **HRMS (ESI, m/z)**: 317.9878 (100%, $[M\text{-}2PF_6]^{2+}$), calculated 318.1000. **IR (ATR)**: (ν_{max}/cm^{-1}) 1552 (C=N), 1432 (C=O), 824 (P-F). **Purity** (HPLC): 96%, (t_R = 2.12 min).

*2.6.5.2 Dirhodium(II,II) bis-κ-(4,4'-(trifluoromethyl)-2,2'-bipyridyl)-μ-bis-(diacetato) bis-(hexafluorophosphate) (**5**)*

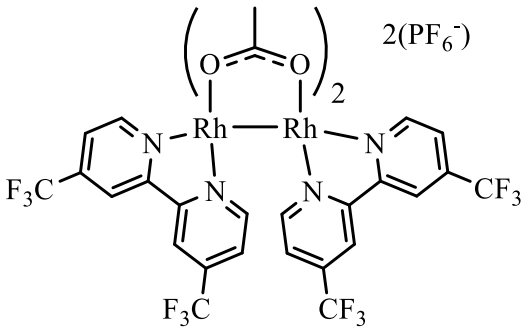

Complex **2** (47 mg, 0.046 mmol) was reacted with ammonium hexafluorophosphate (16 mg, 0.096 mmol) in an EtOH/DCM solution in a ratio of 1:1 under N_2 atmosphere for 5 hours. **Yield**: 41 mg (0.034 mmol, 74%). **Melting Point:** Decomposition without melting, onset at 256 ˚C. **^{1}H NMR (300 MHz, CD$_3$OD)**: δ (ppm) = 8.71 (4H, d, ^{3}J = 5.6 Hz, C-**H**$_{ar}$), 8.67 (4H, s, C-**H**$_{ar}$), 7.78 (4H, d, ^{3}J = 5.1 Hz, C-**H**$_{ar}$), 2.55 (6H, s, μ-O$_2$CC**H**$_3$). **^{13}C{^{1}H} NMR (101 MHz, CD$_3$OD)**: δ (ppm) = 191.8 (s, μ-O$_2$C**C**H$_3$), 156.5 (s, **C**$_{ar}$), 153.2 (s, **C**$_{ar}$), 139.6 (d, $^{2}J_{CF}$ = 37 Hz, **C**$_{ar}$), 123.9 (s, **C**$_{ar}$), 121.9 (q, $^{1}J_{CF}$ = 274 Hz, **C**F$_3$), 119.9 (s, **C**$_{ar}$), 22.7 (μ-O$_2$C**C**H$_3$). **^{19}F NMR** (**377 MHz, CD$_3$OD**): δ (ppm) = -66.22 (s, CF$_3$) -74.05 (d, $^{1}J_{FP}$ = 707 Hz, P**F**$_6$) **^{31}P{^{1}H} NMR** (**162 MHz, CD$_3$OD**): δ (ppm) = -144.58 (hept, $^{1}J_{PF}$ = 707 Hz, **P**F$_6$). **HRMS (ESI, m/z)**: 453.9631 (100%, [M-2PF$_6$]$^{2+}$), calculated 453.9600. **IR (ATR)**: (ν_{max}/cm^{-1}) 1557 (C=N), 1447 (C=O), 1128 (C-F), 828 (P-F). **Purity** (HPLC): 99%, (t_R = 2.41 min).

*2.6.5.3 Dirhodium(II,II) bis-κ-(4,4'-(dimethoxy)-2,2'-bipyridyl)-μ-bis-(di-acetato) bis-(hexafluorophosphate) (**6**)*

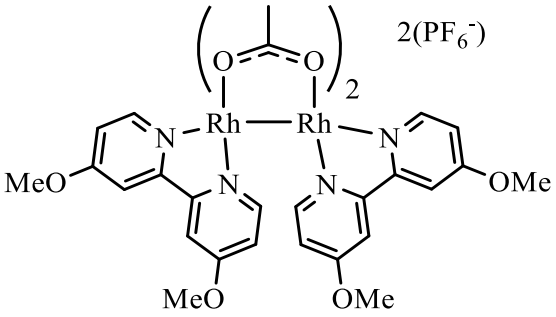

Complex **3** (61 mg, 0.069 mmol) was reacted with ammonium hexafluorophosphate (23 mg, 0.14 mmol) in an EtOH/DCM solution in a ratio of 1:1 under N_2 atmosphere for 6 hours. **Yield**: 49 mg (0.047 mmol, 68%). **Melting Point:** Decomposition without melting, onset at 391 ˚C. **^{1}H NMR (600 MHz, DMSO-d$_6$)**: δ (ppm) = 7.83 (4H, br s, C-**H**$_{ar}$), 7.78 (4H, s, C-**H**$_{ar}$), 6.98

(4H, br s, C-**H**$_{ar}$), 3.96 (12H, s, OC**H**$_3$), 2.37 (6H, s, μ-O_2CC**H**$_3$). **^{13}C{^{1}H} NMR (151 MHz, DMSO-d$_6$)**: δ (ppm) = 189.6 (s, μ-O_2C**C**H$_3$), 166.5 (s, **C**$_{ar}$), 156.7 (s, **C**$_{ar}$), 151.2 (s, **C**$_{ar}$), 113.1 (s, **C**$_{ar}$), 109.9 (s, **C**$_{ar}$), 56.9 (s, O**C**H$_3$), 24.0 (s, μ-O_2C**C**H$_3$), **^{19}F NMR (377 MHz, DMSO-d$_6$)**: δ (ppm) = -70.13 (d, $^1J_{FP}$ = 707 Hz, P**F**$_6$). **^{31}P{^{1}H} NMR** (**162 MHz, DMSO-d$_6$**): δ (ppm) = -144.58 (hept, $^1J_{PF}$ = 707 Hz, **P**F$_6$). **HRMS (ESI, m/z)**: 378.0121 (100%, [M-2PF$_6$]$^{2+}$), calculated 378.0100. **IR (ATR)**: (ν max/cm^{-1}) 1556 (C=N), 1442 (C=O), 1254 (C-F), 832 (P-F). **Purity** (HPLC): 97%, (t_R = 2.17 min).

2.7 References

1. G. A. Rempel, P. Legzdins, H. Smith and G. Wilkinson, *Inorg. Synth.*, 1972, **13**, 90-91.

2. E. B. Boyar and S. D. Robinson, *Coord. Chem. Rev.,* 1983, **50**, 109-208.

3. R. Hrdina, E*ur. J. Inorg. Chem.,* 2021, 501-528.

4. S. de Doncker, A. Casimiro, I. A. Kotze, S. Ngubane and G. S. Smith, *Inorg. Chem.,* 2020, **59**, 12928-12940.

5. Y. Lou, T. P. Remarchuk and E. J. Corey, *J. Am. Chem. Soc.,* 2005, **127**, 14223-14230.

6. T. Yoshimura, K. Umakoshi and Y. Sasaki, *Inorg. Chem.,* 2003, **42**, 7106-7115.

7. M. Cwikowska, F. P. Pruchnik, R. Starosta, H. Chojnacki, A. Wilczok and S. Ulaszewski, *Inorganica Chim. Acta.,* 2010, **363**, 2401-2408.

8. S. E. Witt, T. A. White, Z. Li, K. R. Dunbar and C. Turro, *Chem. Commun.*, 2016, **52**, 12175-12178.

9. J. D. Aguirre, A. M. Angeles-Boza, A. Chouai, J. P. Pellois, C. Turro and K. R. Dunbar, *J. Am. Chem. Soc.,* 2009, **131**, 11353-11360.

10. K. Sorasaenee, P. K. Fu, A. M. Angeles-Boza, K. R. Dunbar and C. Turro, *Inorg. Chem.,* 2003, **42**, 1267-1271.

11. C. A. Crawford, J. H. Matonic, J. C. Huffman, K. Folting, K. R. Dunbar and G. Christou, *Inorg. Chem.,* 1997**, 36**, 2361-2371.

12. H. D. Manamperi, C. E. Moore and C. Turro, *Chem. Commun.*, 2021, **57**, 1635-1638.

13. C. T. Eagle, D. G. Farrar, G. N. Holder, W. T. Pennington and R. D. Bailey, *J. Organomet. Chem.,* 2000, **596**, 90-94.

14. J. L. Bear, T. P. Zhu, T. Malinski, A. M. Dennis and K. M. Kadish, *Inorg. Chem.,* 1984, **23**, 674-678.

15. C. A. Crawford, J. H. Matonic, W. E. Streib, J. C. Huffman, K. R. Dunbar and G. Christou, *Inorg. Chem.,* 1993, **32**, 3125-3133.

16. F. A Cotton, C. Murillo and R. Walton, *Multiple bonds between metal atoms*, Springer, Boston, MA, 2005, 3rd edition, Chapter 12, pp. 465-589.

17. M. E. Prater, L. E. Pence, R. Clérac, G. M. Finniss, C. Campana, P. Auban-Senzier, D. Jérome, E. Canadell and K. R. Dunbar, *J. Am. Chem. Soc.,* 1999, **121**, 8005-8016.

18. G. A. Morris, 2009. Diffusion-Ordered Spectroscopy. Encyclopedia of Magnetic Resonance. DOI: 10.1002/9780470034590.emrstm0119.pub2.

19. I. I. M. Schuster, *J. Magn. Reson.,* 1969, **17** (1), 104-111.

20. A. Welsh, L. Rylands, V. B. Arion, S. Prince and G. S. Smith, *Dalton Trans.,* 2020, **49**, 1143-1156.

21. U. Mayer, V. Gutmann and W. Gerger, *Monatsh. Chem.,* 1975, **106**, 1235-1257.

22. M. A. Beckett, G. C. Strickland, J. R. Holland and K. S. Varma, *Polymer.*, 1996, **37**, 4629-4631.

Chapter 3

Catalytic evaluation of dirhodium(II,II) acetato-bipyridyl complexes as precursors for hydroformylation reactions

This chapter forms part of a publication entitled "*Heteroleptic dirhodium(II,II) acetato-bipyridyl complexes: evaluation as catalyst precursors for hydroformylation reactions",* cited as: **S. de Doncker**, G. S. Smith and S. Ngubane, *Appl. Catal. A Gen.*, 2023, **667**, 119440.

3.1 Introduction

Hydroformylation is a useful reaction utilised to form value-added chemicals such as aldehydes and alcohols for use as precursors in a variety of chemical applications (Scheme 3.1).[1] Commonly referred to as the 'Oxo process', this homogeneous transition-metal catalysed reaction is carried out under a synthesis gas ($CO:H_2$) atmosphere. Discovered by Otto Roelen in 1938, hydroformylation was observed to occur during investigations into the production of oxygenated products resulting from the Fischer-Tropsch reaction.[2]

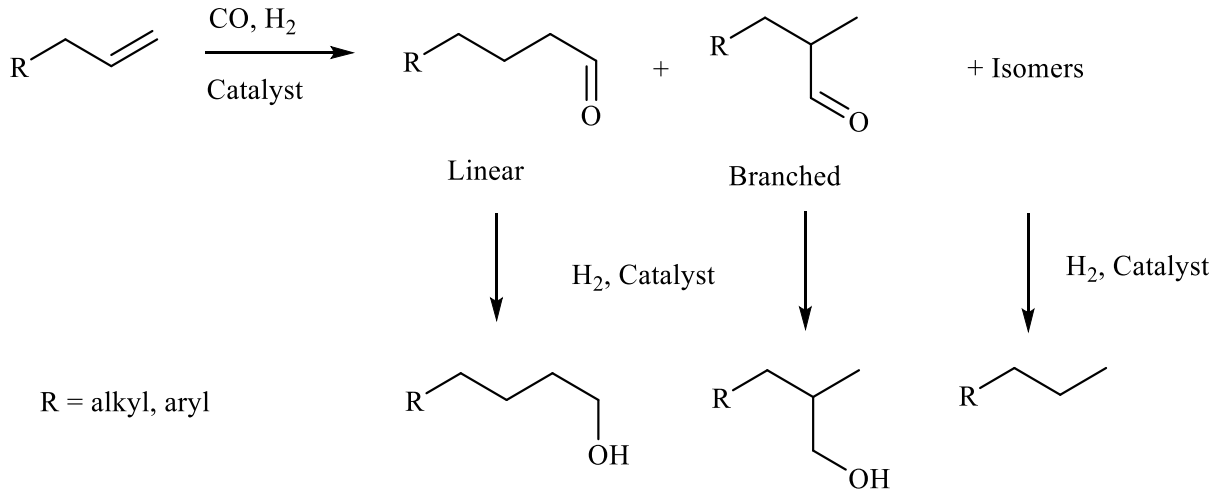

Scheme 3.1. Depiction of the possible products formed in the hydroformylation reaction.

Since the inception of the hydroformylation reaction, research efforts to determine crucial factors influencing product distribution to maximize economic benefit have been undertaken.[3] Further research into enhancing the efficiency of catalytic processes is ongoing, driven by the need to improve selectivity, reactivity and recyclability owing to the rising cost of precious platinum group metals such as rhodium, used as catalysts.[4-6] Toward improving and optimising the hydroformylation reaction, rhodium-containing catalysts are employed, providing enhanced reactivity under milder reaction conditions when compared to other metal-based catalysts, such as cobalt for example.[7,8] Incorporating ligands containing phosphorous donor atoms have led to improvements in reaction conditions for a variety of metal centres. The phosphine-modified rhodium catalysts investigated by Wilkinson and co-workers are well known, showing enhanced product selectivity compared to rhodium carbonyl complexes, in addition to minimising the isomerisation of the substrate.[9,10]

Catalyst precursors exploiting multinuclearity with discrete metal centres incorporated into the molecule have been employed in attempts to enhance the activity or recyclability of catalytic reactions.[11-14] In terms of the exploiting multinuclearity of metal complexes, the use of bimetallic metal-metal bonded complexes, such as the dirhodium(II,II) class, has become more prominent as catalyst precursors in reactions such as hydroformylation in both homogeneous and heterogeneous reactions.[15-17] The wide scope in the application of these complexes is attributed to the plethora of electronic characteristics and coordination geometries accessible when suitable ligands are incorporated. Furthermore, the presence of a metal-metal bonded core and vacant axial sites, a characteristic not exhibited by the more classical mono nuclear rhodium-based complexes, makes this class of bimetallic complex very attractive for applications in catalytic reactions such as allylic oxidation, diazo coupling, carbenoid NH insertion, dehydrogenative silylation and hydroformylation (Figure 3.1, *overleaf*).[18]

For example, Claver and coworkers explored the effects of degrees of substitution of a dirhodium(II,II) acetato complex containing ortho-metallated phosphine ligands on the hydroformylation activity.[15] Generally they reported catalytic activity showed quantitative conversion of styrene, albeit at high catalyst loading (1:400 complex:styrene) with greater formation of branched aldehyde when increasing the number of phosphine ligands bound to the complex. As an extension of the scope of these complexes, Nowotny and coworkers reported similar phosphine substituted complexes immobilised to amorphous silica supports.[16]

Comparable selectivity was obtained for the untethered complexes, favouring the branched aldehyde (up to 15:1) for the free complexes, but the immobilized analogue **3** showed a reduction in activity and selectivity after 4 cycles due to leeching. The complex **4** showed a less dramatic decrease in activity, with similar reduction in the selectivity of product. In our previous work, the effects of complexes bearing bridging ligands containing *N,N* donor atoms showed exceptional homogeneous catalytic ability, with axial interaction of the 2-fluoro substituted complex found to affect the regioselectivity substantially. In other work, the axial occupancy of ligands, solvent and other molecules bearing suitable donor atoms to these vacant sites have shown a profound mechanistic effect in respective applications.[19]

There are significant energy requirements associated with conventional catalyst recovery in homogeneous reactions, by distillation for example, particularly in cases such as the hydroformylation of higher molecular weight olefins. Coupled with the ever-increasing cost of rhodium precursors, this necessitates improving catalyst recovery while maintaining the activity and selectivity of the reaction, culminating in research efforts routinely carried out regarding recyclability.[7,20,21]

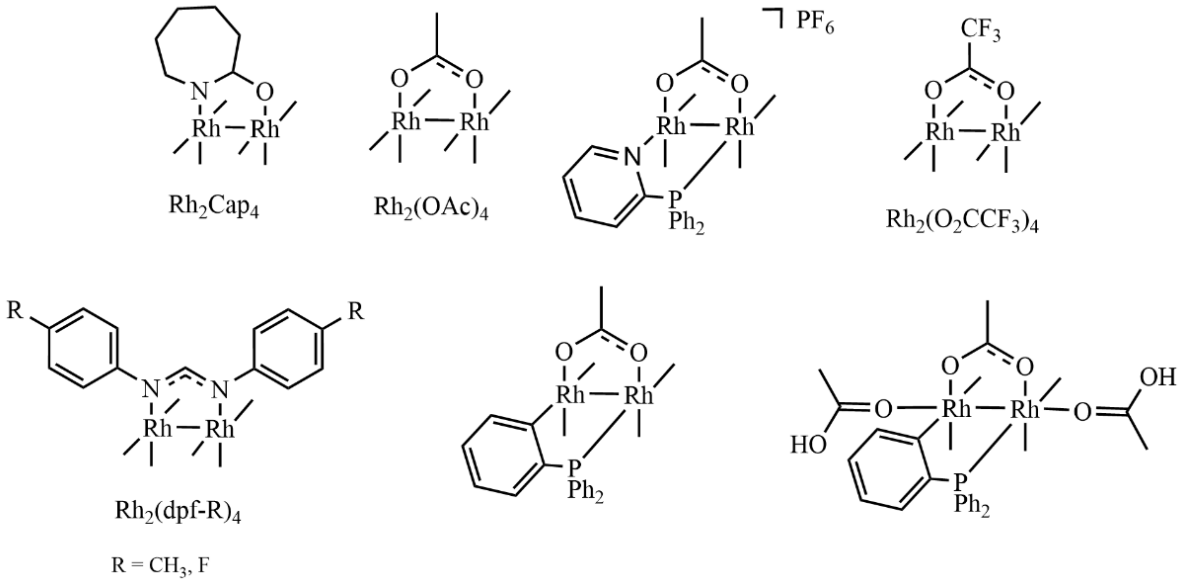

Figure 3.1. Examples of dirhodium(II,II) complexes employed as catalyst precursors for catalytic reactions such as allylic oxidation, diazo coupling, carbenoid NH insertion, dehydrogenative silylation and hydroformylation.[15,17,22-25] Additional bridging ligands omitted for clarity.

By way of example, a few of these strategies include biphasic systems based on aqueous or fluorous-based partitions with the chosen organic solvent,[26-28] supercritical CO_2-based media,[29] and the combination of water soluble moieties and macromolecular systems such as dendrimers.[12,30,31] Additionally, the introduction of suitable ligands to exploit key physicochemical properties such as solubility, and catalyst immobilisation onto insoluble supports are reported in an attempt to recover precursors efficiently.[32] A requirement for efficient biphasic catalytic systems is that catalyst degradation must be minimised in both phases, however, some reports on rhodium-based catalysts show such deactivation over a number of cycles, seen from the reduction in activity over the recyclability experiments.[33,34] Additionally, due to interfacial exposure of the catalyst during the reaction in biphasic media, leaching of the catalyst precursor and/or active catalysts species may contribute to the observed reduction in activity throughout recyclability studies.[35,36]

This chapter will discuss the applicability of the synthesised heteroleptic dirhodium(II,II) acetato-bipyridyl chelate complexes (Figure 3.2) as efficient catalyst precursors for homogeneous hydroformylation. The influence of counterion hemi-lability, electronic and structural features affecting the selectivity and activity is described. Furthermore, modification of the physicochemical properties through a combination of bipyridyl ligand substituent and counterion toward the efficient mono-phasic recyclability of the catalyst recyclability is also described.

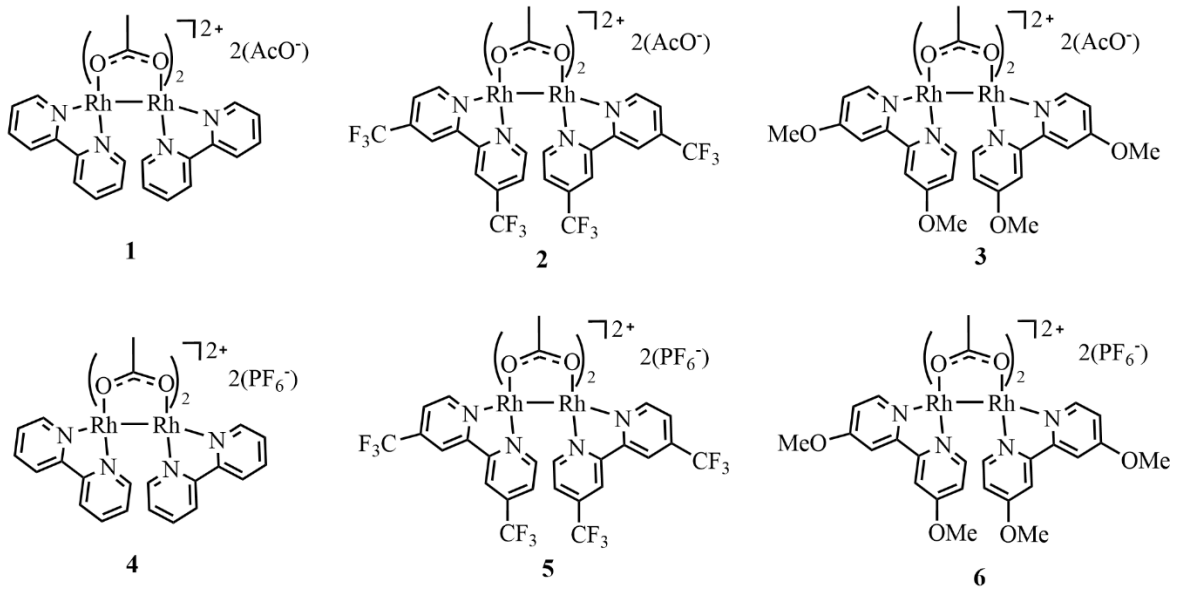

Figure 3.2. Representation of the molecular structures of the complexes described in this chapter.

3.2 Optimisation of the conditions for the hydroformylation of 1-octene

The optimisation of the reaction conditions for the synthesised heteroleptic complexes in the hydroformylation of 1-octene was initiated by reactions carried out under 50 bar syngas pressure at 95 °C for 4 hours.[17] The unsubstituted complex **1** was utilised as a model catalyst precursor, benchmarked against the fully substituted $Rh_2(OAc)_4$ complex, previously reported under these conditions.[17]

*3.2.1 Comparison of the catalytic performance of $Rh_2(OAc)_4$ to complex **1** under identical reaction conditions*

As described for the homoleptic precursor $Rh_2(OAc)_4$ complex, optimisation of the reaction conditions is necessary to determine the sensitivity of the catalytic reaction on variables such as pressure, time and temperature.[16] For comparison, the conditions previously reported were employed for the evaluation of complex **1** relative to the parent complex $Rh_2(OAc)_4$.[17] Initially, temperatures of both 85 °C and 95°C while maintaining 50 bar pressure and 4-hour reaction time were adopted for these experiments. This allows for a direct comparison of the catalytic differences between the fully substituted $Rh_2(OAc)_4$ complex against the unsubstituted complex **1** (Table 3.1).

Table 3.1. Comparison of the Hydroformylation data obtained from temperature variation experiments between $Rh_2(OAc)_4$ and complex **1**.

Entry	Complex	Temperature (˚C)	Conversion (%)	Total aldehydes (%)	Total *iso*-octenes (%)	TOF (hr^{-1})	*n:iso*
1[17]	$Rh_2(OAc)_4$	95	99	98	2	613	0.78
2[17]	$Rh_2(OAc)_4$	85	94	85	15	506	2.45
3	**1**	95	99	99	1	621	0.71
4	**1**	85	99	99	1	618	0.78

Hydroformylation of 1-octene in toluene (5 mL), 1:1 $CO:H_2$, 50 bar pressure, reaction time of 4 hours and catalyst loading of 2.87×10^{-3} mmol. GC conversions were obtained using an internal standard of *n*-decane. Total aldehydes are composed of linear and branched aldehydes in a mixture with percentage sum of 100. TOF = (mmol aldehydes per mmol Rh_2)/ time. Reactions carried out in triplicate with an average error value of 2.18%

The data obtained shows that the combination of bridging acetate ligand with the bipyridyl chelate ligand results in a higher conversion (99%) at the lower temperature of 85 °C (Table 3.1, entry 4), compared to the fully substituted acetate complex where only 94% conversion of substrate is observed (Table 3.1, entry 2). Comparably, this suggests that the energy requirement for the reaction carried out with catalyst precursor **1** is reduced, likely due to the presence of the bipyridyl chelate and consequentially the corresponding electronic effects thereof. Additionally, comparison of the data obtained for chemoselectivity shows a substantial decrease in aldehyde production, from 98 to 85%, with the corresponding decrease in temperature for $Rh_2(OAc)_4$. Complex **1** shows comparable aldehyde production at both 85 and 95 °C with 99% conversion and aldehyde produced in both respective cases (Table 3.1, entries 3 and 4). The small differences in TOF values for the same reaction time is due to small changes in the averaging of the experimental data and the associated error for reactions carried out in triplicate.

A decrease in the temperature resulted in a corresponding decline in the conversion of 1-octene observed, coupled to an increase in the *n:iso* ratio for the fully substituted complex (Table 3.1, entry 2). This suggests that a significantly higher energy requirement exists for the conversion of branched olefins to aldehydes in the presence of $Rh_2(OAc)_4$ compared to the bipyridyl chelate complex **1**. Due to the significant effects of temperature variation compared to the previously optimised reaction conditions, further optimisation of the temperature was carried out with complex **1** as a model for the heteroleptic dirhodium(II,II) bipyridyl chelate complexes.

3.2.2 The effect of temperature on catalyst performance

The temperature optimisation for the hydroformylation reaction was carried out by varying the reaction temperature from 55 to 95 °C with complex **1** as a catalyst precursor. This is necessary to determine the temperature at which the conversion limit and aldehyde production would be observed (Table 3.2, *overleaf*).

Although the conversion of 1-octene and production of aldehydes are observed to be unaffected at 95 and 85 °C with catalyst precursor **1**, a significant decrease in conversion is noted once the reaction temperature is reduced to 75 °C (Table 3.2, entry 3). The decrease in the conversion between 85 and 75 °C is accompanied by a notable decrease in the observed formation of

aldehyde from 99 to 91% respectively (Table 3.2 entries 2 and 3). Additionally, comparable conversion of substrate between 75 and 65 °C is observed, with a corresponding drop in chemoselectivity for aldehyde (Table 3.2, entries 3 and 4). This suggests that there is a substantial decline in catalyst performance for the hydroformylation reaction from this temperature range. Furthermore, the limit for the conversion of substrate has not been reached and moderate conversion is maintained across the temperature range, with the onset of significant decline in conversion appearing at only 55 °C (Table 3.2, entry 5) at 85%.

A further decrease in the production of aldehyde products is observed for reactions carried out at 65 and 55 °C. This confirms that the energy requirement of the production aldehyde products by complex **1** is not being met for optimal aldehyde production. Therefore, the optimised temperature for the hydroformylation of 1-octene with complex **1** as a catalyst precursor is observed at 85 °C. Furthermore, the observed change in the regioselectivity upon temperature variation, coupled with the rise in detected isomerised octenes can be attributed to the additional energy requirements for the hydroformylation of internal olefins for this catalyst precursor. The combined data suggests that for appreciable conversion of substrate and for the production of aldehyde products to be maintained, the reaction temperature for subsequent time and pressure optimisation experiments is 85 °C.

Table 3.2. Comparison of the Hydroformylation data obtained from temperature variation experiments carried out with model complex **1**.

Entry	Temperature (˚C)	Conversion (%)	Total aldehydes (%)	Total *iso*-octenes (%)	Linear aldehydes (%)	Branched aldehydes (%)	TOF (hr^{-1})
1	95	99	99	1	41	59	621
2	85	99	99	1	44	56	618
3	75	94	91	9	52	48	536
4	65	94	79	21	55	45	495
5	55	85	72	28	57	43	451

Hydroformylation of 1-octene in toluene (5 mL), 1:1 $CO:H_2$, 50 bar pressure, reaction time of 4 hours and catalyst loading of 2.87 x 10^{-3} mmol. GC conversions were obtained using an internal standard of *n*-decane. Total aldehydes are composed of linear and branched aldehydes in a mixture with percentage sum of 100. TOF = (mmol aldehydes per mmol Rh_2)/ time. Reactions carried out in triplicate with an average error value of 3.78%.

3.2.3 The effect of syngas pressure on catalyst performance

The hydroformylation reaction requires an atmosphere containing a mixture of CO and H_2 (syngas), and changes in the pressure of syngas is an important factor for maximising the product yield of the reaction. The production of aldehyde strongly depends on the pressure of CO for the addition of the formyl entity to the olefin substrate.[37,38] To determine the critical pressure limit of the hydroformylation reaction at the previously optimised temperature of 85 °C, the pressure was lowered systematically from 50 to 20 bar, until a significant drop in aldehyde production was observed (Table 3.3, *overleaf*).

The data obtained from the variation of the gas pressure shows that in this instance, the relationship between regioselectivity and gas pressure is negligible. This is attributed to the comparable production of linear and branched aldehyde observed for reactions carried out between 50 and 20 bar syngas pressure (Table 3.3, entries 1 to 4). This indicates that regioselective control is not significantly influenced by changes in pressure and is likely due to steric influence around the catalytically active site. A slight decline in the formation of aldehyde product from 99 to 97% is observed for reactions carried out at 50 and 40 bar respectively (Table 3.3, entries 1 and 2) and further reduction in the pressure to 30 bar results in a significant reduction of aldehyde products formed (87 %) (Table 3.3, entry 3).

Additionally, further reduction of the gas pressure to 20 bar results in a significant decrease in aldehyde products and a decrease in conversion of substrate (Table 3.3, entry 4). This is speculated to be due to a dependence on the gas pressure for the active catalyst required to consume substrate for either isomerisation or hydroformylation. At lower pressure the chemoselectivity toward aldehydes decreases, with the related increase in isomerised octene from 13 to 39% when the pressure is altered from 30 to 20 bar respectively (Table 3.3, entries 3 and 4).

The isomerisation of the substrate may occur through several pathways. The catalyst mediated isomerisation reactions may proceed *via* coordination of the olefin through a dissociative mechanism to form a metal-alkyl-hydrido complex followed by rearrangement through the intramolecular migration of a hydride, and elimination of the isomerised product (Scheme 3.2 - pathway A, *vida infra*).

Table 3.3. Comparison of the Hydroformylation data obtained from pressure variation experiments carried out with model complex **1** at the optimised temperature of 85 °C.

Entry	Pressure (bar)	Conversion (%)	Total aldehydes (%)	Total *iso*-octenes (%)	Linear aldehydes (%)	Branched aldehydes (%)
1	50	99	99	1	44	56
2	40	99	97	3	44	56
3	30	94	87	13	43	57
4	20	84	61	39	42	58
5	40 (N_2)	0	-	nd	-	-

Hydroformylation of 1-octene in toluene (5 mL),1:1 CO:H_2 syngas atmosphere, reaction temperature of 85 °C, reaction time of 4 hours and catalyst loading of 2.87 x 10^{-3} mmol. GC conversions were obtained using an internal standard of *n*-decane. Total aldehydes are composed of linear and branched aldehydes in a mixture with percentage sum of 100. TOF = (mmol aldehydes per mmol Rh)/ time. Reactions carried out in triplicate with an average error value of 3.21%. nd- not detected.

Alternatively, the coordination of the olefin to an activated metal-hydride species may then undergo rearrangement and elimination of the products of the isomerisation of 1-octene. To corroborate that the isomerisation is promoted by some activated catalyst species in the presence of syngas, the reaction was carried out under 40 bar N_2 atmosphere. The rationale behind this is that should the isomerisation reaction proceed *via* the rearrangement pathway without an active metal-hydrido species, some isomerisation would occur in the absence of syngas. Both cycles for the isomerisation mechanism are proposed in Scheme 3.2 (*overleaf*).

The results obtained show no significant *iso*-octene formation under these conditions (Table 3.3, entry 5). This confirms that the isomerization of substrate requires the active catalyst, likely a metal hydride active species formed *in-situ*, opposed to substrate coordination to the metal followed by dissociation of an olefinic C-H bond and the corresponding hydride shift step proposed. The optimised pressure was determined where maximum conversion and aldehyde production was observed, in this case at 40 bar pressure with a syngas (CO:H_2) ratio of 1:1.

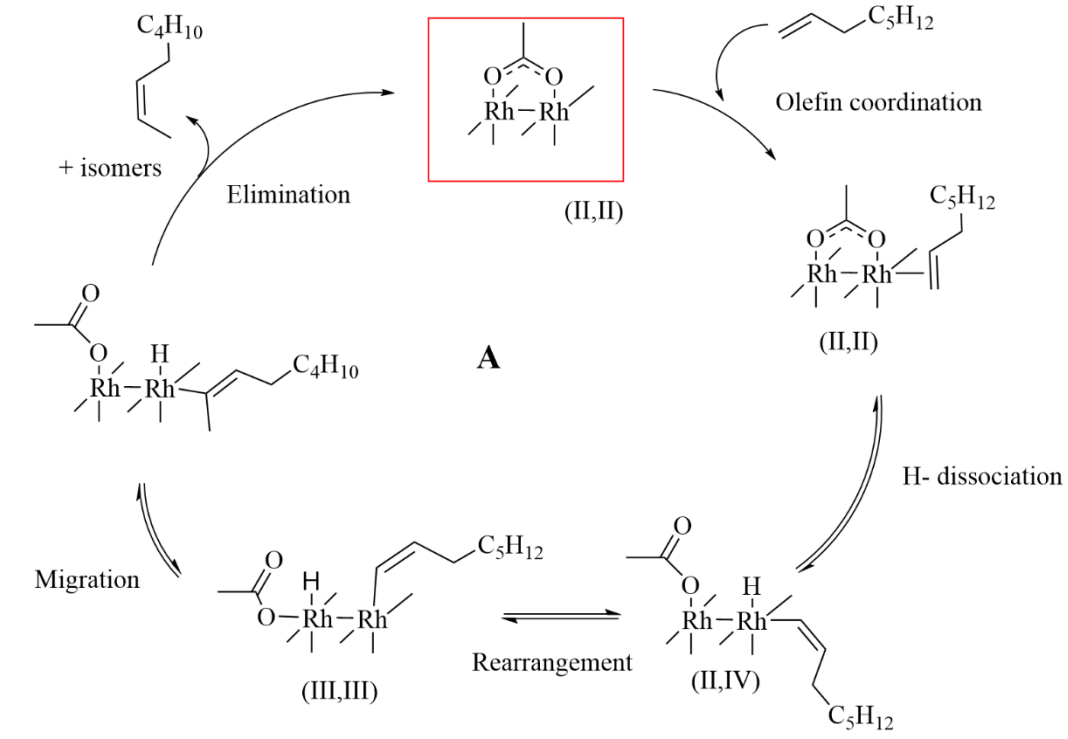

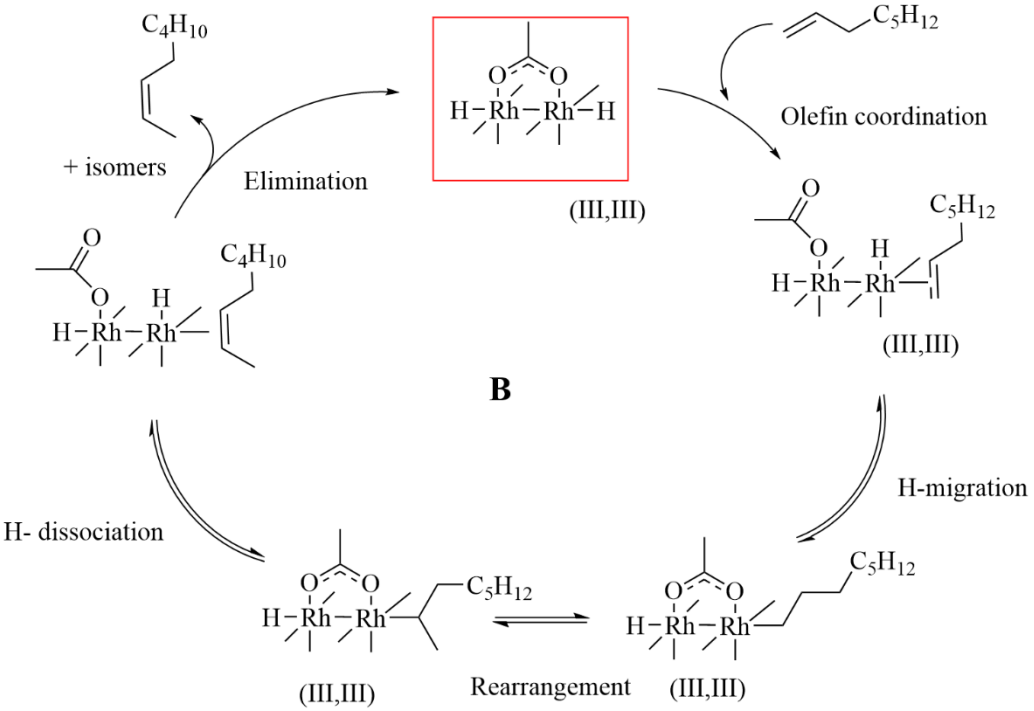

Scheme 3.2. Depiction of the proposed dissociative pathway (**A**) and the active metal hydride pathway (**B**) for the isomerisation of the alkene substrate.

3.2.4 The effect of time variation on catalyst performance

As previously reported in the time-dependent study carried out for the homoleptic acetate complex, the effects on the consumption of substrate, chemo- and regioselectivities were elucidated by changing the reaction time.[17] The effect on the hydroformylation of 1-octene with model complex **1** at the previously optimised temperature of 85 °C and 40 bar syngas pressure at different time intervals was carried out. The results (Table 3.4) show that from 1 - 4 hours reaction time, the conversion increases steadily from 44% to 99% indicating a lower average rate of substrate consumption compared to the $Rh_2(OAc)_4$ catalyst precursor.[17] The data obtained for the chemoselectivity suggests that the isomerisation and hydroformylation reactions proceed at similar rates in the first hour, with total aldehyde production and *iso*-octene formation at 48 and 52 % respectively (Table 3.4, entry 4). Analysis of the changes in the regioselectivity data across this time-period shows preferential formation of the linear aldehyde in the first hour with an observed *n:iso* ratio of 2.65. This is attributed to the lower energy requirements for the hydroformylation of terminal olefins compared to internal olefins.

Table 3.4. Comparison of the Hydroformylation data obtained from time variation experiments carried out with model complex **1** at the optimised temperature of 85 °C and pressure of 40 bar.

Entry	Time (h)	Conversion (%)	Total aldehydes (%)	Total *iso*-octenes (%)	Linear aldehydes (%)	Branched aldehydes (%)	*n:iso*
1	4	99	96	4	44	56	0.71
2	3	97	90	10	45	55	0.81
3	2	78	79	21	62	38	1.65
4	1	44	48	52	73	27	2.65

Hydroformylation of 1-octene in toluene (5 mL), reaction temperature of 85 °C, 40 bar gas (1:1 $CO:H_2$) pressure and catalyst loading of 2.87 x 10^{-3} mmol. GC conversions were obtained using an internal standard of *n*-decane. Total aldehydes are composed of linear and branched aldehydes in a mixture with percentage sum of 100. Reactions carried out in triplicate with an average error value of 3.21%.

The higher energy requirement for the hydroformylation of internal olefins is supported by the amount of terminal and internal octenes detected, at 56 and 52% respectively. Additionally, under these conditions both the hydroformylation and isomerisation of the substrate proceeds at similar rates. This is substantiated by the observed aldehyde and isomerised products detected in comparable amounts of 48 and 52% respectively. The increase in conversion

between reactions carried out for 1- and 2-hours is observed, from 44 to 78% with a comparable increase in the total aldehydes produced from 48 to 79% (Table 3.4, entry 3). A substantial decrease in the amount of *iso*-octenes detected for the reaction carried out in 2 hours, from 52 to 21%, and a corresponding reduction in the *n:iso* ratio from 2.65 to 1.65 is observed (Table 3.4, entries 3 and 4). The combined data shows that a large proportion of the isomerised alkenes are converted by the hydroformylation reaction in the 2 - 4-hour period. Additionally, the data indicates that the bulk of the linear aldehyde product is formed within the first 2 hours. Furthermore, near-quantitative consumption of the substrate is observed for the reaction run for 3 hours (Table 3.4, entry 2). The associated increase in the amount of aldehyde products detected at this time (90%) and the aldehyde formation of 96% observed after 4 hours (Table 3.4, entry 1) suggests that the majority of the hydroformylation has taken place after 3 hours. Additionally, the comparable *n:iso* ratio observed between reactions run for 3- and 4-hours shows that at this point, the consumption of terminal and internal octenes are consumed by the hydroformylation reaction. A graphical representation of the conversion, chemo- and regioselectivity data at each time interval is shown in Figure 3.2.

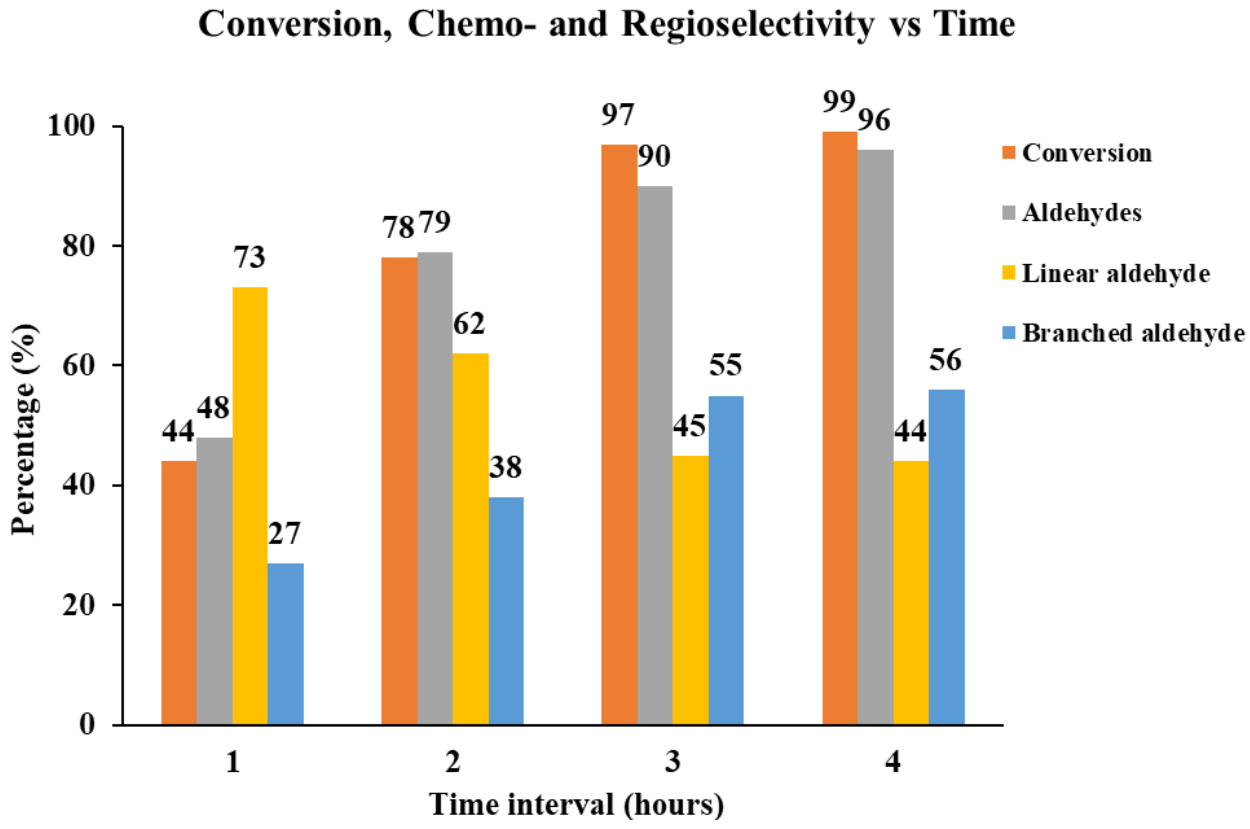

Figure 3.2. Representation of the conversion, chemo- and regioselectivity during time variation experiments with model catalyst precursor **1** for the hydroformylation of 1-octene.

Although changes in the conversion, chemo- and regioselectivity are observed over different reaction times, the maximum conversion of substrate and chemoselectivity for aldehyde is observed for the reaction carried out for 4 hours. Therefore, the optimal reaction time for further hydroformylation experiments is 4 hours.

3.2.5 Ligand additive (co-ligand) and mercury poisoning experiments: effects on the hydroformylation of 1-octene

Ligands bearing donor atoms from group 15 such as nitrogen and phosphorous are regularly employed as co-ligands or additives in some hydroformylation reactions.[39] These exert influence by binding to the metal centre and enhancing the stability of the complex, in turn affecting the conversion ability, chemo-, regioselectivity and activity of catalytic systems.[39] Often, the effect of pre-forming a catalyst precursor incorporating similar ligands over proceeding with reactions in combination with co-ligands is less advantageous. Reactions carried out in this way may require separate reaction optimisation and purification steps, depending on the additive, and may present additional waste generated compared to prior synthesis of the catalyst precursor.

To determine any differences in the reaction outcome for preformed heteroleptic dirhodium(II,II) catalyst precursors, co-ligand experiments were carried out with results presented in Table 3.5 (*overleaf*). This was achieved by loading $Rh_2(OAc)_4$ into reactors with 2, 4 or 10 equivalents of 2,2'-bipyridyl ligand under the optimised reaction conditions of 85°C, 40 bar and 4 hours (Table 3.5, entries 1 - 3). The results obtained show that the addition of 2 equivalents of ancillary ligand to a reaction vessel charged with the $Rh_2(OAc)_4$ complex presents a negative effect on the chemoselectivity for aldehyde compared to pre-formed complex **1**. This can be deduced by comparison of the production of aldehyde whereby a decrease in selectivity from 96 to 72% (Table 3.5, entries 1 and 4) is observed.

Additionally, an improvement in the regioselectivity for reactions carried out in the presence of bipyridyl co-ligand is observed, with 55% nonanal produced compared to the 44% obtained for the reaction carried out with complex **1**. This shows that *in-situ* binding of the bipyridyl ligand to the $Rh_2(OAc)_4$ has a steric influence on the catalytically active site, favouring the production of linear products at the expense of efficient hydroformylation of the 1-octene substrate.

Table 3.5. Comparison of the hydroformylation data obtained from co-ligand experiments carried out with $Rh_2(OAc)_4$ and 2,2'-bipyridyl compared to the data obtained from model complex **1** under optimised conditions.

Entry	Complex	Conversion (%)	Total aldehydes (%)	Total *iso*-octenes (%)	Linear aldehydes (%)	Branched aldehydes (%)	TOF (hr^{-1})	*n:iso*
1	$Rh_2(OAc)_4$[a]	97	72	28	55	45	449	1.21
2	$Rh_2(OAc)_4$[b]	47	55	45	71	29	345	2.44
3	$Rh_2(OAc)_4$[c]	35	53	47	70	30	328	2.50
4	**1**	99	97	3	44	56	609	0.77
5	**1** + Hg	97	97	3	44	56	602	0.78

Hydroformylation of 1-octene in toluene (5 mL), 1:1 $CO:H_2$, 40 bar syngas (1:1 $CO:H_2$) pressure, reaction time of 4 hours and catalyst loading of 2.87 x 10^{-3} mmol. GC conversions were obtained using an internal standard of *n*-decane. Total aldehydes are composed of linear and branched aldehydes in a mixture with percentage sum of 100. TOF = (mmol aldehydes per mmol Rh_2)/ time. Reactions carried out in triplicate with an average error value of 2.29%. [a] 2 equivalents of 2,2'-bipyridyl. [b] 4 equivalents of 2,2'-bipyridyl. [c] 10 equivalents of 2,2'-bipyridyl.

An increase in the equivalents of bipyridyl ligand (4 eq.) resulted in further reduction in the conversion to 47% and a reduction in chemoselectivity to 55% aldehyde (Table 3.5, entry 2). Furthermore, a substantial increase in the regioselectivity toward linear aldehydes (71%) is observed under these conditions. This is speculated to be due to competitive binding of the excess bipyridyl ligand and incoming substrate, resulting in further steric influence and therefore the lower observed activity.

To substantiate this speculation, an experiment was carried out with 10 equivalents of the bipyridyl ligand to further saturate the catalytic system. The results obtained with 10 equivalents of co-ligand show a further decline in conversion with comparable chemo- and regioselectivity observed to the reaction carried out with 4 equivalents of co-ligand (Table 3.5, entries 2 and 3). This supports the premise of competitive binding between the substrate and co-ligand, rationalised by a corresponding the decrease in conversion to 35%. The comparable observed regioselectivity is attributed to a sufficiently long-lived coordinatively saturated catalyst species. The reduction in chemoselectivity, conversion and activity for all co-ligand experiments with $Rh_2(OAc)_4$ compared to catalyst precursor **1** illustrates the benefits of preforming the catalytic precursor prior to application in the hydroformylation reaction.

During some catalytic reactions, degradation of the active catalyst may lead to agglomeration of elemental metals such as rhodium, which may significantly influence the data obtained in the hydroformylation reaction.[34,40] Should this occur during the reaction, the observed catalytic data would be a result of the proposed catalyst precursor in combination with the liberated rhodium metal. To determine the homogeneity of the heteroleptic dirhodium(II,II) catalyst precursors under evaluation, a mercury poisoning test was carried out. The addition of elemental mercury to the reaction vessels results in the formation of an amalgam with any deposited rhodium metal, rendering any such particles inactive in the reaction. Comparison of the conversion, chemo- and regioselectivity obtained with, and without mercury shows no significant reduction in the reactivity of the complex in both reactions (Table 3.5 entries 4 and 5). This suggests that the reaction is facilitated by a molecular species and not a combination of the catalyst precursor and rhodium particles.

3.3 Evaluation of the synthesised complexes as catalyst precursors in the hydroformylation reaction under optimised conditions

The data obtained from the catalytic optimisation experiments where temperature, pressure and time were varied, resulted in the conditions of 85 °C, 40 bar and 4 hours being selected for the evaluation and comparison of complexes **1** - **6** as catalyst precursors in the hydroformylation of 1-octene.

3.3.1 The effects of the ancillary ligand substituents and counter ions on the catalytic activity for acetate- and hexafluorophosphate-containing complexes

The choice of ligands incorporating substituents at the 4 and 4’ positions showed the expected trend in variation of the electronic character of the complexes, as shown in the electrochemical analysis section of Chapter 2. The product distributions obtained from hydroformylation reactions are usually reported due to a combination of electronic and steric influences. However, due to the coordination geometry adopted by bipyridyl chelate complexes as previously reported,[41] the differences in the steric influence may be minimised around the axial positions of the bimetallic core. The summarised catalytic data obtained for complexes **1** - **6** is shown in Table 3.6 (*overleaf*).

Comparison of the data obtained for complexes with acetate counter ions show that near quantitative conversion (97 - 99%) is achieved, regardless of the substituent or counter ion interaction under the optimised conditions. In accordance with the electrochemical data, an inverse trend in the amount of aldehyde produced is observed relative to the reduction potential, with complex **2** showing the highest aldehyde production of 99% (Table 3.6, entry 2). Conversely, catalyst precursor **3** displays the lowest chemoselectivity for aldehyde at 84% (Table 3.6, entry 3) with the highest measured reduction potential. A graphic representation of the chemoselectivity is shown in Figure 3.3 (*overleaf*).

Interestingly, the comparable chemoselectivity observed for complexes **3** and **4** are corroborated by the electrochemical analysis, where the reduction potential of complex **3** was determined to be 0.95 V, suggesting that the electronic factors play a crucial role in the chemoselectivity for this class of complex. Additionally, the results obtained for regioselectivity show that the highest linear aldehyde formation is observed for catalyst precursor **3** (Table 3.6, entry 3). The graphic representation of the regioselectivity of all the tested complexes shown in Figure 3.4 (*overleaf*).

Table 3.6. Comparison of the Hydroformylation data obtained from reactions carried out with complexes **1 - 6** as catalyst precursors.

Entry	Catalyst precursor	Conversion (%)	Total aldehydes (%)	Total *iso*-octenes (%)	Linear aldehydes (%)	Branched aldehydes (%)	TOF (h^{-1})	*n:iso*
1	**1**	99	96	4	44	56	602	0.77
2	**2**	99	99	1	40	60	620	0.66
3	**3**	99	84	16	54	46	529	1.17
4	**4**	97	83	17	49	51	573	0.96
5	**5**	99	90	10	45	55	565	0.82
6	**6**	99	89	11	46	54	556	0.85

Hydroformylation of 1-octene in toluene (5 mL), 1:1 CO:H_2, 40 bar pressure, reaction time of 4 h and catalyst loading of 2.87 x 10^{-3} mmol. GC conversions were obtained using an internal standard of *n*-decane. Total aldehydes are composed of linear and branched aldehydes in a mixture with a percentage sum of 100. TOF = (mmol aldehydes per mmol Rh_2)/ time. Reactions carried out in triplicate with an average error value of 3.73%.

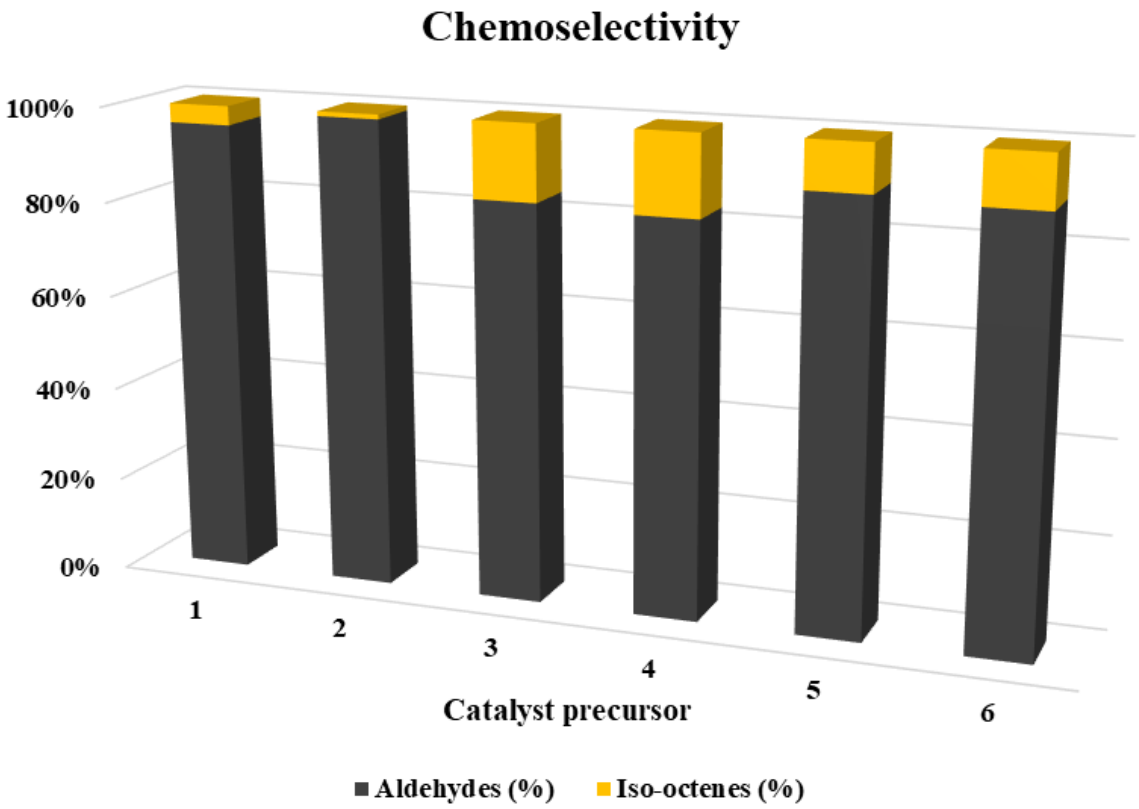

Figure 3.3. Representation of the chemoselectivity in the hydroformylation of 1-octene with complexes **1 - 6** as catalyst precursors.

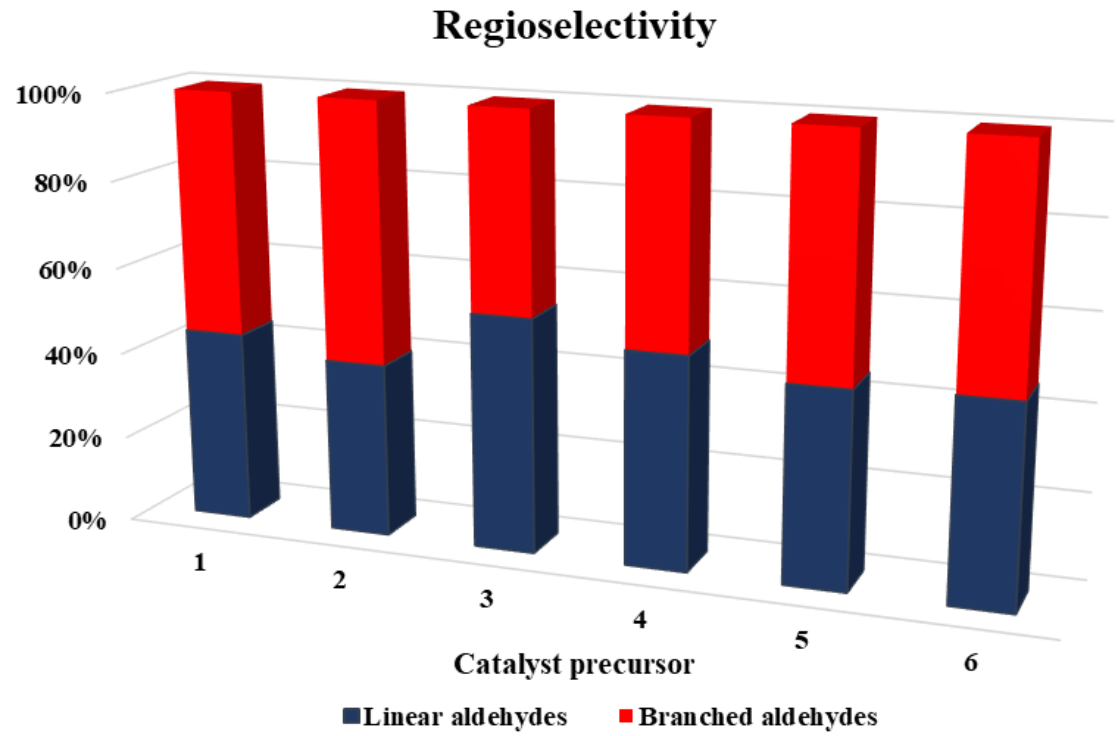

Figure 3.4. Representation of the regioselectivity in the hydroformylation of 1-octene with complexes **1 - 6** as catalyst precursors.

Although a mechanism for the hydroformylation reaction is not yet established for dirhodium(II,II) complexes, the presence of steps such as reductive elimination and oxidative addition are presumed to occur at key points during the cycle. The combination of these results suggests that throughout the catalytic cycle, the reducibility of the complex under similar conditions plays a significant role in the production of aldehydes. This infers that an important step in the catalytic cycle for the title complexes is reductive elimination.

As further support for this speculation, comparison of the catalytic data obtained for complexes **1** and **4** shows a significant decrease in the number of aldehydes produced, from 96 to 83% (Table 3.6, entries 1 and 4). This can be attributed to the increase in the reduction potential observed for complex **4**, at 0.96 V compared to the 0.91 V reduction potential obtained for complex **1**.

Classically, the formation of branched aldehyde products is due to a combination of steric and electronic factors. Comparison of the regioselectivity of complexes **1** and **2** (Table 3.6, entries 1 and 2) show similar product distribution although a marked difference in the reduction potential was previously described. This suggests some differences in the steric interaction of the substrate and complexes, and since the bipyridyl ligand steric influence is assumed to be similar, the effect due the presence of the hemilabile counter ion is suggested. This speculation is substantiated by comparison of the product distributions observed when the hexafluorophosphate congeners are applied to the hydroformylation reaction, with comparable regioselectivity observed for complexes **4 - 6** (Table 3.6, entries 4 to 6).

Furthermore, although the steric influence is suggested to be the major contributor for regioselectivity, comparing the data obtained for complexes **2** and **5** where the acetate was shown to have negligible binding affinity, show that more linear aldehyde is obtained for the hexafluorophosphate complex (Table 3.6, entries 2 and 5). The combination of these results suggests that although steric influence is the dominant interaction for regioselectivity, the electronic nature of the complex may have a small effect on the regioselectivity for complexes containing trifluoromethyl-substituted bipyridyl ligands.

3.4 The evaluation and development of recyclability of dirhodium(II,II) chelate complexes in the hydroformylation of 1-octene

The recovery of expensive metal-based catalyst precursors through simplistic, clean and energy efficient methods is under constant development.[42,43] Due to the pronounced increase in aqueous solubility relative to the previously reported homoleptic catalyst systems[17] and the high chemoselectivity observed for complex **2**, the aqueous biphasic approach was investigated with the results given in Table 3.7. The reactions were carried out by charging each reactor with catalyst, internal standard, substrate and solvent (toluene) as described for the hydroformylation reaction, with the addition of 5mL of distilled water.

The results obtained show that comparable activity and chemoselectivity is observed upon comparison of reactions in monophasic (toluene) and the first aqueous biphasic (toluene/H_2O) reaction cycle (Table 3.7, entries 1 and 2). A more significant change in the regioselectivity is observed, favouring the production of linear aldehyde in the biphasic system, compared to the reaction run in organic medium only. This likely arises due to the coordination of water molecules changing the geometry and electronic environment around the bimetallic core.

Table 3.7. Preliminary biphasic hydroformylation data obtained using complex **2** as a catalyst precursor.

Entry	Conversion (%)	Total aldehydes (%)	Total *iso*-octenes (%)	Linear aldehydes (%)	Branched aldehydes (%)	TOF (h^{-1})	*n:iso*
1	99	99	1	40	60	620	0.66
2	99	95	1	47	53	597	0.88
3[a]	18	54	46	69	31	339	2.23
4[b]	87	63	37	71	29	393	2.45
5[c]	28	60	40	68	32	375	2.12

Hydroformylation of 1-octene in toluene (5 mL) and H_2O (5 mL), 1:1 $CO:H_2$, 40 bar pressure, reaction time of 4 h and catalyst loading of 2.87 x 10^{-3} mmol. GC conversions were obtained using an internal standard of *n*-decane. Total aldehydes are composed of linear and branched aldehydes in a mixture with a percentage sum of 100. TOF = (mmol aldehydes per mmol Rh_2)/ time. Reactions carried out in triplicate with an average error value of 2.14 %. [a] biphasic cycle 2, [b] biphasic cycle 1 in the absence of toluene, [c] biphasic cycle 2 in the absence of toluene.

Upon subjecting the aqueous phase to a second cycle, a drastic decrease in the conversion of the system was observed, from 99 to 18% with a corresponding decrease in the

chemoselectivity for aldehyde from 95 to 54% (Table 3.7, entries 2 and 3). To determine the cause of this reduction in catalytic efficiency, electronic absorption spectra of the aqueous phase was recorded after each run. The spectra collected was then compared to the spectrum obtained for the complex in deionised water (Figure 3.5).

Initially, the stability of complex **2** in H_2O was monitored over 72 hours by UV-vis spectral analysis, displaying no changes in the spectrum. Comparison of the spectra obtained for the catalyst precursor in water show distinctive maximum absorbances at 280 and 250 nm (blue), shifting to 280 and 240 nm (grey) after the first reaction cycle. This suggests that some changes to the catalyst precursor occurs after the first cycle, corresponding to either a hydrated active catalyst species or some stabilised resting state of the catalyst.

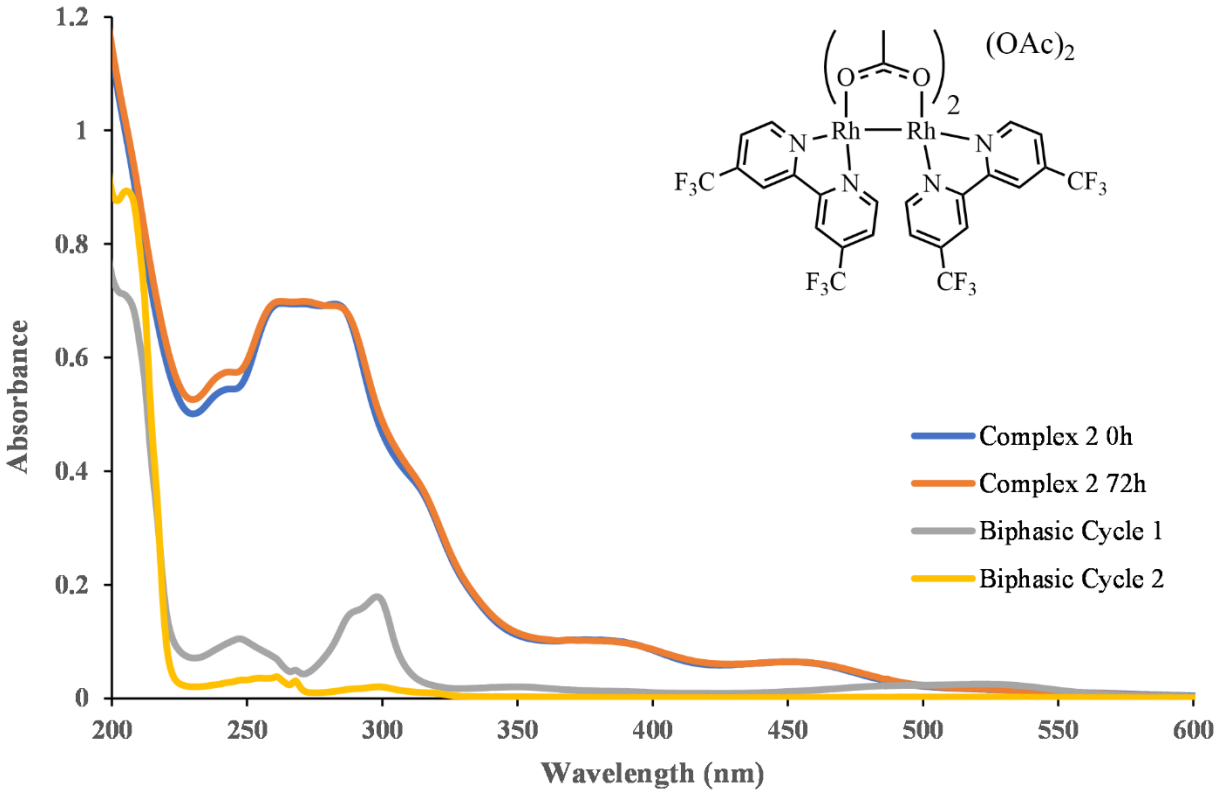

Figure 3.5. Electronic absorption spectra recorded for catalyst precursor **2** in water between 0 (blue) and 72 h (orange), and the aqueous fractions after biphasic cycle 1(grey) and cycle 2 (yellow).

The spectrum obtained for the aqueous layer from the 2nd cycle shows significant diminishing in the absorbances, possibly arising from catalyst deactivation or incomplete separation of the catalyst species from the organic phase. In either case, this effectively reduces the catalyst

loading in subsequent cycles. To substantiate the leeching of the catalyst into the organic layer, the aqueous layer was separated and a further 5 mL aliquot of distilled water was added to the remaining organic layer. The spectrum recorded after 24 hours presents the same profile as that obtained for the second cycle, indicating that some corresponding species is indeed present in the organic phase.

Since the catalyst precursor shows appreciable solubility in the organic solvent (toluene) used for these reactions, another reaction was attempted in the absence of toluene to determine whether any improvement would be observed. The results show reduced overall conversion in the absence of toluene for the first biphasic catalytic cycle, ascribed to the unfavourable catalyst-substrate interaction at the boundary between organic and aqueous phases (Table 3.7, entry 4). This is further supported by the significant decrease in the aldehyde products produced at 63% relative to the 97% observed for the first biphasic cycle in the presence of toluene. Additionally, carrying out a second cycle under these conditions showed a pronounced decline in the conversion of substrate to 28% (Table 3.7, entry 5), however the chemo- and regioselectivity is maintained. This suggests that mass transfer between the organic and aqueous phases still occurs under neat conditions, although to a lesser effect in the absence of toluene. The combination of these observations and the inherent solubility characteristics of this complex therefore renders it unsuitable as a candidate for aqueous biphasic catalysis.

Due to the significant variation in the solubility when the bipyridyl substituent and counter ion is altered, changing these in the appropriate manner may allow for solubility characteristics necessary for mono-phasic catalyst recycling. The described characteristics of complex **6** showed limited solubility in toluene at ambient temperature, with no aqueous solubility observed unless additives such as DMSO or acetone are added. It was noted during the catalyst precursor evaluation that a homogeneous solution was obtained after the hydroformylation reaction was carried out with complex **6**. Furthermore, cooling this solution to below 0 °C resulted in the formation of a light green precipitate. From this mixture, the supernatant was removed, and the precipitate washed with cold toluene in 3 cycles, before reintroducing the recovered solid to the corresponding reactor with fresh standard, substrate, and solvent. This process was carried out in 5 cycles, and the results are shown in Table 3.8 (*overleaf*).

Table 3.8. Preliminary mono-phasic hydroformylation recyclability data obtained with complex **6** as a catalyst precursor.

Entry	Catalyst precursor	Conversion (%)	Total aldehydes (%)	Total *iso*-octenes (%)	Linear aldehydes (%)	Branched aldehydes (%)	TOF (h^{-1})	*n:iso*
1	**6**[a]	99	89	7	49	51	530	0.96
2	**6**[b]	99	85	15	47	53	557	0.88
3	**6**[c]	98	83	17	52	48	520	1.08
4	**6**[d]	99	85	15	48	52	534	0.92
5	**6**[e]	97	87	13	53	47	516	1.13

Hydroformylation of 1-octene in toluene (5 mL), 1:1 CO:H_2, 40 bar pressure, reaction time of 4 h and catalyst loading of 2.87 x 10^{-3} mmol. GC conversions were obtained using an internal standard of *n*-decane. Total aldehydes are composed of linear and branched aldehydes in a mixture with a percentage sum of 100. TOF = (mmol aldehydes per mmol Rh_2)/ time. Reactions carried out in triplicate with an average error value of 5.71%. [a-e] cycles 1 to 5 of recyclability study.

The recorded data indicates that the catalyst activity is maintained, seen by TOF values of above 500 h^{-1}, and the differences observed between runs were found to be within experimental error. This indicates that excellent tolerance toward exposure to repeated hydroformylation cycles for complex **6** can be achieved with this method. Graphic representations of the activity and selectivity (chemo- and regio-) are depicted in Figures 3.6 and 3.7 respectively, over the recyclability evaluation. The comparable results obtained for the TOF, chemo- and regioselectivity over the 5-cycle study indicate that the active catalyst species is stable to the hydroformylation reaction and the recyclability method.

The solid recovered after the 5th cycle was further analysed by ^{1}H-NMR spectroscopy and compared to the spectrum obtained for complex **6** since any significant changes in the signals would suggest complex degradation or possibly the presence of an activated catalyst species. Comparison of the ^{1}H-NMR spectra obtained before and after the recycling study (Figure 3.8, *vida infra*) shows signals corresponding to the catalyst precursor after 5 cycles. This is evidence that the catalyst precursor is indeed reformed at the end of each catalytic run. Furthermore, coupled to the mercury drop test previously carried out, this shows that the complex is stable under the optimised conditions for hydroformylation.

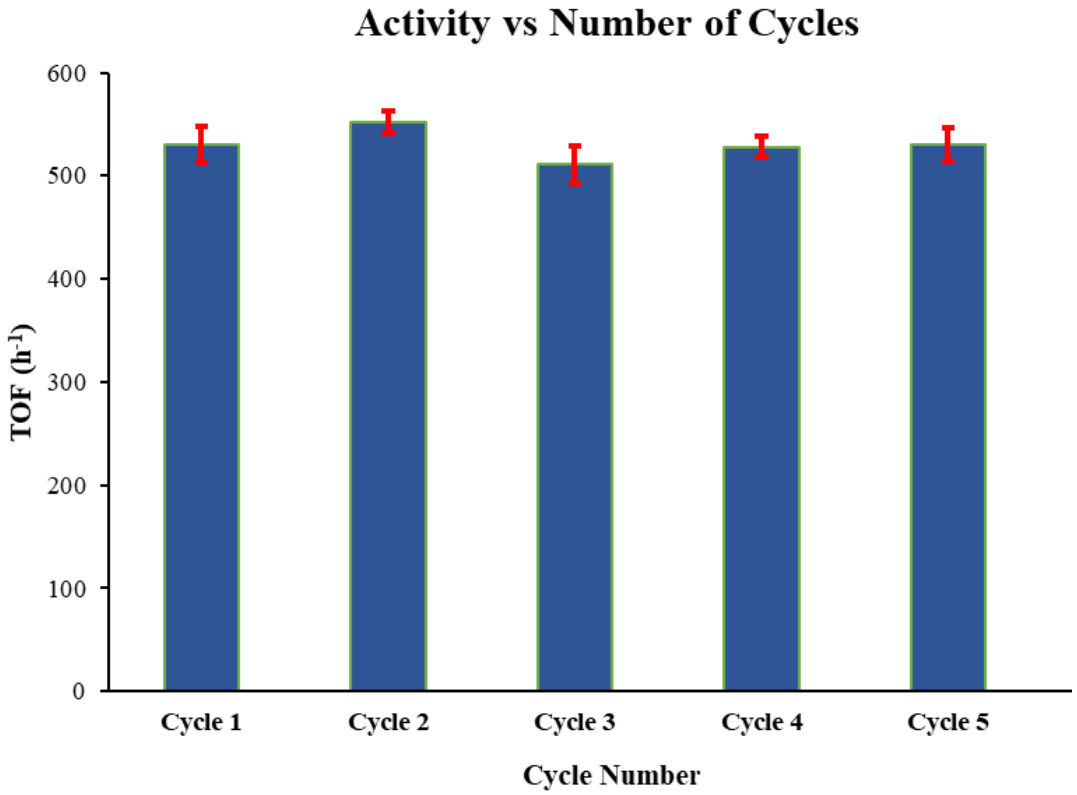

Figure 3.6. Graphic representation of the changes in catalyst activity over 5 cycles with catalyst precursor **6**. Reactions were carried out in triplicate with error bars shown in red.

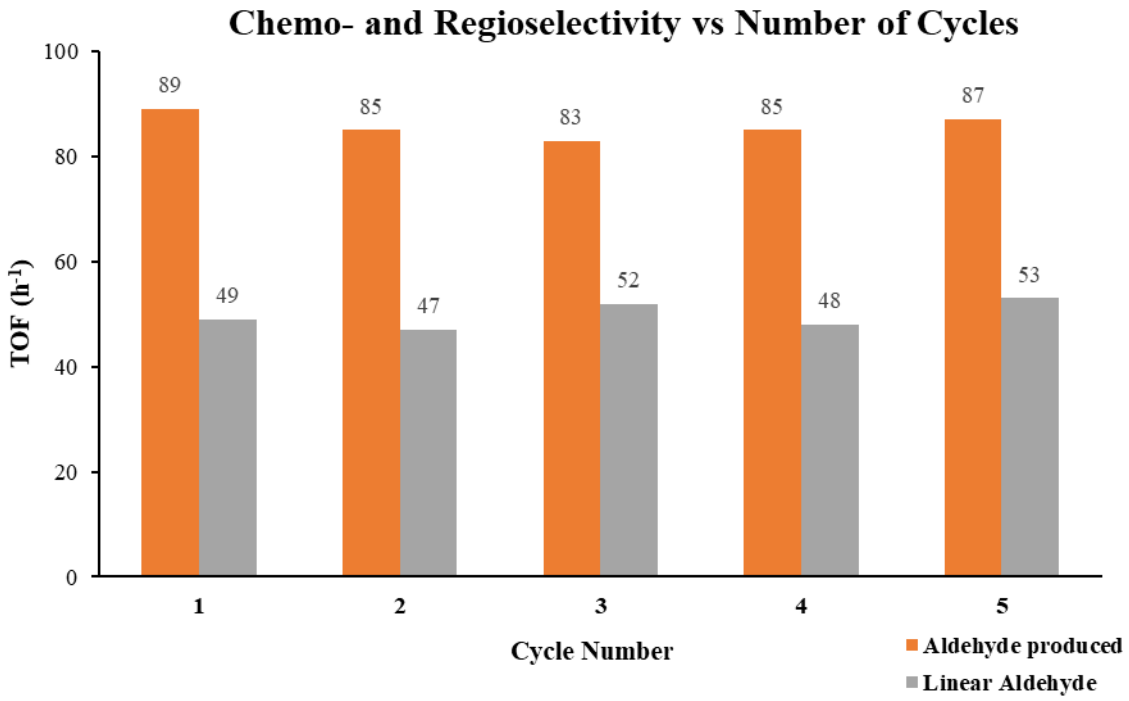

Figure 3.7. Graphic representation of changes in the chemo- and regioselectivity over 5 cycles with catalyst precursor **6**.

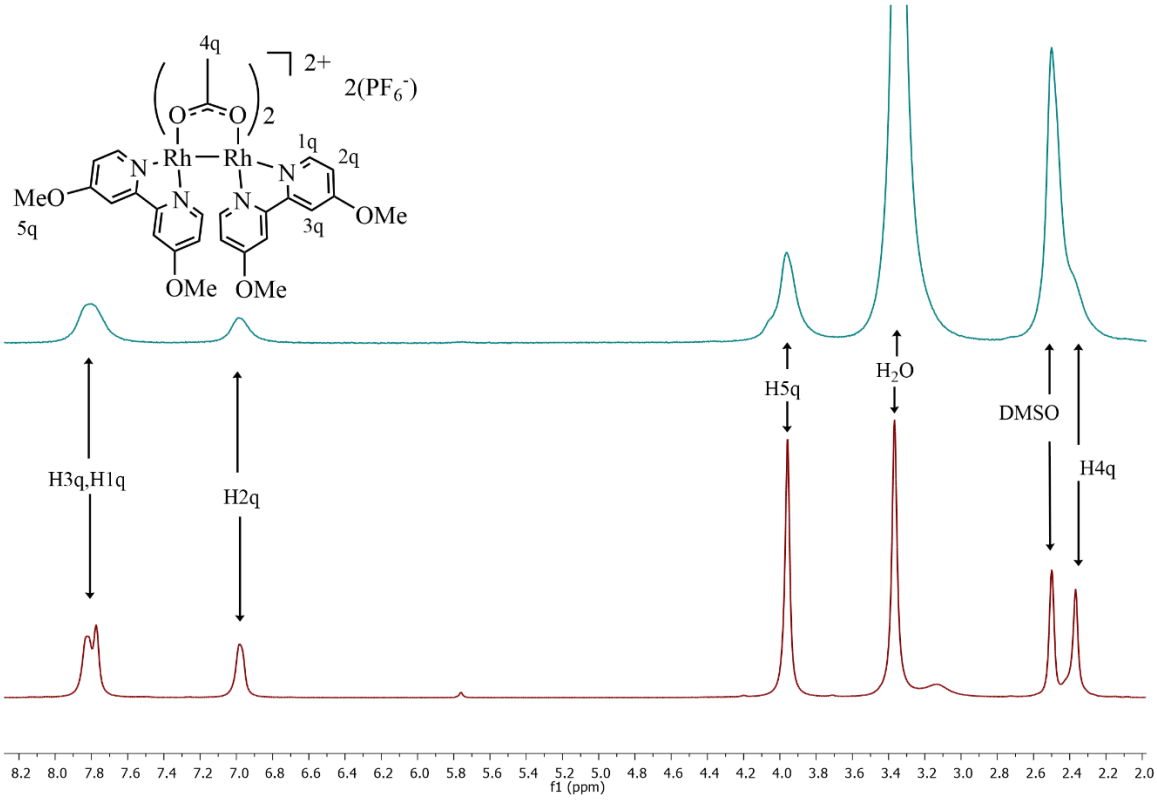

Figure 3.8. ^{1}H-NMR spectral comparison of catalyst precursor **6** before (bottom) and after (top) 5 cycles.

3.5 Substrate scope for the hydroformylation reaction with dirhodium(II,II) chelate complex 2 as a catalyst precursor

The sensitivity of the catalytic system to the nature of the substrate was explored for the best performing catalyst precursor complex **2**, in the hydroformylation of styrene, cyclohexene and 7-tetradecene (7-TDC) as substrates. Initially, the reactions carried out with 7-TDC and cyclohexene under the optimised temperature of 85 °C showed low conversion. This is attributed to the rigid half-chair conformation of cyclohexene and the higher energy requirements for the conversion of long-chain internal olefins such as 7-TDC. [9,44] Thus, to satisfy the energy requirements for hydroformylation of these substrates the reactions were carried out at 105 °C. The obtained results are shown in Table 3.9.

Near quantitative conversion (98%) was observed in the hydroformylation of styrene with no isomerised products observed due to the nature of the substrate. Interestingly, similar regioselectivity is observed under the same conditions with 1-octene as a substrate. Due to stabilisation of the benzylic position by the phenyl ring, anti-Markovnikov addition of the metal complex to the olefin is expected, usually resulting in a larger proportion of branched aldehydes formed. A schematic representation of this is shown in Scheme 3.3 (*overleaf*).

Table 3.9. Results from hydroformylation reactions with varying substrates (styrene, cyclohexene, 7-tetradecene) obtained with complex **2** as catalyst precursor.

Entry	Temperature (˚C)	Conversion (%)	Total aldehydes (%)	Total isomerized products (%)	Linear aldehydes (%)	Branched aldehydes (%)	TOF (h^{-1})	*n:iso*
1[a]	85	98	100	0	43	57	615	0.75
2[b]	105	76	84	16	-	-	404	-
3[c]	105	88	100	-	-	100	582	-

Hydroformylation of 1-octene in toluene (5 mL), 1:1 CO:H_2, 40 bar pressure, reaction time of 4 h and catalyst loading of 2.87 x 10^{-3} mmol. GC conversions were obtained using an internal standard of *n*-decane. Total aldehydes are composed of linear and branched aldehydes in a mixture with a percentage sum of 100. TOF = (mmol aldehydes per mmol Rh_2)/ time. Reactions carried out in triplicate with an average error value of 2.81%. [a]- Styrene substrate. [b]- 7-tetradecene substrate. [c]- Cyclohexene substrate.

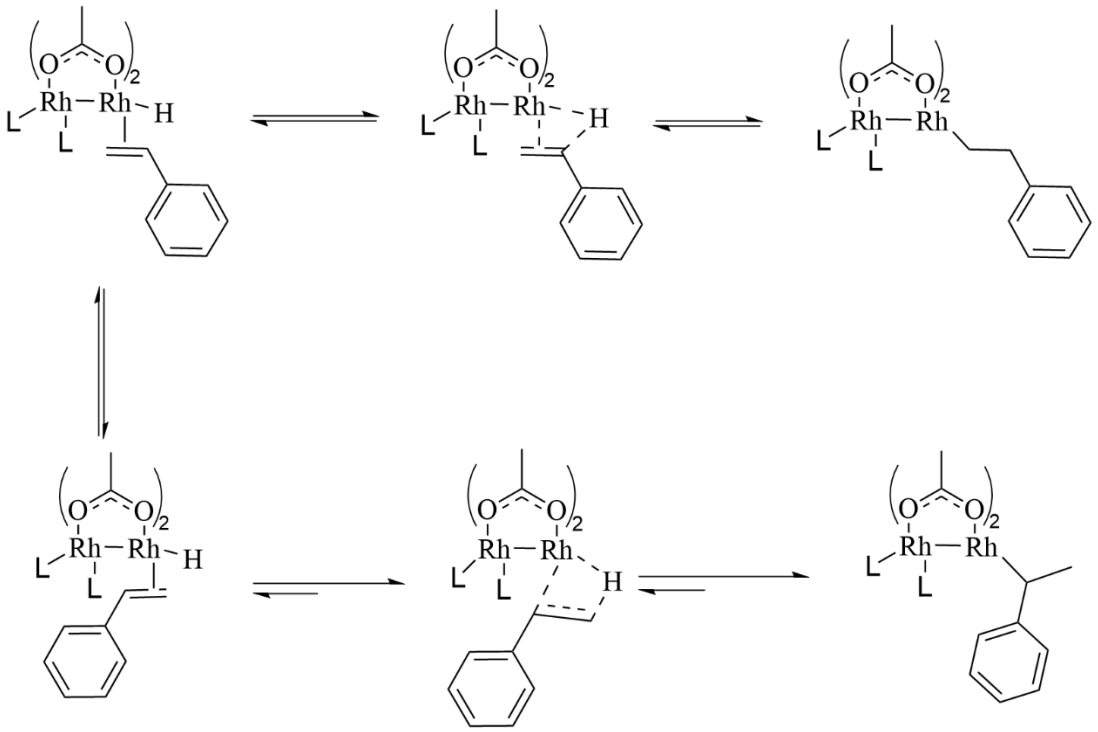

Scheme 3.3. Depiction of the proposed anti-Markovnikov addition of the metal complex to styrene following hydride transfer for heteroleptic dirhodium(II,II) compounds.

The reaction carried out with cyclohexene as substrate shows good conversion (88%) of the alkene to form cyclohexanecarboxaldehyde (branched product) exclusively (Table 3.9, entry 3). This is due to the nature of the substrate, whereby a shift in the double bond results in no difference to the substrate.

Furthermore, the reaction carried out with 7-TDC shows good conversion (76%) with 84% chemoselectivity toward aldehyde products with only 16% isomers detected (Table 3.9, entry 2). This is due to the substrate being fully internalised, whereby any isomerisation leads to the formation of less branched isomers, which are not as thermodynamically favoured compared to the fully internalised olefin. The results show good to excellent applicability for varying substrates for complex precursor **2**, provided the energy requirements for the hydroformylation reaction are satisfied.

3.6 Proposed mechanism for the hydroformylation of alkenes with heteroleptic dirhodium(II,II) acetato-bipyridyl catalyst precursors

Although there is no catalytic cycle reported for the hydroformylation reaction with dirhodium(II,II) complexes, the accepted catalytic cycle for the classical rhodium-based hydroformylation reaction employs key steps such as reductive elimination, oxidative addition and migratory insertion.[45] These steps facilitate key changes in the complex electronics, oscillating between Rh(I) and Rh(III), thereby allowing the coordination of substrate and the subsequent transformation to the desired aldehyde products.

In this chapter, the isomerisation was shown to be dependent on the presence of syngas to provide a catalytically active species which is then able to undergo isomerisation of the substrate through a proposed metal hydride species. Therefore, some activation of the catalyst precursor must occur (Step 1). Similarly, since the catalyst precursor was recovered and characterised, the active catalyst must be reformed in a final step, through reductive elimination.

Unlike mono-metallic catalyst precursors, the dirhodium(II,II) core offers the possibility of a cooperative effect, whereby hydride transfer may occur from one rhodium atom to the other. Alternatively, the homolytic addition of dihydrogen to the metal complex may occur as observed in the hydrogenation of alkenes.[46] Should the addition of dihydrogen occur, this would allow for homolytic bond cleavage of the incoming dihydrogen molecule across the bimetallic core, resulting in the formation of two metal hydrides and a corresponding increase in the core oxidation state from (II,II) to (III,III).

This leads to a coordinatively saturated species, which is then only able to undergo olefin addition by breaking a metal-ligand bond which may occur through either a bridging or chelating ligand. The creation of the required coordinatively unsaturated species may also occur through breaking of the metal-metal bond. The latter is less likely due to orbital mixing of the bridging acetate ligands with the bimetallic core[47] and, as such increases the probability of chelate ligand lability pathway.

The observed reduction potential of each complex with acetate counter ions and the corresponding effects on the formation of aldehyde products suggests that the proposed mechanism should place emphasis on reductive elimination as a likely rate determining step. Should the formation of the acyl-hydrido complex form as depicted (Scheme 3.4), reductive elimination may occur once a suitable ligand arrangement occurs whereby both the acyl and hydrido groups are *syn*- to the bimetallic core. This arrangement allows for reductive elimination to occur, reforming the catalyst precursor and liberate the aldehyde product. The proposed mechanism for the hydroformylation reaction with heteroleptic dirhodium(II,II) catalyst precursors is shown in Scheme 3.4, constructed from the combined electrochemical, synthetic, and catalytic data obtained in this study.

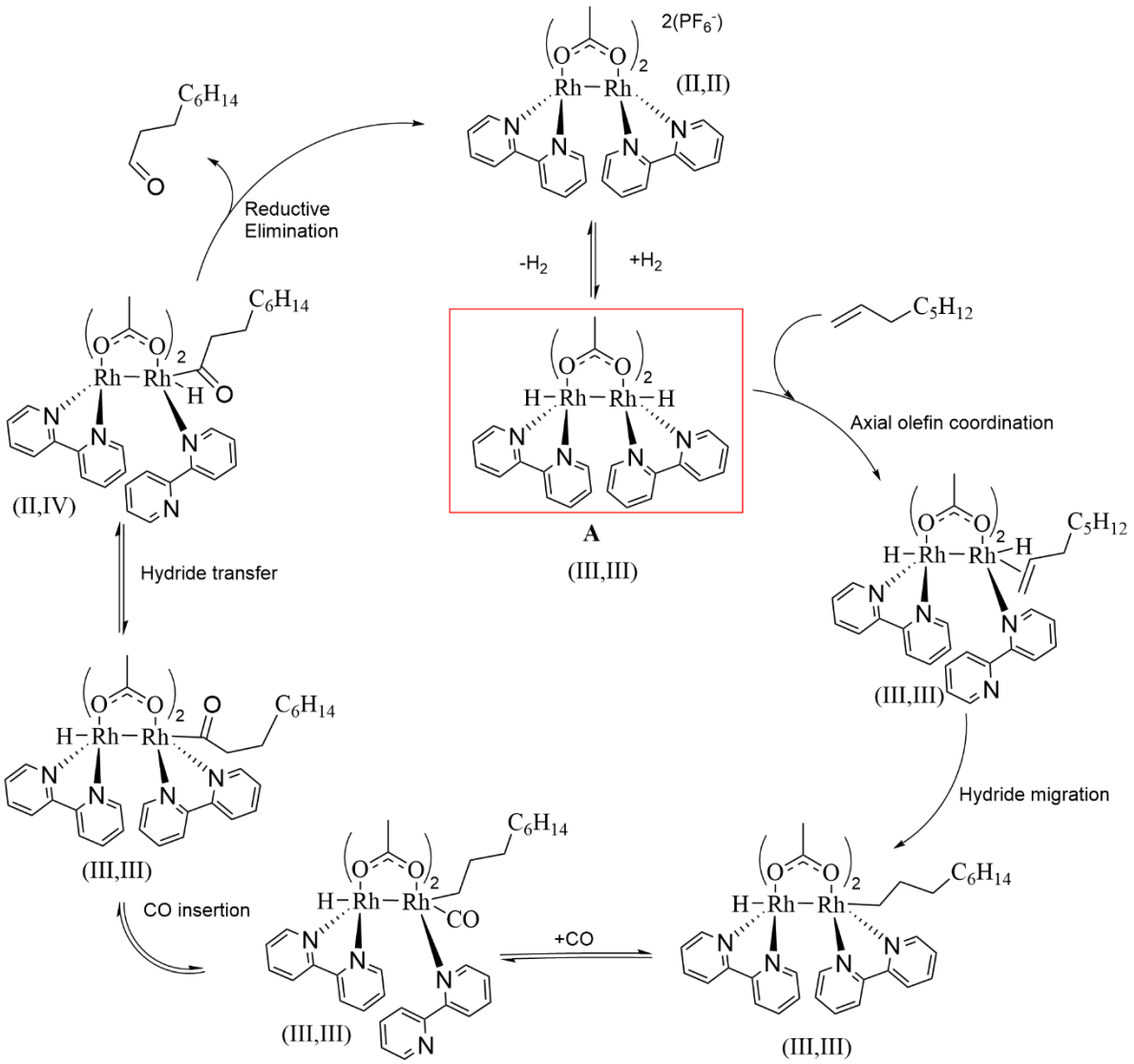

Scheme 3.4. Proposed mechanism for the hydroformylation reaction with heteroleptic dirhodium(II,II) complexes as catalyst precursors. Counter ions omitted in individual steps of the cycle for clarity.

3.7 Summary

In summary, three dirhodium(II,II) acetato-bipyridyl complexes with acetate counter ions (**1** - **3**), and three hexafluorophosphate analogues (**4** - **6**) were evaluated as catalyst precursors in the hydroformylation of 1-octene. Complex **1** was used as a model for the optimisation of the reaction conditions (temperature, pressure, and time) with comparable performance under milder conditions compared to the previously reported dirhodium(II,II) tetraacetate. Hydroformylation reactions carried out using the prototypical $Rh_2(OAc)_4$ complex with varying equivalents of 2,2'-bipyridyl ligand additive showed a reduction in catalyst performance compared to the preformed complex **1**. The presence of additional ligand resulted in pronounced effects on conversion, chemo- and regioselectivity, attributed to the increased steric interactions when excess ligand is present in the reaction medium. Trends in the chemoselectivity for complexes with acetate counter ions were attributed to the redox characteristics of complexes **1** - **3**. The hemi-labile counter ion provides favourable steric and electronic interactions, resulting in higher aldehyde production compared to hexafluorophosphate analogues. Additionally, the highest regioselectivity was observed for complex **3** presenting the highest production of linear aldehyde due to steric influence of the counter ion acetate group. Furthermore, the counter ion interactions were corroborated by the catalytic data obtained for hexafluorophosphate complexes (**4** - **6**) whereby comparable regioselectivity was observed across this series, independent of substitution of the bipyridyl ligands at the 4 and 4' position. The catalyst precursor which showed the greatest chemoselectivity for aldehyde production (**2**) was applied toward substrate scope evaluation in the hydroformylation of styrene, 7-tetradecene and cyclohexene with good conversion and production of aldehyde observed, provided the energy requirements for the internal and cyclic olefins were satisfied. The aqueous solubility of complex **2** prompted an initial study to determine whether the catalyst could be recycled, however the solubility of the catalyst precursor in the organic layer resulted in poor catalyst recovery. Temperature dependent solubility in toluene was observed for complex **6**, allowing for the prospect of catalyst precursor recyclability *via* a simplistic separation method. This post-catalytic precipitation at low temperature was achieved in aid of catalyst recyclability, whereby the recovered solid was re-used over 5 cycles. Comparable results were observed regarding activity and selectivity, with spectroscopic analysis of the recovered residue showing no degradation of the catalyst precursor after recycling.

3.8 Experimental details and Instrumentation

3.8.1 Equipment and instrumentation

Nuclear magnetic resonance (NMR) spectra were recorded on a Varian Mercury 300 (^{1}H: 300.08 MHz) spectrometer and were recorded using tetramethylsilane (TMS) as the internal standard. Coupling constants are reported in Hz and chemical shifts are reported in ppm relative to residual solvent signals. Analysis of the hydroformylation samples of reactions were carried out on a Perkin Elmer Clarus 580 GC equipped with a flame-ionisation detector (FID). The products were confirmed in relation to authentic standards for the hydroformylation products of 1-octene (internal-octenes and isomers of nonanal), styrene, cyclohexene and 7-tetradecene.

3.8.2 General method for hydroformylation reactions

Hydroformylation reactions were carried out in stainless steel pipe reactors (90 mL) equipped with a Teflon-coated magnetic stirrer bar. Each reactor was charged with toluene (5 mL), substrate (7.2 mmol), internal standard n-decane (1.26 mmol) and catalytic precursor (2.87 x 10^{-3} mmol), calculated per dirhodium core unit, equivalent to a rhodium metal loading of 5.74 x 10^{-3} mmol. The pipe reactor was purged with nitrogen three times, followed by purging with syngas (1:1, CO:H_2) three times. The reactor was pressurised to the required pressure, followed by heating to the required temperature. Samples were collected at the beginning and end of each reaction. All reactions were performed in triplicate and are recorded as an average of three identical experiments.

3.8.3. Mercury poisoning study

Mercury poisoning experiments were carried out in a 90 mL stainless steel pipe reactor charged with toluene (5 mL), 1-octene (7.2 mmol), internal standard n-decane (1.26 mmol) and catalytic precursor (complex 1) (2.87 x 10^{-3} mmol). To each reactor was added one drop of mercury, after which the reactors were sealed. The reactors were purged with N2 three times followed by purging with syngas three times, followed by pressurization to 40 bar and heating to 85 ˚C for 4 hours.

3.8.4. Recycling method

The method for recycling was modified from a previously reported method[28] and carried out as follows:

Following cooling to ambient temperature and de-pressurisation, the reactor contents were decanted into separate vials and analysed by GC-FID. The vials were then cooled to 0 °C overnight following precipitation of a green solid. The supernatant was removed and the remaining solid washed with cold toluene in 3 cycles. The solid was then transferred to the reactor with fresh substrate, and internal standard before purging with nitrogen and syngas as described in section 3.6.2 and heating to the required temperature. All reactions were performed in triplicate and are recorded as an average of three identical experiments.

3.9 References

1. R. Franke, D. Selent and A. Börner, *Chem. Rev.*, 2012, **112** (11), 5675-5732.

2. B. Cornils, W. A. Herrmann and M. Rasch, *Angew. Chem. Int. Ed.*, 1994, **33**, 2144-2163.

3. B. Zhang, D. Peña Fuentes and A Börner, Hydroformylation. *ChemTexts.*, 2022, **8**, 2.

4. B. Cornils, W. A. Herrmann, I. T. Horvath, W. Leitner, S. Mecking, H. Olivier-Bourbigou and D. Vogt, in *Multiphase Homogeneous Catalysis*, Wiley-VCH Verlag GmbH & Co. KGaA, Weinheim, 2nd edn., 2005, pp. 3-21.

5. D. J. Cole-Hamilton, *Catalysis.*, 2003, **299**, 1702-1707.

6. P. Tundo and A. Perosa, *Chem. Soc. Rev.*, 2007, **36**, 532-550.

7. B. R. James, P. W. N. M. van Leeuwen and C. Claver, in *Rhodium Catalyzed Hydroformylation*, Kluwer Academic Publishers, New York, 1st edn., 2002, pp. 6-27.

8. A. Börner and R. Franke, *Hydroformylation: Fundamentals, Processes and Applications in Organic Synthesis*, Wiley-VCH, Weinheim, 2016.

9. M. Vilches-Herrera, L. Domke and A. Börner, *ACS Catal.*, 2014, **4**, 1706-1724.

10. J. Hagen, in *Industrial catalysis: A practical approach*, Wiley-VCH, Weinheim, 2015, pp. 59-67.

11. N. N. Omosun, S. Ngubane and G. S. Smith, *Appl. Catal. A Gen.*, 2021, **610**, 117950.

12. S. Siangwata, N. J. Goosen and G. S. Smith, *Appl. Catal. A Gen*., 2020, **603**, 117736.

13. C. Williams, M. Ferreira E. Monflier, S. L. Mapolie and G. S. Smith, *Dalton Trans.*, 2018, **47**, 9418-9429.

14. P. Govender, S. Ngubane, B. Therrien and G. S. Smith, *J. Organomet. Chem.*, 2017, **848**, 281-287.

15. C. Claver, N. Ruiz, P. Lahuerta, and E. Peris, *Inorg. Chim. Acta.*, 1995, **233**, 161-164.

16. N. Nowotny, T. Maschmeyer, B. F. G. Johnson, P. Lahuerta, J. M. Thomas and J. E. Davies, *Angew. Chem. Int. Ed.*, 2001, **40** (5), 955-958.

17. S. de Doncker, A. Casimiro, I. A. Kotze, S. Ngubane and G. S. Smith, *Inorg. Chem.*, 2020, **59**, 12928-12940.

18. J. L. Bear, E. Van Caemelbecke, S. Ngubane, V. Da-Riz, and K. M. Kadish, *Dalton Trans.*, 2011, **40** (11), 2486-2490.

19. T. J. Whittemore, H. J. Sayre, C. Xue, T. A. White, J. C. Galucci and C. Turro, *J. Am. Chem. Soc*., 2017, **139**, 14724-14732.

20. J. Hagen, in *Industrial Catalysis*, Wiley-VCH Verlag GmbH & Co. KGaA, Weinheim, 2nd edn., 2006, pp. 9-14.

21. X. Jin, J. Feng, S. Li, H. Song, C. Yu, K. Zhao and F. Kong, *Mol. Catal.*, 2019, **475**, 110503.

22. A. J. Catino, R. E. Forslund and M. P. Doyle, *J. Am. Chem. Soc*., 2004, **126**, 13622-13623.

23. H. M. L. Davies, A. M. Walji and T. Nagashima, *J. Am. Chem. Soc.*, 2004, **126**, 4271-4280.

24. R. Ohnishi, H. Ohta, S. Mori and M. Hayashi, *Organometallics*., 2021, **40**, 2678-2690.

25. H. K. Kisan and R. B. Sunoj, *J. Org. Chem.*, 2015, **80,** 2192-2197.

26. Q. Chu, M. S. Yu and D. P. Curran, *Tetrahedron.*, 2007, **63** (39), 9890-9895.

27. W. Keim, *Green Chem.*, 2003, **5**, 105-111.

28. L. Maqeda, B. C. E. Makhubela and G. S. Smith, *Polyhedron.*, 2015, **91**, 128-135.

29. J. Fang, H. Jin, T. Ruddy, K. Pennybaker, D. Fahey and B. Subramaniam, *Ind. Eng. Chem. Res.*, 2007, **46**, 8687-8692.

30. S. Siangwata, N. C. C. Breckwoldt, N. J. Goosen and G. S. Smith, *Appl. Catal. A Gen.*, 2019, **585**, 117179.

31. N. N. Omosun and G. S. Smith. *Eur. J. Inorg. Chem.*, 2019, 2558-2564.

32. C. Li, L. Yan, L. Lu, K. Xiong, W. Wang, M. Jiang, J. Liu, X. Song, Z. Zhan, Z. Jiang, Y. Ding, *Green Chem.*, 2016, **18**, 2995-3005.

33. S. Siangwata, N. Baartzes, B. C. E. Makhubela and G. S. Smith, *J. Organomet. Chem.*, 2015, **796**, 26-32.

34. L. C. Matsinha, S. F. Mapolie and G. S. Smith, *Dalton Trans.*, 2015, **44**, 1240-1248.

35. Y. Brunsch and A. Behr, *Angew. Chem. Int. Ed.*, 2013, **52**, 1586-1589.

36. S. Paganelli, M. Marchetti, M. Bianchin and C. Bertucci, *J. Mol. Catal. A Chem.*, 2007, **269**, 234-239.

37. A. M. Kluwer, M. J. Krafft, I. Hartenbach, B. de Bruin and W. Kaim, *Top. Catal.*, 2016, **59**, 1787-1792.

38. P. W. N. M. Van Leeuwen and C. Claver, in *Rhodium catalyzed hydroformylation*, Kluwer Academic Publishers, Dordrecht, 2000.

39. Y. Jiao, M. S. Torne, J. Gracia, J. W. (Hans) Niemantsverdriet and P. W. N. M. van Leeuwen, *Catal. Sci. Technol.*, 2017, **7**, 1404-1414.

40. V. J. Guanipa Q., L. G. Melean, M. Modroño Alonzo, A. Gonzalez, M. Rosales, F. Lopez-Linares and P. J. Baricelli, *Appl. Catal. A Gen.*, 2009, **358** (1), 21-25.

41. C. A Crawford, J. H. Matonic, J. C. Huffman, K. Folting, K. R. Dunbar and G. Christou, *Inorg. Chem.*, 1997, **36**, 2361-2371.

42. A. E. C. Collis and I. T. Horváth, *Catal. Sci. Technol.*, 2011, **1**, 912-919.

43. N. N. Omosun and Gregory S. Smith, *J. Organomet. Chem.*, 2021, **951**, 122022.

44. L. Le Goanvic, J. Couturier, J. Dubois and J. Carpentier, *Catalysts.*, 2018, **8**, 148.

45. S. Gladiali, J. Carles Bayón and C. Claver, *Tetrahedron: Asymmetry.*, 1995, **6**, 1453-1474.

46. B. C. Hui and G. L. Rempel, *J. Chem. Soc. D.*, 1970, 1195-1196.

47. J. Lloret, J. J. Carbo, C. Bo, A. Lledos and J. Perez-Prieto, *Organometallics.*, 2008, **27**, 2873-2876.

Chapter 4

The development of heteroleptic dirhodium(II,II) acetato-bipyridyl complexes as catalyst precursors for hydroaminomethylation reactions

4.1 Introduction

Amines are a useful class of compounds with a variety of applications in industrial, pharmaceutical and academic research due to their nucleophilic properties.[1,2] Precursor compounds incorporating the amine functionality for synthetic applications are often derived from fossil fuel sources, however, bio-sourced amines are of great interest particularly for pharmaceutical purposes.[3,4] The synthesis of amines is conventionally carried out by reactions such as the reductive amination of alcohols, amination of aryl halides or through the reduction of nitriles.[5-7] In recent times, the need for sustainable synthetic procedures of fine chemicals is often met by the inclusion of catalytic processes or steps in the synthetic protocol, and may be tailored specifically toward the synthesis of amines. Research efforts into compounds incorporating amine functionalities such as Cu-catalysed or photoredox mediated coupling reactions, Buchwald-Hartwig amination and Fe-catalysed reductive amination are a few areas routinely explored.[8-11] Furthermore, the consumption of alkene feedstocks through carbonylation reactions such as hydroformylation offer a versatile means of synthesising aldehydes and corresponding carboxylic acids, alcohols, and amines through additional chemical processes.[12] These extrinsic reaction steps often include stoichiometric amounts of harsh reagents, unfavourable reaction conditions, intensive purification procedures and the formation of unwanted or toxic by-products.[12]

The hydroaminomethylation (HAM) reaction, reported by Reppe and Vetter in 1953, involves the reaction of the aldehydes produced from a hydroformylation reaction with an amine reagent *in-situ*, leading to the formation of intermediary imines or enamines.[13] Subsequent catalytic reduction of the condensation intermediates occurs in the presence of the catalyst and H_2 to form amines as major products (Scheme 4.1). This allows for a more straightforward way of obtaining amines from suitable alkene feedstocks with a significant reduction in the environmental impact. The hydroaminomethylation reaction increases atom economy substantially, since the tandem process utilises two catalytic steps, producing water as the major by-product.[14]

The advantage of the atom economy of the hydroformylation reaction, which forms an integral part of the HAM process, allows for an efficient approach to obtaining amines directly from low-value industrial feedstock alkenes.[14,15] Additionally, since the condensation step liberates water as a byproduct, the stability of the catalyst precursor to an aqueous environment may be required since deactivation of the active hydride species may hinder the catalytic steps and therefore significantly reduce the yield. Ideally, catalyst precursors may be recycled by means of aqueous biphasic catalysis, similar to hydroformylation reports, where the catalyst precursor remains in the aqueous layer and the reaction occurs at the interphase between the organic and aqueous phases, facilitated by rapid stirring and heating.[16,17] Other attempts at improving the selectivity, activity and recyclability of the catalyst species includes the incorporation of the active metal centre into large coordination assemblies or the use of micellar catalytic systems.[18,19]

The use of multifunction catalyst systems such as hetero-bimetallic rhodium/iridium complexes have shown an increased efficiency compared to homo-metallic complexes.[20,21] These catalyst systems utilise rhodium as the primary hydroformylation catalytic centre and iridium or other transition metals as the hydrogenation centre due to the affinity for each metal to carry out specific transformations.[20-22] Despite these advances, the inclusion of additives such as cyclodextrins, HBF_4, $Zn(OTf)_2$ and H_3PO_4 or other ligand additives result in higher condensation and hydrogenation efficiency in hydroaminomethylation, and are often reported in conjunction with transition metal-based catalyst precursors.[23-27]

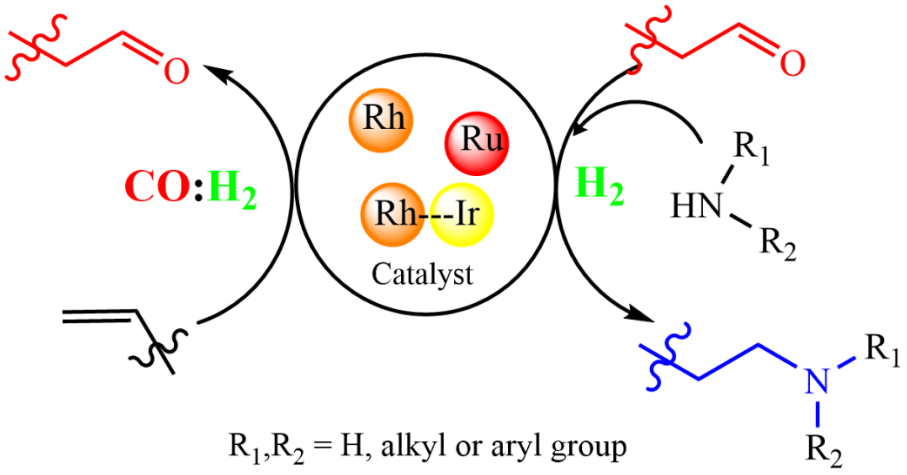

Scheme 4.1. An example of the hydroaminomethylation process incorporating some of the transition metals employed as catalysts.[20,21,23,25]

Furthermore, the addition of ligands and additives bearing donor atoms such as phosphorous and nitrogen are often utilised toward enhancing the reduction capabilities of rhodium-based catalysts in hydroaminomethylation. However, fewer reports on pre-formed nitrogen-containing rhodium-based complex catalysts exist.[28,29] Recently, October and co-workers reported the synthesis and activity of Rh(I) based imino-pyridyl complexes with good activity and selectivity using aliphatic olefins.[30] Comparable conversions were obtained with good regioselectivity under milder conditions, and at lower catalyst loading when compared to previous reports. In a subsequent study, suitable substrates reported for obtaining products *via* hydrogenolysis of benzyl groups to afford the target amines in good yield.[30,31]

To our knowledge, reports on substituent variation of the ancillary ligands in heteroleptic dirhodium(II,II) acetato-bipyridyl complexes remain unexplored, particularly in terms of the effects on homogeneous tandem catalytic reactions such as hydroaminomethylation. Furthermore, the inclusion of catalyst precursors showing no hydrogenation activity when applied in the hydroformylation reaction are prime candidates for the catalytic hydrogenation of imines under certain conditions. Should these conditions and nature of the catalyst be suitably optimised, this system may be utilised as chemoselective catalysts for the hydrogenation of imines and enamines exclusively thereby increasing the selectivity of the reaction.

This chapter will discuss the development and optimisation of a hydrogenation model reaction by altering gas composition, thermal parameters, counter ion nature, bipyridyl substituent and catalyst loading to favour production of target amine products. The optimised system will be applied toward the hydroaminomethylation of olefins using the title heteroleptic dirhodium(II,II) complexes as catalyst precursors for obtaining secondary and tertiary amines from a range of alkene and amine substrates. Finally, discussion of the optimised catalyst system and conditions toward incorporation of the hydroaminomethylation reaction in the synthetic protocol of analogues of a known API, Tramadol® is described.

4.2 The optimisation of reaction conditions (Temperature, Pressure, Time, Catalyst loading) for the selective hydrogenation of imines

The previous reports for both homo- and heteroleptic dirhodium(II,II) complexes as catalyst precursors in hydroformylation reactions showed no appreciable formation of alkanes or alcohols from the hydrogenation of alkenes and aldehydes throughout the course of the reactions.[32,33] This attribute of the reported complexes may be exploited toward increasing the selectivity of a tandem reaction such as hydroaminomethylation, provided suitable conditions are developed for the hydrogenation of imine and/or enamine intermediates. Considerations regarding the aqueous stability of the complexes have been discussed in Chapter 3, however, the effects of the presence of the catalyst on the Schiff-base reaction and formation of the intermediary products needs to be determined in this context.

4.2.1 The initial evaluation of dirhodium(II,II) complexes as catalyst precursors for catalytic imine hydrogenation

The model reaction for evaluating the hydrogenation capabilities of the previously synthesised complexes was carried out by reacting benzaldehyde with n-propylamine in toluene in the presence of the catalyst precursor. This allows for simplistic means of determining the effects of the presence of the catalyst on the condensation and hydrogenation steps in a one-pot reaction. Additionally, the reaction outcome with a substrate such as benzaldehyde infers the enhancement in the reactivity of the aliphatic aldehydes for Schiff-base condensation, due to the higher electrophilicity of the carbonyl carbon atom in aliphatic aldehydes obtained from hydroformylation. The heteroleptic complex **1** was used as a model catalyst precursor under identical conditions as reported for the hydroformylation reaction (85 °C, 40 bar syngas

pressure and 4-hour reaction time) with benzaldehyde and propylamine substrates in a 1:1 molar ratio (Scheme 4.2, *overleaf*).

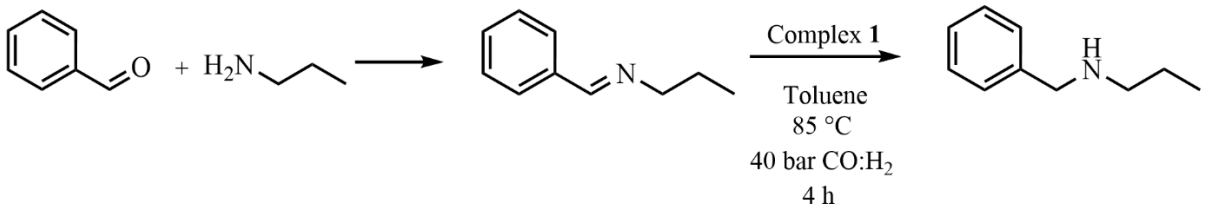

Scheme 4.2. Outline of the model catalytic reduction reaction using complex **1** as a catalyst precursor.

Analysis of the chromatograms obtained by gas chromatography of the reaction mixture show signals corresponding to unreacted benzaldehyde (t_R = 24.63 min) and imine product (t_R = 30.32 min), with an average substrate consumption percentage of 85%, and low amine yield (<5%). These signals were compared to authenticated standards of both substrates and intermediates which were synthesised by reported methods and characterised prior to catalytic evaluation.[34] The toluene was removed under reduced pressure before further analysis by NMR spectroscopy (Figure 4.1). The relative integration of each signal shown in the expanded spectra, confirm the reaction of benzaldehyde and n-propylamine into the expected imine product, with the relative aldehyde (H_{1r}, 9.86 ppm) to imine proton (H_{1s}, 8.17 ppm) signal integration observed in a 0.29:1 ratio. This corresponds to approximately 80% conversion, in agreement with the conversion calculated from the GC-FID chromatogram. In the same manner, the conversion of imine to amine was calculated by comparing the benzylic (H_{1t}) and methylene (H_{2s}) proton signals in the obtained mixture, resulting in an approximate 6% conversion to the required amine.

The reaction was repeated under a hydrogen atmosphere of 40 bar to determine any influence on the production of amine products (Table 4.1). Under this pure hydrogen atmosphere at 40 bar pressure and 85 °C, the conversion to imine intermediate and amine yield increased to 99 and 15% respectively (Table 4.1, entry 1). Comparison of these data suggests that the increase in conversion is a result of the absence of the carbon monoxide, likely influencing the catalytic hydrogenation activity by strong coordination of CO to the metal centre. This indicates that the system may be further optimised for maximal amine production, from the reduction of the imine formed *in-situ* and would need to include a lower concentration of CO relative to H_2 in the reaction atmosphere.

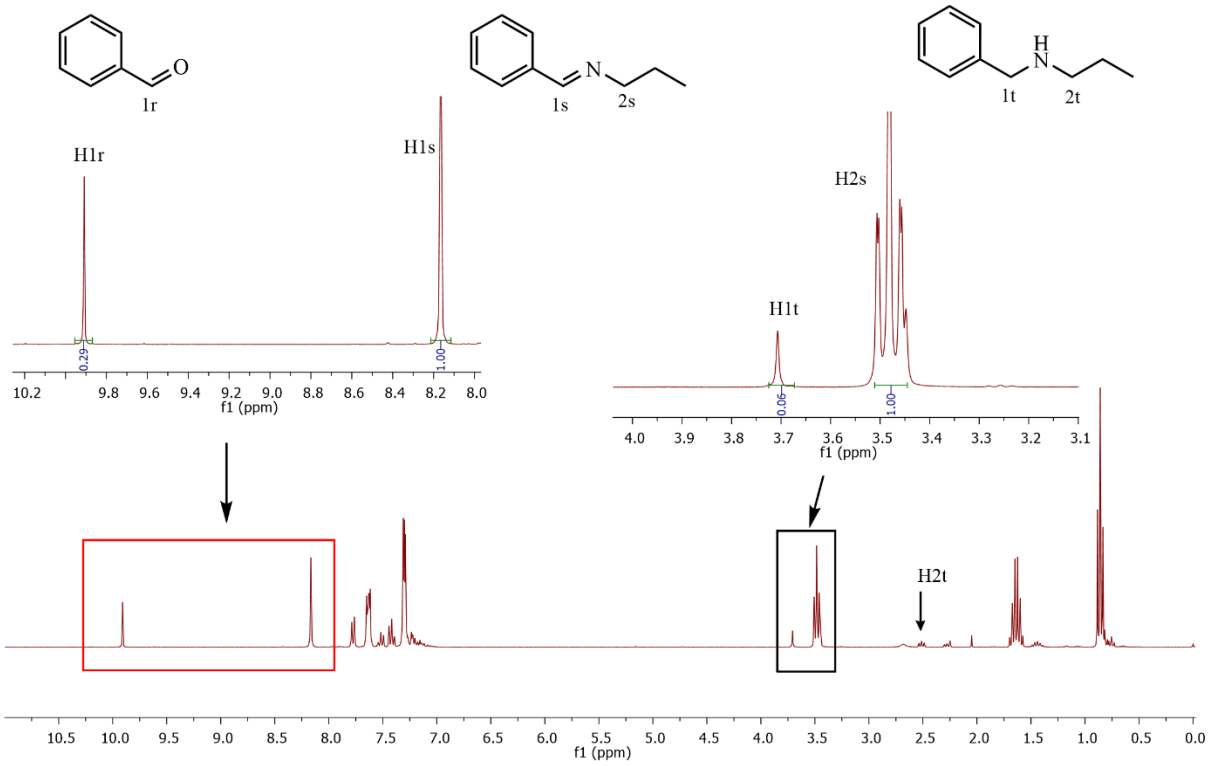

Figure 4.1. A comparison of the recorded ^{1}H-NMR spectrum of the products obtained from the model catalytic reaction highlighting the characteristic signals, in $CDCl_3$.

Temperature optimisation for the hydrogenation reaction was carried out at 40 bar hydrogen pressure in 10 °C increments from 85 up to 115 °C (Table 4.1, entries 1 - 4). The results obtained show the consumption of the substrate remains near quantitative (>99%) across the tested temperature range. This indicates that the thermal requirements for the condensation of benzaldehyde with n-propylamine are satisfied from 85 °C under H_2 atmosphere. Additionally, a substantial increase in the catalytic production of amine products is observed at 95 and 105 °C with amine product production of 31 and 41% respectively (Table 4.1, entries 2 and 3).

Table 4.1. Temperature optimisation data obtained using complex **1** as a catalyst precursor for the catalytic hydrogenation of n-propylbenzylimine.

Entry	Temperature (˚C)	Consumption of substrate (%)	Imine (%)	Amine (%)	Im:Am
1	85	99	85	15	5.67
2	95	99	69	31	2.23
3	105	99	59	41	1.43
4	115	99	69	31	2.23
5[a]	105	99	51	49	1.04
6[b]	105	99	>99	<1	NC

Hydrogenation model reaction in toluene (5 mL), 40 bar H_2 pressure, 4 h reaction time, varying the temperature and catalyst loading of 0.04%. GC conversions were obtained using an internal standard of n-decane. Reactions were carried out in duplicate or triplicate with average error values of 5.23 %. NC – not calculated.

[a] Reaction carried out for 8 hours

[b] Reaction carried out in the absence of catalyst precursor

Increasing the reaction temperature to 115 °C resulted in a decrease in the amine production (31%) relative to the reaction run at 105 °C (Table 4.1, entry 4). This decrease is ascribed to exceeding the boiling point of toluene (*ca.* 110 °C), used as the solvent for the reaction. The boiling of the solvent results in visible deposition of the catalyst precursor on the walls of the reactor, effectively reducing the amount of catalyst precursor in the reaction medium and, hence, the production of amine. ^{1}H-NMR spectral analysis of the mixture of products obtained at each temperature increment agrees with the data obtained from GC analysis whereby increasing intensity of the signals corresponding to the amine product is observed (Figure 4.2).

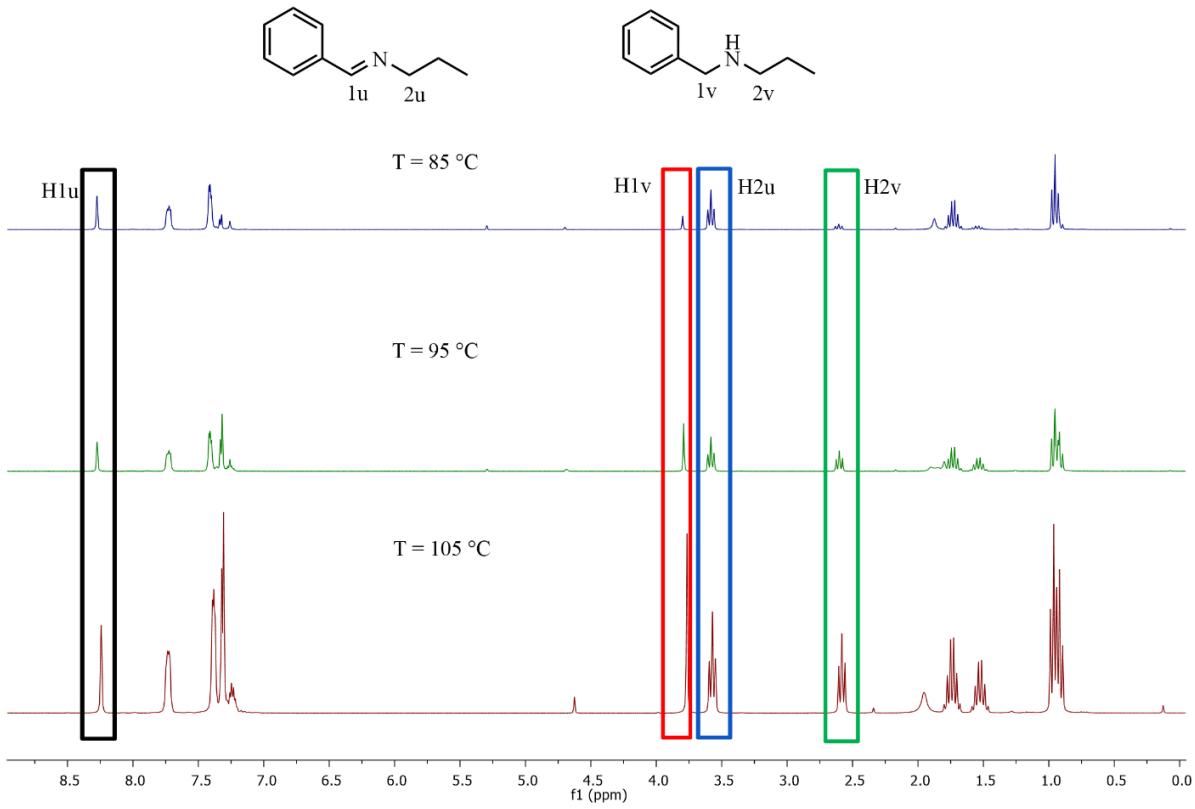

Figure 4.2. A comparison of the obtained ^{1}H-NMR spectra of the product mixture obtained from the model catalytic hydrogenation reactions carried out at 85, 95 and 105 °C, recorded in $CDCl_3$.

Thus, the obtained data clearly shows that the optimised temperature where maximum amines are produced (105 °C) would be used for subsequent optimisation experiments. Increasing the reaction time to 8 hours yielded a marginal improvement in the amine product obtained at 49% (Table 4.1, entry 5). This disproportionate increase of 8% amine relative to extending the reaction time under identical conditions suggests that time is not the limiting factor for the hydrogenation of imines in the presence of the model catalyst precursor.

Furthermore, the reaction carried out without catalyst precursor under 105 °C and 40 bar pressure shows near quantitative consumption of the substrates with a quantitative amount of Schiff-base (>99%) detected (Table 4.1, entry 6). This confirms that the presence of the catalyst is required for the hydrogenation reaction to form the target amine product, and the Schiff-base condensation reaction proceeds uninhibited in the presence or absence of the catalyst precursor. The combined optimisation data dictates that further evaluation of the catalyst precursors will be carried out under 105 °C, 40 bar H_2 pressure and 4-hour reaction time.

4.2.2 The effect of electron-withdrawing and electron-donating substituents of benzaldehyde on the hydrogenation activity

The effects of electron-withdrawing and electron-donating groups on the hydrogenation activity were probed by carrying out the hydrogenation reaction using 4-nitrobenzaldehyde or 4-methoxybenzaldehyde with n-propylamine under the optimised conditions. The results are given in Table 4.2 (*overleaf*).

The results obtained for the reaction with 4-nitrobenzaldehyde shows low substrate consumption (22%) compared to that obtained for the reaction with the unsubstituted benzaldehyde substrate (Table 4.2, entries 1 and 2). This is attributed to the strong electron-withdrawing effect of the nitro-substituent, hindering the formation of condensation products through lower stability of the imine intermediate. Additionally, the major product observed is the corresponding tertiary amine with no secondary amine products detected in the reaction mixture. This indicates that the hydrogenation reaction is largely uncompromised by the presence of the electron-withdrawing nitro substituent and the reaction of the more nucleophilic secondary amine, produced from the initial hydrogenation reaction of n-propylamine with 4-nitrobenzaldehyde, occurs with lower efficiency.

Table 4.2. The evaluation of catalyst precursor **1** for the hydrogenation of imines formed from the condensation of substrates with nitro and methoxy substituents.

Entry	Substrate	Consumption of substrate (%)	Imine/ enamine (%)	Secondary Amine (%)	Tertiary Amine (%)
1	benzaldehyde	99	32	68	-
2	4-nitrobenzaldehyde	22	14	-	86
3	4-methoxybenzaldehyde	99	-	4	96

Hydrogenation reactions carried out in toluene (5 mL), 40 bar total pressure, 105˚C, reaction time of 4 h and catalyst loading of 5.74×10^{-3} mmol. GC conversions were obtained using an internal standard of n-decane. Reactions carried out in duplicate with an average error value of 3.46%.

Conversely, when substituted with a methoxy group (Table 4.2, entry 3) the consumption of substrate increases to near quantitative amounts (99%). This occurs due to favourable mesomeric donation from the methoxy group allowing for unhindered Schiff-base

condensation, followed by a reduced hydrogenation rate due to a less electrophilic imine. Scheme 4.3 describes the proposed factors and their influence on the product distributions.

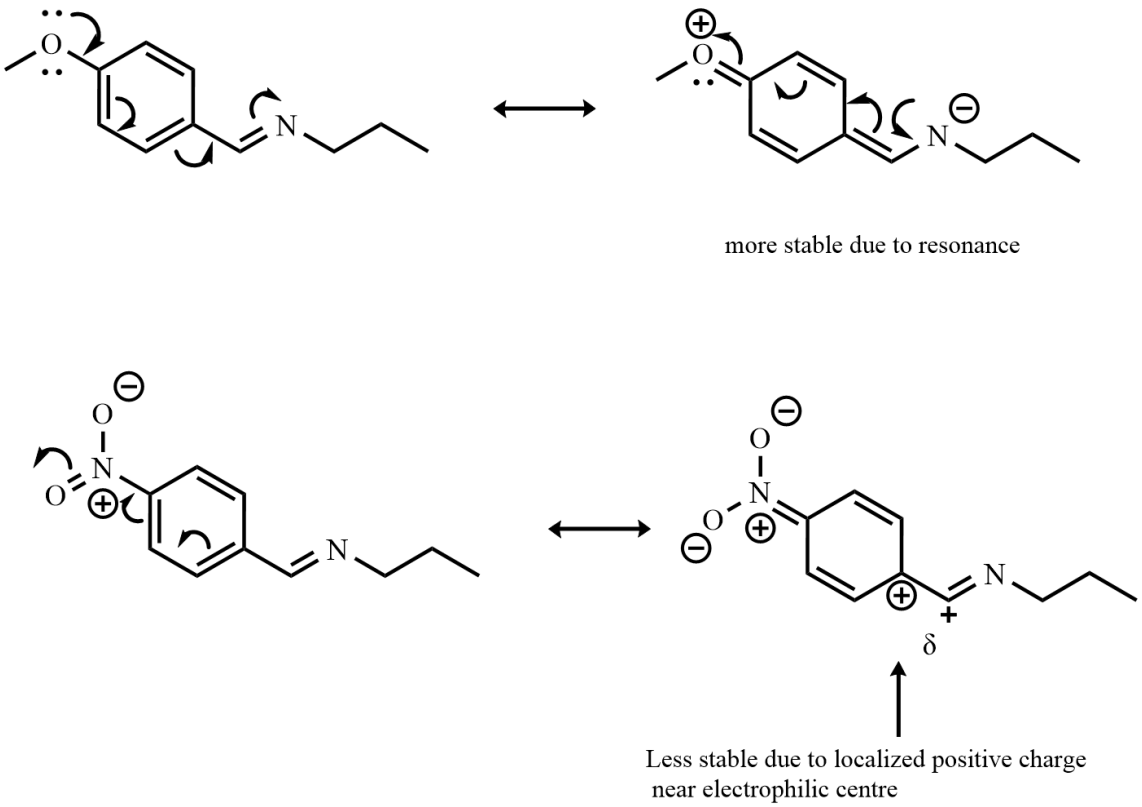

Scheme 4.3. The effect of resonance on the imine stability relative to the aldehyde substituent.

The combination of these factors results in the buildup of aldehyde relative to the secondary amine produced by the hydrogenation step. This facilitates condensation reactions between the more nucleophilic secondary amine and the aldehyde to form enamines, which then undergo hydrogenation to form tertiary amine products. The combination of these data suggests that sensitivity of the proposed catalytic hydrogenation reaction to changes in the appended aldehyde functional group depends primarily on the substituents ability to inhibit the Schiff base formation and therefore amine product produced.

4.2.3 The evaluation of heteroleptic dirhodium(II,II) acetato-bipyridyl complexes for the hydrogenation of imines

Under the previously optimised hydrogenation reaction conditions, the effects of counter ion type and bipyridyl substituent were explored by evaluating each catalyst precursor for applicability in the model hydrogenation reaction (Table 4.3). The influence of the counter ion was explored by evaluation of the hexafluorophosphate congener (complex **4**, Table 4.3, entry

1) and comparing the data to that obtained for complex **1**. The results show a significant increase in the production of the target amine product (58%) for complex **4**. This observation is ascribed to the combination of the steric and electronic influence of the hemi-labile acetate, as concluded from the reported hydroformylation study.[33] This is likely a consequence of competitive binding between the acetate counter ion and the imine product to the bimetallic core, or the presence of the basic acetate group influencing catalytic hydrogenation.

Table 4.3. The evaluation of catalyst precursor complexes **4** - **6** for the catalytic hydrogenation of n-propylbenzylimine.

Entry	Catalyst precursor	Consumption of substrate (%)	Imine (%)	Amine (%)	Im:Am
1	**4**	99	42	58	0.72
2[a]	**4**	99	38	62	0.61
3[a]	**5**	99	32	68	0.47
4[a]	**6**	99	69	31	2.23

Hydrogenation model reaction in toluene (5 mL), 40 bar H_2 pressure, 4 h reaction time varying the temperature and catalyst loading of 0.04%. GC conversions were obtained using an internal standard of n-decane. Reactions were carried out in duplicate or triplicate with average error values of 5.23 %.

[a] Reaction carried out at 0.08 mol% catalyst loading.

As part of further optimisation, the catalyst loading was increased from 0.04 to 0.08 mol% for catalyst precursor **4** under the optimised conditions (Table 4.3, entry 2). The results show a marginal increase in the formation of amine product of 62%, indicating that the catalyst loading has a small effect on the production of amine under these conditions.

To maximise product yield, further evaluation of the title dirhodium(II,II) bipyridyl chelate complexes was carried out at 0.08 mol% catalyst loading. The typical catalyst loading reported for efficient hydroaminomethylation using rhodium-based catalyst precursors is between 0.5-1 mol%.[30,35-37] The proposed catalytic system thus represents a substantial improvement toward efficient rhodium catalysed hydroaminomethylation reactions without the addition of ligands or additives.[23] The influence of the bipyridyl substituent on the hydrogenation reaction was elucidated by evaluating hexafluorophosphate complexes **5** and **6** under the optimised conditions and comparing the data to that obtained for complex **4**.

The results show that a strong dependence on the catalytic reduction relative to the substituent exists, with trifluoromethyl-containing complex **5** presenting the highest amine yield of 68% (Table 4.3, entries 3 and 4). This can be ascribed to a combination of the lower reduction potential imparted by the electron-withdrawing trifluoromethyl group, and the lower steric interaction resulting from competitive axial binding, allowing facile substrate binding before hydrogenation takes place. The former may be corroborated by the result obtained for complex **6**, with the lowest catalytic conversion of the imine corresponding to the methoxy-substituted complex, which showed the highest observed reduction potential of the series.

Additionally, the Schiff-base condensation proceeds in a near quantitative manner, affected by neither the change in catalyst loading, nor the counter ion nature as evidenced by the near quantitative consumption of substrate overall. The combined data suggests that under these conditions the trifluoromethyl-substituted hexafluorophosphate complex (**5**) is the best candidate for further application and optimisation toward the hydroaminomethylation reaction. Furthermore, since the hydrogenation reaction proceeds under 40 bar H_2 atmosphere and it is necessary that CO will at some point need to be included in the reaction atmosphere, the reaction total pressure would be carried out at 50 bar for further experiments and the model hydroaminomethylation reaction.

4.3 Optimisation of partial gas pressures ($CO:H_2$) and equivalents of n-propylamine substrate for the hydroaminomethylation of cyclohexene with complex 5 as a catalyst precursor

The previously discussed findings obtained from the optimisation reactions prompted that a model hydroaminomethylation reaction be attempted with a suitable olefin substrate. The temperature requirement for the hydrogenation reaction (105 °C) and the previously reported hydroformylation data regarding substrate scope makes cyclohexene a suitable candidate for the model alkene substrate. This choice is exemplified by the formation of one aldehyde product and no extraneous formation of hydrogenated products, as observed from the hydroformylation reaction data previously obtained.[33] The model reaction was carried out as depicted in Scheme 4.4 below with the results reported in Table 4.4 (*overleaf*). Additional NMR spectra of isolated major products are given in the Appendix.

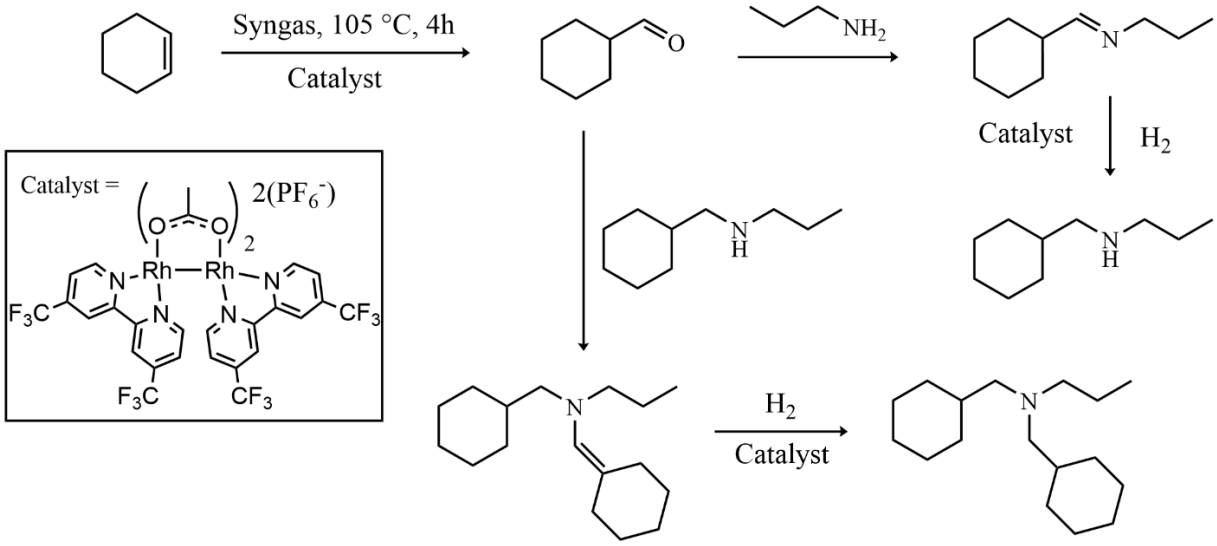

Scheme 4.4. Outline of the model hydroaminomethylation reaction and possible product formation using complex **5** as a catalyst precursor.

Under the control reaction conditions, no aldehyde, imine or amine was obtained for the reaction carried out under 50 bar H_2 atmosphere only (Table 4.4, entry 1). This is rationalised by the dependence of the hydroformylation reaction on the presence of CO required for addition of the acyl group. Since no aldehyde is produced under these conditions, there is no primary substrate for the condensation reaction to proceed and therefore no downstream intermediates such as imines or enamines and their corresponding amine products from the hydrogenation step are detected.

Additionally, under the higher pressure of H_2 no cyclohexane was observed, indicating that under the mildly elevated reaction temperature and pressure conditions no hydrogenation of the alkene occurs. This observation, in combination with the hydroformylation and hydrogenation reaction results supports the fact that the catalytic system may be utilised for chemoselective hydrogenation of imines and enamines under catalytic conditions. Furthermore, the application of the proposed catalytic system may therefore be modified in terms of the ratio of CO:H_2 required for activity, since at the higher temperature and pure H_2 atmosphere no alkane or alcohol products should be formed during the course of the reaction.

Table 4.4. Results obtained from the model hydroaminomethylation reactions under varying syngas partial pressure and equivalents of amine substrate carried out at 105 °C for 4 hours using complex **5** as a catalyst precursor.

Entry	$CO:H_2$ Ratio	Olefin conversion (%)	Aldehyde (%)	Imine/ enamine (%)	Amines (%)	Secondary Amine (%)	Tertiary Amine (%)
1	0:1	-	-	-	-	-	-
2	1:4	66	<1	53	47	99	1
3	2:3	98	<1	35	65	90	10
4	1:1	74	<1	36	64	>99	<1
5[a]	2:3	69	<1	<1	>99	>99	<1

Hydroaminomethylation of cyclohexene in toluene (5 mL), 50 bar total pressure, 105˚C, reaction time of 4 h and catalyst loading of 5.74×10^{-3} mmol. GC conversions were obtained using an internal standard of n-decane. Total amines are composed of secondary and tertiary amines in a mixture with a percentage sum of 100. Reactions carried out in duplicate with an average error value of 5.12 %.

[a] 1.5 equivalents of n-propylamine

Increasing the partial pressure of CO relative to H_2 to a 1:4 ratio (Table 4.4, entry 2) results in 66% consumption of substrate through the hydroformylation reaction, however, no aldehyde product was detected after the reaction. This is ascribed to the condensation reaction between the aliphatic aldehyde and the amine substrate occurring efficiently, supported by the detection of intermediary imine/enamine products and amine products at 53 and 47% respectively. Interestingly, the secondary to tertiary amine distribution was observed to be 99:1 under these conditions. The formation of tertiary amines from the hydroaminomethylation reaction of an alkene with a primary amine is a consequence of the condensation reaction occurring between the secondary amine product with the aldehyde forming an enamine (Scheme 4.4, *vida supra*).

Subsequently, reduction of the enamine by the catalyst precursor yields the corresponding tertiary amine and may be primarily influenced by two factors. Firstly, should the hydrogenation reaction liberate secondary amine at a higher rate than the condensation reaction between the primary amine and the aldehyde, this would result in the production of both secondary and tertiary amines as products. Alternatively, if the hydroformylation reaction proceeds at a higher relative rate to the condensation reaction, a higher concentration of aldehyde in the reaction medium is available for condensation to form either the imine or enamine. Since the reaction under these conditions consumes only 66% of the alkene, it can be

concluded that the less efficient hydroformylation step influences the low production of tertiary amine under these conditions. Therefore, it can be deduced that under these conditions, the condensation and hydrogenation reactions proceed more efficiently compared to the hydroformylation reaction.

Further increasing the $CO:H_2$ partial pressure ratio to 2:3 results in the near quantitative conversion of substrate (98%) with no detectable aldehydes present in the reaction medium (Table 4.4, entry 3). The increased substrate consumption is directly correlated to the higher CO pressure, facilitating higher hydroformylation activity, while the negligible amount of aldehyde detected indicates that the condensation reaction still proceeds quantitatively. An increase in the amount of amine products is observed (65%) under these conditions with an increase in the amount of tertiary amine detected relative to the reaction carried out under the 1:4 $CO:H_2$ ratio. The higher production of tertiary amine product supports the previous speculation of the influence of the relative rates of each reaction step on the products formed. This is ascribed to the availability of the catalyst precursor for each catalytic reaction step, assuming that the active species cannot be involved in both reactions simultaneously.

Evidence for this phenomenon may be shown by the presence of amide products formed from the reductive elimination of the amine and an acyl intermediate. These amide products are not detected after reactions carried out under optimised conditions, indicating that the hydroformylation and hydrogenation reactions do not occur simultaneously. The increase in the hydrogenation rate is therefore proposed to be dependent on the concentration of substrate (imine and/or enamine) and the availability of the catalytically active species. The higher proportion of tertiary amine produced (10%) under these conditions suggests a higher relative rate of the hydroformylation reaction compared to the condensation reaction.

A lower consumption of substrate is observed for the reaction carried out under a $CO:H_2$ ratio of 1:1 (Table 4.4, entry 4) with similar amounts of imine and amine produced. In this case, only secondary amine product was detected as compared to the reaction previously described (Table 4.4, entry 3). The lower conversion obtained at the higher CO partial pressure of this reaction contradicts the previous hypothesis regarding relative rates of the hydroformylation, condensation and hydrogenation reactions. However, the comparable production of imine and amine observed suggests that the hydrogenation reaction proceeds in a similar manner under

these conditions. The exclusive production of secondary amine under these conditions indicates that up to a certain level, the relative hydrogenation rate is slowed, possibly due to the higher concentration of CO in the reaction medium. The lower substrate consumption (74%) under these conditions is therefore ascribed to some deactivation of the hydroformylation catalyst, likely due to the faster formation of amines which may coordinate to the metal centre and hinder the hydroformylation reaction.

An increase in the equivalents of the amine substrate (Table 4.4, entry 5) resulted in a decrease in the conversion to 69% with excellent conversion to specifically secondary amine product. This selectivity for secondary amine is attributed to favouring the formation of the Schiff base by Le Chatellier's principle, therefore reducing the amount of aldehyde in the reaction medium to react with the formed secondary amine. The combined data from the optimisation of the partial pressure of CO relative to H_2 suggests that for efficient hydroaminomethylation, the ratio of CO:H_2 for further experiments should be 2:3.

4.4 Performance of the optimised catalytic system while varying amine substrate

The optimised conditions and complex precursor **5** were further evaluated in the hydroaminomethylation reaction with cyclohexene while varying the amine substrate. This was carried out to determine applicability of the catalytic process in terms of sensitivity toward substrate scope for primary and secondary amines of the alkyl and aryl category.

4.4.1 The effects of primary or secondary alkyl or aryl amine substrates

The effects of varying alkyl amines were explored by reacting cyclohexene under the optimised catalytic conditions with secondary amines (piperidine and dibenzylamine) for comparison with the results obtained for n-propylamine. The results are given in Table 4.5. Comparison of the results obtained for the hydroaminomethylation of n-propylamine with piperidine (Table 4.5, entries 1 and 2) show a decrease in the conversion from 98 to 81%, while the reaction with dibenzylamine shows 97% conversion of substrate (Table 4.5 entry 3). The binding of amines to metal catalysts often results in the reduction or complete deactivation in certain reactions and as such, amines such as piperidines may be considered as poisons in some catalytic reactions.[35,36] Since some binding between the amine substrate and the catalyst precursor may

occur, the lower observed conversion for piperidine is attributed to a combination of ligation and the cyclic structure providing steric interference to the cyclohexene substrate for the hydroformylation reaction step.

Table 4.5. Comparison of the results obtained for hydroaminomethylation reactions of cyclohexene with varying alkyl amines under optimised conditions.

Entry	Amine substrate	Olefin conversion (%)	Aldehyde (%)	Imine/ enamine (%)	Amines (%)	Secondary Amine (%)	Tertiary Amine (%)
1	propylamine	98	<1	35	65	90	10
2	piperidine	81	<1	<1	99	0	100
3	dibenzylamine	97	<1	<1	99	0	100
4	dimethylamine·HCl	99	97	<1	<1	-	-

Hydroaminomethylation of cyclohexene in toluene (5 mL), 50 bar total pressure, 105˚C, reaction time of 4 h and catalyst loading of 5.74 x 10^{-3} mmol. GC conversions were obtained using an internal standard of n-decane. Total amines are composed of secondary and tertiary amines in a mixture with a percentage sum of 100. Reactions carried out in duplicate with an average error value of 3.45%.

The results obtained with dibenzylamine substrate show an increase in conversion due to free rotation of the aromatic groups which may alter the conformation to allow facile substrate binding under catalytic conditions (Scheme 4.5).

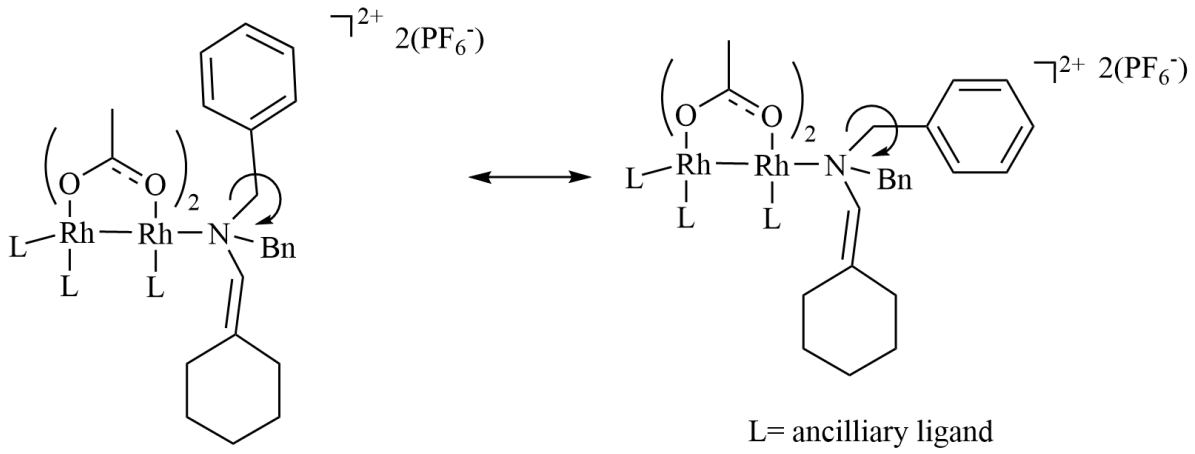

Scheme 4.5. Depiction of the steric implications of amine substrate binding to the metal complex and the proposed effects on the olefin substrate coordination for hydroformylation.

Since no imine formation is possible for the hydroaminomethylation of secondary amine substrates, the exclusive production of enamines and tertiary amine products is expected for both dibenzylamine and piperidine (Table 4.5 entries 2 and 3). The near quantitative consumption of the enamine in both cases confirms that the hydrogenation of enamine intermediates proceeds efficiently under the optimised conditions.

Furthermore, the hydroaminomethylation reaction carried out with dimethylammonium chloride shows no formation of intermediary or target amine products (Table 4.5, entry 4). This is attributed to a combination of insufficient nucleophilicity and low solubility of the salt in this form. This results in no reaction occurring with the aldehyde products under the catalytic conditions in an organic solvent such as toluene, as expected.

The applicability of the catalyst for the hydroaminomethylation of aromatic primary and secondary amines was evaluated by reacting cyclohexene with either aniline or diphenylamine. The results obtained from the reaction with aniline substrate (Table 4.6, entry 1) shows a substantial reduction in the olefin conversion (57%) and the hydrogenation capability, with 9% amine product formed. This is attributed to the deactivation of the active catalyst by the coordination of aniline coupled with lower nucleophilicity due to delocalisation of the lone pair by the aromatic ring. An increase in the conversion (98%) of olefin is observed for the reaction carried out with diphenylamine substrate (Table 4.6, entry 2), with 87% aldehyde observed.

Table 4.6. Comparison of the results obtained for hydroaminomethylation reactions of cyclohexene with varying aryl amines under optimised conditions.

Entry	Amine substrate	Olefin conversion (%)	Aldehyde (%)	Imine/ enamine (%)	Amines (%)	Secondary Amine (%)	Tertiary Amine (%)
1	aniline	57	<1	<1	9	>99	0
2[a]	diphenylamine	98	87	<1	13	0	>99

Hydroaminomethylation of cyclohexene in toluene (5 mL), 50 bar total pressure, 105˚C, reaction time of 4 h and catalyst loading of 5.74 x 10^{-3} mmol. GC conversions were obtained using an internal standard of n-decane. Total amines are composed of secondary and tertiary amines in a mixture with a percentage sum of 100. Reactions carried out in duplicate with an average error value of 2.53%.

[a] Reaction mixture analysed by LC-MS.

This result is ascribed to a further decrease in nucleophilicity, and steric implications of both phenyl groups bonded directly to the nitrogen atom which results in a significantly reduced poisoning effect of the catalyst in the hydroformylation step. Furthermore, this reduction in nucleophilicity was found to directly affect the efficiency of the condensation step, seen by the 87% aldehyde product observed. This is further supported by the observed formation of the proposed tertiary amine product, at a low level of 13%. The results obtained from experiments varying the amine substrate indicate good applicability of primary and secondary aliphatic amines with a lower conversion ability for the aromatic amine substrates under these conditions.

4.5 Performance of the optimised catalytic system with various olefin substrates

Further hydroaminomethylation reactions were carried out by varying the olefin substrate to styrene, cyclohex-2-en-1-one and cyclohex-2-en-1-ol. This was carried out to determine any factors which may affect the catalytic reaction outcome and product distributions relating to the nature of the substrate.

4.5.1 The hydroaminomethylation of Styrene

The hydroformylation of styrene described in Chapter 3 showed the formation of both the linear and branched aldehyde products under the optimised reaction conditions. It is expected that increasing the number of aldehyde products may result in the formation of multiple imines and/or enamines formed and their associated hydrogenation products, particularly for primary amine substrates (Scheme 4.6, *overleaf*).

The results obtained show near quantitative conversion of the alkene substrate with high production of amine products, indicating a highly efficient overall transformation of the substrates into the target amine products. Interestingly, the reaction which utilised n-propylamine as the amine substrate showed the greatest regioselectivity, with near quantitative conversion of branched product detected (Table 4.7, entry 1).

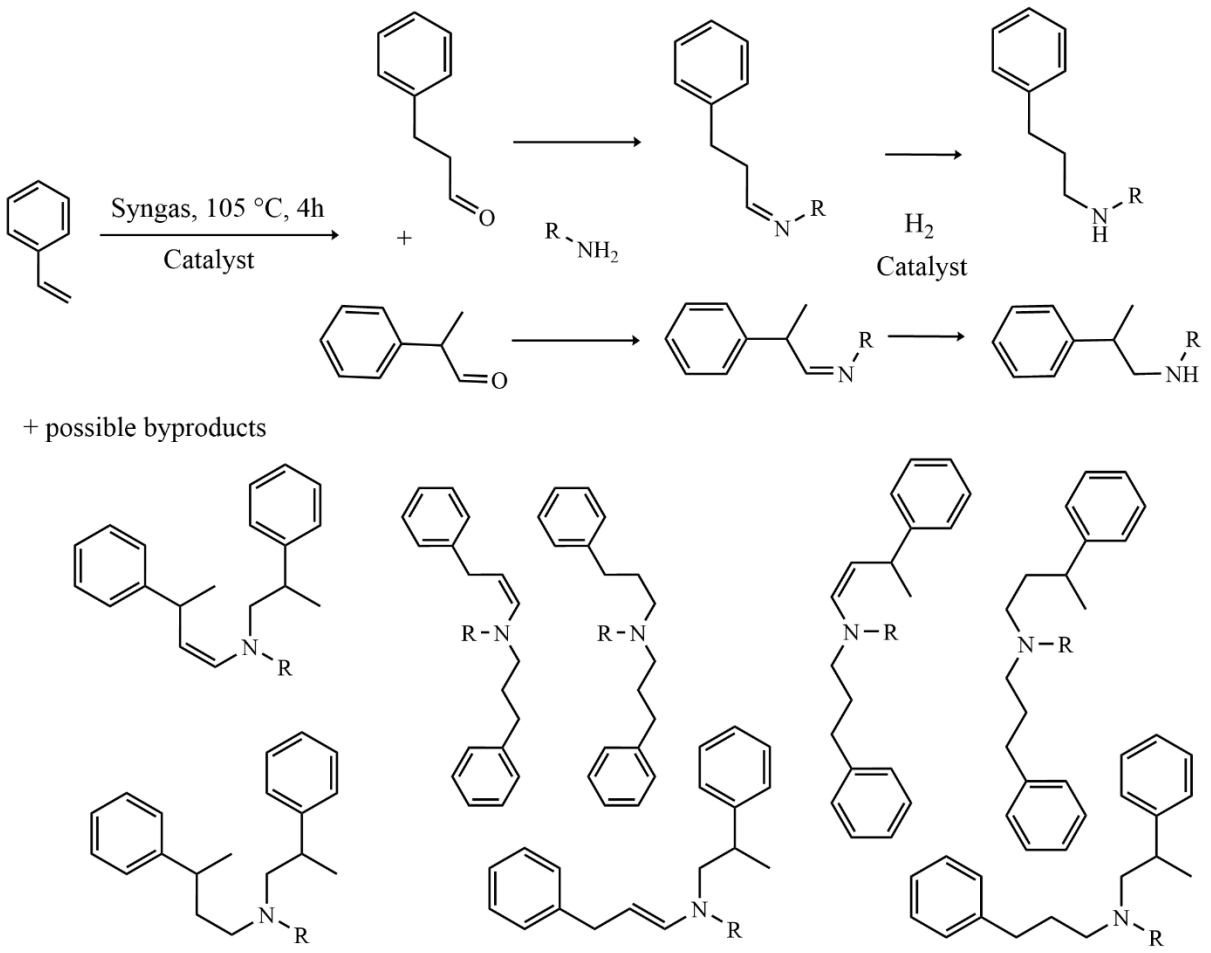

Scheme 4.6. Depiction of the possible product formation of the hydroaminomethylation of styrene with a primary amine and the possible byproducts from reactions of the target secondary amines with the aldehyde intermediates.

The higher proportion of branched product produced under these conditions is attributed to the higher reaction temperature compared to the previously reported hydroformylation of styrene, favouring formation of the branched aldehyde. The near quantitative consumption of the aldehyde and the selectivity for branched secondary amine product can be attributed to a balance in the formation of the imine with the branched aldehyde relative to the hydrogenation step.

This reduces the possibility of extraneous reactions occurring between the formed secondary amine and the aldehyde hydroformylation products. In this example, a product incorporating the phenylethylamine motif is obtained. This class of compound are known to have biological applications, suggesting that this reaction may be used to produce valuable compounds of pharmaceutical relevance. Further analysis and verification were carried out by ^{1}H-NMR

(Appendix, Figure A11) and LC-MC analysis where the expected proton signals corresponding to the branched secondary amine was observed. The obtained mass spectral data shows a base peak at *m/z* = 178.2, corresponding to an $[M+H]^+$ protonated molecular ion (Appendix, Figure A12).

Table 4.7. Results obtained for the hydroaminomethylation reactions of styrene with propylamine or piperidine under optimised conditions.

Entry	Amine substrate	Olefin conversion (%)	Aldehyde (%)	Imine/ enamine (%)	Amines (%)	Secondary Amine (%)	Tertiary Amine (%)
1	propylamine	99	<1	<1	>99	<1 (lin) >99 (br)	-
2	piperidine	99	<1	<1	>99	-	15 (lin) 85 (br)

Hydroaminomethylation of cyclohexene in toluene (5 mL), 50 bar total pressure, 105˚C, reaction time of 4 h and catalyst loading of 5.74 x 10^{-3} mmol. GC conversions were obtained using an internal standard of n-decane. Total amines are composed of secondary and tertiary amines in a mixture with a percentage sum of 100. Reactions carried out in duplicate with an average error value of 2.53%.

The data obtained for the reaction carried out with piperidine (Table 4.7, entry 2) shows lower regioselectivity toward the branched products, with an observed 85% formation of the branched tertiary amine product. This is attributed to the presence of the piperidine during the hydroformylation reaction exerting larger steric influence in the condensation reaction with the branched aldehyde, increasing the formation of linear product. Theoretically, the comparative steric influence of n-propylamine would be significantly lower, supporting the regioselectivity observed the reaction carried out with n-propylamine. The combination of the observed data shows that the product distribution of the hydroaminomethylation of styrene can be suitably influenced by the nature of the amine and the reaction conditions to produce target amine products in good to excellent yields.

Separation of the mixture *via* column chromatography and subsequent analysis shows the expected signals in the ^{1}H-NMR spectra collected for both the linear and branched products (Appendix, Figures A13 and A14), with base peaks observed at *m/z* = 204.2 in the LC-MS spectra for each respective product corresponding to the $[M+H]^+$ protonated molecular ion (Appendix, Figures A15 and A16). This shows that the hydroaminomethylation reaction may

be used to produce compounds from the phenylethylamine class with good selectivity, provided a suitable substrate is utilised.

4.5.2 The hydroaminomethylation of cyclohex-2-en-1-one and cyclohex-2-en-1-ol

Further probing into the effect of the substrate nature on the product distribution was carried out by applying the catalytic system to substrates cyclohex-2-en-1-one and cyclohex-2-en-1-ol in hydroaminomethylation reactions with piperidine. Due to the unsymmetrical nature of the alkenes in this case, addition of the formyl group in the hydroformylation step is expected to produce two possible aldehydes, thereby introducing the possibility of regioisomers. The results are shown in Table 4.8.

Table 4.8. Results obtained for the hydroaminomethylation reactions of cyclohex-2-en-1-ol and cyclohex-2-en-1-one with piperidine under optimised conditions with complex **5** as a catalyst precursor.

Entry	Cyclic olefin substrate	Olefin conversion (%)	Aldehyde (%)	Imine/ enamine (%)	Amines (%)	Secondary amine (%)	Tertiary amine (%)
1	cyclohex-2-en-1-ol	91	<1	5	95	-	100 (α-product)
2[a]	cyclohex-2-en-1-one	99	<1	mixture of difunctionalised enamine and amine products			

Hydroaminomethylation of cyclohexene in toluene (5 mL), 50 bar total pressure, 105˚C, reaction time of 4 h and catalyst loading of 5.74 x 10^{-3} mmol. GC conversions were obtained using an internal standard of n-decane. Total amines are composed of secondary and tertiary amines in a mixture with a percentage sum of 100. Reactions carried out in duplicate with an average error value of 2.53%.

[a] Reaction mixture analysed by LC-MS.

High conversion of the olefin was observed for the reaction carried out with cyclohex-2-en-1-ol (91%) with near quantitative consumption of the cyclohex-2-en-1-one substrate observed at 99% (Table 4.8, entries 1 and 2). This suggests that the catalyst may be used to good effect on substrates containing ketones and alcohol groups. No observed aldehyde was detected for the reactions of either substrate, however, the results for cyclohex-2-en-1-ol present a conversion to 95% amine product and 100% α-product formed. This is supported by the obtained NMR and mass spectral data (Appendix, Figures A17 and A18) the latter showing a base peak at *m/z* = 198.2 corresponding to the $[M+H]^+$ protonated molecular ion. Should both regioisomers be

present, this would present with two signals in the LC chromatogram with the same corresponding masses and diagnostic proton signals corresponding to both regioisomers. The regioselectivity can be rationalised by the presence of the hydroxyl group, which may coordinate to the bimetallic core resulting in directing the formation of the α metal-acyl intermediate to form the corresponding aldehyde. The subsequent reactions steps would then result in the regioselectivity observed. Conversely, the reaction carried out with cyclohex-2-en-1-one showed multiple products formed, with the mass spectral analysis indicating the mixture of condensation products occurring at the ketone and aldehyde functionalities under catalytic conditions.

The combined data shows that the regioselectivity may be influenced by directing groups through speculated interactions of the hydroxyl group leading to the bimetallic core, leading to the formation of only one aldehyde isomer with low sensitivity of the hydrogenation reaction toward the presence of an OH substituent on the substrate.

4.6 The application of the catalyst system toward the synthesis of analogues of Tramadol® *via* hydroaminomethylation

The data obtained from the optimisation and substrate variation of the hydroaminomethylation reaction suggest that the catalyst precursor and the conditions may be exploited for the synthesis of a suitable active pharmaceutical ingredient (API). Typically, the addition of a formyl group followed by a reductive amination cascade may provide a synthetic pathway to obtaining opioid-class analgesics such as Fentanyl®, Tapentadol® and Tramadol® through a catalytic process (Figure 4.3, *overleaf*).[37-39] Tramadol® is a class IV scheduled substance used for short term relief from moderate to severe pain, and is widely used due to a less addictive drug profile compared to codeine and morphine.[39]

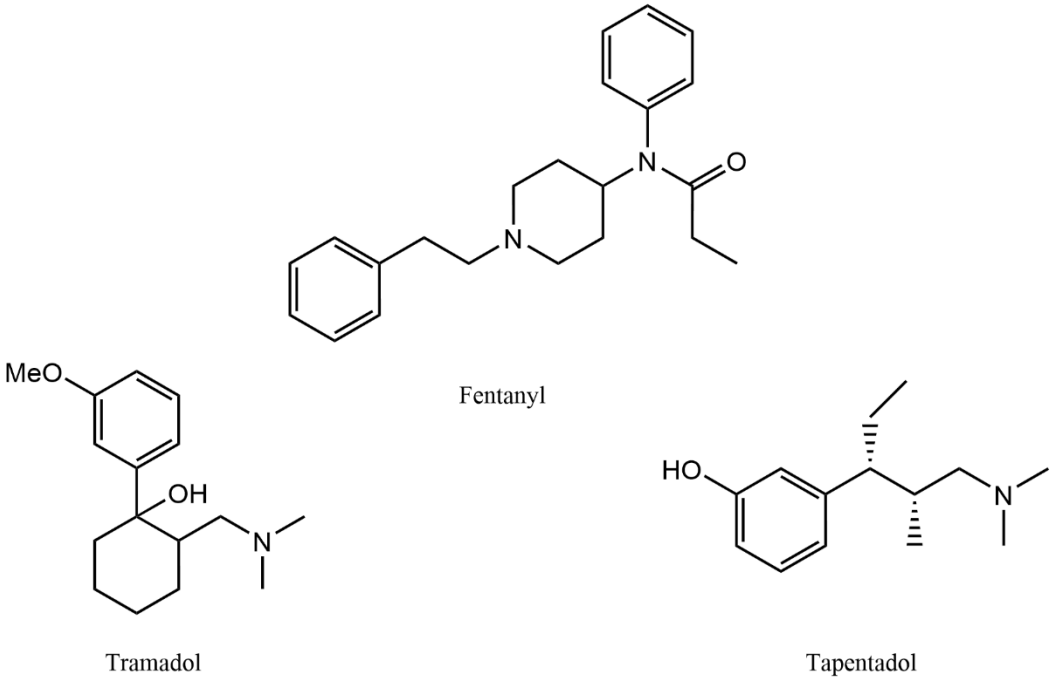

Figure 4.3. Examples of the molecular structures of a few opioid class analgesics which may be obtained by incorporating catalytic hydrogenation or hydroaminomethylation reactions as key steps.

A synthetic route has been reported by Alvarado and co-workers following a multistep protocol with harsh reagents, incorporating no catalytic reactions. Firstly, a Mannich condensation reaction of the suitable amine to cyclohexanone is described, followed by addition of the methoxy benzene moiety *via* an organolithium reagent to the resulting ketone.[39] The crystallisation to form the hydrochloride ammonium salt may be carried out by crystallisation in HCl/ether in an additional step. If dimethylammonium hydrochloride is used as the amine reagent, the hydrochloride salt may be formed in fewer steps.[40]

The direct formation of an active pharmaceutical in this class catalytically is economically and environmentally beneficial and may significantly reduce by-product formation and the cost of production. Furthermore, mitigation of the harsh reaction conditions and time associated with stoichiometric synthetic procedures and extraneous purification is often an advantage associated with catalytic reactions. An analogue of Tramadol®, 1-phenyl-2-(piperidin-1-ylmethyl)cyclohexan-1-ol, was retro-synthetically analysed and suitable synthons were identified as illustrated in Scheme 4.7.

The first disconnection shows that the hydroaminomethylation of a suitable substrate, 3,4-dihydro-[1,1'-biphenyl]-1(2H)-ol, with piperidine could be used as a final key step for obtaining the proposed tramadol analogue. Further analysis of the olefin shows that this synthon may be obtained in a Grignard reaction between bromobenzene and cyclohex-2-en-1-one. Since the hydroaminomethylation of cyclohex-2-en-1-one resulted in the formation of multiple products, the addition of the phenyl group and the subsequent formation of the hydroxy substituent after the Grignard addition reaction should reduce the formation of multiple products.

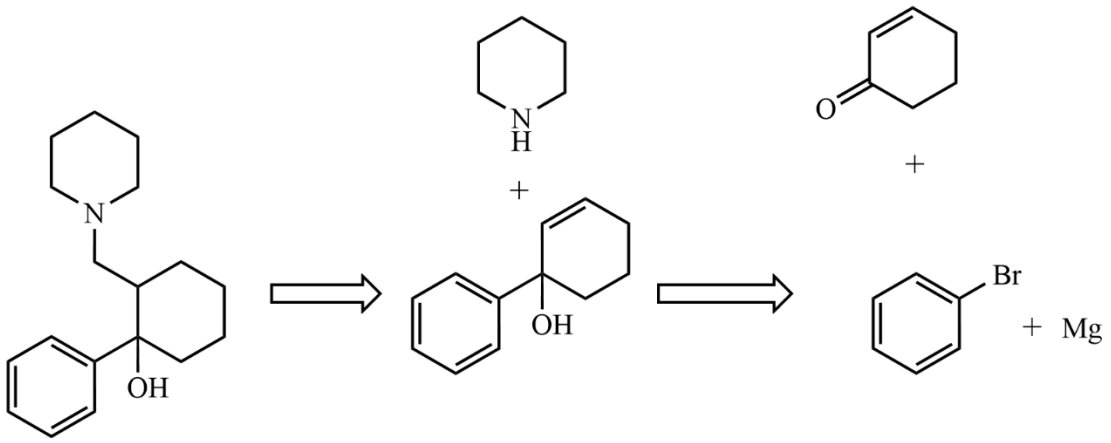

Scheme 4.7. Retro-synthetic analysis and identification of possible synthons for the synthesis of 1-phenyl-2-(piperidin-1-ylmethyl)cyclohexan-1-ol using hydroaminomethylation as a key step.

Furthermore, as was observed for the hydroaminomethylation of cyclohex-2-en-1-ol, the regioselectivity of this reaction should be directed by the presence of the hydroxy group to favour the α-substituted regio-isomer. Therefore, the proposed route for the synthesis of the analogue requires the synthesis of the 3,4-dihydro-[1,1'-biphenyl]-1(2H)-ol olefin (**S1**) as a substrate.

*4.6.1 Synthesis and characterisation of precursor olefin substrate (**S1**)*

The proposed substrate was synthesised *via* a Grignard addition reaction between cyclohex-2-en-1-one and bromobenzene in the presence of Mg, catalytic I_2 and using THF as a solvent.[41] It is widely accepted that ethereal solvents such as THF stabilise the formed magnesium alcoholate, which allows for the alkyl or aryl transfer through either a polar or radical type

mechanism.[42] The desired product is then obtained after protonation of the alkoxide and subsequent purification by column chromatography. The overall reaction outline is given in Scheme 4.8, and the resulting product **S1** was obtained as a light yellow crystalline solid in a moderate yield of 61%.

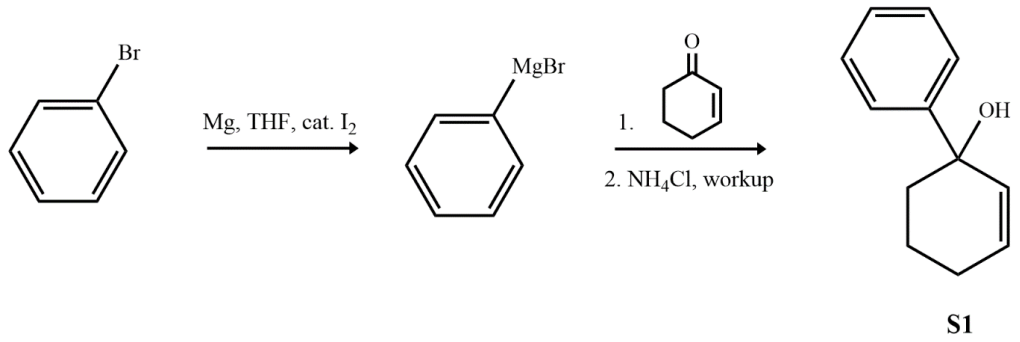

S1

Scheme 4.8. Reaction outline for the formation of 3,4-dihydro-[1,1'-biphenyl]-1(2H)-ol by a Grignard addition reaction between bromobenzene and cyclohex-2-en-1-one.

Analysis of the obtained ^{1}H-NMR spectrum (Figure 4.4, *overleaf*) confirms the proposed structure, with the aromatic protons integrating for a total of 5H relative to the 1H integration for each olefin proton. The broad signals resonating in the 2.5 to 1.7 ppm region integrating for a combined 6H, agrees with the aliphatic protons in the proposed structure, with a broad signal resonating at around 1.6 ppm ascribed to residual H_2O from the workup procedure. The former broadening of these signals is ascribed to conformational differences in the half-chair molecular structure, averaging out the explicit axial and equatorial proton signals over the NMR timescale. The presence of the olefin proton signals supports the chemoselectivity of the Grignard reaction for the ketone functionality in this case, whereby addition to the carbonyl group over the alkene is observed.

Further analysis by LC-MS indicates a purity of 95.15% and shows a base peak at *m/z* = 157.2 assigned to the $[M\text{-}OH]^+$ molecular ion (Appendix, Figure A19). This agrees with the ^{1}H-NMR data and confirms the proposed structure for use as a substrate for the hydroaminomethylation reaction.

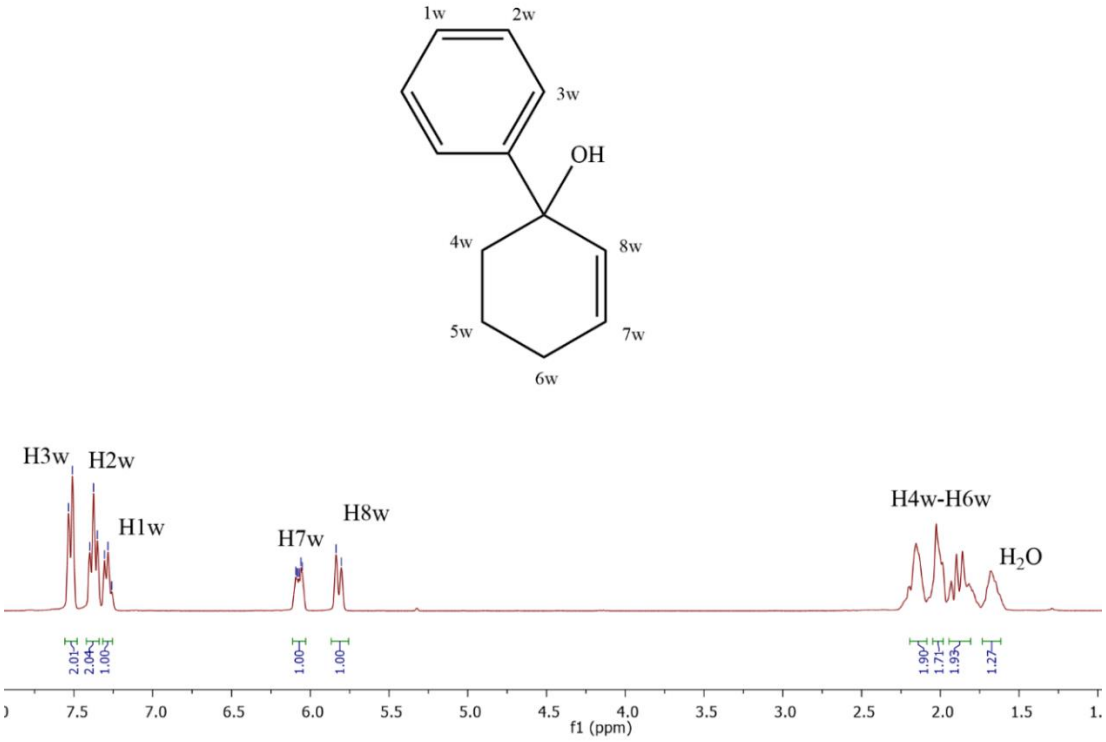

Figure 4.4. ^{1}H-NMR spectrum obtained for **S1** recorded in $CDCl_3$.

4.6.2 Hydroaminomethylation as a key step toward the synthesis of Tramadol® analogues

The hydroaminomethylation of the synthesised substrate (**S1**) was carried out with piperidine and dibenzylamine as amine substrates to afford two analogues of Tramadol®, using complex **5** as a catalyst precursor. Since no amine products were observed in the initial model reaction with dimethylammonium chloride, the inclusion of the dibenzyl group may be subsequently reduced to form the amine moiety through Pd/C hydrogenolysis.[31]

Furthermore, the inclusion of the additional phenyl groups on dibenzylamine offers further evaluation of the steric parameters which may hinder formation of the desired product due to interaction with the phenyl substituent on the olefin substrate. After the reaction was completed, the solvent was evaporated before analysis of the crude mixture was carried out by LCMS. The data obtained after reactions with both amine substrates is given in Table 4.9, with structures shown in Figure 4.5 (*overleaf*).

Table 4.9. Results obtained for the hydroaminomethylation reactions of the synthesised substrate (**S1**) with piperidine or dibenzylamine under optimised conditions.

Entry	Amine substrate	Conversion (%)	Target product (%)	Regio-isomer ratio α : β
1	piperidine	99	74	4:1
2	dibenzylamine	51	36	3:1

Hydroaminomethylation of **S1** in toluene (5 mL), 50 bar total pressure, 105˚C, reaction time of 4 h and catalyst precursor (complex **5)** at a loading of 5.74 x 10^{-3} mmol. Reactions carried out in duplicate with an average error value of 4.75%. Reaction mixtures analysed by LC-MS.

The chromatogram obtained for **S1** shows a peak at a retention time of 0.915 min with the corresponding mass, which was used to determine the conversion of the substrate by LC-MS analysis. The observed yields for reactions carried out with **S1** and piperidine or dibenzylamine indicates that under catalytic conditions, the piperidine analogue (**P11**) was obtained in a 74% yield (*m/z* = 274.2), while the reaction with dibenzylamine yielded the target product (**P12**) in a lower 36% yield (*m/z* = 386.2) (Appendix, Figure A20 and A21). This is attributed to steric interactions of the large dibenzyl group with the phenyl substituent on the substrate, hindering the formation of the enamine intermediate under these conditions.

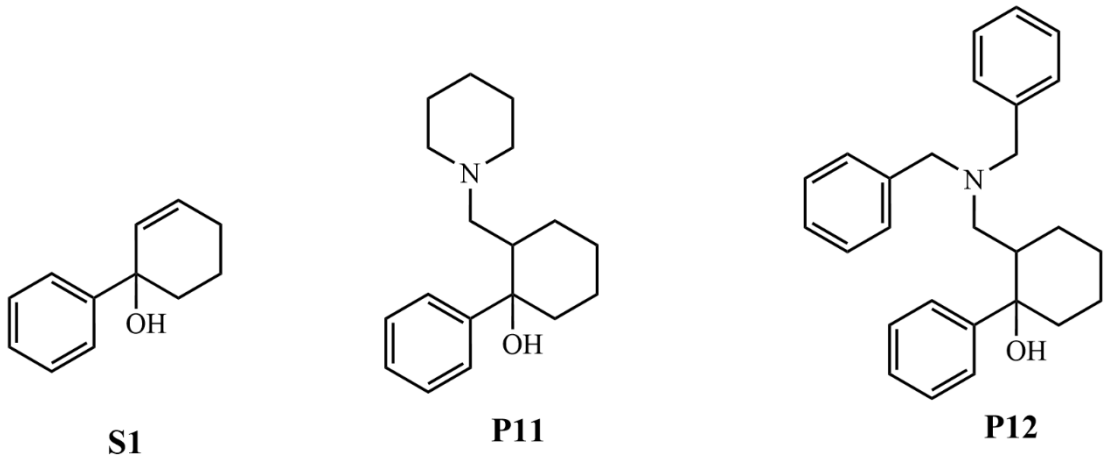

S1 **P11** **P12**

Figure 4.5. Representation of the structures of **S1**, **P11** and **P12**.

In both cases, crystallisation of the products with HCl/ether and subsequent product analysis resulted in LC-MS data which exclusively shows the expected signals at *m/z* = 274.2 and 386.2 for the $[M+H]^+$ protonated molecular ions, confirming the data obtained from crude mixture analysed. Furthermore, mass spectral analysis indicates two base peaks with *m/z* corresponding

to the target products at different retention times. This is attributed to the formation of regio-isomers, calculated as a ratio of 4:1 and 3:1 in favour of the product substituted α- to the hydroxyl substituent, for reactions carried out with piperidine and dibenzylamine respectively.

Since some coordination of the amine to the active catalyst is expected during the reaction, this suggests that the regioselectivity and product production is due to steric implications of the large dibenzyl group, unfavourably interacting with the phenyl substituent on the substrate, not seen for the reaction carried out with piperidine. Compared to the reaction carried out with piperidine and cyclohex-2-en-1-ol where only the α-substituted product was detected, this suggests that the presence of the phenyl group plays a steric role in directing the regioselectivity.

4.7 Summary

The extension on further application of the synthesised dirhodium(II,II) acetato-bipyridyl chelate complexes to the hydroaminomethylation reaction was achieved by determining the conditions required for catalytic hydrogenation of imines. The optimisation of the catalytic conditions was explored using a model reaction with complex **1** as a catalyst precursor showing that under catalytic conditions, the *in-situ* formation of the model imine complex occurs readily between 85 and 115 °C. Additionally, a temperature dependent increase in the hydrogenation was observed resulting in a maximum occurring at 105 °C indicating the optimal reaction temperature. A reaction carried out in the absence of the catalyst precursor shows no detectable hydrogenation product with full consumption of the substrate, confirming that the catalyst precursor is required for hydrogenation. Exchange of the acetate counter ion for the hexafluorophosphate congener (complex **4**) resulted in a 17% increase in amine product production. Further evaluation of the complexes revealed the highest production of amine at 68% at 105 °C, 40 bar total pressure and 4h reaction time at 0.08 mol% catalyst loading was achieved for the trifluoromethyl-substituted complex (**5**).

The hydroaminomethylation model reaction carried out with cyclohexene and n-propylamine as substrates was further optimised by altering the partial pressure of CO relative to H_2 in the syngas mixture. The data indicated the importance of the CO:H_2 ratio on both the hydroformylation and hydrogenation capabilities, culminating in the highest amine production at a 2:3 ratio of CO:H_2 with a total pressure of 50 bar. The evaluation of aliphatic primary and

secondary amines showed good conversion, with low conversion of aromatic amines or ammonium salts to the target products. The olefin substrate scope was varied (styrene, cyclohex-2-en-1-one, cyclohex-2-en-1-ol) and showed good applicability and selectivity except in the reaction with cyclohex-2-en-1-one, which resulted in the formation of bis-substituted amine and enamine product mixtures. The application was then extended toward the synthesis of two analogues of Tramadol®, using the hydroaminomethylation reaction as a key step. Retrosynthetic analysis of the products and synthesis of the required substrate *via* a Grignard addition reaction of bromobenzene and cyclohex-2-en-1-one afforded the substrate (**S1**) in good yield with excellent purity. The hydroaminomethylation of **S1** with piperidine or dibenzylamine resulting in the target compounds formed in moderate (74%) and low (36%) yields respectively, with distributions in regio-isomers correlated to the steric bulk of the amine substrate and the presence of the hydroxyl group.

4.8 Experimental details

4.8.1 General information

All chemicals/reagents were purchased from Merck and used without purification unless stated otherwise. Solvents of analytical grade were used as received or freshly distilled, where necessary, and were stored over molecular sieves. All reactions were carried out under Ar or N_2 inert conditions, prepared using standard Schlenk line techniques.

4.8.2 Equipment and instrumentation

Nuclear magnetic resonance (NMR) spectra were recorded on a Varian Mercury 300 (^{1}H: 300.08 MHz) spectrometer and were recorded using tetramethylsilane (TMS) as the internal standard. Coupling constants are reported in Hz and chemical shifts are reported in ppm relative to residual solvent signals. Analysis of the hydroaminomethylation samples of reactions were carried out on a Perkin Elmer Clarus 580 GC equipped with a flame-ionisation detector (FID) or an analytical Agilent HPLC 1260 equipped with an Agilent infinity diode array detector (DAD) 1260 UV-Vis detector, with an absorption wavelength range of 210 – 640 nm. The compounds were eluted using a mixture of solvent A (10 mM NH_4OAc/H_2O) and solvent B (10 mM NH_4OAc/MeOH) at a flow rate of 0.9 mL min^{-1}. The gradient elution conditions were as follows: 10% solvent B from 0 - 1 min, 10 – 95% solvent B from 1 - 3 min, 95% solvent B from 3 - 5 min. Mass spectrometry was carried out using Electron Impact (EI) on a JEOL

GCmatell instrument or using a Waters Synapt G2 equipped with an ESI probe with data recorded in positive mode. The reaction products were confirmed in relation to authenticated standards.

4.8.3 General methods for hydrogenation and hydroaminomethylation reactions

Hydrogenation reactions were carried out in stainless steel pipe reactors (90 mL) equipped with a Teflon-coated magnetic stirrer bar. Each reactor was charged with toluene (5 mL), benzaldehyde, 4-nitrobenzaldehyde or 4methoxy benzaldehyde (7.2 mmol), propylamine (7.2 mmol), internal standard n-decane (1.26 mmol) and catalytic precursor (2.87×10^{-3} mmol). The pipe reactor was purged with nitrogen three times, followed by purging with hydrogen (40 bar) three times followed by heating to the required temperature. All reactions were performed in duplicate or triplicate and are recorded as an average of 3 identical experiments.

Hydroaminomethylation reactions were carried out in stainless steel pipe reactors (90 mL) equipped with a Teflon-coated magnetic stirrer bar. Each reactor was charged with toluene (5 mL), olefin substrate (7.2 mmol), amine substrate (7.2 mmol), internal standard n-decane (1.26 mmol) and catalytic precursor (5.74×10^{-3} mmol). The pipe reactor was purged with nitrogen three times, followed by purging with syngas corresponding to a partial pressure ratio of (2:3, $CO:H_2$) three times. The reactors were then heated to the required temperature whilst stirring for 4 hours. All reactions were performed in duplicate and are recorded as an average of two identical experiments.

*4.8.4 Synthesis of reference imine and amine compounds for the hydrogenation model reaction and the synthesis of 3,4-dihydro-[1,1'-biphenyl]-1(2H)-ol (**S1**)*

4.8.4.1 n-Propylbenzylimine [43]

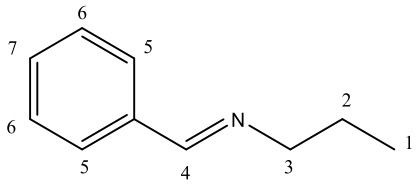

To a 50 cm^3 round bottomed flask was added $MgSO_4$ (0.300 g) and CH_2Cl_2 (5 mL) The flask was then charged with benzaldehyde (0.197 g, 1.86 mmol) and *n*-propylamine (0.100 g, 1.69 mmol). The reaction mixture was stirred at ambient temperature for 17 hr. The mixture was

diluted to 20 mL, filtered, and washed with deionised H_2O (3 x 20 mL). The organic layer was collected and dried over $MgSO_4$ and filtered by gravity, washing with an additional 20 mL CH_2Cl_2. The solvent was removed under reduced pressure and the residue dried *in vacuo* to produce a yellow oil. **Yield**: 0.087 g (0.587 mmol, 34 %) **^{1}H NMR (400 MHz, DMSO-*d*$_6$)**: δ (ppm) = 8.32 (1H, s, H_4), 7.74-7.72 (2H, m, H_6), 7.44-7.42 (3H, m, H_7, H_5), 3.52 (2H, t, ^3J = 6.8 Hz, H_3), 1.63 (2H, sxt, ^3J = 7.1 Hz, H_2), 0.89 (3H, t, ^3J = 6.8 Hz, H_1). **IR (ATR)**: (ν max/ cm^{-1}) 1646 (C=N), 1542 (C_{Ar}-N). **Purity**: 98.86% by LC (t_R = 0.57 min). **MS (EI, m/z)**: 148.1 (35%, $[M]^+$), calculated 148.0.

4.8.4.2 n-Propylbenzylamine [43]

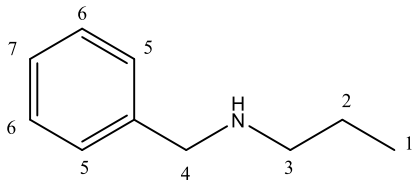

A round bottomed flask equipped with magnetic stirrer bar was charged with a solution of benzaldehyde (0.197 g, 1.86 mmol) in dry dichloromethane (5 mL) and anhydrous magnesium sulfate (0.300 g). A solution of N-propylamine (0.100 g, 1.67 mmol) in dry dichloromethane (5 mL) was added dropwise while to the mixture while stirring. The reaction mixture was stirred at ambient temperature for 16 hours. The reaction mixture was filtered by gravity and the solid washed with dichloromethane (3 x 5 mL). The solvent was removed under reduced pressure and the residue was dried under vacuum for 1 hour. The flask was then purged with vacuum and filled with N2 in three cycles. Dry methanol (10 mL) was added to the flask under inert atmosphere. The reaction vessel was submerged in an ice bath before sodium borohydride (0.100 g, 2.63 mmol) was slowly added. The reaction mixture was stirred for 12 hours. The reaction was quenched with cold deionised H_2O (15 mL) and the resulting mixture was extracted using dichloromethane (20 mL) before washing the organic layer with deionised water (3 x 30 mL). The organic fraction was collected and dried over anhydrous magnesium sulfate. The mixture was filtered, washed with dichloromethane (20 mL) before reducing the filtrate volume under reduced pressure. The resulting residue was dried under vacuum to afford a viscous yellow oil. **Yield**: 0.067 g (0.47 mmol, 28 %). **^{1}H NMR (400 MHz, DMSO-*d*$_6$)**: δ (ppm) = 7.33-7.19 (5H, m, H_5-H_7), 3.67 (2H, s, H_4), 2.43 (2H, t, ^3J = 7.1 Hz, H_3) 1.46-1.38 (2H, m, H_2), 0.86 (3H, t, ^3J = 6.8 Hz, H_1). **IR (ATR)**: (ν max/ cm^{-1}) 3328 (N-H).

*4.8.4.3 3,4-Dihydro-[1,1'-biphenyl]-1(2H)-ol (**S1**)* [44]

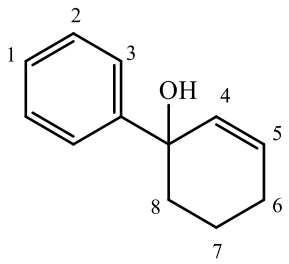

A round bottomed flask equipped with magnetic stirrer bar was charged with anhydrous THF (50 mL) to which magnesium (0.845 g, 34.1 mmol) was added whilst flushing with continuously with N_2. The flask was then heated to 40 °C following the addition of bromobenzene (2.00 g, 12.7 mmol) followed by I_2 (0.032 g, 0.13 mmol) before heating to 60 °C and stirring continuously for 30 min. A colour change in the solution was observed, from yellow to dark brown. To this stirring mixture was added cyclohex-2-en-1-one (1.11 g, 11.5 mmol) dropwise after which the reaction was removed from the heating mantle and stirred continuously for an additional 2 hours. After this period, a change in the colour of the solution was observed from dark brown to yellow. The reaction mixture was quenched by the addition of NH_4Cl (30 mL). The THF was removed under reduced pressure and the organic components extracted using CH_2Cl_2 (3 x 30 mL), before washing with deionised H_2O (3 x 30 mL). The organic layer was dried over anhydrous $MgSO_4$ before filtering the mixture and the excess solvent removed by rotary evaporation. The resulting residue was purified by column chromatography (100 % CH_2Cl_2, R_f = 0.55) before drying under vacuum to produce a pale yellow solid. **Yield**: 0.988 g (5.67 mmol, 61 %). **Melting Point**: 43.4-43.8 °C. **^{1}H NMR (400 MHz, $CDCl_3$)**: δ (ppm) = 7.48 (2H, d, ^3J = 7.0 Hz, H_3), 7.33 (2H, t, ^3J = 7.1 Hz, H_2), 7.25 (1H, d, ^3J = 8.3 Hz, H_1), 6.02 (1H, d, ^3J = 9.9 Hz, H_4), 5.78 (1H, d, ^3J = 9.9 Hz, H_5) ,2.42-1.84 (6H, m, H_6-H_8). **IR (ATR)**: (ν max/ cm^{-1}) 3102 (O-H), 1321 (C=C). **Purity**: 95.19% by LC (t_R = 0.915 min). **MS (EI, m/z)**: 157.2 (100 %, $[M\text{-}OH]^+$), calculated 157.1.

4.8.5 Further characterization of hydroaminomethylation products

*4.8.5.1 N-(Cyclohexylmethyl)propan-1-amine (**P1**)* [45]

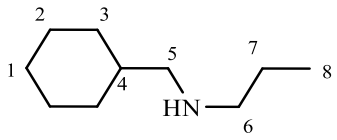

Cyclohexene (7.2 mmol) was reacted with n-propylamine (7.2 mmol) in toluene at 105 °C for 4 hours under catalytic conditions. The product was isolated by column chromatography (100% CH_2Cl_2, R_f = 0.55) before drying under vacuum to produce a clear oil. **^{1}H NMR (300 MHz, $CDCl_3$)**: δ (ppm) = 2.53 (2H, t, ^3J = 7.2 Hz, H_6), 2.41 (2H, d, ^3J = 6.6 Hz, H_5), 1.78-1.64 (4H, m, H_3), 1.55-1.45 (4H, m, H_2), 1.30-1.18 (3H, m, ^3J, H_1, H_7) ,0.95-0.81 (4H, m, H_4,H_8). **IR (ATR)**: (ν max/ cm^{-1}) 3280 N-H. **LC**: t_R = 0.528 min. **MS (EI, m/z)**: 156.2 (100 %, $[M+H]^+$), calculated 156.1.

*4.8.5.2 N,N-Bis(cyclohexylmethyl)propan-1-amine (**P2**)*

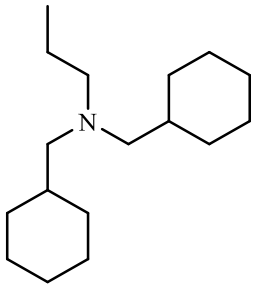

Cyclohexene (7.2 mmol) was reacted with n-propylamine (7.2 mmol) in toluene at 105 °C for 4 hours under catalytic conditions. **LC**: t_R = 0.855 min. **MS (EI, m/z)**: 252.2 (100%, $[M+H]^+$), calculated 251.2.

*4.8.5.3 1-(Cyclohexylmethyl)piperidine (**P3**)* [25]

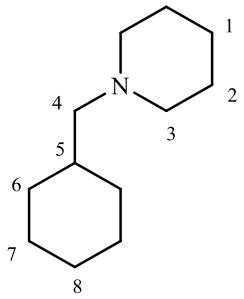

Cyclohexene (7.2 mmol) was reacted with piperidine (7.2 mmol) in toluene at 105 °C for 4 hours under catalytic conditions. Product was isolated by column chromatography (0 to 5% MeOH:CH_2Cl_2) before drying under vacuum to produce a viscous clear oil. **^{1}H NMR (300 MHz, $CDCl_3$)**: δ (ppm) = 2.31 (4H, s, H_3), 2.07 (2H, d, ^3J = 6.8 Hz, H_4), 1.83-1.28 (15H, m, H_1, H_2, H_5-H_7) ,0.85 (2H, m, H_4,H_8). **IR (ATR)**: (ν max/ cm^{-1}) 3280 N-H. **LC**: t_R = 0.418 min). **MS (EI, m/z)**: 182.2 (100 %, $[M+H]^+$), calculated 181.2.

*4.8.5.4 N,N-Dibenzyl-1-cyclohexylmethanamine (**P4**)* [46]

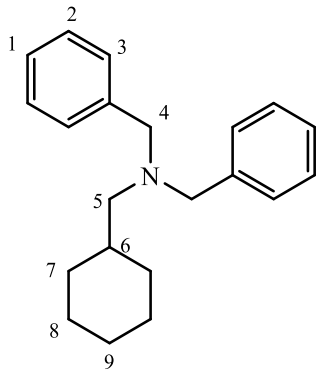

Cyclohexene (7.2 mmol) was reacted with dibenzylamine (7.2 mmol) in toluene at 105 °C for 4 hours under catalytic conditions. The product was isolated by column chromatography (100 % CH_2Cl_2, R_f = 0.11) before drying under vacuum to produce a pale yellow solid. **^{1}H NMR (300 MHz, $CDCl_3$)**: δ (ppm) = 7.40-7.12 (10H, m, H_1-H_3), 3.54 (4H, s, H_4), 2.21 (2H, d, ^3J = 6.8 Hz , H_5), 1.87 (1H, d, ^3J = 12.9 Hz , H_6), 1.65 (4H, m, H_7) 1.40-1.11 (4H, m, H_8) 0.77 (2H, m, H_9). **IR (ATR)**: (ν max/ cm^{-1}) 3280 N-H. **LC**: t_R = 0.884 min. **MS (EI, m/z)**: 294.3 (100%, $[M+H]^+$), calculated 293.2.

*4.8.5.5 N-(Cyclohexylmethyl)aniline (**P5**)* [46]

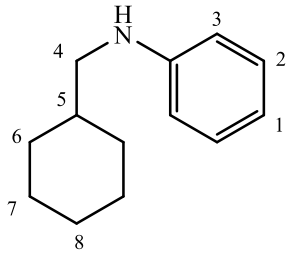

Cyclohexene (7.2 mmol) was reacted with aniline (7.2 mmol) in toluene at 105 °C for 4 hours under catalytic conditions. **LC**: 9% t_R = 1.091 min. **MS (EI, m/z)**: 190.2 (100%, $[M+H]^+$), calculated 189.2.

*4.8.5.6 N-(Cyclohexylmethyl)-N-phenylaniline (**P6**)* [46]

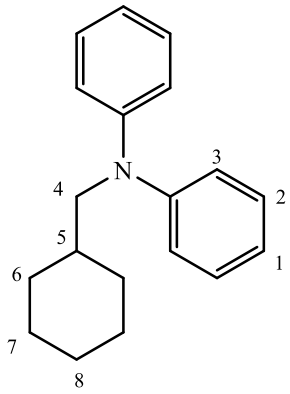

Cyclohexene (7.2 mmol) was reacted with diphenylamine (7.2 mmol) in toluene at 105 °C for 4 hours under catalytic conditions. **LC**: 14%, t_R = 1.511 min. **MS (EI, m/z)**: 266.2 (100%, $[M+H]^+$), calculated 265.2.

*4.8.5.7 2-(Piperidin-1-ylmethyl)cyclohexan-1-ol (**P7**)* [47]

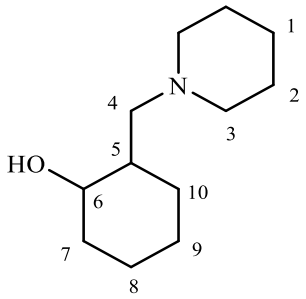

Cyclohex-2-en-1-ol (7.2 mmol) was reacted with piperidine (7.2 mmol) in toluene at 105 °C for 4 hours under catalytic conditions. Product was isolated by column chromatography (100% EtOAc, R_f = 0.10) before drying under vacuum to produce a viscous clear oil. **^{1}H NMR (300 MHz, $CDCl_3$)**: δ (ppm) = 3.40 (1H, br s, H_6), 2.61 (2H, br s, H_4), 2.32 (4H, m, H_3), 1.97 (1H, br s, H_5), 1.74-0.67 (14H, m, H_7-H_{10}, H_1-H_2). **LC**: t_R = 0.295 min. **MS (EI, m/z)**: 198.2 (100%, $[M+H]^+$), calculated 197.2.

*4.8.5.8 2-Phenyl-N-propylpropan-1-amine (**P8**)*

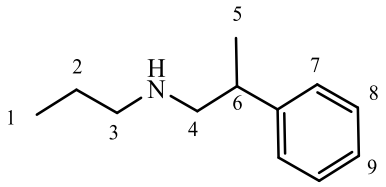

Styrene (7.2 mmol) was reacted with propylamine (7.2 mmol) in toluene at 105 °C for 4 hours under catalytic conditions. Product was isolated by column chromatography (100 % EtOAc, R_f = 0.11) before drying under vacuum to produce a pale-yellow emulsion. **^{1}H NMR (300 MHz, $CDCl_3$)**: δ (ppm) = 7.44-7.02 (5H, m, H_7-H_9), 2.97 (1H, m, H_6), 2.80 (2H, d, ^3J = 7.2 Hz , H_4), 2.54 (2H, m, H_3), 1.46 (3H, br m, H_2, NH), 1.29 (3H, d, ^3J = 6.1 Hz , H_5) 0.87 (3H, t, ^3J = 7.2 Hz, H_1). **LC**: t_R = 0.451 min. **MS (EI, m/z)**: 178.2 (100%, $[M+H]^+$), calculated 177.2.

*4.8.5.9 1-(3-Phenylpropyl)piperidine (**P9**)*[20,48]

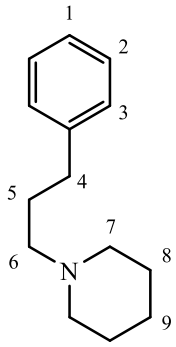

Styrene (7.2 mmol) was reacted with piperidine (7.2 mmol) in toluene at 105 °C for 4 hours under catalytic conditions. Product was isolated by column chromatography (100 % EtOAc, R_f = 0.15) before drying under vacuum to produce a pale-yellow oil. **^{1}H NMR (300 MHz, $CDCl_3$)**: δ (ppm) = 7.30-7.01 (5H, m, H_1-H_3), 2.54 (2H, t, ^3J = 7.7 Hz, H_4), 2.38-2.16 (6H, m, H_6, H_7), 1.87-1.68 (2H, m, H_3), 1.57-1.42 (4H, m, H_8), 1.36-1.23 (2H, br s, H_9) **LC**: t_R = 0.442 min. **MS (EI, m/z)**: 204.2 (100 %, $[M+H]^+$), calculated 203.2.

*4.8.5.10 1-(2-Phenylpropyl)piperidine (**P10**)* [49]

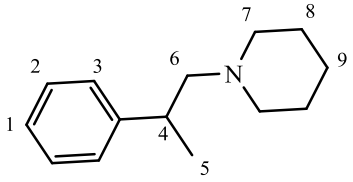

Styrene (7.2 mmol) was reacted with piperidine (7.2 mmol) in toluene at 105 °C for 4 hours under catalytic conditions. Product was isolated by column chromatography (100% EtOAc, R_f = 0.4) before drying under vacuum to produce a yellow oil. **^{1}H NMR (300 MHz, $CDCl_3$)**: δ (ppm) = 7.43-7.12 (5H, m, H_1-H_3), 3.01 (1H, dd, ^3J = 13.3, 6.6 Hz , H_4), 2.48 (4H, m, H_7), 2.37 (2H, br s, H_6), 1.60 (4H, br s, H_8), 1.45 (2H, m, H_9), 1.31 (3H, d, ^3J = 6.1 Hz , H_5). **LC**: t_R = 0.562 min. **MS (EI, m/z)**: 204.2 (100%, $[M+H]^+$), calculated 203.2.

*4.8.5.11 1-Phenyl-2-(piperidin-1-ylmethyl)cyclohexan-1-ol (**P11**)*[50]

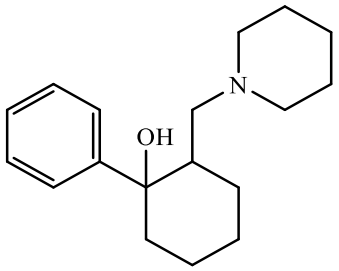

3,4-Dihydro-[1,1'-biphenyl]-1(2H)-ol (7.2 mmol) was reacted with piperidine (7.2 mmol) in toluene at 105 °C for 4 hours under the optimised catalytic conditions. **LC**: 74%, t_R = 0.691 min. **MS (EI, m/z)**: 274.2 (100 %, $[M+H]^+$), calculated 273.2.

*4.8.5.12 2-((Dibenzylamino)methyl)-1-phenylcyclohexan-1-ol (**P12**)*

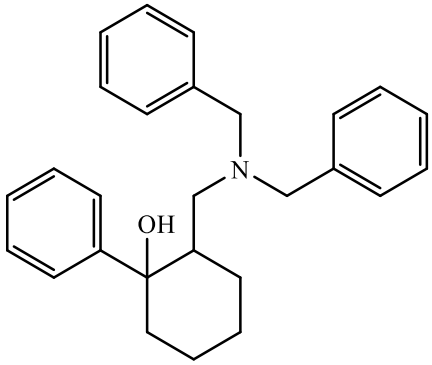

3,4-Dihydro-[1,1'-biphenyl]-1(2H)-ol (7.2 mmol) was reacted with dibenzylamine (7.2 mmol) in toluene at 105 °C for 4 hours under the optimised catalytic conditions. **LC**: 36%, t_R = 0.861 min. **MS (EI, m/z)**: 386.2 (100%, $[M+H]^+$), calculated 385.2.

4.9 References

1. M. Pelckmans, T. Renders, S. Van de Vyver and B. F. Sels, *Green Chem.,* 2017, **19**, 5303-5331.

2. K. S. Hayes, *Appl. Catal. A. Gen.,* 2001, **221**, 187-195.

3. F. Albericio, M. Álvarez, C. Cuevas, A. Francesch, D. Pla, J. Tulla-Puche, in *Molecular imaging for integrated medical therapy and drug development*, Springer, Boston, MA, 2010, p. 237.

4. S. Chen, G. Ravindran, Q. Zhang, S. Kisely, D. Siskind, *CNS Drugs*, 2019, **33**, 225-238.

5. H. Liu, D. L. Wang, X. Chen, Y. Lu, X. L. Zhao and Y. Liu, *Green Chem.* 2017, **19** 1109-1116.

6. S. Shekhar, P. Ryberg, J. F. Hartwig, J. S. Mathew, D. G. Blackmond, E. R. Strieter, and S. L. Buchwald, *J. Am. Chem. Soc.*, 2006, **128** (11), 3584-3591.

7. C. Bornschein, S. Werkmeister, B. Wendt, H. Jiao, E. Alberico, W. Baumann, H. Junge, K. Junge, M. Beller, *Nat. Commun*., 2014, **5**, 4111-4122.

8. D. Ma, Y. Zhang, J. Yao, S. Wu and F. Tao *J. Am. Chem. Soc.*, 1998, **120** (48), 12459-12467.

9. S. Tivari, P. K. Singh, P. P. Singh and V. Srivastava, *RSC Adv.*, 2022, **12** (54), 35221-35226.

10. R. Dorel, C. P. Grugel and A. M. Haydl, *Angew. Chem., Int. Ed.,* 2019, **58**, 17118-17129.

11. K. Natte, H. Neumann, R. V. Jagadeesh and M. Beller, *Nat. Commun.*, 2017, **8** (1),1344, 1-9.

12. H. Elsen, C. Färber, G. Ballmann and S. Harder, *Angew. Chem. Int. Ed.*, 2018, 57, 7156-7160.

13. W. Reppe and H. Vetter, *Ann. Chem.*, 1953, **582**, 133-163.

14, M. J. Schneider, M. Lijewski, R. Woelfel, M. Haumann, P. Wasserscheid, *Angew. Chem., Int. Ed.*, 2013, **52**, 6996-6999.

15. P. Kalck and M. Urrutigoïty, *Chem. Rev.*, 2018, **118**, 3833-3861.

16. E. A. Karakhanov and A. L. Maksimov, *Russ. J. Gen. Chem.*, 2009, **79**, 1370–1383.

17. S. Siangwata, N. J. Goosen and G. S. Smith, *Appl. Catal. A. Gen.*, 2020, **603**, 117736.

18. C. Qian, Q. Zheng, J. Chen, B. Tu and T. Tu, *Green Chem.***,** 2023, **25**, 1368-1379.

19. F. Migliorini, E. Monciatti, G. Romagnoli, M. L. Parisi, J. Taubert, M. Vogt, R. Langer and E. Petricci, *ACS Catal.*, 2023, **13** (4), 2702-2714.

20. H. Liu, D. Yang, Y. Yao, Y. Xu, H. Shang and X Lin, *Mol. Catal.*, 2020, **485**, 1-8.

21. B. Zimmermann, J. Herwig and M. Beller, *Angew. Chem. Int. Ed.*, 1999, **38**, 2372-2375.

22. J. I. van der Vlugt, *Eur. J. Inorg. Chem.*, 2012, 363-375.

23. Y. Sun, M. Ahmed, R. Jackstell, M. Beller and W. R. Thiel, *Organometallics.*, 2004, **23**, 5260-5267.

24. J. Meng, X. H. Li and Z. Y. Han, *Org. Lett.*, 2017, **19** (5), 1076-1079.

25. L. Wu, I. Fleischer, R. Jackstell and M. Beller, *J. Am. Chem. Soc.*, 2013, **135**, 3989-3996.

26. K. U. Künnemann, D. Weber, C. Becquet, S. Tilloy, E. Monflier, T. Seidensticker, and D. Vogt, *ACS Sustain. Chem. Eng.*, 2021, **9** (1), 273-283.

27. T. Roth, R. Evertz, N. Kopplin, S. Tilloy, E. Monflier, D. Vogt and T. Seidensticker, *Green Chem.*, 2023, **25**, 3680-3691.

28. Z. Nairoukh and J. Blum, *J. Chem. Org.*, 2014, **79**, 2397-2403.

29. T. O. Vieira and H. Alper *Chem. Commun.*, 2007, **26**, 2710-2711.

30. J. October and S. F. Mapolie, *Catal. Lett.*, 2020, **150**, 998 -1010.

31. J. October and S. F. Mapolie, *Tetrahedron Lett.*, 2021, **70**, 153018.

32. S. de Doncker, A. Casimiro, I. A. Kotze, S. Ngubane and G. S. Smith, *Inorg. Chem.*, 2020, **59**, 12928-12940.

33. S. de Doncker, G. S. Smith and S. Ngubane, *Appl. Catal. A. Gen.*, 2023, **667**, 119440.

34. D. Giffard, E. Fischer-Fodor, C. Vlad, P. Achimas-Cadariu and G. S. Smith, *Eur. J. Med. Chem.*, 2018, **157**, 773-781.

35. E. B. Maxted and M. S. Biggs. *J. Chem. Soc.*, 1957, 3844-3847.

36. P. Marcazzan, B. O. Patrick and B. R. James. *Organometallics.*, 2003, **22**, 1177-1179.

37. F. C. Braga, T. O. Ramos, T. J. Brocksom, and K. T. de Oliveira *Org. Lett.*, 2022, **24** (45), 8331-8336.

38. Q. Zhang, J. F. Li, G. H. Tian, R. X. Zhang, J. Sun, J. Suo, X. Feng, D. Fang, X. R. Jiang and J. S. Shen, *Tetrahedron: Asymmetry.*, 2012, **23** (8), 577-582.

39. C. Alvarado, Á. Guzmán, E. Díaz, and R. Patiño, *J. Mex. Chem. Soc.,* 2005, **49** (4), 324-327.

40. E.T. Jarvi, N.A. Grayson, R.E. Halvachs, Synthesis and Purification of (r*,r*)-2-[(dimethylamino) Methyl]-1-(3-methoxyphenyl) Cyclohexanol Hydrochloride, US6399829 B1 (2002).

41. D. Seyferth, *Organometallics.,* 2009, **28** (6), 1598-1605.

42. R. M. Peltzer, J. Gauss, O. Eisenstein and M. Cascella, *J. Am. Chem. Soc.*, 2020, **142** (6), 2984-2994.

43. C. L. Bumgardner, E. L. Lawton and J. G. Carver, *J. Org. Chem.*, 1972, **37** (3), 407-409.

44. W. Zhang, P. C. Zhang, Y. L. Li, H. H. Wu and J. Zhang, *J Am Chem Soc.*, 2022, **144** (42), 19627-19634.

45. L. Jiang, P. Zhou, Z. Zhang, Q. Chi and S. Jin, *New J. Chem.,* 2017, **41** (20), 11991-11997.

46. J. An, Z. Gao, Y. Wang, Z. Zhang, J. Zhang, L. Li, B. Tang and F. Wang, *Green Chem.*, 2021, **23** (7), 2722-2728.

47. R. H. K. Foster and A. J. Carman, *J. Pharmacol. Exp. Ther.*, 1947, **91**, 195-209.

48. A. F. M. Iqbal, *Helv. Chim. Acta.*, 1971, **54** (5), 1440-1445.

49. A. M. Seayad, K. Selvakumar, M. Ahmed and M. Beller, *Tetrahedron Lett.*, 2003, **44** (8), 1679-1683.

50. A. L. Morrison and H. Rinderknecht, *J. Chem. Soc.*, 1950, 1510-1513.

Chapter 5

Summary, conclusions, and future outlook

5.1 Overall summary and conclusions

The objectives of this project were to synthesise and characterise a series of heteroleptic dirhodium(II,II) acetate-bipyridyl complexes for application in hydroformylation and hydroaminomethylation reactions. Two known compounds (**1** and **4**)[1] and four new compounds (**2**, **3**, **5** and **6**) were obtained in moderate to excellent yields. The complexes were characterised by an array of spectroscopic and analytical techniques such as NMR spectroscopy (^{1}H-, ^{13}C{^{1}H}-, ^{19}F-,^{31}P- and DOSY), IR spectroscopy in addition to electrochemical (Cyclic voltammetry) and analytical (mass spectrometry, conductivity, melting point) techniques. The interaction of the acetate ligands with the bimetallic core was determined by spectroscopic (DOSY and ^{31}P-NMR) and conductivity measurements. This involvement was shown to significantly affect the electronics of the complexes, whereby cyclic voltammetry shows that exchange of the acetate for hexafluorophosphate resulted in a higher observed reduction potential for the Rh_2^{4+}/Rh_2^{3+} redox couple.

The first application of bis-substituted dirhodium(II,II) bipyridyl chelate complexes for hydroformylation reactions has been reported herein. The title complexes were evaluated as catalyst precursors in the hydroformylation of 1-octene and compared to the $Rh_2(OAc)_4$ complex previously reported. Optimisation of the reaction conditions resulted in a reduction in the temperature and pressure required for the hydroformylation reaction compared to $Rh_2(OAc)_4$ for the model complex.[2] Under these conditions, near quantitative conversion and excellent chemoselectivity for aldehyde products was achieved. The regioselectivity was found to be strongly dependent on the interaction of the acetate counter ion, likely through increased steric influence, with the greatest regioselectivity observed for complex **3**. Under the optimised conditions, recyclability was attempted with a preliminary aqueous biphasic system, however

the tested complex showed poor recyclability due to leaching into the organic phase. Further analysis of the solubility of the complexes resulted in complex **6** showing suitable temperature dependent solubility in toluene. The separation of the catalyst precursor from the reaction medium was thereby achieved by cooling to 0 °C to induce precipitation in toluene, the solvent used in the hydroformylation reaction. Complex **6** was then evaluated for recyclability over 5 cycles showing good activity and selectivity throughout. This finding allows for prospective reuse of the catalyst precursor, unreported for dirhodium(II,II) complexes in this application. Furthermore, the substrate scope was extended to long-chain internal (7-tetradecene), cyclic (cyclohexene) and benzylic (styrene) utilising the catalyst precursor with the greatest chemoselectivity for aldehydes (complex **2**). The results obtained from these substrates showed moderate to excellent activity (> 74%) with no hydrogenated alkene or aldehyde products (alkanes or alcohols) detected in any hydroformylation reactions, eluding candidacy of these complexes for tandem reactions such as hydroaminomethylation.

The application of heteroleptic dirhodium(II,II) bipyridyl chelate complexes as catalyst precursors for hydroaminomethylation reactions has been reported herein for the first time. Toward the development of the title complexes for hydroaminomethylation reactions, the hydrogenation capabilities were initially evaluated in a model reaction between benzaldehyde and propylamine under a variety of conditions. The *in-situ* Schiff-base condensation reaction was found to proceed quantitatively across the tested temperature range, with hydrogenation of the formed imine intermediate occurring effectively at 105 °C. An increase in the hydrogenation capability of the catalyst precursor was observed when the counter ion was exchanged from acetate (**1**) to hexafluorophosphate (**4**) in the model hydrogenation reaction. The maximal increase in the hydrogenation activity (68%) was observed for trifluoromethyl-containing complex **5** at a 0.08 mol% catalyst loading at 105 °C, with no observed production of alcohol by-products. The hydrogenation reaction was found to occur independent of the substituent on the benzaldehyde substrate however, the stability of the Schiff-base significantly influences the yield of target amine product.

Complex **5** was evaluated further as a catalyst precursor in the hydroaminomethylation of cyclohexene and propylamine as a proof of concept. To maximise the production of the target compounds from a combination of the hydroformylation and hydrogenation reactions, the partial pressure of the CO and H_2 components of syngas were varied. This optimisation resulted

in a 2:3/CO:H_2 ratio providing near quantitative conversion of substrate from the hydroformylation step and good hydrogenation activity without additional co-ligands or additives. This shows that under the optimised conditions, this catalytic system provides a route to produce amines from alkenes in good to excellent yields without the use of additives and at lower catalyst loading compared to currently reported homogeneous systems.

Variation in the amine substrate showed good activity and selectivity for both primary and secondary aliphatic amine substrates, with poor product formation for aryl amine substrates. Variation in the olefin substrate to styrene showed excellent conversion and good selectivity for branched amine formation (<85%). Reactions carried out cyclohex-2-en-1-ol and cyclohex-2-en-1-one, showed good hydroformylation conversion with excellent regioselectivity (100% α-product) observed for cyclohex-2-en-1-ol. The reaction carried out with cyclohex-2-en-1-one resulted in the formation of mixed products through condensation occurring at the aldehyde and ketone functionalities. Therefore, it can be deduced that the regioselectivity of the reaction may be enhanced by inclusion of suitable directing substituents such as OH on the substrate, provided that the substituent does not take part in the condensation reaction. The hydroaminomethylation reaction was then applied toward the synthesis of two analogues of Tramadol®, from a suitably structured substrate (**S1**). The substrate (**S1**) was obtained from a Grignard addition reaction and characterised prior to application in the hydroaminomethylation reaction. The production of the piperidinyl and *N*,*N*-dibenzyl derivatives was carried out under catalytic conditions, affording the respective products in yields of 74 and 36% respectively. Further factors influencing the regioselectivity were found, and the steric influence of the amine substituent relative to the phenyl moiety on the substrate (**S1**) was found to negate the effect of the presence of the proposed directing of the hydroxyl group. The data indicates that this complexes and the corresponding reaction conditions can be used to obtain small libraries of compounds such as APIs for structure-activity studies by suitable modification of the substrate catalytically.

5.2 Future outlook

This study has investigated some of the intricacy and nuance associated with the synthesis, characterisation, and application of heteroleptic dirhodium(II,II) acetato-bipyridyl complexes in catalytic transformations. Although these compounds show appreciable activity in the hydroformylation reaction, further development and investigation into the recyclability of the

expensive rhodium-based catalyst precursors should be investigated. Strategies into catalyst recovery may include the addition of further solubilising groups such as sulfonates to improve the aqueous solubility whilst supressing the solubility of the complexes in organic medium.[3-5] Kinetic factors should also be determined and the reaction modified accordingly to enhance the selectivity of the reactions, and the introduction of modified *N*,*N* bridging ligands such as anilinopyridinates or diphenylformamidinates could result in further refinement for the application as catalyst precursors for hydroformylation.[2,6] Additionally, the incorporation of ligands which reduce the temperature requirement for the hydroaminomethylation may be crucial to extend the substrate scope to aliphatic olefins for minimising the isomerisation of substrates.[7] The trifluoromethyl-containing complexes showed promise in hydroformylation and hydroaminomethylation reactions, suggesting that the catalyst precursors containing chelating bipyridyl ligands may benefit from the inclusion of bridging ligands which favour reductive elimination. Insights into the mechanistic and kinetic details for both the hydroformylation and hydroaminomethylation reactions should be investigated toward increasing the efficiencies, poisoning effects, activity and the nature of the proposed species formed in the presence of the catalyst precursors.

Furthermore, should the additional solubilising groups show promise, the hydroaminomethylation reactions may be extended to ammonium salts in an aqueous-biphasic reaction, which proved challenging in the current study. Furthermore, the inclusion of suitably modified ligands capable of directing transformations to chiral substrates may be of interest, particularly in hydroaminomethylation toward obtaining pharmaceutical applications with high enantioselectivity.[8,9]

The complexes may also be evaluated in the catalytic production of amides from alkenes, such as described in hydroaminocarbonylation reactions with palladium catalysts, for example. The comparative improvements in catalyst loading and reaction conditions in such instances may be beneficial, where typical metal loading of around 3 mol% in the presence of strong acid and ligand additives are reported.[10] Additionally, these complexes may then be suitable for the direct formation of key components of Guerbet-type surfactants and the formation of precursors for various polymers with extensive applications.[11-13]

5.3 References

1. C. A Crawford, J. H. Matonic, J. C. Huffman, K. Folting, K. R. Dunbar and G. Christou, *Inorg. Chem.,* 1997**, 36**, 2361-2371.

2. S. de Doncker, A. Casimiro, I. A. Kotze, S. Ngubane and G. S. Smith, *Inorg. Chem.*, 2020, **59**, 12928-12940.

3. S. Siangwata, N. J. Goosen and G. S. Smith, *Appl. Catal. A Gen*., 2020, **603**, 117736.

4. S. Siangwata, N. Baartzes, B. C. E. Makhubela and G. S. Smith, *J. Organomet. Chem.*, 2015, **796**, 26-32.

5. N. N. Omosun, S. Ngubane, G. S. Smith, *Appl. Catal. A Gen.*, 2021, **610**, 117950.

6. R. Hrdina, *Eur. J. Inorg. Chem.,* 2021, 501-528.

7. J. October and S. F. Mapolie, *Catal. Lett.*, 2020, **150**, 998-1010.

8. T. Miyazawa, T. Suzuki, Y. Kumagai, K. Takizawa, T. Kikuchi, S. Kato, A. Onoda, T. Hayashi, Y. Kamei, F. Kamiyama, M. Anada, M. Kojima, T. Yoshino and S. Matsunaga, *Nat. Catal.*, 2020, 3, 851–858.

9. C. Qian, Q. Zheng, J. Chen, B. Tu and T. Tu, *Green Chem.*, 2023, **25**, 1368-1379.

10. H. Yang, Y. Yao, M. Chen, Z. Ren and Z. Guan. *J. Am. Chem. Soc.*, 2021, **143** (19), 7298–730.

11. Li. Yan, Y. Li, Z. Cui, Bing. Song, X. Pei and J. Jiang, *Energy Fuels.,* 2017, **31** (9), 9319-9327.

12. T. Vanbesien, E. Monflier and F. Hapiot, *Green Chem.*, 2017, **19**, 1940-1948.

13. A. Behr, T. Seidensticker and A. J. Vorholt, *Eur. J. Lipid Sci. Technol.*, 2014, **116**, 477-485.

Appendix

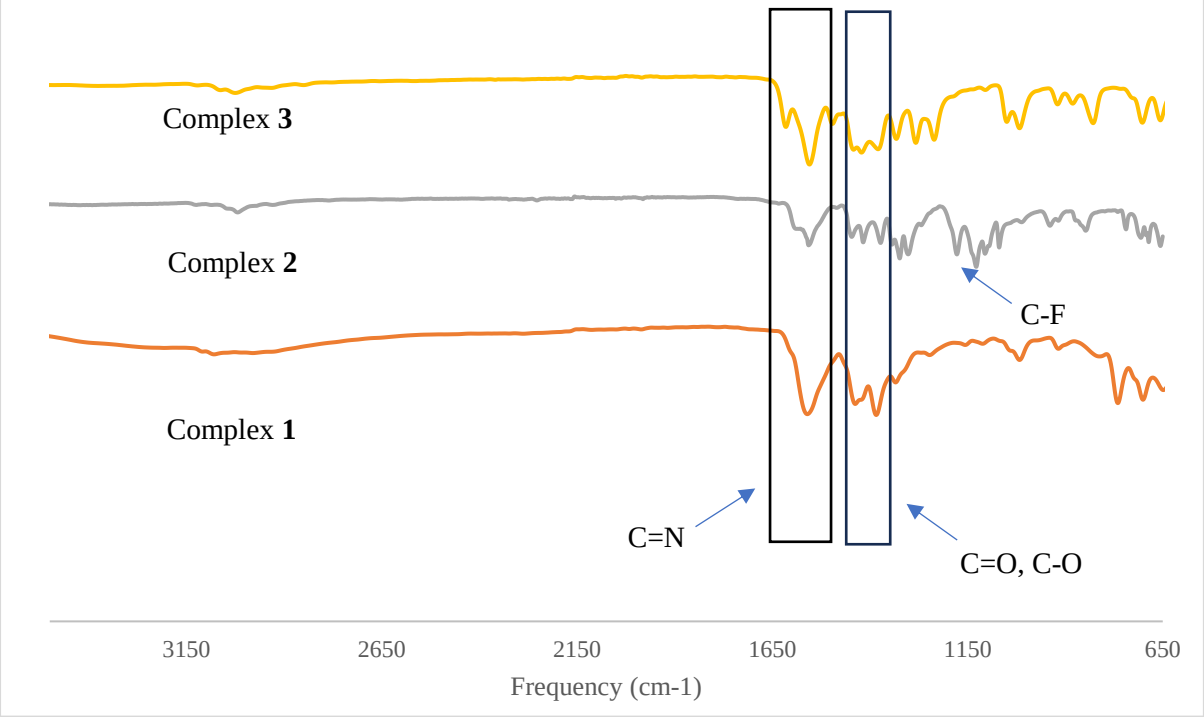

Figure A1. Infrared spectra recorded for complexes **1** - **3**.

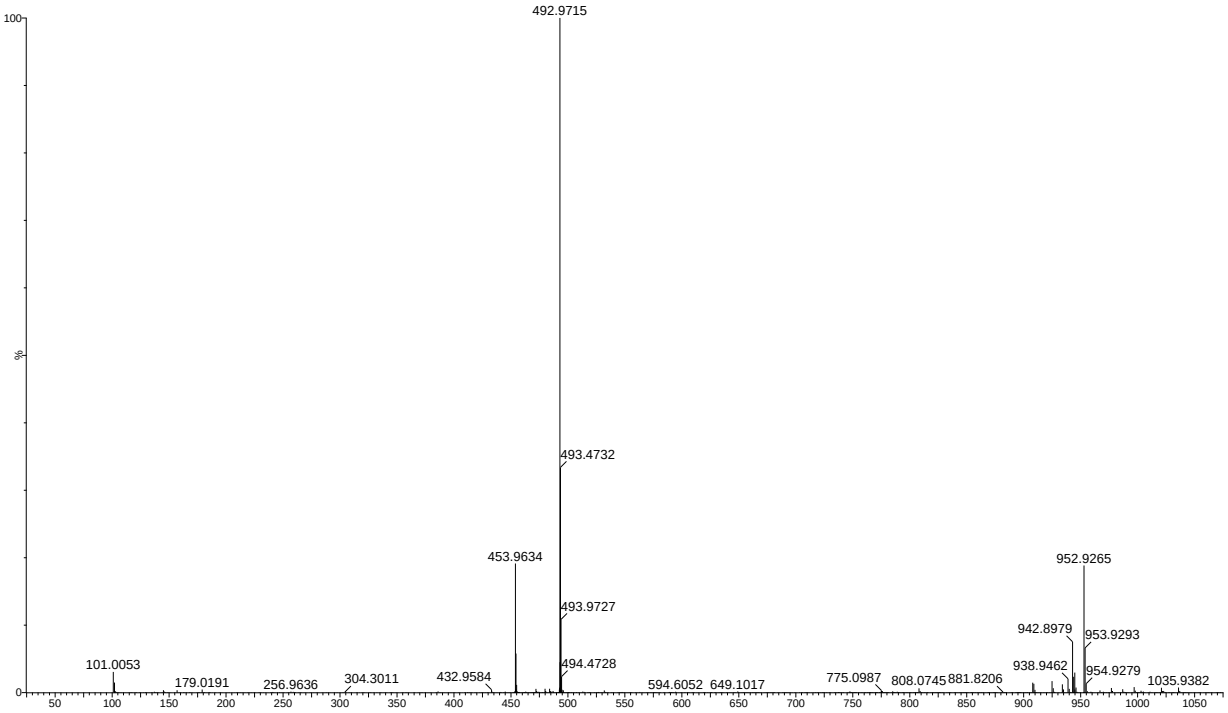

Figure A2. HR-ESI-MS spectrum obtained for complex **2**.

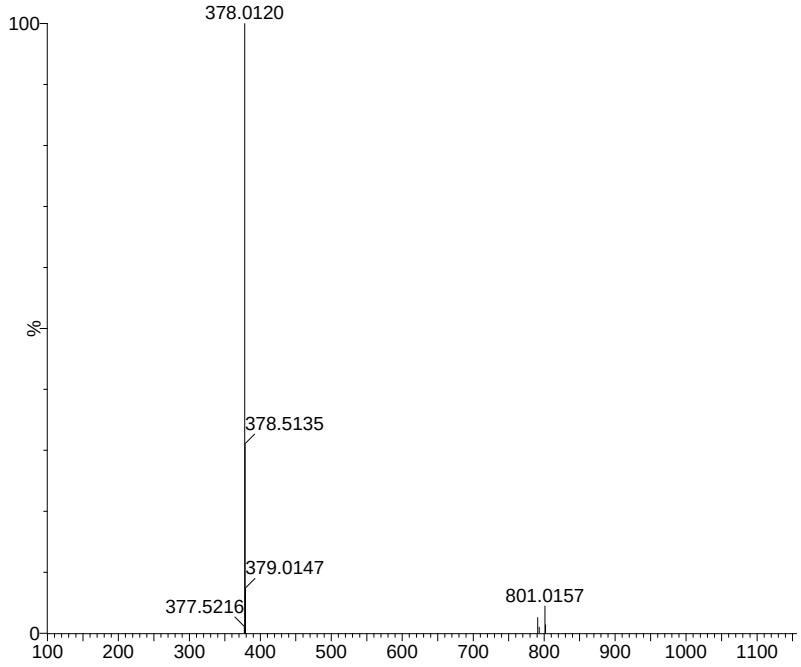

Figure A3. HR-ESI-MS spectrum obtained for complex **3**.

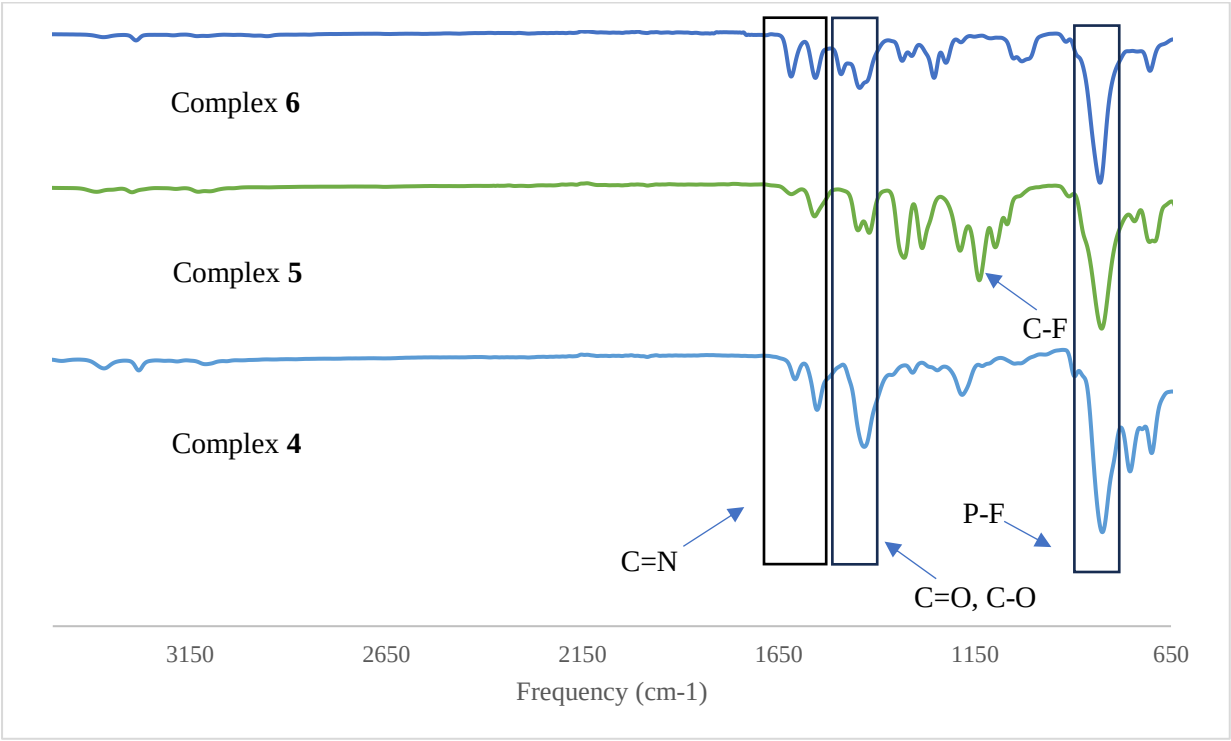

Figure A4. Infrared spectra recorded for complexes **4 - 6**.

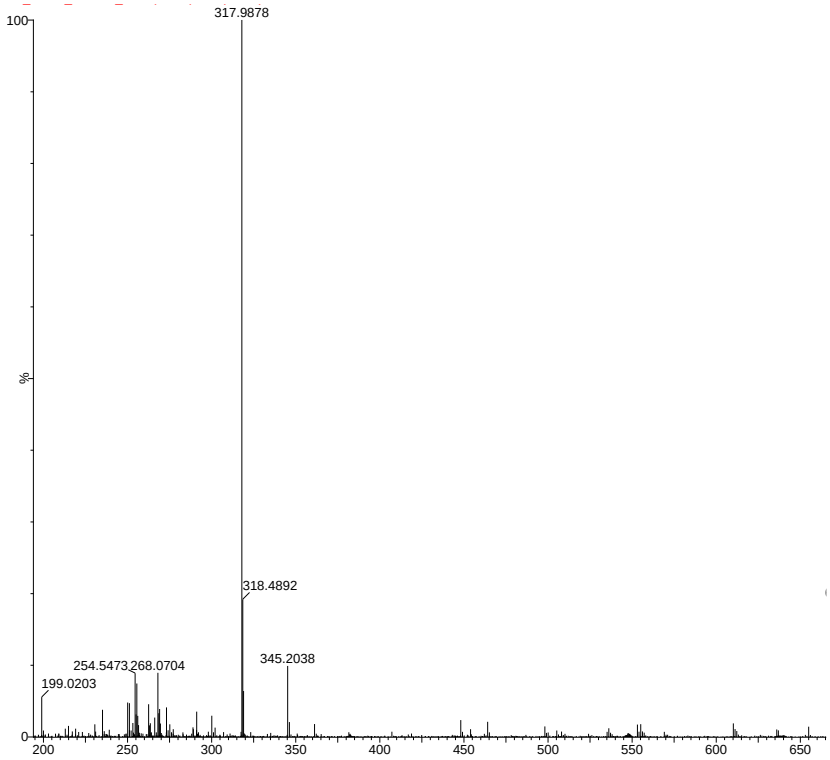

Figure A5. HR-ESI-MS spectrum obtained for complex **4**.

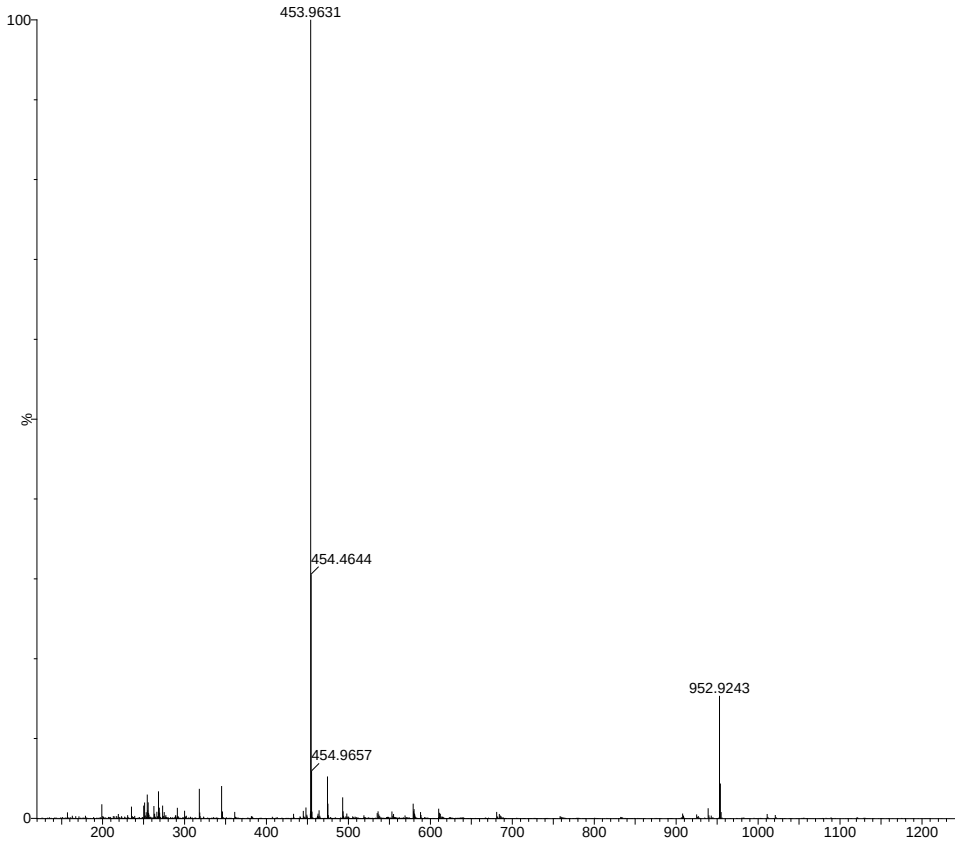

Figure A6. HR-ESI-MS spectrum obtained for complex **5**.

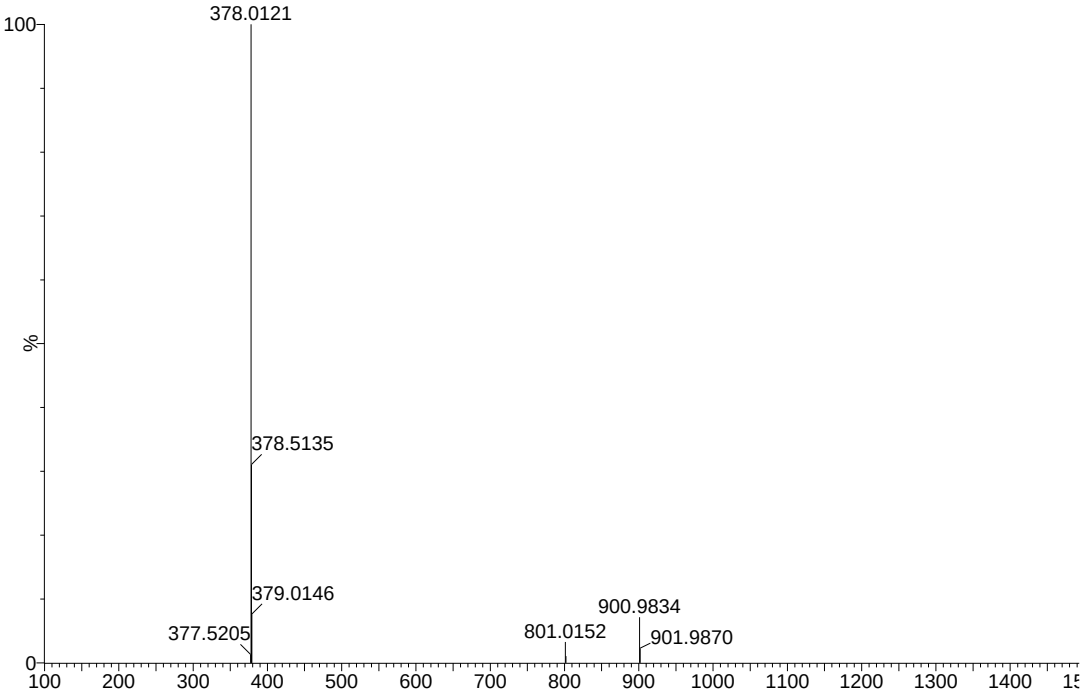

Figure A7. HR-ESI-MS spectrum obtained for complex **6**.

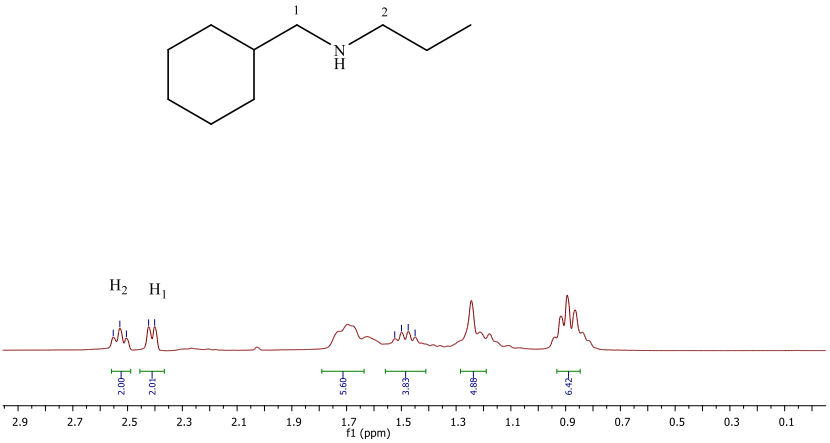

Figure A8. ^{1}H-NMR spectrum obtained for **P1** recorded in $CDCl_3$.

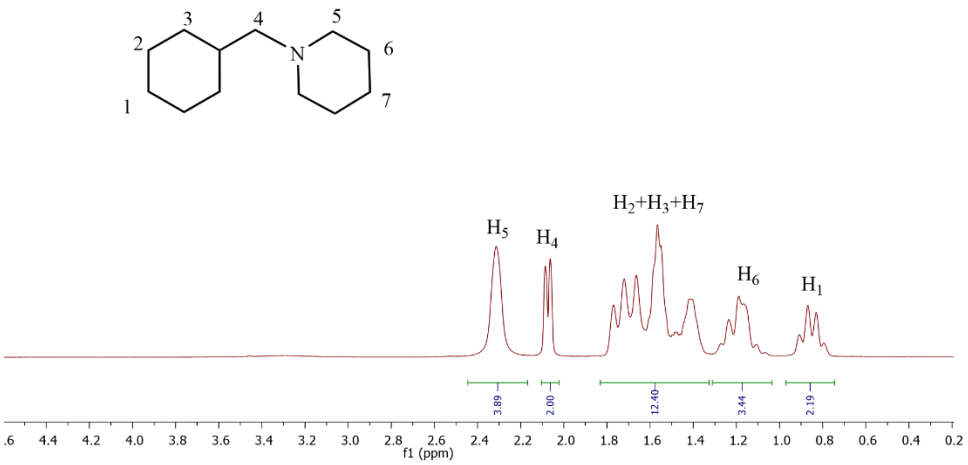

Figure A9. ^{1}H-NMR spectrum obtained for **P3** recorded in $CDCl_3$.

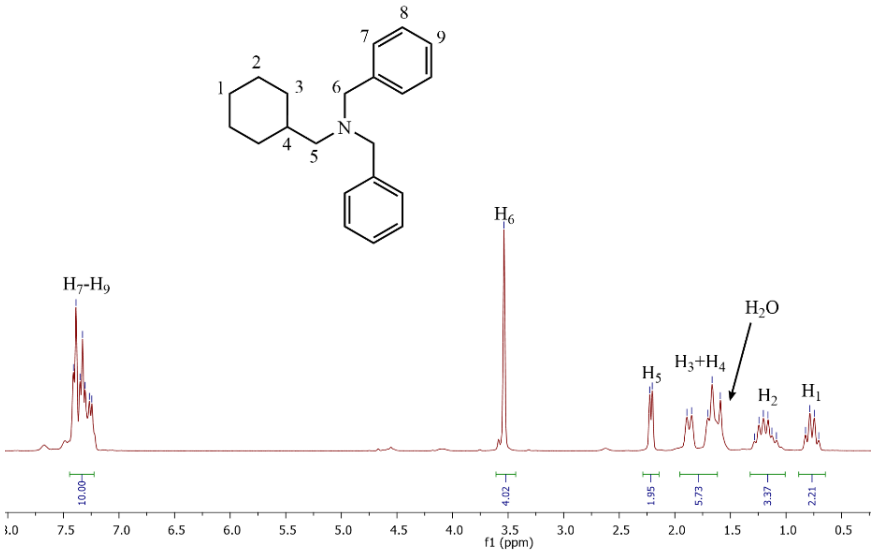

Figure A10. ^{1}H-NMR spectrum obtained for **P4** recorded in $CDCl_3$.

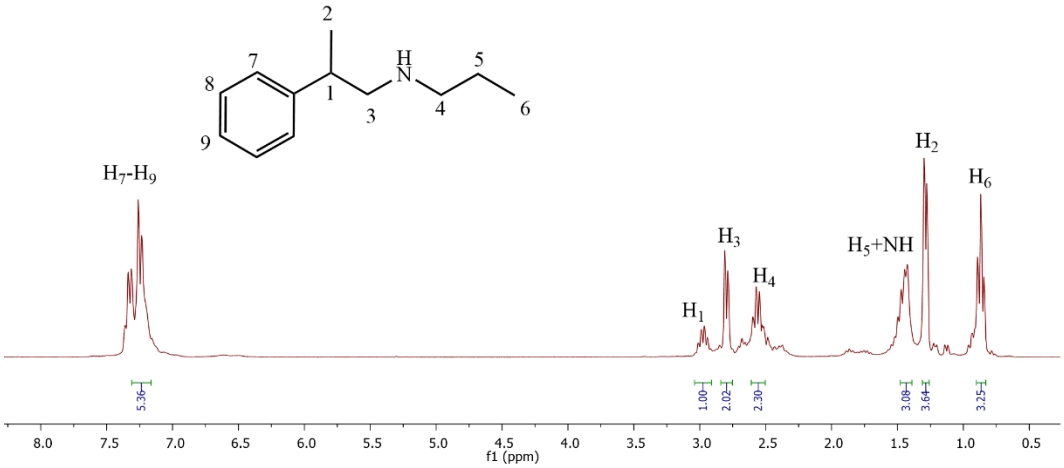

Figure A11. ^{1}H-NMR spectrum obtained for **P8** recorded in $CDCl_3$.

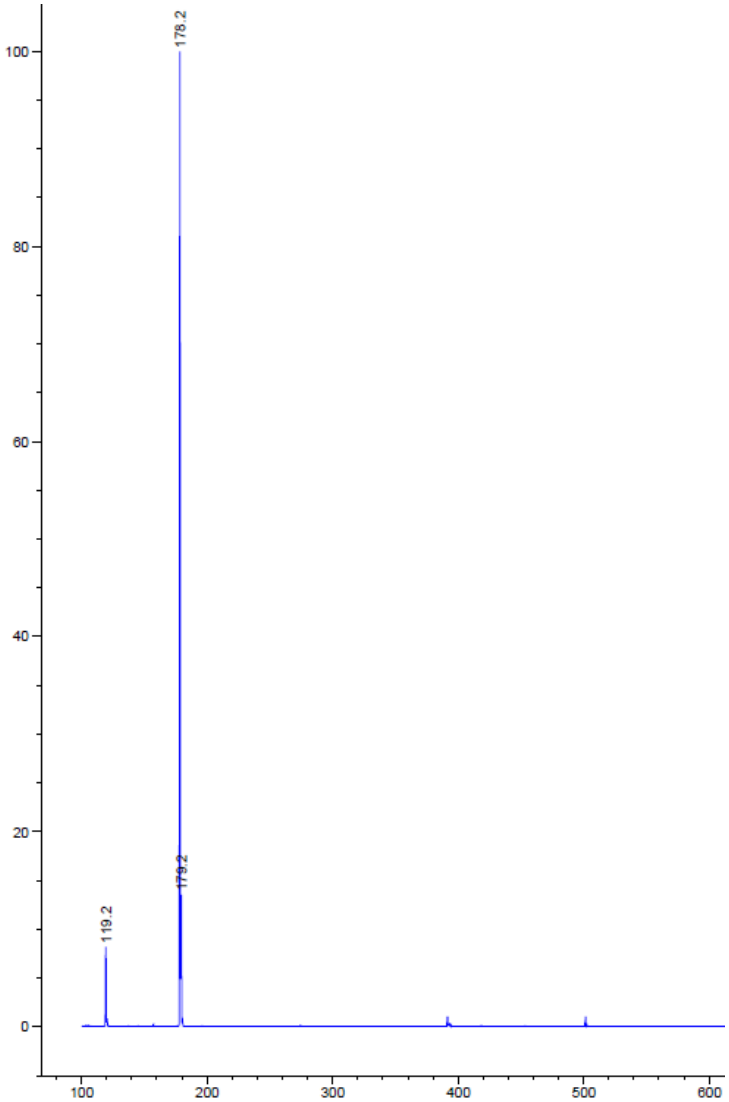

Figure A12. Mass spectrum obtained for **P8.**

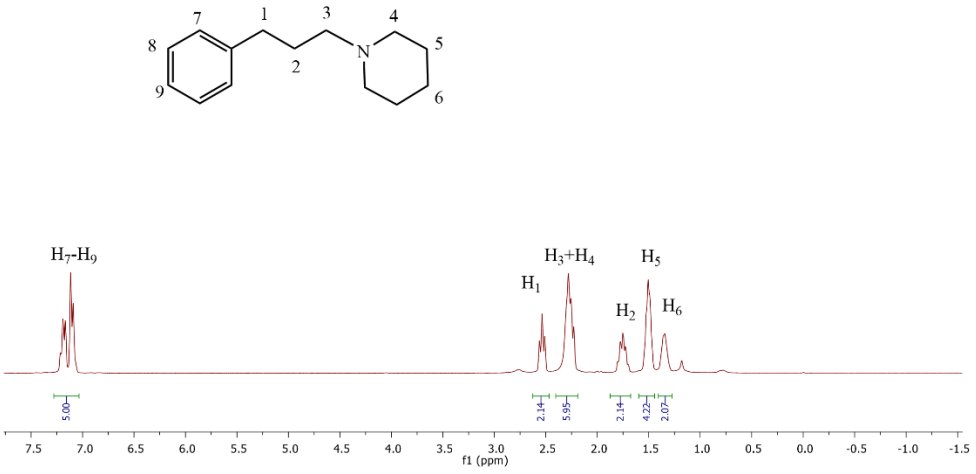

Figure A13. ^{1}H-NMR spectrum obtained for **P9** recorded in $CDCl_3$.

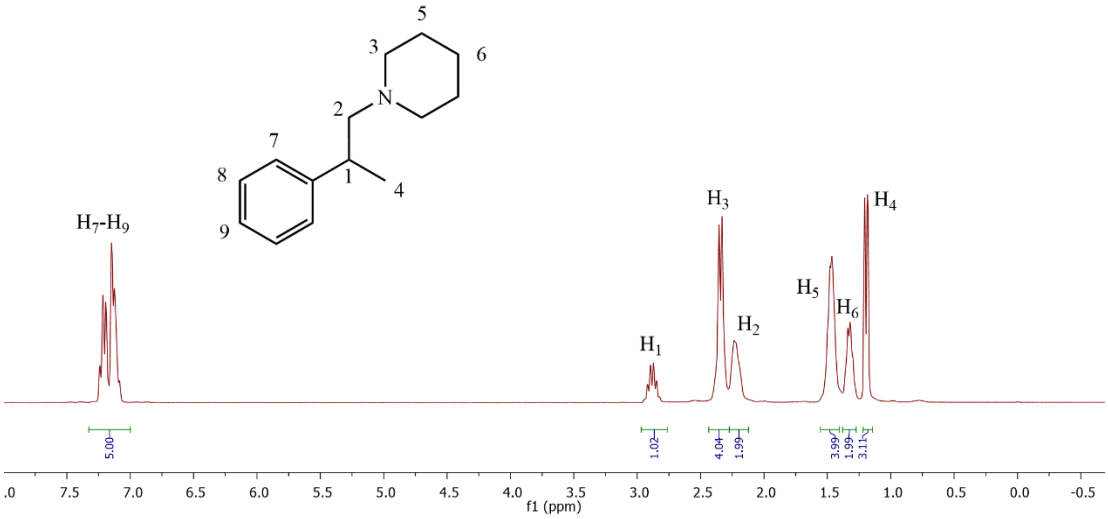

Figure A14. ^{1}H-NMR spectrum obtained for **P10** recorded in $CDCl_3$.

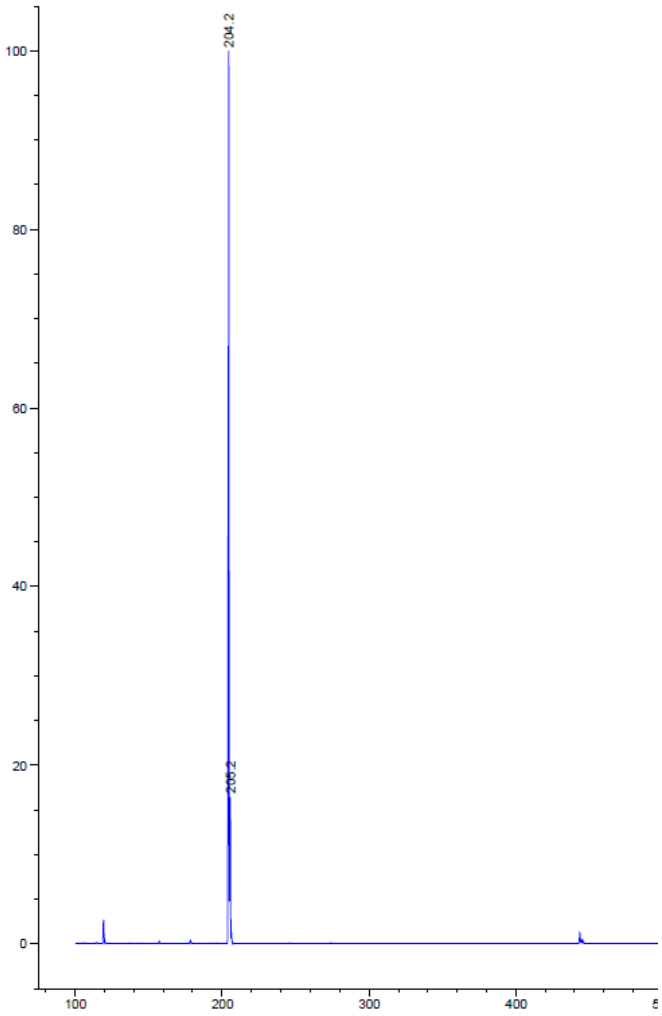

Figure A15. Mass spectrum obtained for **P9.**

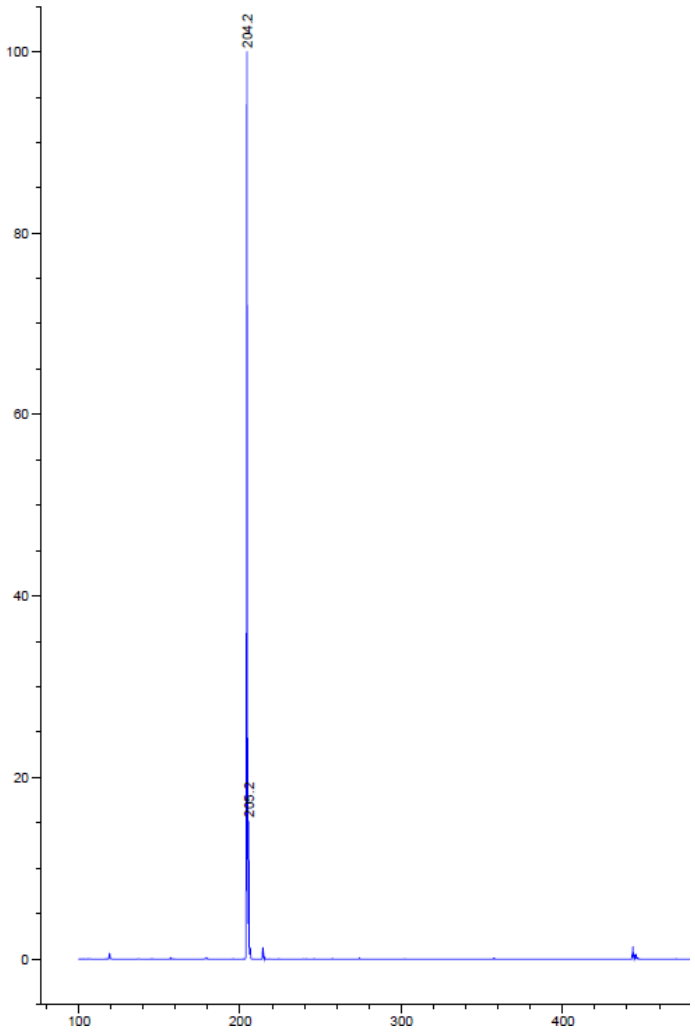

Figure A16. Mass spectrum obtained for **P10.**

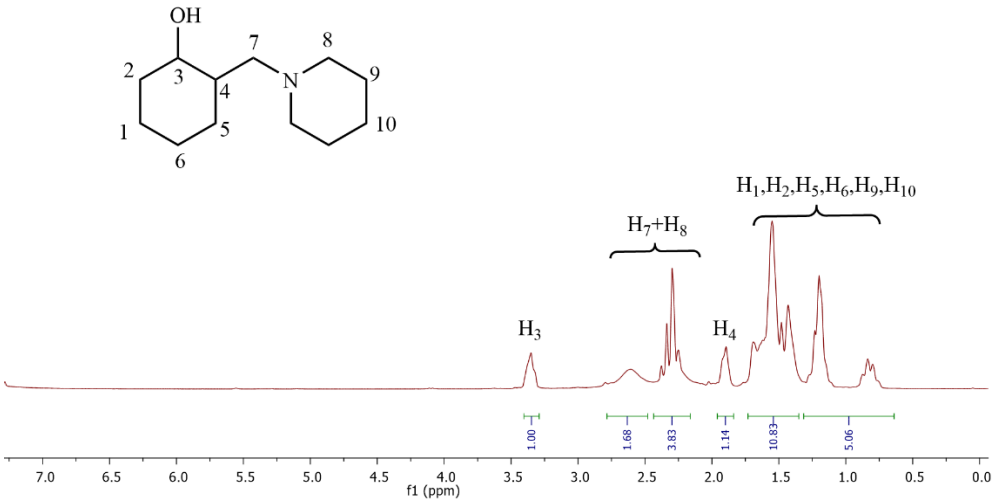

Figure A17. ^{1}H-NMR spectrum obtained for **P7** recorded in $CDCl_3$.

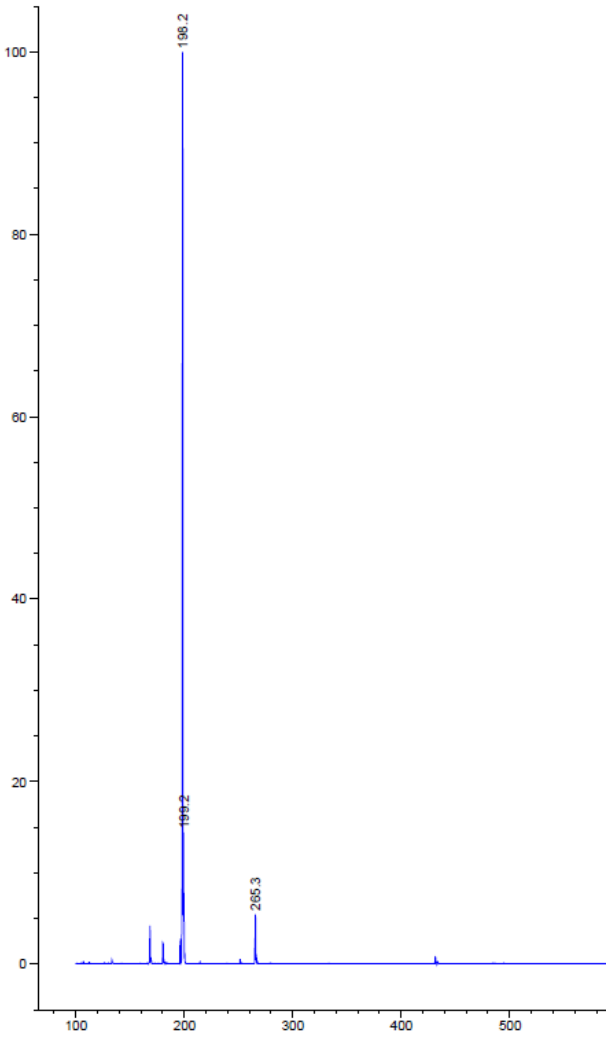

Figure A18. Mass spectrum obtained for **P7.**

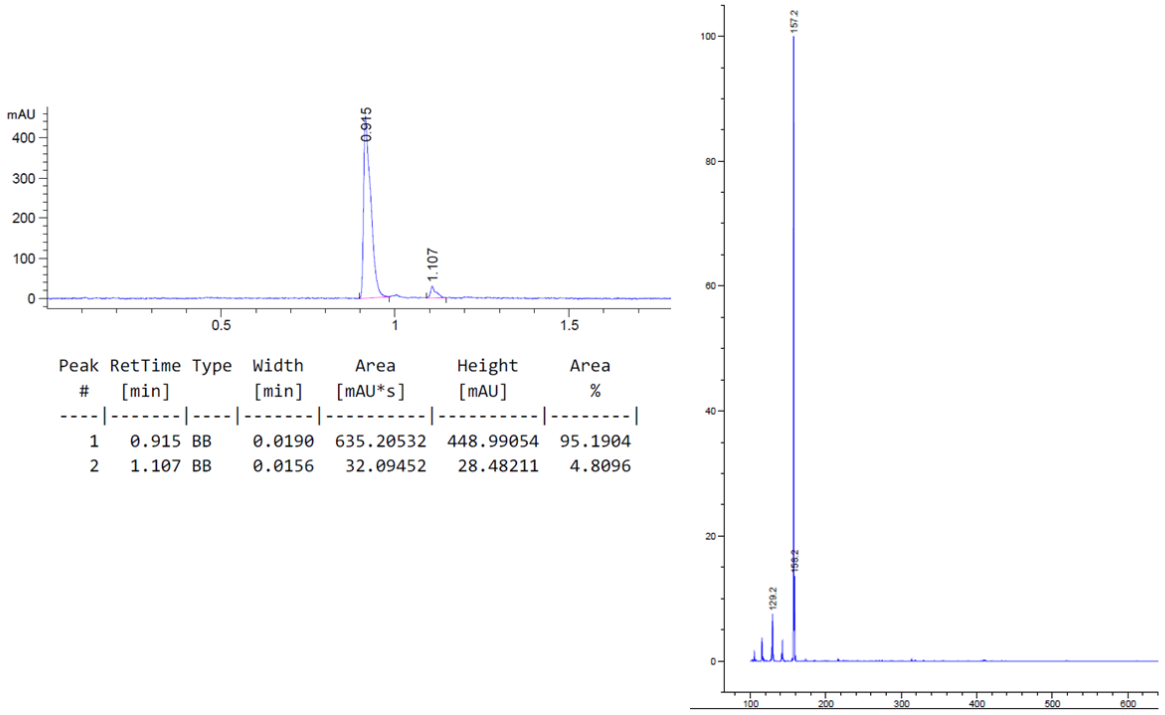

Peak #	RetTime [min]	Type	Width [min]	Area [mAU*s]	Height [mAU]	Area %
1	0.915	BB	0.0190	635.20532	448.99054	95.1904
2	1.107	BB	0.0156	32.09452	28.48211	4.8096

Figure A19. LC-MS data obtained for **S1.**

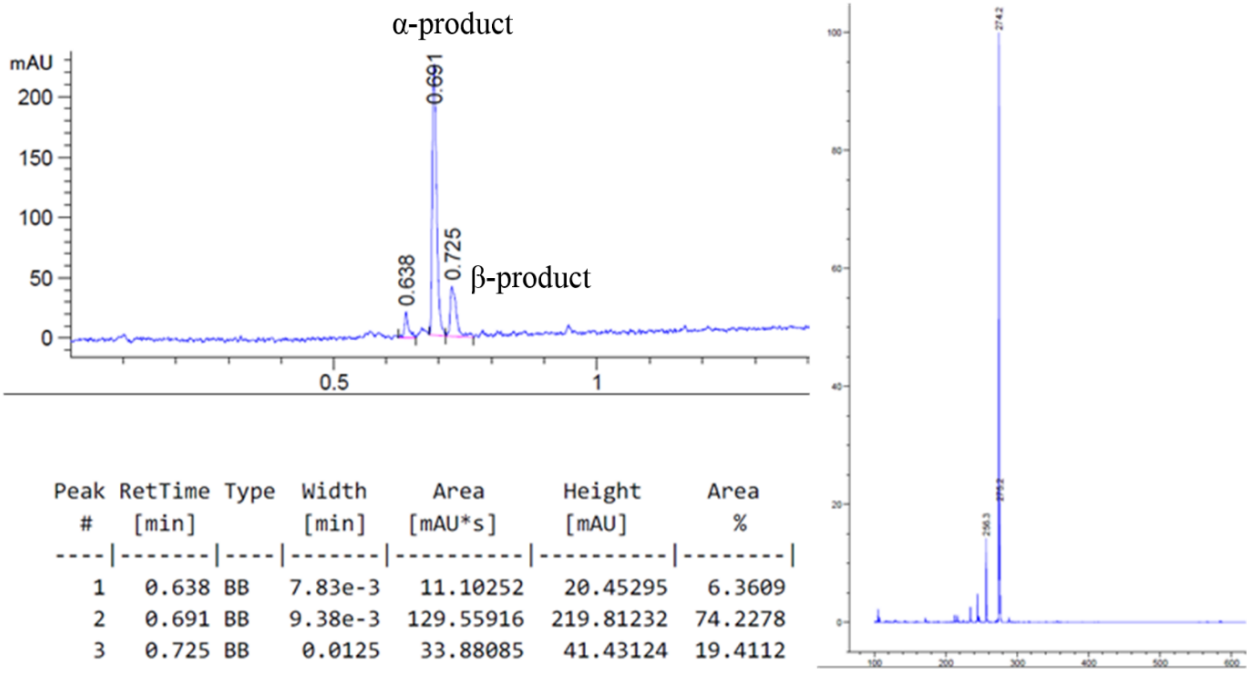

Peak #	RetTime [min]	Type	Width [min]	Area [mAU*s]	Height [mAU]	Area %
1	0.638	BB	7.83e-3	11.10252	20.45295	6.3609
2	0.691	BB	9.38e-3	129.55916	219.81232	74.2278
3	0.725	BB	0.0125	33.88085	41.43124	19.4112

Figure A20. LC-MS data obtained for **P11.**

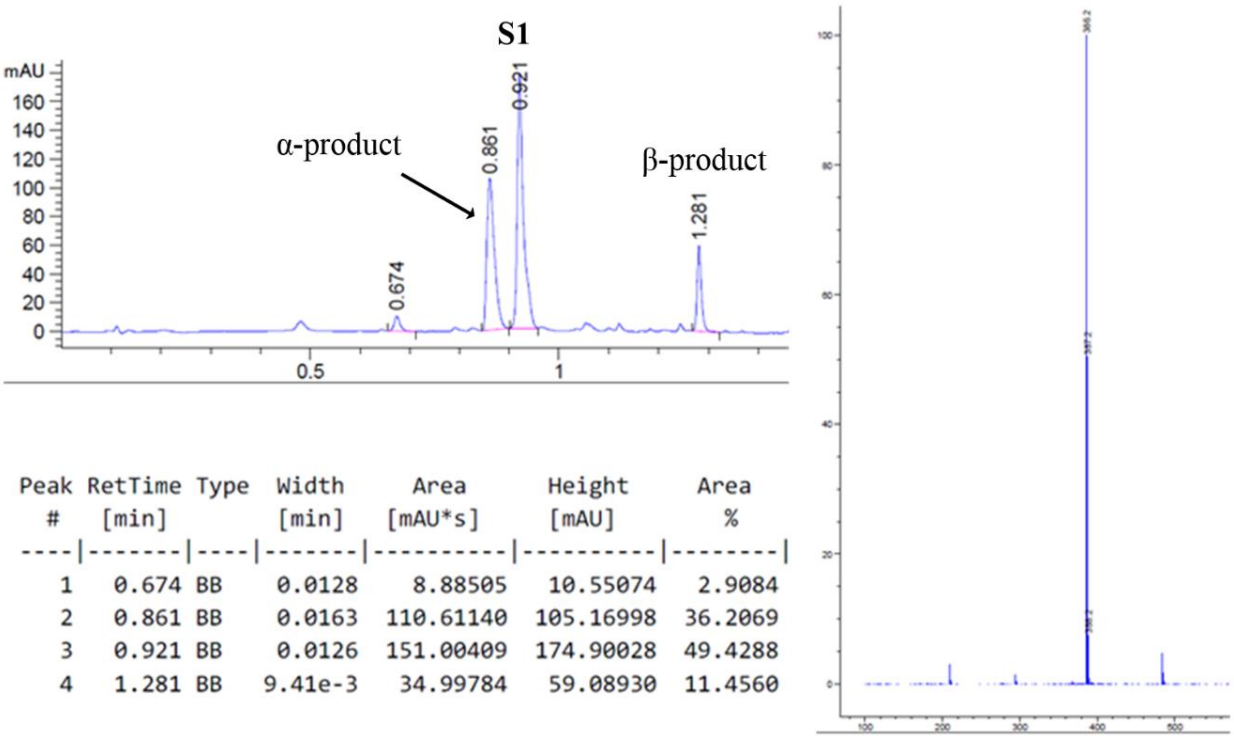

Peak #	RetTime [min]	Type	Width [min]	Area [mAU*s]	Height [mAU]	Area %
1	0.674	BB	0.0128	8.88505	10.55074	2.9084
2	0.861	BB	0.0163	110.61140	105.16998	36.2069
3	0.921	BB	0.0126	151.00409	174.90028	49.4288
4	1.281	BB	9.41e-3	34.99784	59.08930	11.4560

.

Figure A21. LC-MS data obtained for **P12**.